Tomas Bata University in Zlín
Centre of Polymer Systems

Doctoral Thesis

Composite materials based on polysaccharides

Kompozitní materiály na bázi polysacharidů

Author: Ing. Simona Káčerová

Degree programme: P3924 Material Sciences and Engineering

Degree course: 3911V040 Biomaterials and Biocomposites

Supervisor: prof. Ing. Petr Humpolíček, Ph.D.

Consultants: doc. Ing. Zdenka Víchová, Ph.D.
Mgr. Jan Vícha, Ph.D.

Zlín, August 2023

ACKNOWLEDGEMENT

First, I would like to express my appreciation to my supervisor, prof. Ing. Petr Humpolíček, Ph.D. for the privilege of being accepted into his esteemed research group. His unwavering guidance, wisdom, support and patience have been instrumental in shaping my academic journey. Additionally, I would like to extend my sincere thanks to my consultants, doc. Zdenka Víchová, Ph.D. and Mgr. Jan Vícha, Ph.D. for invaluable advices, wisdom and mentorship, which greatly influenced my research skills. Their expertise and dedication have played a pivotal role in shaping the success of my work. I am truly grateful to my supervisor and consultants for their belief in my potential and for providing me opportunities to learn and grow as a researcher. Lastly, a special note of appreciation goes to them for their forgiveness regarding the broken probes of the pH meter.

I would also like to extend my heartfelt appreciation to all of my colleagues from the Centre of Polymer Systems for their support, exchange of ideas, collaborations and emotional support throughout this research journey. Especially, I would like to thank Ing. Kateřina Skopalová, Ph.D. and Ing. Lukáš Münster, Ph.D. for willingness to share their knowledge, help in the laboratory and for their assistance in collecting and organizing data.

Moreover, I am grateful to doc. Ing. Věra Kašpárková, CSc. for her invaluable help, advices and kindness. My thanks also tend to Mgr. Ondřej Vašíček, Ph.D. for introducing me to the world of immunology and for measurement of my samples.

I would like to thank to all of the wonderful friends I made during my abroad internship in Aveiro, Portugal. Their friendship created cherished memories that will forever hold a special place in my heart.

I am also very grateful to my close friends and family for their encouragement, love and great support. To all of you, thank you for unwavering belief in me and for bringing joy and laughter to my life. My heartfelt thanks go to my partner Luba, who has always been here for me. His constant cheer, and thoughtful gestures, like bringing me a home-brewed beer to lift my spirits, have been priceless. I am truly grateful to have such a loving and supportive partner by my side.

Finally, I would like to thank to the Centre of Polymer Systems for its financial support during my studies. The presented thesis was supported by the projects: IGA/CPS/2019/004, IGA/CPS/2020/001, IGA/CPS/2021/001, IGA/CPS/2022/00 and IGA/CPS/2023/001. This dissertation work was also supported by the Czech Science Foundation (19-16861S and 20-28732S). The financial support granted to my research work by the funding is also addressed and acknowledged in the published or submitted papers.

ABSTRACT

One of the most important aspects of effective regenerative medicine is the design of biologically active materials with appropriate biological and material properties. Hydrogels have been receiving great attention as one of the most attractive form of biomaterials. The main reasons are their versatility allowing them to mimic the natural extracellular matrix composition and mechanical properties, their ability to support cell proliferation, migration, differentiation, and allowing of transport of oxygen and nutrients within their structure. Moreover, hydrogels can be engineered according to the demand of specific applications, such as scaffolds for treating various tissues or drug delivery and wound healing systems. In addition, various molecules can be incorporated into the hydrogel to provide specific bioactive properties. The conducting polymers, which could be important in treating nervous or cardiac tissues, are one of the possible bioactive agents.

Experiments described in this thesis were focused on the preparation of biomaterials based on polysaccharides due to their biocompatible, non-immunogenic, and tunable properties. Furthermore, colloidal dispersions of conducting polypyrrole were prepared in order to successfully fabricate bioactive composites for wound healing. This work also focused on the determination of the cytocompatibility of all prepared materials.

Key words: *regenerative medicine, biomaterials, composites, hydrogels, conducting polymers*

ABSTRAKT

Jedním z nejdůležitějších aspektů regenerativní medicíny je příprava biologicky aktivního biomateriálu s vhodnými biologickými, ale i materiálovými vlastnostmi. Jednou z nejaktraktivnějších forem biomateriálů jsou hydrogely, kterým se dostává velké pozornosti z důvodu jejich podobnosti s přirozeným extracelulárním matrixem, ale také pro jejich schopnost podporovat buněčnou proliferaci, migraci, diferenciaci a umožnění transportu kyslíku a živin. Hydrogely mohou být navíc navrhovány podle požadavků konkrétních aplikací, jako jsou například scaffoldy pro léčení různých tkání, nebo systémy pro cílené dodávání léčiv. Kromě toho mohou být do hydrogelu inkorporovány různé molekuly, které poskytují specifické bioaktivní vlastnosti. Jedním z bioaktivních činidel jsou vodivé polymery, které mohou být důležité při léčbě nervových nebo srdečních tkání.

Experimenty popsané v této práci byly zaměřeny na přípravu hydrogelů na bázi polysacharidů, jelikož vykazují dobrou biokompatibilitu a zároveň jsou neimunogenní. Dále byly připraveny koloidní disperse vodivého polypyrrolu za účelem vytvoření bioaktivních kompozit pro hojení ran. Tato práce se také zaměřila na stanovení cykompatibility všech připravených materiálů.

Klíčová slova: *tkáňové inženýrství, biomateriály, kompozity, hydrogely, vodivé polymery*

TABLE OF CONTENT

1. INTRODUCTION

Regenerative medicine (RM) including tissue engineering are rapidly growing multidisciplinary fields. These disciplines have great potential for better treatment of health issues. Furthermore, they have been improved by progress in bioengineering over the last few decades. RM and tissue engineering (TE) are realizing their full potential through the utilization of cells and tissue scaffolds (alone or in combination), as well as the support of the natural healing process by controlled release of bioactive compounds. Numerous methodologies for the preparation of scaffolds, drug delivery systems or wound dressings are currently used depending on the used materials and aimed application. However, the key property that distinguishes materials from each other is the ability to cohabit and interrelate with the tissues and biological systems (e.g. interstitial fluids, blood, immune cells and molecules) without causing any harmful effects. Hydrogels are excellent biomaterial candidates which can accomplish mentioned criteria. They are unique biocompatible polymeric substances that can operate as scaffolds and mimic the properties of diverse biological tissues. Moreover, hydrogels can be also used in desired drug delivery systems and wound healing applications (Chamkouri, 2021; Ebhodaghe, 2020; Guan et al., 2017; Mantha et al., 2019).

Therefore, this doctoral thesis focused on methods of fabrication of hydrogels based on polysaccharides, and the preparation of colloidal dispersions based on conducting polymers (CPs) in order to prepare smart and functional composites. The second part then focused on the determination of the biocompatibility of prepared biomaterials.

2. HYDROGELS

Hydrogels can be defined as cross-linked polymeric materials containing hydrophilic structure which makes them able to retain high amounts of water within their three-dimensional networks (Ahmed, 2015; Pina et al., 2019). The high hydrophilicity is caused by hydrophilic groups, such as hydroxyl, carboxyl, amide and amine which are distributed along the backbone of polymeric chains (El-Sherbiny and Yacoub, 2013). Hydrogels play an important role in biomedicine for more than half a century. For example, Wichterle and Lím invented the first hydrogel soft contact lenses, based on cross-linked poly(2-hydroxyethyl methacrylate), in 1960 (Wichterle and Lím, 1960).

One of the reasons why hydrogels get continuous attention is their similarity with natural tissues, e.g. flexibility and high content of water. The high-water content is one of the common properties of living organisms (considering both the cells and extracellular matrix). Hydrogels are therefore the ideal material to mimic the extracellular matrix (ECM). Water in organisms, and thus even in hydrogels, is an important medium for providing the high permeability of oxygen, nutrients, and, last but not least, water-soluble metabolites (Drury and Mooney, 2003). Another very important aspect of the successful application of hydrogels in biomedicine is biocompatibility and appropriate biodegradability (Ahmed, 2015).

3. HYDROGELS APPLICATION

Hydrogels are very desirable materials due to their previously outlined unique features (high-water content, flexibility, and biocompatibility) and are well established in the fields of RM, TE, and, last but not least, drug delivery and wound healing (Caló and Khutoryanskiy, 2015).

3.1 Tissue engineering

The term “tissue engineering” originated in 1987 at a bioengineering panel meeting at the National Science Foundation. Then, in early 1988 the first TE meeting was held at Lake Tahoe, California and TE was officially defined as “the application of the principles and methods of engineering and the life sciences toward the fundamental understanding of the structure-function relationship in normal and pathological mammalian tissues and the development of biological substitutes to restore, maintain, or improve functions” (Nerem, 1991).

TE is a fast-growing interdisciplinary field including biomaterial science, cell biology, cell-material interactions, and surface characterization. This research area aims to restore, maintain, or improve tissue functions. Furthermore, TE also targets replacing diseased or damaged organs, as well as tissues that have become dysfunctional or lost due to accidents or disease. TE should meet four key

elements:1) selected and isolated cells, 2) biomaterial scaffolds, 3) signaling molecules (proteins, growth factors - GF), and 4) bioreactors that mimic living systems for cell expansion and differentiation (O'Brien, 2011). Figure 1 shows the general tissue engineering approaches currently being employed in clinical practice (El-Sherbiny and Yacoub, 2013).

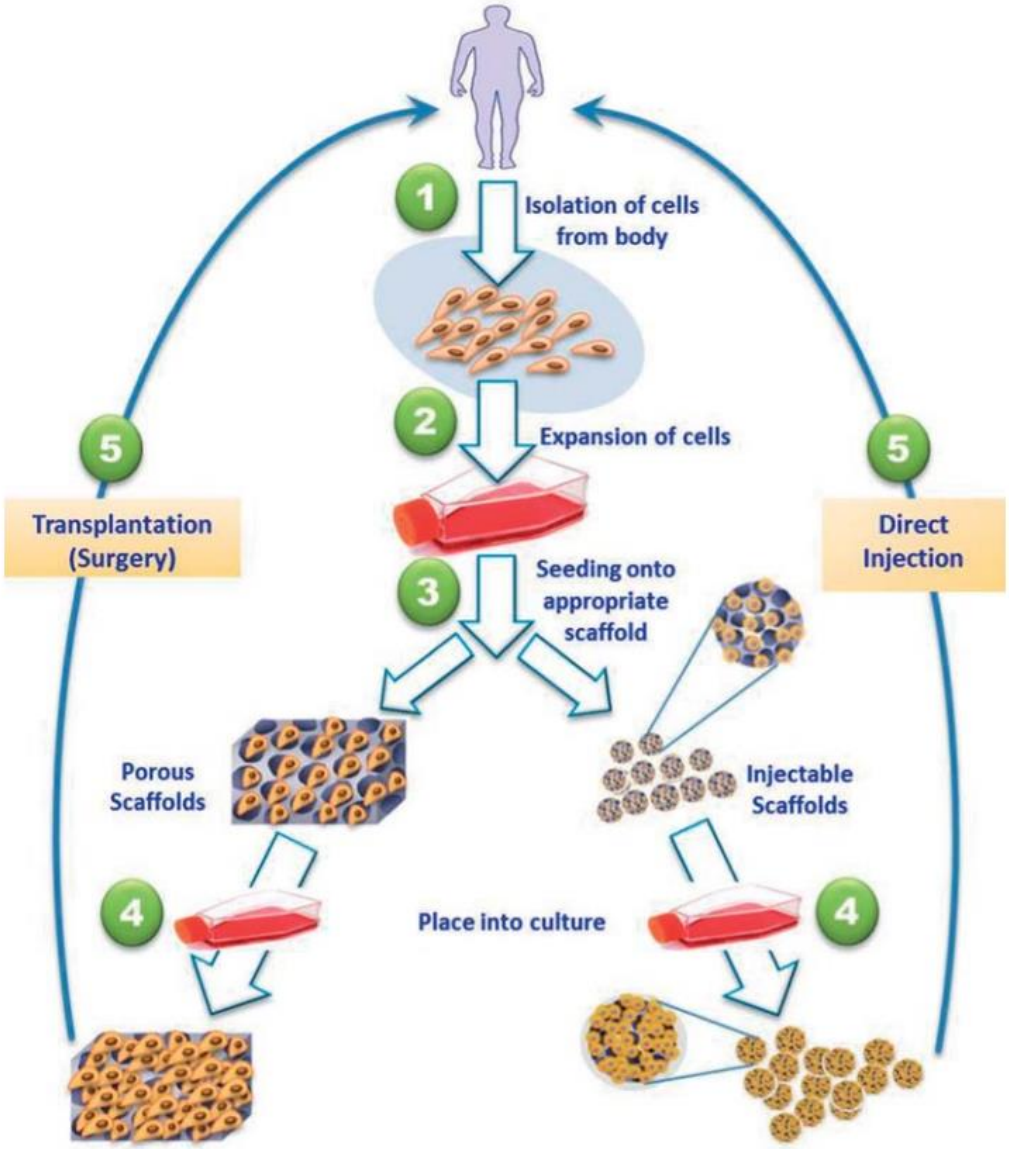

Figure 1: *A schematic illustration of TE approaches (El-Sherbiny and Yacoub, 2013)*

3.1.1 Cells for TE

Cells can be isolated directly from the patient and subsequently expanded *in vitro* and used for treatment. The advantage is that no immune response is observed after transplantation, however, in diseased stages or with elderly patients, autologous cells are not often appropriate for transplantation (Heath, 2000). Thus, another promising method is the use of undifferentiated cells - stem cells. They can renew themselves but also can differentiate into many phenotypes if suitable conditions are provided. There is a number of different stem cell (SC) lineages. They can be divided, for example, according to their differentiation potential:

1) Totipotent stem cells are formed after fertilization of an egg cell by a sperm cell. They provide the foundation for the entire organism. After four days totipotent cells become pluripotent cells.

2) Pluripotent stem cells can give rise to all of the cell types that make up the human body.

Embryonic stem cells are an example of pluripotent stem cells. They can be collected from early embryos. However, this type of harvesting cells was ethically controversial, and thus the technology of production of **induced pluripotent stem cells** (iPSC) is used instead, as they are made from adult cells. iPSC are already differentiated cells that are reprogrammed back.

3) Multipotent stem cells form later and can also differentiate into other cell types but in a limited way. Multipotent stem cells are for example mesenchymal (MSCs), neural, and hematopoietic stem cells. These cells can be isolated from the tissues of adult mammals (bone marrow, peripheral blood, brain, spinal cord, blood vessels, liver, skeletal muscle etc.) (Howard et al., 2008; Rodriguez et al., 2005; Zakrzewski et al., 2019).

For illustration, decellularized scaffolds loaded with autologous adipose-derived stem cells were found to be suitable for cell repopulation and support the formation of cartilage tissue (Kang et al., 2014).

3.1.2 Extracellular matrix components

As it was already mentioned, hydrogels make good options for ECM mimicking. The crucial functions of a native ECM scaffold are its effect on cell attachment, proliferation, migration, differentiation, and apoptosis (Naahidi et al., 2017). This is connected to the concrete composition of ECM within the concrete tissue. ECM is formed from different biomacromolecules such as structural proteins (fibronectin, collagen), signaling proteins and peptides (e.g. GF), and polysaccharides (e.g. hyaluronate, glycosaminoglycans). From tissue to tissue, ECM composition varies. ECM can be classified into two groups, interstitial and pericellular. The interstitial matrices have a part in surrounding cells, on the other

hand, pericellular matrices are in close contact with cells (Hernandez-Gordillo and Chmielewski, 2014). The main structural molecules of ECM are:

1) Collagen is the most plentiful fibrous protein. It is synthesized and secreted by fibroblasts. The family of collagens is made of twenty-eight collagen types composed of at least 46 distinct polypeptide chains. The main types of collagen in ECM are collagen type I which constitutes tissues, such as the dermis, and collagen type II which is mainly associated with cartilage. For more details see chapter 6.2.1.

2) Fibrin polymer forms by thrombin cleavage of fibrinogen. Fibrin, unlike collagen, is not a major part of mature tissue, but it is more associated as a temporary repair stage ECM component. Fibrin generally takes place in healing and tissue repair (Alovskaya et al., 2007). For more details see chapter 6.2.2.

3) Hyaluronan (HA) is a linear glycosaminoglycan (GAGs) that exists either as a free GAG or non-covalently bound to proteoglycans (PGs) in the ECM. HA plays an important role in many functions such as tissue osmosis, viscosity, and wound healing. It also ensures normal water balance, tissue hydration, and elasticity. (Ward et al., 2002). Important is also the effect of HA on cell behaviour, such as migration, proliferation, and differentiation (Dovedytis et al., 2020). For more details see chapter 7.

Besides HA, are many more GAGs that bind GF, which are molecules that moderate cell behaviour, are in ECM. Components of the ECM as well as their placement outside the cell, can be seen in Figure 2 (Badylak et al., 2009).

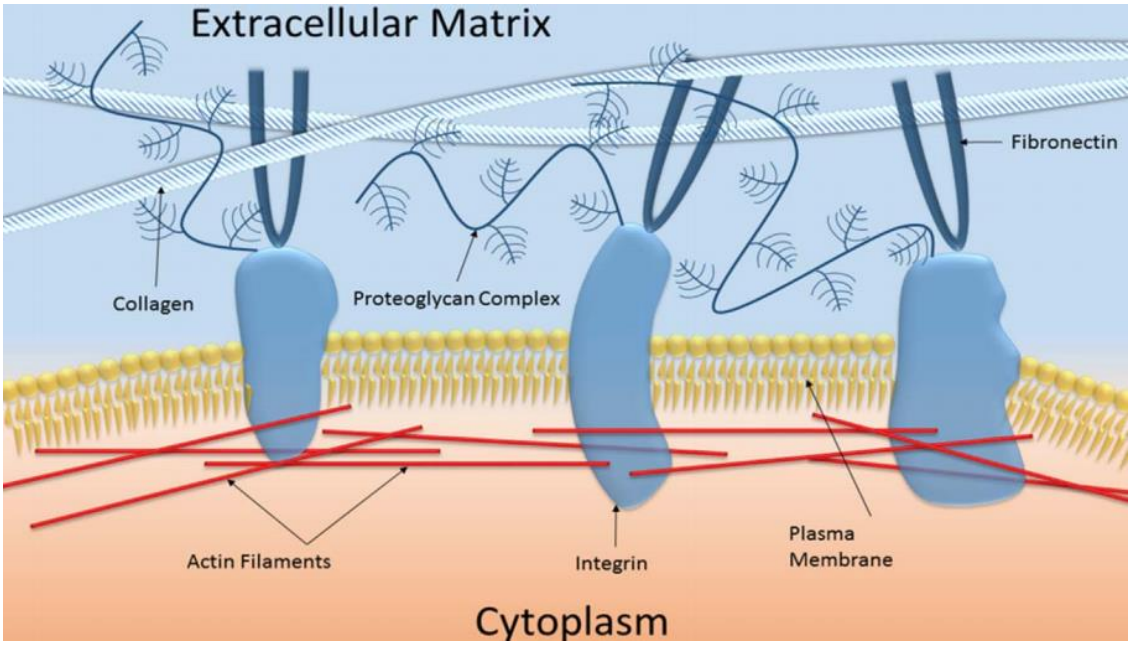

Figure 2: *Scheme of ECM components (protein proteoglycan, polysaccharide), as well as the cell receptors (integrins) that interact with them (Naahidi et al., 2017)*

3.1.2.1 ECM/cell signalization

Cell communication relies on direct interactions of molecules and on the secretion of hormones or mediators that locally or systematically modulate cell functions (Silva et al., 2009). ECM provides spatial context for signaling actions given by cell GF receptors and adhesion molecules (Kim et al., 2011). For instance, cell-ECM adhesion is mediated by integrin family members. Tripeptide Arg-Gly-Asp (RGD) is a well-known motive, that is critical in cell adhesion. First, it was found in fibronectin and later also in other ECM proteins (laminin, fibronectin, vitronectin, etc). (Milner and Campbell, 2002; Saltzman, 2004) Other adhesive peptides are for example IKVAV or YIGSR (Hernandez-Gordillo and Chmielewski, 2014).

GF, a group of polypeptides, are also very important substances that act as signaling molecules between cells. Together with ECM, these are regulating many cellular processes including cell proliferation, migration, differentiation, and gene expression (De et al., 2013).

For a better illustration of the variability of ECM components, neural ECM (n-ECM) and cardiac ECM (c-ECM) are described below.

3.1.2.2 ECM composition of neural ECM

ECM composition of n-ECM is not uniform and varies in embryonic stages, as well as in matured ECM - basement membrane (BM), central nervous system (CNS), and peripheral nervous system (PNS).

During early natal and late embryonic stages of ECM, HA serves as the backbone for the versicans, neurocan, laminins, tenascin-C, and cartilage link proteins (HAPLN1) to assemble and interact in neural stem cells (NSCs), glia cells and neurons (Mouw et al., 2014). Subsequently, the juvenile ECM is replaced by other variant ECM molecules. For instance, versican V1 is replaced by another splice variant versican V2. BM is composed of collagen IV, laminin-nidogen complexes, fibronectin, dystroglycan, agrin, and perlecan (Thomsen et al., 2017). On the other hand, PNS is majorly composed of proteoglycans, tenascin-R, hyaluronan, and link proteins in the brain parenchyma (Lau et al., 2013). In parenchyma, the neural interstitial matrix is distributed and mainly comprised of proteoglycans, HA, tenascins, proteins, and also collagen XV, elastin, laminin, and fibronectin forming fibrous structures. PNS consists of collagen types I, II, IV, and XV, laminins, nidogen-1, heparin sulfate proteoglycans, and fibronectin in a tubular form surrounding Schwann cells along the axon (Jain et al., 2020).

3.1.2.3 ECM composition of cardiac ECM

As well as the composition of n-ECM, c-ECM differ depending on the stages of tissue and on individual cardiac tissues.

In the development of cardiac tissues, ECM mostly consists of HA, proteoglycans, collagens, elastin, fibrillin, tenascin, fibronectins, and laminins (Lockhart et al., 2011). However, HA is not the only glucosaminoglycan playing an important role in the structure of the c-ECM. For example, heart tissue also consists of chondroitin sulfate / dermatan sulfate, heparan sulfate, and keratin sulfate linked to proteoglycan core proteins (Luong et al., 2021). In addition, it is known, that proteoglycans, such as versican, aggrecan, and neurocan are expressed in the developing heart tissue (Kern et al., 2006). Besides proteoglycans, growth factors, and cytokines, such as VEGF, BMPs, FGFs, and TGF-βs bound to heparan sulfate chains, are also unreplaceable for cardiac development. Among these components, protein agrin, localized at the neuromuscular junction, glypican family poteoglcans, and collagens have also significant functions in c-ECM (Lockhart et al., 2011). For instance, collagen types I, III, V, and VI are in the ventricular myocardium, developing valves and cordae tendineae. Contrastingly, collagen II, IV, XI, and XIII are important in valve structures and tendonous apparatus development. Furthermore, collagen types XV and XVIII are expressed in the developing and adult hearts (Halfter et al., 1998; Icardo and Colvee, 1995).

3.1.3 Hydrogel-based scaffolds

Artificial scaffolds themselves can play a significant role in regulating cell behaviour (cell-instructive properties) e.g. cell proliferation, migration, and, last but not least, ECM production. This is connected to their chemistry, architecture, mechanical properties, and surface properties. They can be also applied as delivery vehicles for bioactive substances which can further modify the cell behaviour. Scaffold material and its properties differ depending on the concrete application and specific tissue. The requirement for every scaffold is its biocompatibility and the formation of a proper environment for cells (bulk and mechanical properties) (Courtney et al., 2006; Slaughter et al., 2009).

Cell adhesion is the first of cell-scaffold interactions occurring after the cell seeding, hence appropriate peptide motives, either on the hydrogel surface or throughout its bulk, are used. A widely used adhesion peptide sequence is the RGD domain, which enhances the cellular (fibroblasts, endothelial cells, smooth muscle cells, chondrocytes, and osteoblasts) proliferation, growth, migration, and organization in tissue regeneration applications (Shin et al., 2003). Other adhesives, such as fibrin glue or hydrogels composed of chitin derivatives of chitosan are used to seal small wounds and to improve the efficacy of wound dressings (Ono et al., 2000; Zhao et al., 2001). Furthermore, components of ECM,

such as fibronectin, vitronectin, and laminin are also used to promote not only cell adhesion but also **cell proliferation**.

It is noticeable, that the high peptide density of materials improves cell attachment but it was shown that it may also impede cell migration and proliferation. However hydrophilic/hydrophobic nature of the material must be considered as well (Drumheller et al., 1994; Massia and Hubbell, 1991; Neff, 1999)

Moreover, scaffolds can also influence **cell differentiation**. Various factors can affect the stem cell fate, for example, hydrogel porosity, different polymer types, stiffness, or growth factors incorporation (Lee et al., 2015; Tsou et al., 2016). For instance, the impact of hydrogels with adjustable stiffness by changing the molecular weight of HA on stem cells was researched. The lowest-strength hydrogel maintained the ability of bone marrow mesenchymal stem cells (BMSCs) to self-renew in a short time. The process also activated the canonical Wnt pathway. BMSCs revealed the potential for chondrogenic differentiation as mechanical strength increased, which required calcium influx mediated by transient receptor potential vanilloid 4 (TRPV4) through the plasma membrane of the BMSCs (Ren et al., 2021).

Many kinds of natural and synthetic polymers have been used to create artificial scaffolds, however, natural polymers have the advantages of biocompatibility and biodegradability, they are environmentally friendly and are abundant in the source. Also, scaffolds fabricated from natural polymers offer binding sides for the interactions between cells and hydrogels (Akilbekova et al., 2018). In contrast, synthetic hydrogels show very often undesirable effects when implanted (Lee et al., 2015).

3.2 Drug delivery

Hydrogels are also used in drug delivery systems because of their specific physical properties. Their porous structure, which can be easily adjusted, allows the loading and subsequently releasing of drugs (Elvira et al., 2002; Vashist et al., 2014). Researchers' attention is also paid to hydrogel's ability to direct drug release over a long period (Hoare and Kohane, 2008).

The medication can be placed into a hydrogel and subsequently released *via* a variety of a process, including diffusion, swelling, chemical control, and environmentally-responsive release.

The diffusion-controlled release devices are described, for example, by either **reservoirs** or **matrix systems**. As can be seen in Figure 3, a **reservoir delivery system** consists of a core that contains a drug coated with a hydrogel membrane (Bierbrauer, 2005).

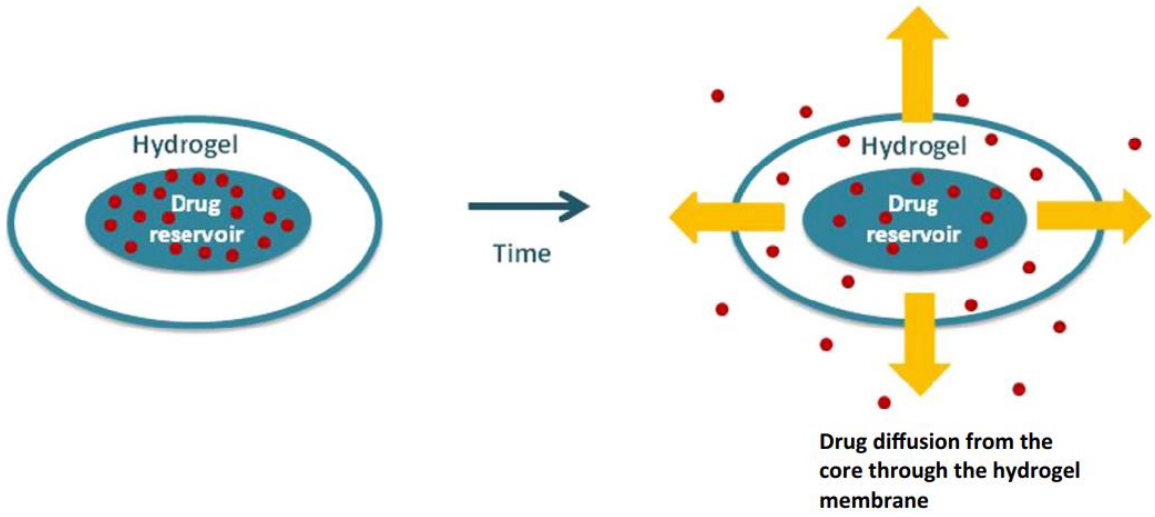

Figure 3: *Drug release through hydrogel membrane in a reservoir system (Caló and Khutoryanskiy, 2015)*

On the other hand, in **matrix systems,** the medication is equally disseminated or dissolved through the three-dimensional structure of the hydrogel. Here, the drug release is carried out through the macromolecular mesh or the pores (Figure 4) (Bierbrauer, 2005).

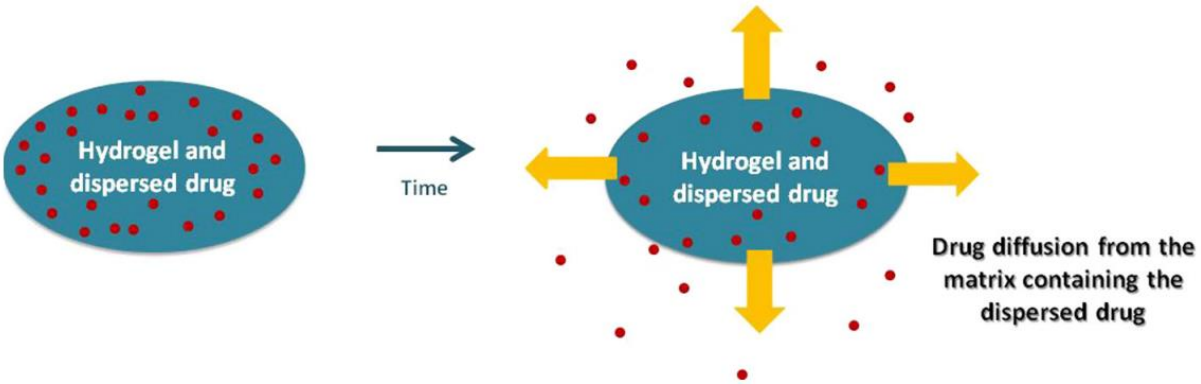

Figure 4: *Drug release from matrix devices (Caló and Khutoryanskiy, 2015)*

Although many patents and academic publications have been published on the potential applications of hydrogels in drug delivery, not many of them contributed to commercial products. For instance, therapeutic hydrogels made of poly(vinyl alcohol) or poly(vinylpyrrolidone) containing an extract from medicinal plants (e.g. *Houttuynia cordata*, elm, celandine) were fabricated for the treatment of atopic dermatitis (Nho et al., 2007)

Hydrogels can also be used as ocular drug delivery carriers. Ocular therapeutics™ produces poly(ethylene glycol) hydrogels for ophthalmic drug delivery systems. Dexamethasone punctum plug, for example, is used for the controlled release of the corticosteroid to lower inflammation and pain ("Ocular

Therapeutix™," 2021). Vaginal insert Cervidil® for cervical ripening is another prosperous example of hydrogels for drug delivery. In addition, it has been on the market since 1995 ("Cervidil," 2021)

Furthermore, many researchers are currently developing systems, that could be employed in cancer treatment. Such delivery systems could be more efficacious than systemic therapies. They arrange a high concentration and a persistent release of the drugs at tumour sites (Tian et al., 2014).

3.3 Wound healing dressings

Another interesting usage of hydrogels is hydrogel dressings for wound healing. Although the skin is the largest organ in the human body serving as a barrier against the outside environment, it must be considered that even the smallest wound could represent a high life risk. Wound healing is a coordinated sequence of controlled stages each of which has a proper duration. The stages are **hemostasis**, **inflammation**, **proliferation,** and **remodeling** (Figure 5) (Firlar et al., 2022; Velnar et al., 2009).

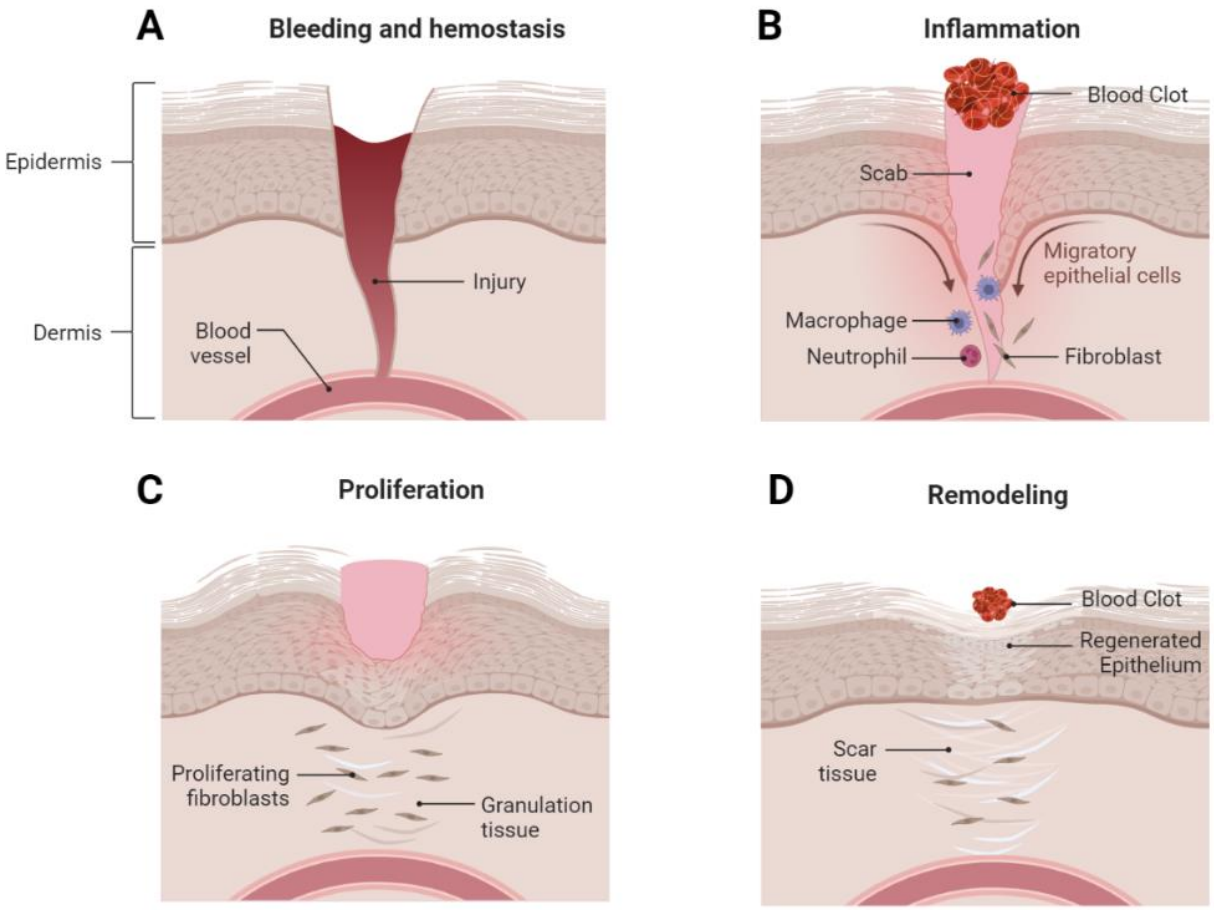

Figure 5: *Wound healing stages: A) – Bleeding and hemostasis; B) Inflammation; C) Proliferation; D) Remodeling (Created with BioRender.com, 2023)*

The first response to the damage is **homeostasis**. The blood clot is created to seal the damaged blood arteries (Han and Ceilley, 2017). Then, the **inflammatory** phase begins, while inflammatory cells (monocytes, lymphocytes, and neutrophils) are activated and respond to chemokines by moving to the wound. Neutrophils are producing reactive oxygen species (ROS) that cause the killing of invading microorganisms. Nevertheless, ROS in high concentrations can cause lipid peroxidation and cell damage and induce the development of chronic wounds. On the other hand, macrophages play an important role in the regeneration of skin tissue. They also clear the apoptotic cells, including neutrophils (Wang et al., 2018). The third phase, **proliferation**, is responsible for granulated tissue with ECM formation. And last but not least, the **remodeling** of tissue to be similar to a healthy one is taking place (Su et al., 2021).

In contrast to gauzes and bandages, hydrogel dressings excel in the similarity to biological tissues including the high-water content which can keep the wound moist and can also absorb the exudate. In addition, hydrogel's mechanical and biochemical properties can be enhanced with various bioactive molecules (Huang et al., 2022).

For illustration, the antibacterial characteristics of hydrogels can be adjusted using, for example, antibiotics and inorganic metals (M. H. Kim et al., 2018; Liang et al., 2019). Adhesion can be improved by polymers containing carboxyl groups (Shin et al., 2019). Moreover, antioxidant and anti-inflammatory properties can be enhanced for example with honey, acacia gum, and polyaniline (Mohd Zohdi et al., 2012; Singh et al., 2017; Zhao et al., 2017). However, polyaniline, as well as polypyrrole, are also used for their conducting properties which improve healing (Lu et al., 2019; Zhao et al., 2017).

Nevertheless, scientists are still developing new and improved hydrogel-based wound dressings, and some of the hydrogel materials are already commercially available. Hydrogel film Suprasorb®G based on acrylic polymers, poly-ethylene, and phenoxyethanol is being used for moisturizing and preventing the formation of necrotic tissue in chronic dry wounds ("Suprasorb®G," 2023). On the other hand, L-Mesitran® is a hydrogel dressing based on acrylic polymer gel with polyurethane film enhanced with a medical grade honey for its antibacterial and anti-inflammatory properties ("L-Mesitran," 2023). Many more hydrogel dressings are already commercially available (Firlar et al., 2022).

4. HYDROGEL PREPARATION

Many 1) **chemical** and 2) **physical** cross-linking methods have been utilized for hydrogel fabrication:

1) **Chemical** cross-links are carried out *via* covalent bonding between separate polymer chains. Hydrogels formed in this manner are forming with elastic

behaviour and better resist mechanical stress (Figure 6a). Chemically crosslinked hydrogels can be prepared by, for example, chain-growth polymerization, polyaddition, and polycondensation, or gamma and electron beam polymerization accompanied by crosslinking but crosslinking copolymerization of monomer and crosslinker is the most used technique (Maitra and Shukla, 2014; Oyama, 2014).

2) On the other hand, **physically** cross-linked hydrogels rely on molecular entanglement and non-covalent (hydrogen bonding, ionic and van der Waals interactions) and hydrophobic interactions to provide coherence (Figure 6b). However, although physical cross-links may not be permanent in nature, they are able to build hydrogels that are permanent in aqueous media. Furthermore, physically cross-linked hydrogels are reversible (Maitra and Shukla, 2014). This reversibility makes the soluble polymer possible to form an insoluble gel in contact with living tissues. This property is widely used for injectable applications, mainly for drug-delivery systems (Hu et al., 2019).

Both the types of gels and degree of cross-linking provide different properties at the nano- and macro-scale (swelling, elastic modulus, and transport of molecules) (Kuo and Ma, 2001).

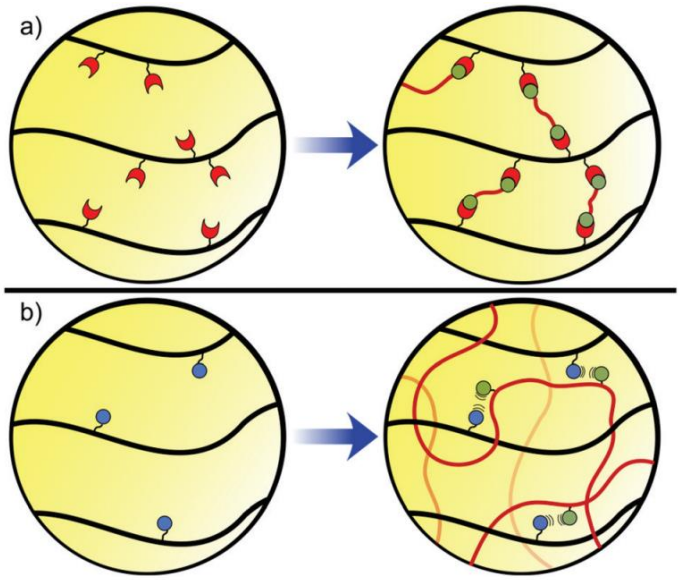

Figure 6: *a) Chemical crosslinking; b) Physical cross-linking (Spicer, 2020)*

5. DESIGN OF HYDROGEL-BASED BIOMATERIALS

Hydrogels are widely used in RM due to their ability to mimic natural tissues. However, as with every biomaterial, hydrogels must fulfil various criteria to function appropriately, such as physical parameters (e.g., mechanical properties, degradation) and also biological parameters (e.g. appropriate cell adhesion and

proliferation) (Gomez-Florit et al., 2020). The most important condition of hydrogels is biocompatibility. Naturally derived polymers usually feature good biocompatibility, on the other hand, synthetic polymers may induce a relevant negative response from the body (Lee and Mooney, 2001).

5.1 Biocompatibility

The key to every biomaterial preparation is biocompatibility. It is "the ability of the material to perform with an appropriate host response in a specific application" (Williams, 1999). However, the application of the hydrogel must be considered, which means that biocompatibility is the characteristic not only of the material but of a biomaterial-host system (Williams, 2014). As the material is supposed to exist within the body, it cannot damage cells or lead to the inflammatory response of the body to the hydrogel. Furthermore, the material must be biocompatible even during degradation (Naahidi et al., 2017).

The basic mechanisms of biocompatibility:

- The consequences of interactions between a substance and a host may relate to the proximity of the material but the impacts can be also distant, impacting the entire body or a specific remote spot (Williams, 2018).

- In some situations, an event has the potential to spontaneously occur, and its impact can be significantly amplified through one or more processes. These processes can rapidly alter the overall nature of the response, leading to a notable transformation within a short period of time (Ekdahl et al., 2011).

- The nature of the material can regulate biocompatibility, but it can vary from patient to patient (Williams, 2018). In the case of hydrogels, it is crucial to examine the preparation process, as toxic components and chemicals might be involved in scaffold fabrication (polymerization, cross-linking precursors). Also, harmful substances, such as unreacted monomers, initiators, stabilizers, or organic solvents, should be considered. To ensure safety, purifying hydrogels from any remaining unreacted substances is desirable before use. Techniques such as solvent washing or dialysis can be used as purification methods. However, certain hydrogels, especially those prepared via in situ gelation, may pose challenges in terms of purification. Hence, it is crucial to utilize non-toxic and safe substances through the fabrication process (El-Sherbiny and Yacoub, 2013).

5.2 Biodegradation

Biodegradability is an important feature in the field of drug delivery and implants for TE applications. There are some ways in which degradation can occur, for instance, thanks to the a) physical or b) chemical processes and also, c) biological processes that rely on biological agents, like enzymes. It is resulting in scaffold disassembling and dissolution of the scaffold bulk or surface degradation. It can occur in a polymer backbone, side chains, or crosslinks. Besides, the degradation rate of a polymer depends on various characteristics of the polymer, such as chemical structure, the presence of hydrolytically unstable bonds, the level of hydrophilicity and hydrophobicity, morphology, the copolymer ratio, and the molecular weight (Jeong et al., 2004; Middleton and Tipton, 2000). Furthermore, degradation can be adjusted by incorporating naturally biodegradable ECM components (hyaluronan, laminin, fibronectin etc.) (Dhandayuthapani et al., 2011; Lutolf and Hubbell, 2005).

However, in some RM applications, biodegradability is not required, such as articular cartilage (Ratner, 2013).

5.3 Bulk properties

Among the bulk properties, the architecture and mechanical properties can be considered.

5.3.1 Architecture

Hydrogels should create a 3D architecture for cell growth. Such architecture more closely resembles natural tissues and enables morphology and gene expression that are impossible to achieve in 2D structures.

A very important factor in scaffold designing and preparing is their porosity. Best hydrogels are those with high **porosities** and an open **interconnected geometry** (Ahumada et al., 2019). The high interconnected porosity is critical for cell ingrowth and cell distribution. Additionally, other characteristics are significant in scaffold designing as well, such as **pore size, volume, size distribution, shape, and wall roughness** (Yang et al., 2001). For instance, small pore sizes may obstruct cellular penetration and ECM production. On the other hand, pore interconnectivity is crucial for cell migration, neovascularization, nutrients, and metabolite transfer (Griffon et al., 2006). Many researches have been studying the optimum of pore sizes. For example, for ingrowth of fibroblasts, it is 5 – 15 μm (Klawitter and Hulbert, 1971), for neovascularization, it is 5 μm (Brauker et al., 1995) and for adult mammalian skin cells 20 – 125 μm (El-Sherbiny and Yacoub, 2013; Yannas et al., 1989).

There are some ways how to control the porosity, one of them is solvent casting or particle leaching. It is based on the dispersion of a porogen with a certain

particle size into a polymer solution. Then the polymer is solidified resulting in a polymer-porogen network. Subsequently, the solute particles are leached or dissolved from the polymer using a specific solvent (Quirk et al., 2004).

Another widely used technique is, for example, lyophilization. Rapid cooling is used to create thermodynamic instability in a system and cause phase separation. Sublimation under a vacuum is used to remove the solvent, which causes the formation of voids in the areas it previously inhabited. For example, a modified lyophilization process was used to fabricate agarose hydrogels with linear pores (Figure 7 A, B) and the linear network of porous paths appropriate for cell infiltration was created. Scaffolds prepared this way were capable to control regeneration in a spinal cord injury model (Figure 7 C-E) (Stokols and Tuszynski, 2004).

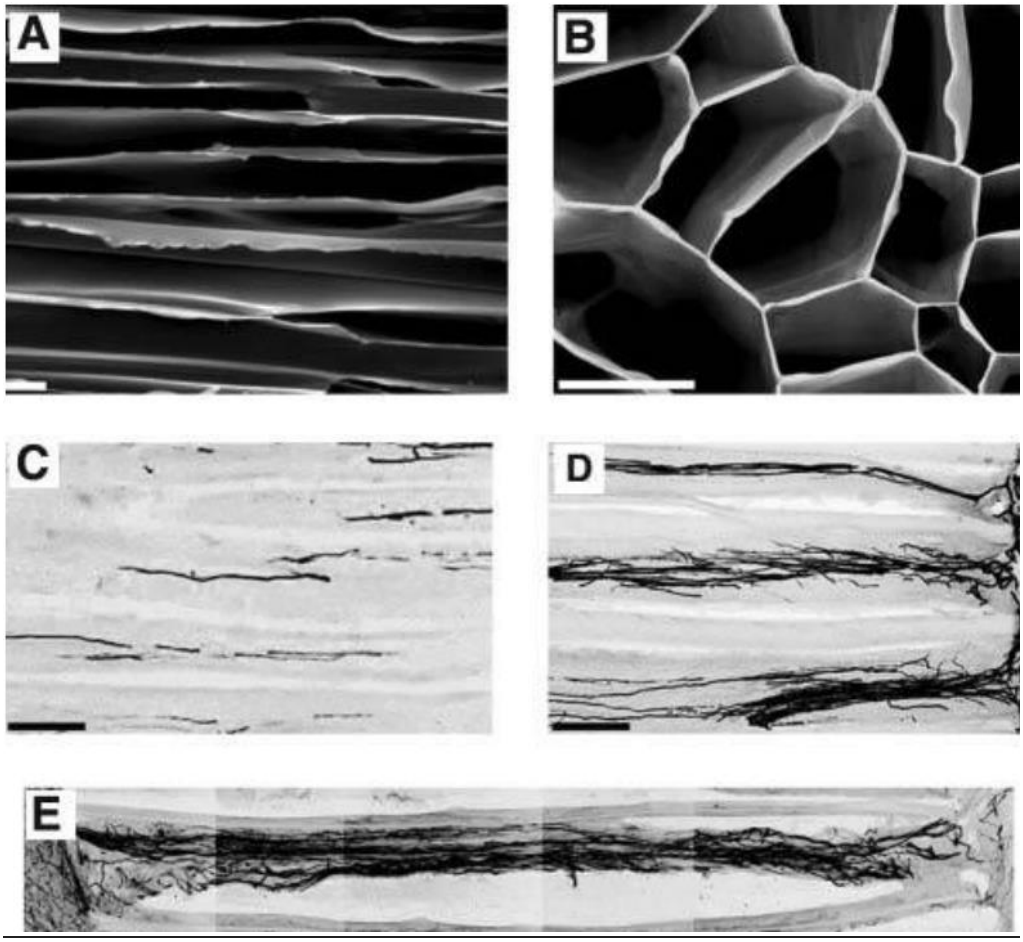

Figure 7: *Morphology and in vivo accomplishment of lyophilized agarose hydrogel scaffolds. Linear porosity can be seen in scanning electron microscopy (SEM) images of longitudinal A) and cross-sectional B) orientations. Axonal penetration after one moth in vivo in a spinal cord injury model in the lack C) and presence D) of brain-derived neurotrophic factor. Axons entirely cross the construct in the best sample obtained E)* (Maccarone et al., 2020; Stokols and Tuszynski, 2004)

5.3.2 Swelling

Moreover, hydrogels can show a detectable change in volume in response to external stimuli – swelling (Figure 8). The capability of the hydrogel network to diffuse water is influenced by the degree of crosslinking. Also, the capacity of hydrogels to take up water needs to be considered (Peppas, 2000). The water capacity is the ratio of the mass of a fully swollen hydrogel (in a state of equilibrium with an aqueous medium) to the mass of a dehydrated hydrogel, where M is hydrogel mass (Brannon-Peppas and Peppas, 1991).

$$\text{Swelling ratio} = \frac{M_{hydrated} - M_{dehydrated}}{M_{dehydrated}}$$

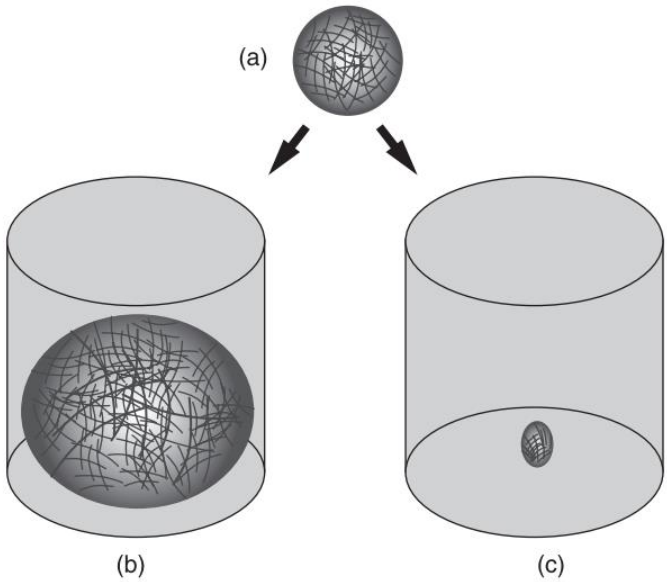

Figure 8: *Small variations in external stimuli, such as temperature, pH or analyte concentration, alter hydrogel hydrophilicity, resulting in dehydrated (a), swollen (b), and shrunken (c) hydrogels (Holback et al., 2011).*

Hydrogels, which are made up of networks of crosslinked hydrophilic polymers, swell, rather than dissolve in water. On the other hand, polyelectrolyte hydrogels swell more because of the charge repulsion across polymer chains. This swelling property is advantageous in environment-sensitive hydrogel swelling for controlled drug release (Holback et al., 2011; Peppas, 2000; Roy and Gupta, 2003).

5.3.3 Mechanical properties

The mechanical properties of scaffolds must be similar to those of native tissues to be replaced. They have a crucial impact on attached cells and encapsulated cells. There is a specific level of isometric tension in the ECM between the cells in a certain tissue (Ingber, 2006). This fact must be considered in the hydrogel

designing, as each tissue has specific mechanical characteristics (Zhu and Marchant, 2011). For example, it has been researched that the differentiation of MSCs can be controlled by the hydrogel stiffness (Engler et al., 2006).

The mechanical properties can be adjusted not only by cross-linker type, cross-linker density, and monomer type but also by incorporating various materials, such as inorganic nanoparticles. For instance, calcium phosphates and silicates have been used for modulating the mechanical strength and osteogenic properties of hydrogels for bone tissue engineering (Drury and Mooney, 2003; Xavier et al., 2015; Zhao et al., 2010).

5.4 Surface properties

Both topographical and chemical characteristics are crucial in controlling cell adhesion and proliferation as the scaffold surface is the initial and primary site of interaction surrounding cells and tissues (Boyan, 1996). For these reasons, a scaffold must be designed to enable cell attachment. This is usually accomplished by various methods, such as film deposition and binding the adhesive bioactive molecules, such as GF, fibronectin, collagen, insulin, and RGD peptides (Figure 9). The biomoieties can be bound to the surface of the scaffold covalently, electrostatically or by self-assembly (Elbert and Hubbell, 1996).

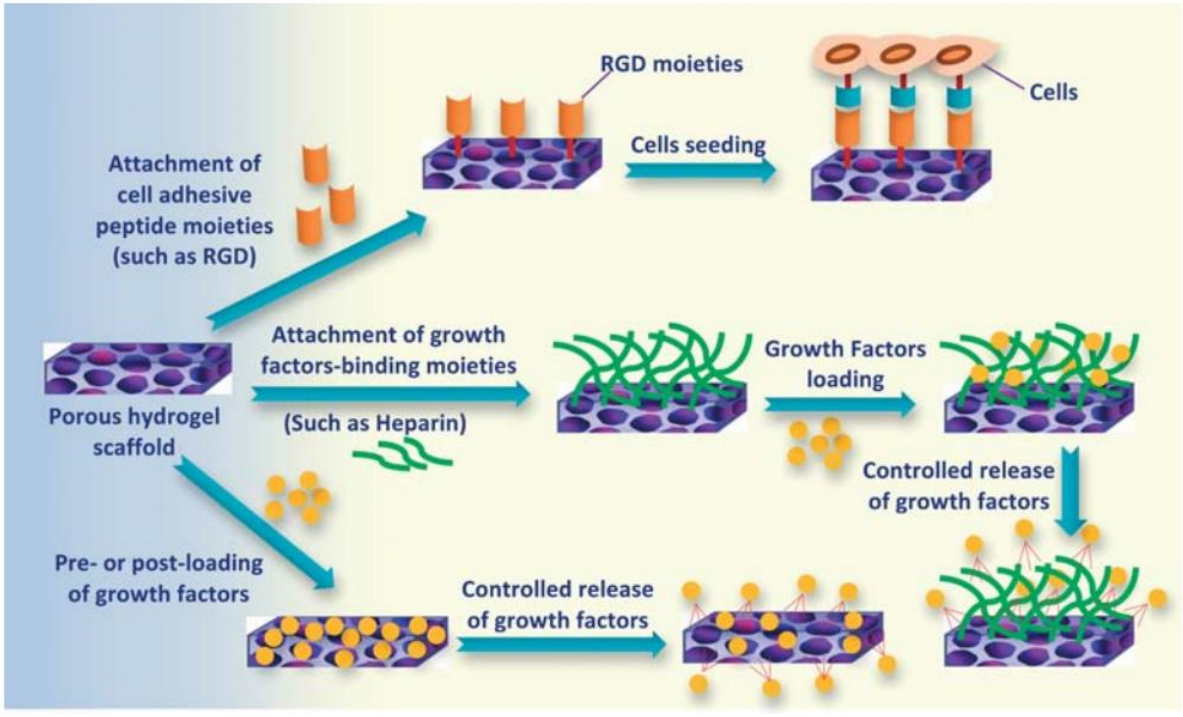

Figure 9: *Some possibilities for selective improvement of surface properties of hydrogel scaffold (El-Sherbiny and Yacoub, 2013)*

6. TYPES OF POLYMERS USED IN BIOMEDICAL APPLICATIONS

Based on the source of material, hydrogels can be divided into natural, synthetic, and hybrid polymer-based hydrogels, which is a combination of both materials (El-Sherbiny and Yacoub, 2013).

6.1 Synthetic polymers

Synthetic polymers offer various physical and chemical structures and synthetic techniques. Their characteristics can be easily managed and altered. Such materials are more effortless to process than natural polymers and have more probable results. On the other hand, synthetic polymers may show less biocompatibility as well as bioactivity, unlike naturally derived polymers (Naahidi et al., 2017).

6.1.1 Poly(lactic acid) (PLA) and poly(glycolic acid) (PGA)

These polyesters with aliphatic chains are one of the most researched synthetic derived polymers in the past and have demonstrated acceptable biocompatibility (Athanasiou, 1996). Furthermore, some of these materials have been approved by the US Food and Drug Administration (FDA) for certain human clinical applications (Ratner, 2013).

Poly(lactic acid) (PLA) and poly(glycolic acid) (PGA) (Figure 10) contain hydrolytic ester groups in their backbone, so their degradation primarily occurs through random hydrolytic chain split (Chandra, 1998).

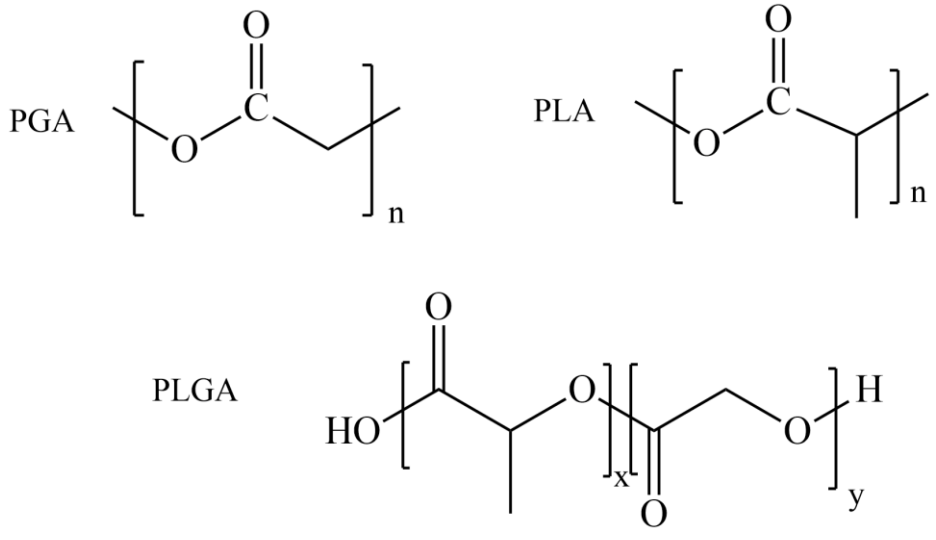

Figure 10: *Chemical structures of PGA, PLA and PLGA*

Application of PLA and PGA and their copolymers, poly(lactic acid-co-glycolic acid) have been found for TE. As these materials have good

biodegradability and mechanical strength, they are primary used for cartilage and bone TE (Gentile et al., 2014). Nevertheless, a problem occurs in their degradation. Intermediate degradation products decrease the local pH resulting in an inflammatory reaction and inducing bone cell damage at the implant emplacement. In addition, the rapid decrease of pH enhances the degradation of polymer (Liu et al., 2006). Lately, nano-hydroxyapatite/PLA scaffolds have been researched to be more biocompatible with human bone marrow-derived MSCs (Zong et al., 2014) and also osteoblast-like human bone fibroblast (MG-63) cells (Cecen et al., 2015).

6.1.2 Poly(ethylene oxide) (PEO) and poly(ethylene glycol) (PEG)

Like PLA and PGA polymers, PEO and PEG (Figure 11) are also materials approved by FDA and are often used as scaffolds for TE (Ratner, 2013).

PEO usually exhibits very low inflammatory reactions, protein binding, and cell adhesion (Lee et al., 1995). Low protein binding is probably caused by the lack of a hydrogen-donating group. PEG, similar to PEO, has a lower molecular weight and became used in the 1970s for its ability to block protein adsorption (Ostuni et al., 2001).

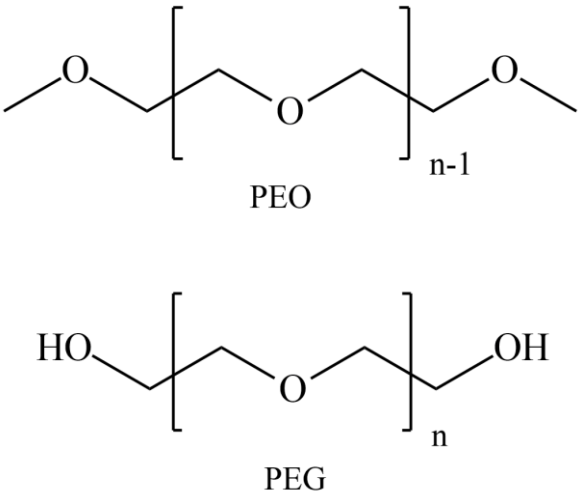

Figure 11: *Chemical structures of PEO and PEG*

Both PEG and PEO can be photocrosslinked by altering the ends of the polymers with acrylates or methacrylates (Cruise et al., 1998). Then, modified PEO or PEG can be mixed with the photoinitiator and crosslinked thanks to UV exposure (Bryant and Anseth, 2001).

To improve cell attachment and spreading, RGD sequences are often used (Zhu, 2010). Bioactive PEG hydrogels enabled the immobilization of different cell lines, such as fibroblasts, chondrocytes, vascular cells, endothelial cells, osteoblasts, neuro cells and stem cells (Kraehenbuehl et al., 2009; Tibbitt and Anseth, 2009).

6.1.3 Poly(vinyl alcohol) (PVA)

PVA (Figure 12) is a biocompatible and biodegradable polymer synthesized through the partial or full hydrolysis of the precursor poly(vinyl acetate) (Spicer, 2020). There are many reasons why PVA became popular among scientists. PVA exhibits high elasticity, which enables hydrogels based on this material to be used in cartilage TE (Jiang et al., 2011). Although pure PVA hydrogels are not able to mimic the soft living tissue strength enough, the usage of vinylpyrrolidone as a co-monomer helped to overcome this limitation (Shi et al., 2016).

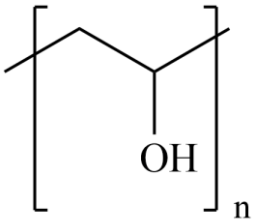

Figure 12: *Structure of PVA*

PVA is a hydrophilic polymer due to its polyhydroxylated nature resulting in low cell and protein adhesion (Nuttelman et al., 2001). Hydroxyl groups are usually chemically modified to get an active hydrogel. As crosslinking agents are used, for example, aldehydes (formaldehyde, glutaraldehyde…) (Chen et al., 1973), di- tri- and polycarboxylic acids (Jian and Xiao Ming, 1987), and others. PVA hydrogels were aslo modified to form complexes with boronic acid-containing copolymers (Konno and Ishihara, 2007). Such hydrogels were able to limit stem cell differentiation and provide control over the cells thanks to the incorporation of soluble factors (Oda et al., 2015). These hydrogels may serve as carriers for the controlled release of cells (Spicer, 2020).

6.2 Natural polymers

Naturally derived polymers originate from living organisms, which is the main reason why they generally possess adequate biocompatibility with low cytotoxicity. For instance, the main proteins of mammalian tissue ECM are collagens and composing about 25 % of the overall protein mass of most mammals (Lee et al., 2001; Vella, 1994). Comparably, hyaluronan (HA) is found in all tissues of adult animals (Lee et al., 2001). Other natural polymers occurring in living organisms are for example chitosan, alginates, and fibrin. Furthermore, these materials do not induce a chronic inflammatory response (Singh et al., 2016).

6.2.1 Collagen and Gelatine

Collagen is the most plentiful fibrous protein found in the ECM of mammalian tissues, such as skin, cartilage, bone, tendon, and ligament. Hence, it is a very attractive material for TE applications (Echave et al., 2017). Collagen has triple-

stranded helical structures held together by covalent and hydrogen bonds. The family of collagens is made of twenty-eight collagen types composed of at least forty-six distinct polypeptide chains. The main types of collagen in ECM are collagen type I, which constitutes tissues, such as the dermis, and collagen type II (Figure 13), which is mainly associated with cartilage (Svensson et al., 2001). However, collagen I is the most used type for hydrogels and it is derived from human or animal sources (Antoine et al., 2014; Wolf et al., 2009). Collagen fibers are easy to operate. The mechanical strength can be controlled by using chemical crosslinkers, crosslinking with physical adjustment, or mixing with other polymers (Dinescu et al., 2019; Slaughter et al., 2009; Weadock et al., 1995).

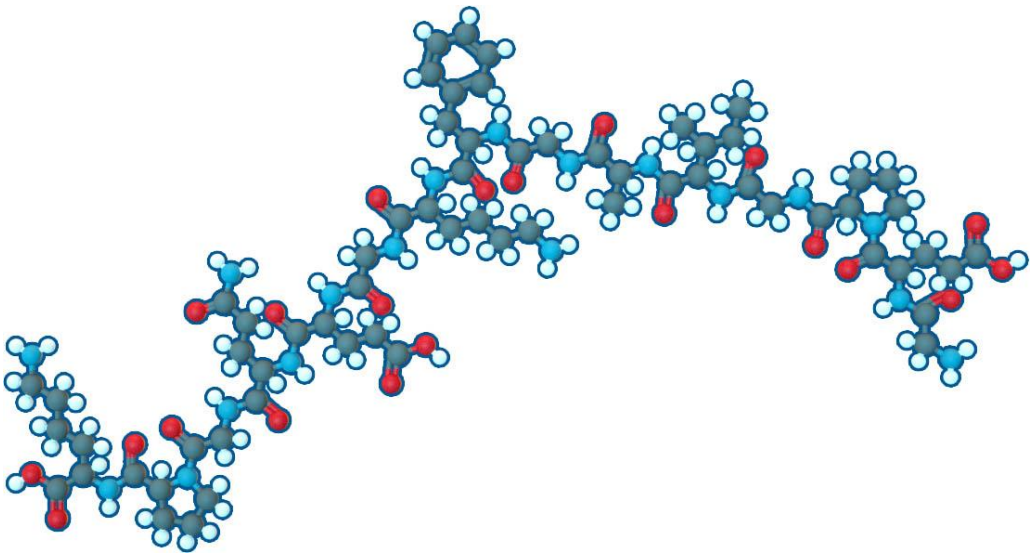

Figure 13: *Collagen type II ("SUPREME PHARMATECH, CO., LTD.," 2021)*

A derivate of collagen is gelatine. It is formed by breaking the natural triple-strand structure of collagen into single-helix molecules (Lee and Mooney, 2001). Gelatine forms gels by changing the temperature of the solution, although it dissolves at body temperature (Panduranga Rao, 1996). As in the case of collagen, the mechanical strength is poor and is usually enhanced by physical or chemical crosslinking. Nevertheless, chemical crosslinking agents, such as carbodiimide, glutaraldehyde or methacrylic anhydride, show often cytotoxic or immunological responses from the host (Choi et al., 1999; Stevens et al., 2002).

6.2.2 Fibrin

Fibrin is a non-globular protein derived from fibrinogen and involved in the blood-clotting process. Fibrin comprises three pairs of polypeptide chains. Fibrinogen is composed of three sets of structures: a central domain made up of fibrinopeptide E with two pairs of fibrinopeptides A and B, and two terminal domains of fibrinopeptide D. Linear fibrils arise due to the cleavage of fibrinopeptides A and B in the presence of thrombin. Fibrinolysis occurs because of the degradation of fibrin clot initiated by enzymes in the human body (Shirwaiker et al., 2014).

Both fibrin and fibrinogen play crucial roles in blood clotting, the inflammatory response and wound healing (Ahmed et al., 2008). As a naturally-derived polymer, fibrin shows good biocompatibility and biodegradability. Furthermore, in the presence of ECM proteins, that improve cell adhesion and proliferation, fibrin is one of the promising biopolymers used in TE. The advantage is also that fibrin hydrogels can be produced from the patient's own blood, so no toxic degradation or inflammatory reactions are awaited. Due to fibrin's injectability and degradability, such materials are suitable as carrier vehicles for bioactive molecules. Fibrin-based materials are usually used for cardiovascular TE or cartilage repair (Janmey et al., 2009; Schense et al., 2000)

6.2.3 Chitin and chitosan

Chitin is the second most plentiful polysaccharide found in the exoskeletons of crustaceans, insects, and fungi. However, chitin is mostly used in its deacetylated form, chitosan, built of N-glucosamine and N-acetyl glucosamine units linked by a β (1→4) glycoside bond (Figure 14). Its molecular weight may scope from 300 to 1000 kDa depending on the source and production process used. Chitosan (Figure 14) is water-soluble only in diluted acid with a pH of less than 6. This fact is caused by the protonated free amino group on glucosamine, which eases the solubility of the molecule, while in water and aqueous solutions above pH 7 chitosan is usually insoluble (Figure 15) (Madihally and Matthew, 1999). The positive charge of the molecule can be used to complex with negatively charged substances, such as GF, nucleic acids, or cytokines (Aibani et al., 2021).

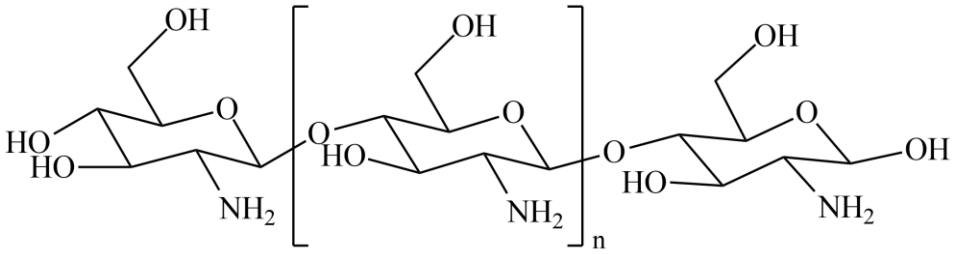

Figure 14: *Structure of chitosan*

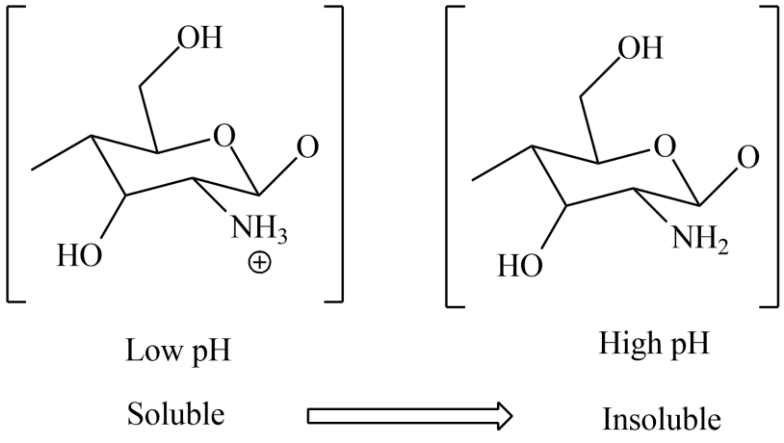

Figure 15: *Schematic illustration of chitosan's versatility*

Chitosan-based materials are well-established in the biomedical field. These substances are biocompatible and show wound-healing and antibacterial properties (Kim et al., 2023). Furthermore, chitosan can be degraded by human enzymes. Lysozymes are primarily responsible for its biodegradation because they can break the linkage between acetylated units and reduce chitosan to monosaccharides (S. Kim et al., 2018). The highly deacetylated form exhibits the lowest degradation rates resulting in a longer-lasting material (up to several months *in vivo*). For this reason, chemical modification of chitosan is desired, as it can remarkably affect its solubility and degradation rate (Shi et al., 2006). One of the possible modifications is the partial re-acetylation of chitosan resulting in the preparation of water-soluble half N-acetylated chitosan. No artificial functional groups are added. Thus, the modification is natural and resulting in low toxicity and good biocompatibility (Kubota et al., 2000; Qin et al., 2006).

Chitosan is also a promising material for bone TE because it supports the adhesion and proliferation of osteoblasts (Khor and Lim, 2003; Przekora and Ginalska, 2014).

6.2.4 Alginate

Alginate is a well-known polysaccharide obtained from brown algae. It is composed of 1,4 linked-β-D-mannuronate and α-L-guluronate residues (Lee and Mooney, 2012). As alginate is negatively charged due to its acid groups, it can react with divalent cations, such as Ca^{2+} which are used as ionic cross-linkers (Figure 16). A problem of ionic crosslinking is in the decrease of concentration of cations due to diffusion resulting in the loss of water from the gel, leading to plastic deformation. Furthermore, alginate hydrogels can be prepared by covalent cross-linking. This method is widely used for its improvement of the physical properties of hydrogels. For example, adipic dihydrazide is used as a covalent cross-linking agent for aldehyde-functionalized alginate (Bouhadir et al., 1999). However, covalent cross-linkers may be toxic.

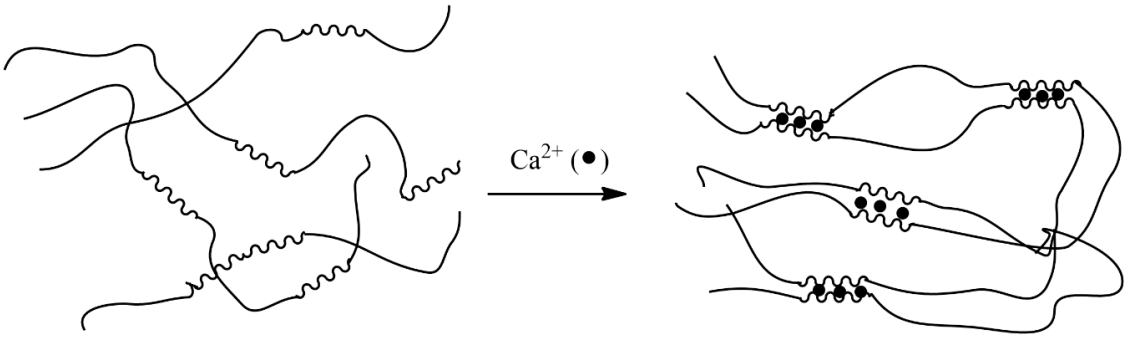

Figure 16: Alginate hydrogels fabricated by ionic cross-linking (egg-box model)

Another type of cross-linking is cell cross-linking. Alginate modified with RGD peptide sequences, which are responsible for cell adhesion, leads to the

binding of multiple polymer chains by cells resulting in reversible network formation without the chemical cross-linkers (Lee et al., 2003).

Alginate hydrogels are receiving considerable attention because of their structural similarity to the ECM of living tissues. The application is potential in wound healing, biological substance delivery, and cell transplantation (Sahoo and Biswal, 2021).

7. HYALURONAN

HA exhibits not only non-immunogenic properties but also the ease of chain modification (Allison and Grande-Allen, 2006).

HA is a linear glycosaminoglycans (GAGs) with disaccharide units consisting of α-1,4-D-glucuronic acid and β-1,3-*N*-acetyl-D-glucosamine. HA is a highly hydrated polyanionic molecule. It exists in molecular weights from 100 000 Da in serum to 8 000 000 Da in the vitreous (Burdick and Prestwich, 2011). HA is a hydrophilic molecule, so it forms hydrogen bonds between water molecules and carboxyl- as well as acetyl-groups. HA is highly viscous in an aqueous solution because of its high molecular weight and strong binding with water (Day and Sheehan, 2001). HA has a negative charge, because of the presence of glucuronic acid, resulting in the binding of cations, such as Ca^{2+}, K^{+}, Na^{+} and H^{+} (Maleki et al., 2008).

HA plays a major role in the structure and composition of the ECM. It is found throughout the body, mainly in synovial fluid and cartilage tissues. Besides giving the tissues their structure, it also provides hydration (Fraser et al., 1997). HA is a biodegradable polymer with a half-life of a maximal 24 h. It is degraded either by the organism's hyaluronidase enzymes or *via* HA cell internalization by CD44 cell surface receptors (Brown et al., 1991). Furthermore, HA can be also cleaved by acidic or alkaline hydrolysis, thermal degradation, and degradation by oxidants (Stern et al., 2007).

7.1 Scaffolds based on HA

In terms of preparing a scaffold for TE, HA without chemical modification and crosslinking could represent a problem. Modification of HA improves not only degradation time but also mechanical stability *in vivo* (Kafedjiiski et al., 2007). The chemical modifications of HA target three functional groups: carboxylic acid of the glucuronic acid, the primary and secondary hydroxyl groups, and the *N*-acetyl group (following deamidation). Mostly **carboxylates** have been modified by carbodiimide-mediated reactions, esterification, and amidation. On the other hand, **hydroxyls** have been altered by etherification, divinylsulfone crosslinking, esterification, and bis-epoxide crosslinking (Figure 17) (Burdick and Prestwich, 2011).

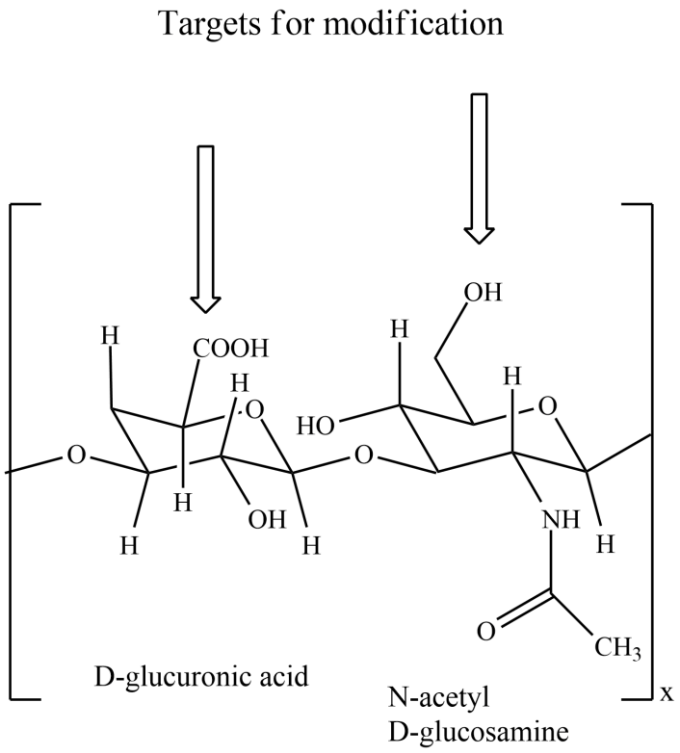

Figure 17: *The structure of unmodified HA backbone and the main targets for modification – carboxylic (–COOH) or the hydroxyl (–OH) group*

7.2 Hydrogels from functionalized HA

HA can be functionalized using for example a) **adipic acid dihydrazide (ADH)**. HA-ADH provides binding sites for ketones, aldehydes, and acylhydrazides with acylating agents, which allows cross-linking, the addition of the hydrophobic moieties, and attachment of drugs, GF, and cytokines (Burdick and Prestwich, 2011; Vercruysse et al., 1997). In addition, hydrogels prepared from HA-ADH and PEG bis(succinimidyl propionate) with incorporated bone morphogenetic protein-2 (BMP-2) exhibited good cell infiltration and chondrogenic differentiation (Bulpitt and Aeschlimann, 1999). Moreover, hydrazide- and aldehyde-functionalized HA resulted in the formation of a prostate cancer model that was used for testing the effectiveness of anticancer drugs (Gurski et al., 2009).

Another possibility of modification of HA is *via* b) **polymerizable methacrylate residues to the hydroxyl group**. The benefit is that photopolymerization allows controlling gel geometry (Walimbe et al., 2017). Hydrogels with good tunability and biocompatibility were prepared by the reaction of photo crosslinkable methacrylate with oxidized HA or oxidized HA with a functional acrylamide (Jia et al., 2004). Such hydrogels promote cell adhesion and proliferation (Hansen et al., 2005).

One of the most promising methods is **c) thiolation**. It involves the modification of the carboxylic group on the HA backbone resulting in thiols as sites for cross-linking. Many researchers are being attracted by disulfide bond hydrogels for the simple way of fabrication, non-toxicity, and *in-situ* gelation properties. Furthermore, these hydrogels can be prepared from a single component. The principle of biodegradation of the disulfide bond of HA relies on dissociation by reductant glutathione (GSH), which can be synthesized in cells (Bian et al., 2016). Biodegradation and mechanical characteristics can be improved, for example, by changing the molecular weight of HA or the degree of thiolation (Burdick and Prestwich, 2011). Moreover, the combination of thiolated-HA with thiolated gelatin or methacrylated collagen to provide cell adhesion motifs resulted in the development of complex patient-specific tumour-derived organoids from a lot of types of tumour biopsies (melanoma, colorectal, etc.) (Devarasetty et al., 2018). A hybrid of HA-based hydrogel constructed of polydopamine and thiolated HA was prepared. The addition of polyamide into HA gel improved the cell affinity and tissue adhesion and potential bacterial inhibition (Yu et al., 2020).

Another potential technique for functionalization of HA is using **d) CPs**, such as polyaniline (PANI) (Figure 18b), poly(3,4-ethylenedioxythiophene) (PEDOT) and polypyrrole (PPy) (Figure 18a), that are popular constituents for biomaterials and their applications where electrical signalling is desirable (Balint et al., 2014).

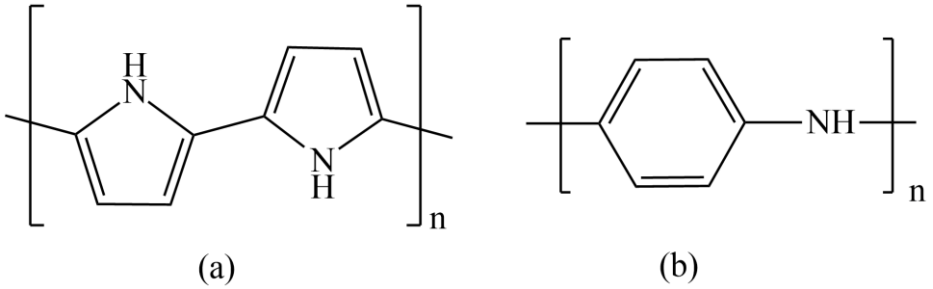

Figure 18: *a) polypyrrole and b) polyaniline*

CPs are simple to work with and to modify (Guimard et al., 2007). Moreover, at the interfaces between cells and conductive surfaces, electrical impulses can be efficiently conveyed, resulting in electrical communication between cells and stimulation of cellular activities, such as differentiation (Thrivikraman et al., 2014).Conductive hydrogels were prepared by the combination of pyrrole-incorporating hyaluronic acid and PPy *via* covalent bond formation and PPy polymerization. These hydrogels showed good cell adhesion and proliferation (Yang et al., 2016). Furthermore, hydrogels based on HA with incorporating single-walled carbon nanotubes (CNTs) and/or PPy were fabricated to support the differentiation of human neural stem/progenitor cells (Shin et al., 2017).

8. AIMS OF DOCTORAL THESIS

The main aims of my experimental work during the Ph.D. study were the preparation of hydrogels based on polysaccharides, the preparation of colloidal dispersions formed from CPs for subsequent incorporation into the hydrogels, and last but not least, the study of interactions between materials and cells, concretely:

- The preparation and characterization of hydrogels based on hyaluronic acid
- The fabrication and characterization of polypyrrole colloids
- The preparation and characterization of smart functional wound dressing composites based on chitosan and polypyrrole colloidal dispersions
- Determination of biocompatibility of above-mentioned materials

9. EXPERIMENTAL PART

The experimental part of this work focused on the preparation of hydrogel composites based on polysaccharides and the testing of interactions between materials and cells. The fabrication of hydrogels based on hyaluronan and/or chitosan was optimized. Furthermore, conducting polymer – polypyrrole –was used for the preparation of colloidal dispersions. CPs are widely used for their unique characteristics, mainly for application where bioelectricity play a role. Here, the PPy colloidal dispersion was used for the preparation of bioactive wound dressing composites based on chitosan. Then, materials were tested using the NIH/3T3 mouse fibroblast cell line to evaluate the cytotoxicity, cell proliferation, and migration. Furthermore, the skin irritation potential of prepared wound dressings was also tested using a 3D reconstructed human epidermal tissue model EpiDerm^{TM}. The following chapters describe the methodology required to assess the experiments during the doctoral study.

9.1 Materials

HA (sodium salt, *Mw* = 1.5 MDa, Contipro), 1-ethyl-3-(3-dimethyllaminopropyl) carbodiimide hydrochloride (EDCl, Sigma Aldrich Co.), N-hydroxysuccinimide (NHS, Sigma Aldrich, Co.) and cysteamine hydrochloride (CSA·HCl, Sigma Aldrich Co.) were used in the HA-SH preparation.

Polypyrrole colloids stabilized by poly(vinylpyrrolidone) (PPy/PVP) were prepared using pyrrole (Sigma-Aldrich Co.), iron (III) chloride (Sigma-Aldrich) and poly(vinylpyrrolidone) (PVP; Fluka, K 90, molecular weight M_w = 360,000).

Cellulose SigmaCell type 20 (Sigma Aldrich Co.), sodium periodate ($NaIO_4$; Penta, Czech Republic), and ethylene glycol (Penta, Czech Republic) were used in the preparation of dialdehyde cellulose (DAC). Low-molecular-weight chitosan (Sigma Aldrich Co.), glacial acetic acid (CH_3COOH; Sigma Aldrich Co.), absolute ethanol (VWR, Czech Republic), acetic anhydride (Ac_2O; Sigma Aldrich Co.), hydrochloric acid (HCl; Penta, Czech Republic) and sodium hydroxide (NaOH; Penta, Czech Republic) were used in the preparation of soluble chitosan.

Sample preparation

Most of the samples were prepared and tested by myself, however, in some cases, the optimization of sample fabrication and testing was done in cooperation with other colleagues and institutes (Institute of Biophysics, Czech Academy of Science).

9.1.1 The fabrication of thiolated hyaluronan

A modified procedure based on research by Bian et al. was used for the preparation of HA-SH (Bian et al., 2016). In the first step, HA was dissolved in

UPW for 24 h. Next, pH was adjusted to 5.5 and NHS and EDCl were transferred into the mixture and let to react for 2 h to activate the carboxylic groups of HA. In the next step, pH was adjusted to 4.75 and CSA·HCl dissolved in UPW was added to the solution (molecular ratio – HA:NHS:EDCl:CSA·HCl = 1:2:2:2). The mixture was stirred for 24 h and then dialyzed against dilute HCl solution (pH 3.5) containing NaCl for 48 h. In the last step, the solution was lyophilized to get the solid HA-SH sample. The synthesis was prepared under the nitrogen atmosphere.

The degree of thiol substitution was analysed by Ellman's test (Ellman, 1959).

Preparation of HA-SH hydrogel

The solution of HA-SH was able to crosslink itself and form the hydrogel thanks to the oxidation reaction of free thiol groups resulting in disulfide bonds. To achieve this, solid HA-SH polymer was dissolved in UPW (pH 3.5). In the next step, the pH value of the solution was adjusted to 7.5 – 8 with the addition of 1.0 M NaOH. Then the solution was immediately injected into a vessel and exposed to the air at room temperature for 1 h. To get stiffer hydrogel, hydrogen peroxide was added (w/v = 0.35%) to oxidize residual thiol groups. Finally, prepared hydrogels were put into reaction flasks with PBS (Phosphate Buffered Saline) and shaken for 24 h.

The gelation time of HA-SH hydrogel

Freshly prepared HA-SH solution in the vessel was determined by inverse tube test, i.e. test tubes inverted after a given time to confirm gel formation. If there was not any observed fluidity after 1 min since the test tube was inverted, it could be considered that the hydrogel was formed. More polymer concentrations were prepared to see the limit concentration when the hydrogel is still formed (w/v = 2%, 3%, and 5%).

9.1.2 The preparation of PPy colloidal dispersions

Solutions of different concentrations of PVP (2 and 4 wt.%) were prepared by dissolving a specific amount of PVP powder in UPW. Then, to each of the PVP solutions, pyrrole was added, and the volume was adjusted to 50 mL. The mixture was put under ultrasonic treatment for 30 min to get a solution. Each solution was mixed with iron(III) chloride to initiate the polymerization of PPy. The mixture was left to polymerize at room temperature for 24 h. Subsequently, the colloidal dispersions were dialyzed against aqueous HCl to remove the unreacted monomer and oxidant ions (Li et al., 2016).

Zetasizer Nano ZS instrument (Malvern Instrument, UK) was used for the determination of the particle sizes by dynamic scattering (DLS).

For more details see the ready-to-submit manuscript **APPENDIX I**.

9.1.3 Synthesis of water-soluble chitosan

A modified synthesis process by Qin et al. was used for the water-soluble half N-acetylated (50%) chitosan (SCN, Soluble ChitosaN) fabrication (Qin et al., 2006). Briefly, low-molecular-weight chitosan was dissolved in 10% acetic acid for 6h. In the next step, a mixture of ethanol and Ac_2O was added dropwise and stirred for 15 h at 40 °C. The pH was set to 8.5 to initiate the formation of gel particles in the solution. The mixture was dialyzed against water for 72 h. Subsequently, the pH was decreased to 6.5 which led to the dissolution of gel particles. The sample was centrifuged, filtered, and lyophilized.

9.1.4 Synthesis of crosslinker – dialdehyde cellulose

$NaIO_4$ was used for cellulose oxidation (molar ratio of anhydroglucose unit: $NaIO_4$ was 1:1:25) (Münster et al., 2018, 2017). Next, ethylene glycol was added to terminate the reaction. Dialdehyde cellulose (DAC) was purified by repeated centrifugation and mechanical homogenization. Subsequently, the DAC was solubilized. In the next step, centrifugation and filtration were used for the removing of insoluble residues. Finally, the sample was dialyzed and the solubilized product was lyophilized.

9.1.5 Wound dressings preparation

The SCN-DAC films were prepared by adding either 2 or 5 mol.% of DAC relative to SCN (SCN-DAC-2% and SCN-DAC-5%).

PPy-containing wound dressings were prepared by adding the 5 or 10 wt.% PPy (relative to SCN) to the SCN solution and subsequently crosslinked with 2 mol.% of DAC (SCN-DAC-PPy5%, SCN-DAC-PPy10%).

For more details see the ready-to-submit manuscript **APPENDIX II.**

9.2 Biological properties

The biological properties of materials were characterized in accordance with ISO standard 10993 Biological evaluation of medical devices.

9.2.1 Cell lines

In this chapter, cell lines used for the biological testing of the materials are described.

Mouse embryonic fibroblast cell line NIH/3T3

The biological testing was exhibited using a mouse embryonic fibroblast cell line NIH/3T3 (EACC 93061524, England). Dulbecco's Modified Eagle's Medium (Biosera, France) with the content of 10% of calf serum (Biosera, France) and 100 U/mL of Penicillin/Streptomycin (Biosera, France) was used for the cultivation of NIH/3T3 cells. Cells were incubated at 37 °C under the 5% CO_2

atmosphere in the humidified air (incubator HERAcell 150i, Thermo Scientific, USA).

Ovarian cancer cell line A2780

The cell line A2780 (EACC, England) was cultivated in RPMI-1640 medium, supplemented with 10% fetal bovine serum (FBS, mycoplasma-free, PAN, Germany), 100 U/mL Penicillin/Streptomycin and hydroxyethyl-piperazine-ethane-sulfonic acid buffer (HEPES, Merck, Germany). The cells were incubated at 37°C in a humified 5% CO_2.

Embryonic stem cell line ESCs

The embryonic stem cell ES R1 line was cultured in an undifferentiated state using gelatinized tussie culture dishes (0.1% gelatine in UPW) in DMEM containing 15% fetal calf serum, 100 U/mL Penicillin/Streptomycin, 100 mM non-essential amino acids solution (Thermo Fisher, USA), 0.05 mM 2-mercaptoethanol (Sigma, USA) and 1000 U/mL of LIF (Gibco, USA).

9.2.2 Biological testing

Material **cytotoxicity** was examined using the MTT assay which evaluates the cell viability (Freimoser et al., 1999; Riss et al., 2004). Extracts from samples were prepared according to ISO standard 10993-12. Cytotoxicity itself was done according to ISO 10993-5 protocol. Furthermore, cell **proliferation** on the samples was researched (Adan et al., 2016). **Skin irritation** of topically applied mateials was studied according to OECD 439 (OECD, 2021) using a 3D reconstructed human epidermal (RhE) tissue model EpiDerm™ (EPI-200, MatTek, Ashland, USA and MatTek In Vitro Science Laboratories, Bratislava, Slovakia). And last but not least, the **migration assay** was used for the evaluation of wound healing activity (Liang et al., 2007).

10. SUMMARY OF RESULTS

The presented doctoral thesis is mainly focused on the preparation, optimization, and biological testing of biomaterials. As was previously discussed in the theoretical part, they must meet many aspects in terms of biochemical, mechanical and physical properties (Pina et al., 2019). Their applicability can be documented by the fact, that they are employed since the 1960s for contact lenses and intraocular lens applications (Singh, 2009). Moreover, hydrogels are used as, for example, 3D scaffolds for the biomimetic 3D microenvironment for cell growth, but also drug delivery and wound healing (Bordbar-Khiabani and Gasik, 2022; Cui et al., 2023; Xu et al., 2020). Though they can be prepared from many different materials, whether natural, synthetic, or their composites, natural ones were chosen in this thesis. The main reasons for this decision were good biocompatibility caused by the natural origin processed from living organisms. However, the naturally derived materials also exhibit some limitations, such as weak mechanical properties. Thus they must be very often chemically modified (Naahidi et al., 2017). Their potential can be also enhanced by the incorporation of various bioactive molecules (Fiorati et al., 2021). Nevertheless, it should be noted that all of the modifications of the materials must depend on the intended field of application while considering biocompatibility.

In my experimental work, I focused on 1) the fabrication and optimization of HA-SH hydrogels for future preparation of scaffolds for reconstituted intestinal tissue; 2) the preparation and biological testing of conducting PPy/PVP colloidal dispersions; and 3) the preparation and biological testing of active hydrogel wound dressing composites based on chitosan and PPy/PVP colloidal dispersions

1) *The fabrication and optimization of HA-SH hydrogels for future preparation of reconstituted intestinal tissue*. Hyaluronic acid is the only non-sulfated glucosaminoglycan found in embryos and the niches of progenitor/neural cells. HA naturally exhibits low stiffness and high degradability, however, researchers all over the world have been studying multiple strategies to improve the control over these properties. Among others, modifications of HA involve the functionalization of hydrazide or thiol groups, or methacrylation (for more information see chapter 7) (Xu et al., 2012). When I began my postgraduate studies, I started researching the modification of HA by thiol groups. This method relies on methods of green chemistry involving non-toxic urea and succinic acid derivatives as by-products. Furthermore, cysteamine is used as a non-toxic crosslinker. The gelation itself is initiated by the controllable formation of –S–S– groups when the precursor solution is set close to neutral pH, –SH groups start to create mentioned disulfide bridges. The gelation can be controlled by the concentration of the polymer as well as the amount of –SH groups (Bian et al., 2016). However, as is common in science, many challenges arose during the modification process that needed to be solved. Hence, I present below the specific

situations that occurred and describe the approaches I employed to overcome them.

The HA-modification in this thesis was inspired by the work of Bian et al. (Figure 19) (Bian et al., 2016). In the first step, HA was dissolved in water, then EDC and NHS were added into the solution to activate the –COOH groups. Subsequently, cysteamine was added as a bearer of thiol and amine groups.

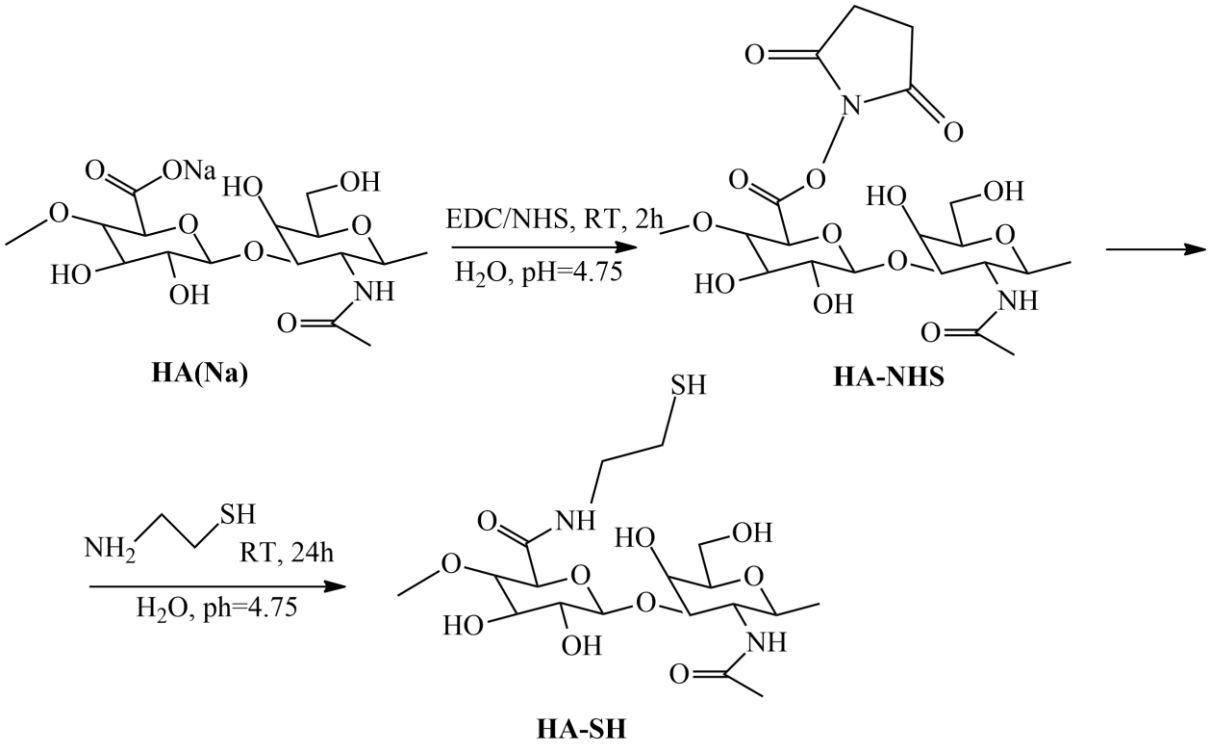

Figure 19: *Scheme of HA-SH synthesis (Bian et al., 2016)*

To obtain the pure product, HA-SH was dialyzed against an aqueous HCl solution (pH = 3.5) and lyophilized. The acidic environment prevented the thiol groups to react with each other. However, it was important to choose the appropriate molar ratio of reactants to prepare the demanded degree of thiolation. The degree of thiol substitution was analyzed according to Ellman's test (Ellman, 1959). The results showed that if the coupling rate was too high (the molar ratio of HA:NHS:EDCl:CSA·HCl = 1:4:4:4), the degree of thiol groups was about 20%, but the sample was not soluble. Carboxyl groups that are providing a negative charge of HA, thus making the molecule hydrophilic, are in this modification substituted with thiol groups. This makes the HA more hydrophobic. Consequently, the molar ratio was adjusted to HA:NHS:EDCl:CSA·HCl = 1:2:2:2 but the degree of thiol groups was only about 4 – 5%. Nevertheless, it was not clear why it was not possible to get higher degrees of thiolation as well as the problems with dissolving the samples occurred again. Thus, the samples were synthesized under the nitrogen atmosphere which prevented oxidation during the fabrication and also during the storage and resulted in higher concentrations of

thiol groups (10 – 11%). Furthermore, according to the research by Cao et al., the dialysis solution was enriched with NaCl solution which decreased the viscosity of the solution and helped with the dissolution of the final product (Cao et al., 2019). After the modification of the HA-SH, the polymer with the exact concentration was dissolved and disulfide-crosslinked in the neutral environment to get hydrogel (Figure 20). Furthermore, to get a firmer hydrogel, hydrogen peroxide was added as it immediately oxidizes all of the residual thiol groups to disulfide.

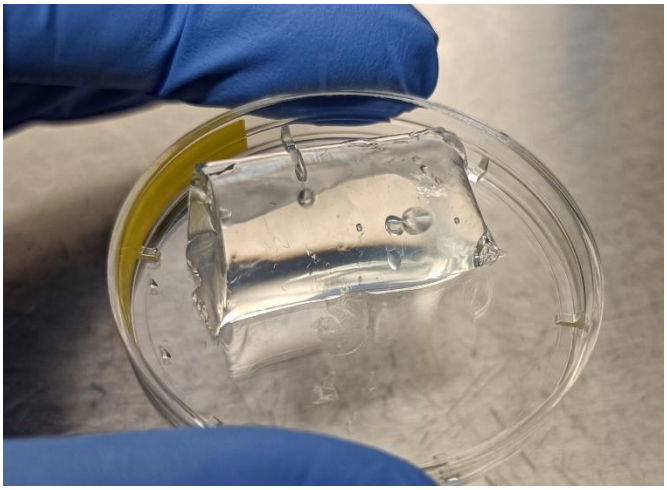

Figure 20: *HA-SH_2% hydrogel sample*

The viscoelastic properties of the samples were studied (the molar ratio of HA:NHS:EDCl:CSA·HCl = 1:2:2:2; degree of thiol groups – 10.44%). The dependence of storage modulus, G', on angular frequency is given in Figure 21. Four types of HA-SH hydrogels were tested; 2%, 3%, 5% and 3% + H_2O_2. It can be observed that the higher the concentration of HA-SH is, the bigger the storage modulus and the elasticity of HA-SH gel. It is because of the denser network of the hydrogel, which can more easily store deformation the energy. Moreover, Bian et. al. have also reported, that the higher the degree of thiol substation, the bigger the G' (Bian et al., 2016).

Nevertheless, it is noticeable that 3% HA-SH hydrogel with the addition of H_2O_2 has a 15 times smaller storage modulus, which is probably caused by side reactions of HA-SH and H_2O_2, causing over-oxidation of SH groups. Also, the decrease of the curve with higher frequency indicates a shearing response and thus more viscous behaviour. This fact rejects our hypothesis about getting a firmer hydrogel after adding the hydrogen peroxide. However, less concentrated H_2O_2 solution could help to overcome this issue, thus further research is needed.

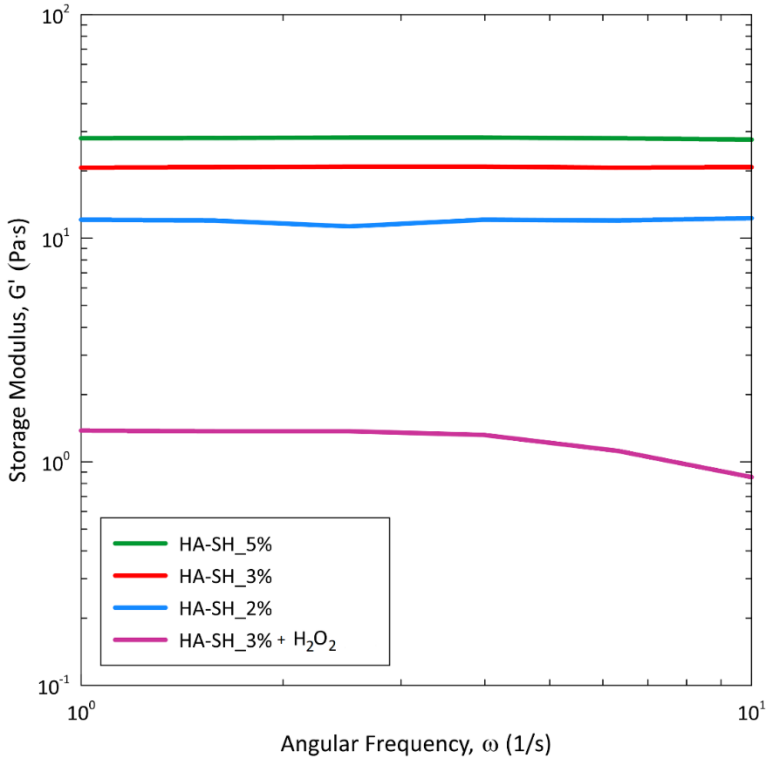

Figure 21: *Dependence of storage modulus (G') of HA-SH hydrogels on the angular frequency*

The cytotoxicity of prepared hydrogels was determined according to ISO 10993-5 using a mouse embryonic fibroblast cell line (NIH/3T3). As expected, the absence of any cytotoxicity (viability of cells higher than 70%) was observed in the case of all samples. This is a confirmation of the successful use of green chemistry methodes in this work. Also, cell proliferation was studied. However, the cells were not able to proliferate on the surface of the hydrogels as a result of a highly hydrophilic and polyanionic surface of HA. This could be overcome by the combination of HA, for example, with growth factors or collagen. For illustration, Gao et al. prepared HA/collagen composite hydrogel with tunable properties resulting in good cell proliferation (Gao et al., 2020).

In conclusion, this pilot study performed by me has led to the idea of the preparation of man-made scaffolds mimicking the mechanical and biochemical composition of small intestine tissue (SIT). The material should be formed by HA-SH and collagen as the main constituents and combined also with appropriate growth factors as well as intestinal stem cells. Currently, this research is being finished and the results will be published in a research article.

Furthermore, after a not-so-simple start to my studies, I moved from hydrogels for a while and focused on the preparation of colloidal PPy.

2) *The preparation and biological testing of conducting PPy/PVP colloidal dispersions*. It is known, that CPs are having unique properties, which are widely used for the preparation of neural implants, biosensors, tissue engineering

scaffolds, and drug delivery systems. For instance, they have not only good electrical properties, but they are also biocompatible, easy to synthesize and work with (Guimard et al., 2007; Jasenská et al., 2021). One of the most popular CPs is PPy. Due to its p-type conductivity, PPy exhibits good electrical conductivity under physiological circumstances. Furthermore, the synthesis of PPy can be done through chemical and electrochemical polymerization (Wang et al., 2004). Even though PPy can be prepared in the forms of colloidal dispersions, insoluble powder, or film, colloidal suspensions are a best choice for further usages, such as scaffold preparation. Colloidal dispersions are prepared using a proper stabilizer. The main reason for stabilizer useage is its ability to create a shell over the particle surface preventing the PPy from precipitation. For example, nanocrystalline cellulose or PVA can be used (Al-Dulaimi and Wanrosli, 2016; Gangopadhyay and Molla, 2011). The reaction medium should not be forgotten either, as water is used the most in the biomedical sciences. Here, PVP was employed as a stabilizer. PVP is a non-toxic biocompatible polymer and is thus widely used as a carrier in biomedical or pharmaceutical fields. Furthermore, this substance was also accepted by the FDA for biomedical applications (Bothiraja et al., 2010; Franco and De Marco, 2020).

The main goal of this study was **to evaluate the biological characteristics of pristine PPy colloidal dispersions** for the first time as only the PPy salts were already studied previously (Humpolíček et al., 2018).

Firstly, in this thesis, the PPy colloidal dispersions were prepared using 2 and 4 wt.% of the PVP stabilizer. According to the literature, the characteristic peaks around 450 nm, corresponding to the π–π* transition from the valence to the antibonding band because of the polaron presence emerged in the **UV-vis spectra**, are confirming the PPy development (Figure 22) (Li et al., 2016; Weng et al., 2011).

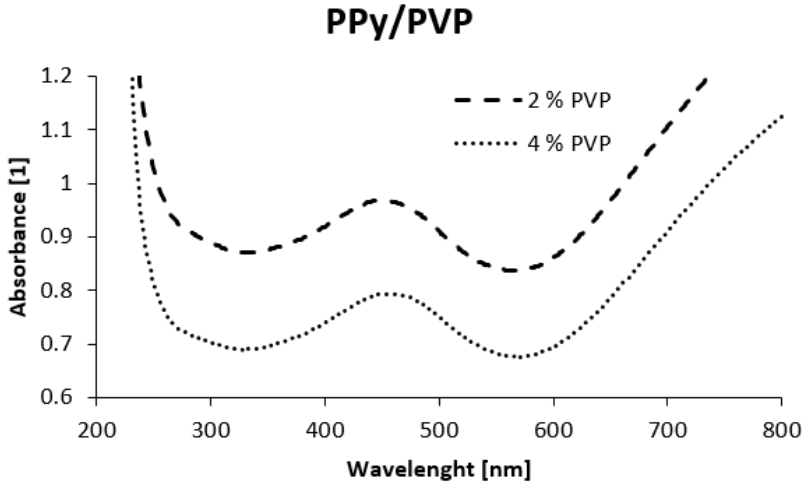

Figure 22: *UV-vis spectra of PPy/PVP colloidal dispersions*

Sizes of the prepared **particles** were also characterized. As illustrated in Table 1, the results showed that the concentration of stabilizer did not significantly affect the z-average diameter of particles. A difference of 50 nm was found between PPy/PVP-2%, where the z-average was 131±7 nm, and PPy/PVP-4% with a value of 179± nm. The polydispersity index (PDI) for both colloids was below 0.3 which is generally considered as polydisperse system with **good homogenity** (Raval et al., 2019).

Table 1: *Size (z-Average Diameter ± SD) and Polydispersity Index (PDI ± SD) of PPy colloids*

	Fresh		**24 months of storage**		**pH 7.4**	
	Z-Ave ± SD **[d.nm]**	**PDI**	**Z-Ave** ± SD **[d.nm]**	**PDI**	**Z-Ave** ± SD **[d.nm]**	**PDI**
PPy/PVP-2%	131±7	0.25±0.03	179±2	0.24±0.03	152±3	0.23±0.01
PPy/PVP-4%	179±7	0.29±0.01	73±1	0.20±0.03	211±4	0.42±0.02

Furthermore, the long-term stability of the colloids was assessed after 24 months of storage at 4°C. Both colloids (PPy/PVP-2% and PPy/PVP-4%) were visually homogenous (Figure 23 a, b). The z-average of PPy/PVP-4% significantly decreased from 179±7 nm to 73±1 nm, as well as the PDI. This suggests that the particles are maturing and creating a new thermodynamic equilibrium state, which was probably made possible by an excess of PVP that could stabilize much smaller particles. Nevertheless, no traces of aggregation or particle sedimentation were found.

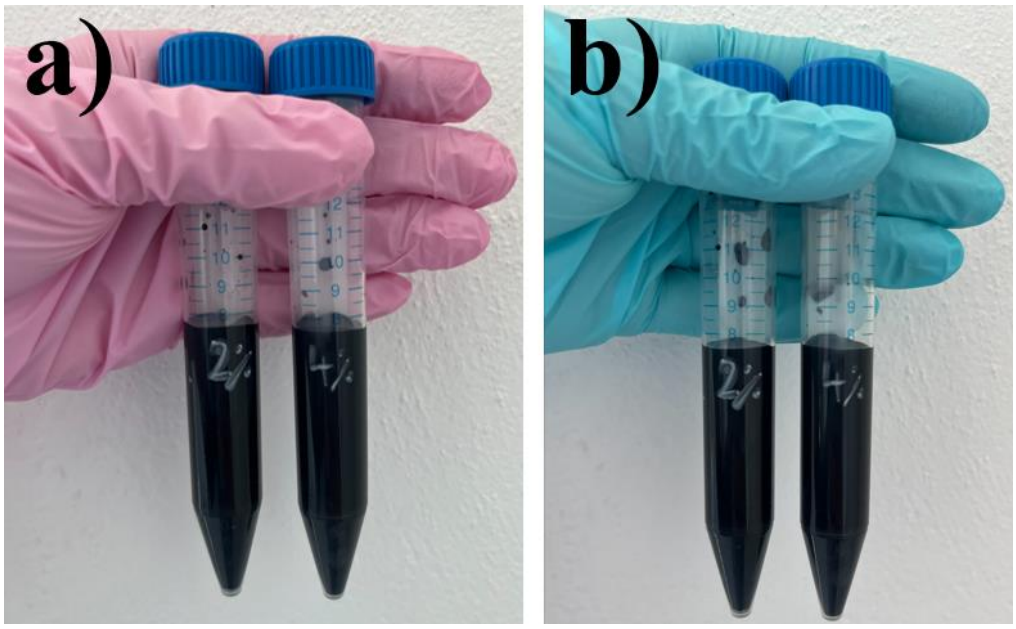

Figure 23: *The long-term stability of the PPy/PVP-2% (left) and PPy/PVP-4% (right): a) freshly prepared samples; b) samples after 24 months storage at 4°C*

The pH stability of materials is another crucial property as it is meant to come in touch with biological systems. For this reason, the z-average diameter and PDI were studied at pH 7.4 in PBS. The results showed that the z-average and PDI of PPy/PVP-2% did not remarkably change. However, good stability cannot be claimed in the case of PPy/PVP-4%. Finally, it is evident from the obtained results that the colloidal particles in PPy/PVP-2% are stable in the physiological setting.

Nevertheless, DLS expresses particle sizes as their hydrodynamic diameter, which includes also the ionic corona etc. Due to this fact, TEM analysis was also used. The results showed that the morphology of colloidal particles was homogenous and the sizes were approximately 35 nm for both colloids.

Finally, the **biological properties** of colloidal PPy particles were evaluated in cooperation with the Institute of Biophysics (Czech Academy of Sciences). As it was previously said, cytotoxicity, antioxidant activity, and antibacterial tests were established and reported for the first time.

The initiative step of biological testing was the **cytotoxicity** evaluation followed by the ISO standard 10993 part 5 using a mouse fibroblast cell line (NIH/3T3). Figure 24 shows the reported data. As can be seen, both of the samples having a concentration of PPy 200 $\mu g.mL^{-1}$ or less did not show any cytotoxicity.

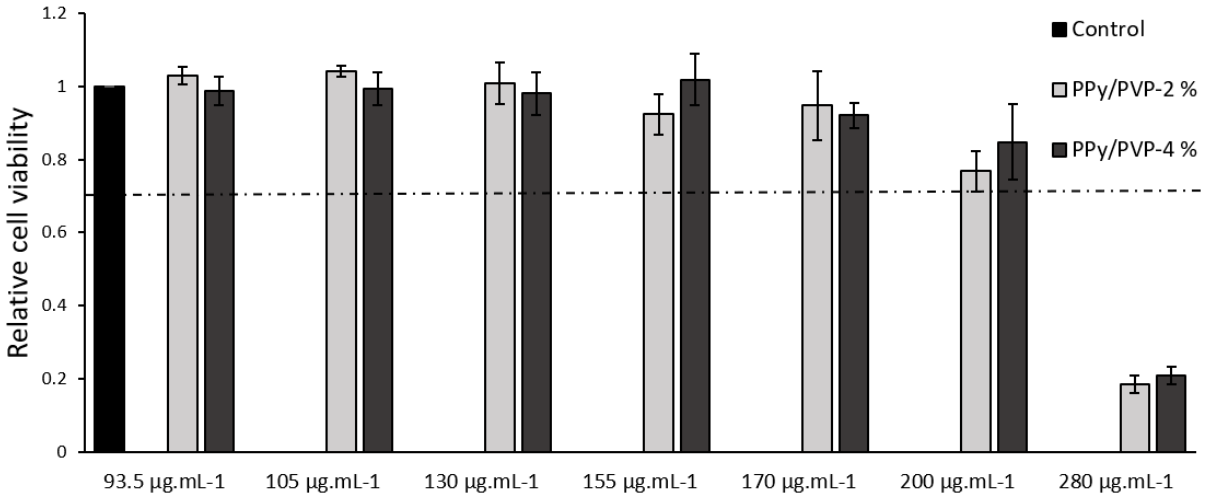

Figure 24: *Cytotoxicity of PPy colloids with different concentrations of PVP. Relative values to the reference (set as 1) are used to express data.*

For illustration, Vaitkuviene et al. studied the PPy nanoparticles prepared by the oxidative polymerization route. The higher concentrations were toxic to mouse hepatoma cells (MH-22A), primary mouse embryonic fibroblast cells (MEF) and human T lymphocyte Jurkat cells, while concentrations lower than 9.7 $\mu g.mL^{-1}$ did not affect cell viability. This value is significantly lower than the concentration of PPy in PPy/PVP colloids thus it can be concluded that PVP improves the biocompatibility (Vaitkuviene et al., 2013). Furthermore, Guo et al. researched the cytotoxicity of PPy nanoparticles mediated by PVP. They found

that the cell lines mouse fibroblasts (L929), pancreatic acinar (266-6) and colorectal adenocarcinoma (HT29) were viable at the tested nanoparticles concentration of 100 $\mu g.mL^{-1}$ (Guo et al., 2019).

As was previously discussed in the theoretical part, biomaterials can be immunomodulatory active and induce a variety of adverse reactions, such as inflammation. This reaction can be activated immediately once the material comes in contact with living tissues. Immune cells start to produce ROS, aiding in the healing process but also having the potential to cause oxidative stress (Tu et al., 2022). The existing studies on the antioxidant activity of PPy are limited. For instance, research paper by Upadhyay et al. examined the antioxidant activity of PPy nanotubes with different diameters. They explored that not only do higher concentrations of PPy have an impact on antioxidant activity, but also that nanotubes with smaller diameter showed enhanced activity (Upadhyay et al., 2014). In our study, we investigated **the antioxidant activity** of colloidal PPy as potential immunomodulatory markers. Based on the obtained data, it was researched that colloidal PPy itself revealed a **significant antioxidant effect** even in low concentrations. Tested concentrations of PPy ranged from 1.87 – 93.5 $\mu g.mL^{-1}$. The concetrations 9.35 – 93.5 $\mu g.mL^{-1}$ showed a nearly complete loss of the signal and the lowest concentration 1.87 $\mu g.mL^{-1}$ reducted the signal below 50 % of the control. Additionally, the production of ROS both before and after the neutrophil activation by opsonized zymosan particles (OZP) was examined. Even the lowest tested concentration of PPy 1.87 $\mu g.mL^{-1}$ significantly reduced both the OZP-activated and spontaneously produced ROS. Furthermore, concentrations 9.35 $\mu g.mL^{-1}$ and above resulted in remarkable reduction of over 90% in spontaneous ROS generation which is a potential counterproductive outcome. As previously researched, basal levels of ROS are essential for maintaining normal cellular functioning (Dunnill et al., 2017). However, in the case of OZP-activated ROS generation, only the highest concentration of PPy (93.5 $\mu g.mL^{-1}$) achieved complete ROS production, indicating promising results. These consequences lead to the conclusion that **PPy colloids make excellent free radical scavengers**.

Biological testing should undoubtedly include **antimicrobial properties**. It is known that bacteria have a negatively charged wall cell thus the positive net charge of PPy chains electrostatically interacts with it (Varesano et al., 2013). Here, in this thesis, the antibacterial activity expressed as a minimal inhibitory concentration (MIC) against both gram-positive (*Staphylococcus aureus*) and gram-negative (*Escherichia coli*) bacteria was investigated. The best results were obtained for PPy/PVP-2% with the MIC value 234 $\mu g.mL^{-1}$ for both gram-positive and gram-negative bacteria. The same value was observed for the PPy/PVP-4% against *S. aureus*, in the case of *E. coli*, the MIC value was higher – 468 $\mu g.mL^{-1}$. For comparison, the research group Sayyah et al. studied the MIC against *E. faecalis* and *S. aureus* and the values ranged from 62,5 to

125 mg mL^{-1}. However, they prepared PPy by a cyclic voltammetry without the usage of stabilizing agent with antibacterial properties (Sayyah et al., 2014).

Based on these results it can be conluded that **PPy in colloidal form** is not only **easy to process** but especically samples PPy/PVP-2% exhibited **good stability** under the physiological conditions and in long-term storage. Furthermore, good results were obtained also in biological testing. **No cytotoxic effect** was found under the concentration of 200 $\mu g.mL^{-1}$ colloidal PPy. As measured by ROS scavenging, samples also demonstrated **high antioxidant effects** and related immunomodulatory activities. The sample PPy/PVP-2% exhibited good **antibacterial activity** against both *E. coli* and *S. aureus*. For more details see the ready-to-submit manuscript **APPENDIX I**.

As this material is suitable for biomedical applications, the second part of this thesis studied the incorporation of PPy/PVP-2% into the hydrogel wound dressings based on chitosan to prepare bioactive composites (see the next part 3).

3) *The preparation and biological testing of active hydrogel wound dressing composites based on chitosan and PPy/PVP colloidal dispersions.* As was previously discussed in chapter 3.3, even though the skin is the body's biggest organ and acts as a protective layer against the external world, it's crucial to consider that even a minor injury can pose a significant risk to life. Traditional wound dressings, such as gauzes and bandages are typically utilized primarily to bleeding and shielding the wound from external factors. However, they provide minimal benefits in terms of enhancing the healing process, preventing infection, or reducing overactive inflammation. For these reasons, bioactive wound dressings intended to promote various aspects of the wound healing process have been created (Das and Baker, 2016). Hydrogels are excellent choices for numerous reasons, such as high-water content, similarity to ECM, mechanical properties, they can keep a moist wound environment and absorb excessive exudate and last but not least, they can be enhanced by a variety of bioactive molecules to generate further therapeutic effects (Bano et al., 2017).

In this thesis, chitosan was chosen as it is considered one of the most potent options for treating wounds due to its favourable qualities, including biocompatibility, antimicrobial, and antioxidant properties. Chitosan-based materials are already well-established in the biomedical fields (Ali Khan et al., 2020). Chitosan, for example, was used in the preparation of sponges, nanoparticles, hydrogels, membranes, and wound dressings (Dev et al., 2010; Portero et al., 2007; Tamura et al., 2011). However, chitosan is soluble in water only if its NH_2 groups are protonated to $–NH_3+$ groups, i.e. while the pH is lower than its pK_a value of ~6.5. At physiological pH, chitosan loses its charge, becomes insoluble and also its antibacterial function associated with the positive charge vanishes (Wang et al., 2006). To overcome these issues, water-soluble chitosan derivatives were studied. In this thesis, the fabrication of water-soluble half N-

acetylated chitosan (SCN) was researched (Qin et al., 2006). SCN, with a degree of deacetylation (DD) adjusted to ~50% is soluble at physiological pH. Moreover, SCN preparation is completely natural without a need to use artificial functional groups and it also exhibits high antioxidant activity (Feng et al., 2007). Properties of chitosan-based materials are also often enhanced with various bioactive substances to improve, for example, antibacterial activity or antioxidant and anti-inflammatory properties (Singh et al., 2017; Zhao et al., 2017). Here, the colloidal conductive PPy stabilized by 2% of PVP was incorporated into the SCN hydrogels resulting in better biological properties, such as good biocompatibility, antioxidant activity, and improved antimicrobial activity. The increased conductivity of the hydrogels further improved their potential for promoting wound healing by stimulating cell migration and proliferation (Talikowska et al., 2019). Furthermore, for the first time, dialdehyde cellulose (DAC) was used not only as a crosslinker of the SCN, but also to covalently anchor the prepared PPy particles (Figure 25). DAC is a crosslinking agent with very low toxicity compared to organic crosslinkers, such as glutaraldehyde (Muchová et al., 2020; Münster et al., 2018).

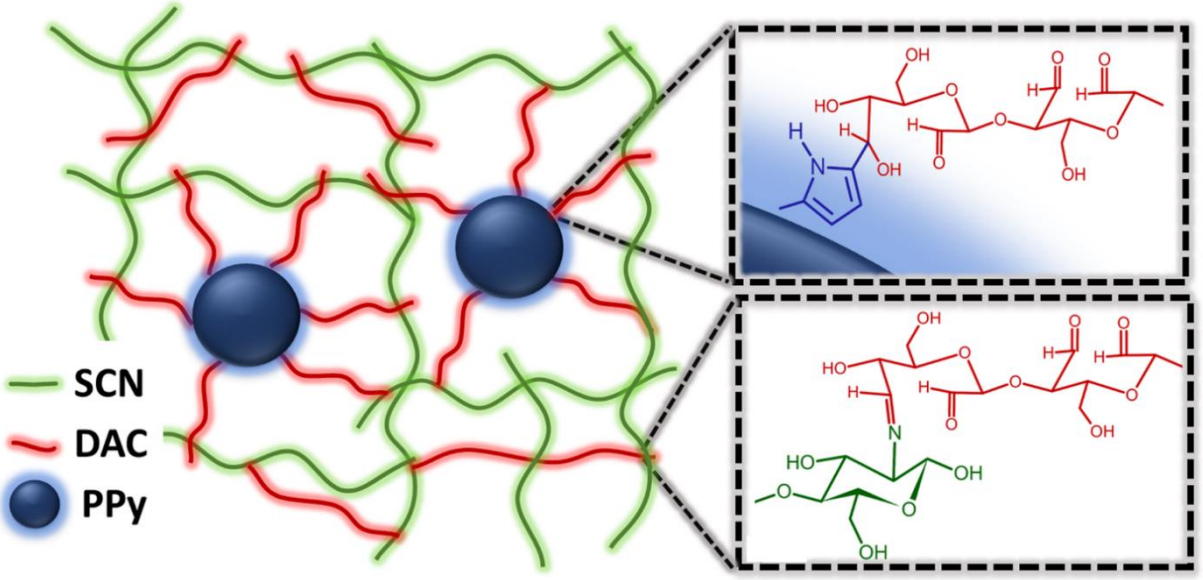

***Figure 25**: Scheme of SCN-DAC-PPy wound dressing hydrogel with details of bonding between DAC+PPy (top) and DAC+SCN (bottom)*

SCN was prepared using a modified method by Qin et al. (Qin et al., 2006), DAC fabrication was based on the works by Münster et al. (Münster et al., 2018, 2017), and finally, colloidal PPy was prepared as described above. The method for determining the degree of deacetylation (DD) of the SCN involved comparing the intensity of H2 signals in ^{1}H NMR spectra (Kasaai, 2010; Kubota et al., 2000), while PPy/PVP-2% characteristics were described previously. The **IR** and **Raman** spcetra DAC, PPy, and their aqueous mixtures (Raman) and dried-out wound dressings (FT-IR) in Figure 26 a, b proves the spontaneous DAC+PPy

reaction by the selective disappearance bands associated with aldehyde groups of DAC. The Raman and FT-IR spectra of DAC showed that the band corresponding to the free carbonyl groups of DAC, which was initially present at 1637 cm^{-1} in Raman and 1732 cm^{-1} in FT-IR spectra, disappeared when DAC was mixed with PPy. Also, the Raman and FT-IR DAC+PPy spectra still clearly show additional DAC bands between 800 and 1200 cm^{-1}.

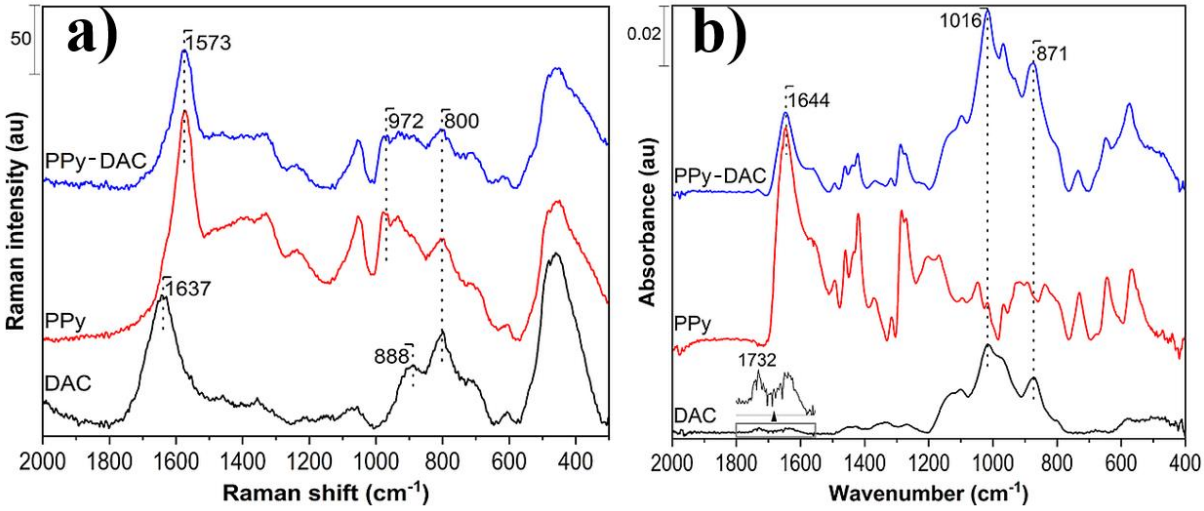

Figure 26: *a) Raman spectra of DAC, PPy, and their mixture, b) FT-IR spectra of DAC, PPy, and wound dressing prepared by drying the PPy-DAC mixture*

Firstly, the right amount of DAC (2 and 5 mol.%) as a crosslinker for the wound dressing preparation was studied. Based on the obtained results, the sample SCN-DAC-2% was chosen for the incorporation of PPy colloid. Mainly for the lower elasticity which allows better adhesion to the skin and also for the higher swelling capacity which allows better exudate absorption and lower cell attachment and growth on the surface.

Subsequently, two different SCN-DAC-2% samples with 5 wt.% of PPy and 10 wt.% of PPy relative to SCN (SCN-DAC-PPy5% and SCN-DAC-PPy10%) were prepared and studied (Figure 27). The network parameters showed that SCN-DAC-PPy5% swelled almost the same as SCN-DAC-2% (31±9 times), with the EWC of 97±1% and gel fraction of 59±2%. On the other hand, SCN-DAC-PPy10% swelled significantly more - 77±9 times, the EWC was 99±0.2% and the gel fraction 62±92%. If compared to SCN-DAC-2%, the storage modulus, loss modulus, and complex modulus of both SCN-DAC-PPy5% and SCN-DAC-PPy10% were higher, which might be explained by the network's integration of stiffer PPy nanoparticles into the network. However, the sample containing 10% of PPy had, for example, a significantly lower storage modulus than the sample with 5% of PPy. The higher SCN-DAC-PPy10% swelling and lower storage modulus may be explained by an increased PPy:DAC ratio. Because as more pyrrole groups are available for aldehyde condensation, more DAC might attach

to the PPy particles and less is available for crosslinking of farther-reaching SCN chains.

Figure 27: *SCN-DAC-PPy5% wound dressing hydrogel samples in UPW*

Moreover, PPy colloids exhibit an ionic/electronic conductivity mechanism, thus the specific conductivity (K) was measured. It is not surprising that no K was observed for dry wound dressings as the ion-conducting environment was missing. However, all swelled samples in UPW showed specific conductivity, between 2.0 $mS.cm^{-1}$ for SCN-DAC-2% and 5.1 $mS.cm^{-1}$ measured for SCN-DAC-PPy10% with an increased quantity of PPy. The hydrogel wound dressings thus possess a conductivity level similar to various human tissues, such as the human epidermis (0.26 $mS.cm^{-1}$), human dermis (2.2 $mS.cm^{-1}$), and muscle (4.1 $mS.cm^{-1}$), as reported in some studies (Duck, 1990; J. Peters, G. Stinstra, M. Hendriks, 2001). Such conductive hydrogels are capable of transmitting bioelectrical signals and potentially aiding in the process of wound healing (Zhao et al., 2017). For example, He et al. prepared hydrogels based on N-carboxyethyl chitosan and benzaldehyde-terminated Pluronic F127/carbon nanotubes with conductivity (1.37 $mS.\ cm^{-1}$ – 8.45 $mS.\ cm^{-1}$) also similar to skin tissue (He et al., 2020).

As illustrated in Figure 28, SEM micrographs of dried samples prepared in this thesis show the amount of PPy particles, represented as the quantity of bright dots, increasing with the initial dose of colloidal PPy. Additionally, the distribution of PPy particles is homogenous because no aggregation of particles was observed.

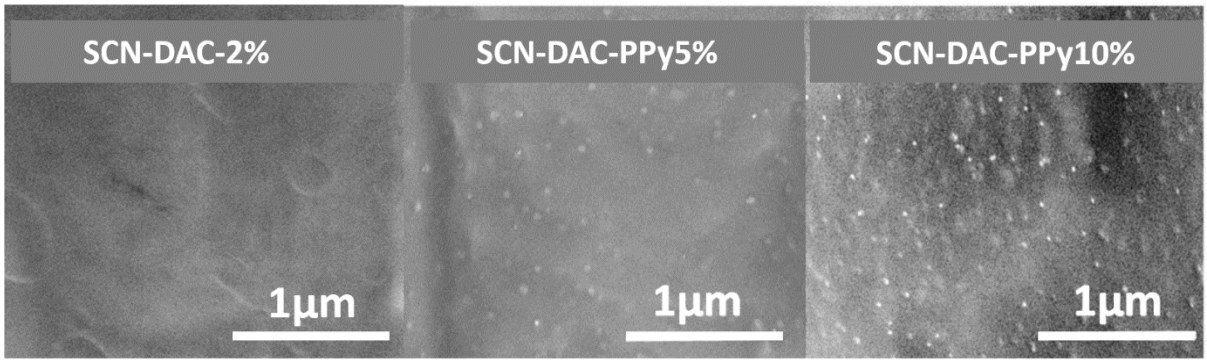

Figure 28: *SEM images of dried samples*

As the prepared wound healing dressings are supposed to interact with living tissues, appropriate **biological tests** were performed in cooperation with the Institute of Biophysics (Czech Academy of Sciences).

The **cytotoxicity testing** using a mouse fibroblast cell line (NIH/3T3) in direct contact with the samples did not show any cytotoxicity. Based on these results, it can be confirmed that PPy in hydrogels does not have a negative impact on cytotoxicity similarly to the previous study. Furthermore, cell **proliferation** was assessed. The morphology of cells on the tissue plastic in the presence of the hydrogels was physiological when compared to the reference (cell proliferation on the tissue plastic). The adhesion and proliferation were not observed on the surface of the hydrogels, especially in the case of SCN-DAC-PPy5%. However, this fact is advantageous in wound healing patches as cell ingrowth is not desirable.

In the next step, **skin irritation** was evaluated. Skin irritation test is crucial as it helps to assess the safety of the materials that come in contact with the skin. Such tests can help identify potential irritants or allergens that could cause undesirable reactions, such as redness, itching, or swelling (Kandarova et al., 2018). Here, *in vitro* skin irritation test was evaluated using a 3D reconstructed human epidermal tissue model EpiDerm^{TM} according to OECD 439 (OECD, 2021). The testing was performed using the neat SCN-DAC hydrogel and the sample with 5% of PPy, which was chosen as the best-performing wound dressing considering its excellent biological and mechanical characteristics. The results showed that both materials have non-irritating properties.

The **wound healing** was studied by a common *in vitro* technique using a **scratch assay** on NIH/3T3 cell line (Liang et al., 2007). Based on the acquired data, it was clear that the presence of all hydrogel wound dressings, even the neat one, significantly enhanced wound healing *in vitro*. It may be expected that the higher the value of PPy, the better results will be observed. However, the best results were observed in the case of SCN-DAC-PPy5% as the percentage of open wound area remaining after 10h of incubation was the lowest (37±2%). In the case of SCN-DAC-PPy10%, the value was comparable to the neat hydrogel. While the

cause behind this behaviour is unclear, the wound healing rate does not increase proportionally with the quantity of PPy.

The development of biomaterials with antioxidant properties has become another important goal in wound dressing preparation. As already discussed in chapter 3.3, excessive ROS production can lead to, for example, deoxyribonucleic acid (DNA)/ribonucleic acid (RNA) damage or cell apoptosis. Antioxidants are a good solution to overcome these limitations as they repair the normal level of ROS (Fadilah et al., 2023). For example, Bektas et al. researched the effects of incorporating vitexin into a gel based on chitosan to enhance wound healing. They observed good results as the material was able to improve the healing process in both *in vitro* and *in vivo* tests (Bektas et al., 2020). In our study, we first focused on the testing of the **antioxidant activity** of the SCN-DAC samples with 0, 5, and 10% of PPy using a luminol-horseradish peroxidase-H_2O_2-free system. The neat SCN-DAC sample showed the signal reduced by a third of the control, thus, the obtained data confirmed the previous research about the antioxidative characteristics of SCN (Feng et al., 2007). However, the samples containing PPy reduced the signal more than twice of the control and the values for both amounts of PPy were nearly the same. Next, the spontaneous and OZP-activated ROS production by neutrophils was researched and similar trends were observed – the antioxidant effect was recorded for all of the samples, including neat SCN-DAC. However, the greater the amount of PPy, the better antioxidant activity. Also, no cytotoxic effect of the samples on macrophages was observed. Moreover, as was observed in nitric oxide (NO) and interleukin 6 (IL-6) production, the tested wound dressings activated and positively modulated macrophage response.

The utilization of antibacterial wound dressings aids can reduce the entry of pathogens into the wound which is resulting in the reduction of inflammatory response. Thus, the **antimicrobial activity** of the SCN-DAC and PPy-containing hydrogels was studied according to ISO standard 22196 using *S. aureus* and *E. coli* bacteria. The results revealed, that neat SCN-DAC hydrogel was not effective against either of the bacterial strains as expected. The reason was already explained previously – materials based on chitosan do not show an antibacterial effect in neutral pH (Qin et al., 2006). On the other hand, the wound dressings containing PPy showed improved antimicrobial activity, for example, both samples exhibited significant activity against *S. aureus* (R ~2) and against *E. coli* the value was 0.8 – 1.0.

Based on obtained results it can be concluded that **active hydrogel dressings** with **non-cytotoxic**, **antioxidant**, **non-irritating**, **antibacterial**, and **conducting properties** were prepared. Furthermore, the samples also exhibited **enhancing *in vitro* wound healing**. Also, it must be noted that in the future the application of the reaction of DAC+PPy could have wide-ranging uses in the development of conductive materials for biomedical applications.

For more details see the ready-to-sumbit manuscript **APPENDIX II.**

During my doctoral studies, I also participated in several cooperations with other researchers to evaluate the biological testing of different biomaterials. Specifically, in a research paper by *Münster L., Fojtů M., Muchová M, Latečka F., **Káčerová S.**, Capáková Z., Juriňáková T., Kuřitka I., Masařík M., Vícha J. Enhancing cisplatin anticancer effectivity and migrastatic potential by modulation of molecular weight of oxidized dextran carrier. Carbohydrate Polymers. 2021, 272, 118461* (**ARTICLE I**) I tested the scratch assay performed on ovarian cancer cell line A2780, which was treated with nanogels based on dextran loaded with cisplatin.

Furthermore, in the work by *Štěpánková K., Ozaltin K., Pelková J., Pištěková H., Karakurt I., **Káčerová S**., Lehocký M., Humpolíček P., Vesel A., Mozetic M. Furcellaran surface deposition and its potential in biomedical applications. International Journal of Molecular Sciences. 2022, 23(13),7439* (**ARTICLE II**) I tested cytotoxicity and cell proliferation of the embryonic stem cell ES R1 line on samples that where prepared by furcellaran deposition onto a poly(ethylene terephthalate) (PET) surface via RF air plasma discharge activation followed by grafting of a N-allylmethylamine (MAAM) monomer.

In a research paper by, *Jasenská D., Kašpárková V., Vašíček O., Münster L., Minařík A., **Káčerová S.**, Korábková E., Urbánková L., Vícha J., Capáková Z., Falleta E., Pina C. D., Lehocký M., Skopalová K., Humpolíček P. Enzyme-catalyzed polymerization process: a novel approach to the preparation of polyaniline colloidal dispersions with and immunomodulatory effect. Biomacromolecules. 2022, 23(8), 3359-3370* (**ARTICLE III**), I tested the effect of biocompatible polymers based on PANI colloidal particles prepared by the enzymatic polymerization of aniline stabilized by PVA or chitosan on NIH/3T3 mouse fibroblast cell viability.

Similarly, in the work by *Martínková M., Hausnerová B., Huba J., Martínek T., **Káčerová S.**, Kašpárková V., Humpolíček P. Powder injection molded ceramic scaffolds: The role of pores size and surface functionalization on the cytocompatibility. Materials and Design. 2022, 224, 111274* (**ARTICLE IV**), I worked on the cytocompatibility tests of ceramic-based scaffolds functionalized by PANI-based films using NIH/3T3 mouse fibroblast cell line.

11. CONTRIBUTION TO SCIENCE

Although biomaterials have unquestionably revolutionized the medicine, their great potential and uncharted territories continue to attract researches towards an exciting journey of exploration and discovery. The presented Ph.D. study contributes to the current knowledge of hydrogels, conducting polymers, and their composites.

The initial phase of this study focused on the modification of carboxylic groups along the hyaluronic acid backbone, leading to the creation of thiol groups that serve as crosslinking sites. Though some problems appeared during the synthesis, appropriate adjustments led to the successful modification of HA with the demanded degree of thiolation. Such materials could be used for the preparation of the model of small intestine tissue where thiolated hyaluronic acid, as well as collagen would be the main structural materials further modified by growth factors. Together the material should promote the desired intestinal stem cells behaviour. It is based on the idea of making the gradients both biochemical and mechanical. This research is being finished and the results will be published in an international journal.

Furthermore, the colloidal dispersions based on conductive polypyrrole stabilized with poly(vinylpyrrolidone) were studied in terms of material and biological properties. While previous investigations explored the biological properties of PPy powders, nanoparticles, films, and composites, the colloidal form of PPy remained unexplored until now. Consequently, the primary objective of this research was to assess the influence of colloidal PPy on cell viability, antioxidant activity, and antibacterial efficacy, marking the first analysis in this field. The obtained data showed an exceptional antioxidative effect of colloidal PPy, positioning it as a highly promising candidate for composite preparation for biomedical applications. Thus, the next study concentrated on the incorporation of PPy into the hydrogels based on chitosan.

The investigation was focused on partially re-acetylated modification of chitosan and subsequently dialdehyde cellulose was used as a low-toxic crosslinker. Additionally, colloidal PPy was employed to enhance the hydrogel properties. The obtained results demonstrated the exceptional capabilities of these samples, as potential wound dressings, exhibiting good ROS scavenging abilities, antibacterial properties, and significant *in vitro* wound healing potential. These findings emphasize the great promise of these bioactive hydrogel dressings in advancing the field of wound care and promoting the accelerated healing process. Furthermore, the condensation reaction between DAC and PPy described here for the first time opens up the doors to the development of many more conductive biomaterials.

REFERENCES

Adan, A., Kiraz, Y., Baran, Y., 2016. Cell Proliferation and Cytotoxicity Assays. CPB 17, 1213–1221. https://doi.org/10.2174/1389201017666160808160513

Ahmed, E.M., 2015. Hydrogel: Preparation, characterization, and applications: A review. Journal of Advanced Research 6, 105–121. https://doi.org/10.1016/j.jare.2013.07.006

Ahmed, T.A.E., Dare, E.V., Hincke, M., 2008. Fibrin: A Versatile Scaffold for Tissue Engineering Applications. Tissue Engineering Part B: Reviews 14, 199–215. https://doi.org/10.1089/ten.teb.2007.0435

Ahumada, M., Jacques, E., Calderon, C., Martínez-Gómez, F., 2019. Porosity in Biomaterials: A Key Factor in the Development of Applied Materials in Biomedicine, in: Martínez, L.M.T., Kharissova, O.V., Kharisov, B.I. (Eds.), Handbook of Ecomaterials. Springer International Publishing, Cham, pp. 3503–3522. https://doi.org/10.1007/978-3-319-68255-6_162

Aibani, N., Rai, R., Patel, P., Cuddihy, G., Wasan, E.K., 2021. Chitosan Nanoparticles at the Biological Interface: Implications for Drug Delivery. Pharmaceutics 13, 1686. https://doi.org/10.3390/pharmaceutics13101686

Akilbekova, D., Shaimerdenova, M., Adilov, S., Berillo, D., 2018. Biocompatible scaffolds based on natural polymers for regenerative medicine. International Journal of Biological Macromolecules 114, 324–333. https://doi.org/10.1016/j.ijbiomac.2018.03.116

Al-Dulaimi, A.A., Wanrosli, W.D., 2016. Preparation of Colloidal Properties and Water Dispersible Conductive Polypyrrole Nanocomposite of Nanocrystalline Cellulose. Polymers and Polymer Composites 24, 695–702. https://doi.org/10.1177/096739111602400904

Ali Khan, Z., Jamil, S., Akhtar, A., Mustehsan Bashir, M., Yar, M., 2020. Chitosan based hybrid materials used for wound healing applications- A short review. International Journal of Polymeric Materials and Polymeric Biomaterials 69, 419–436. https://doi.org/10.1080/00914037.2019.1575828

Allison, D.D., Grande-Allen, K.J., 2006. Review. Hyaluronan: A Powerful Tissue Engineering Tool. Tissue Engineering 12, 2131–2140. https://doi.org/10.1089/ten.2006.12.2131

Alovskaya, A., Alekseeva, T., Phillips, J.B., King, V., Brown, R., 2007. Fibronectin, Collagen, Fibrin - Components of Extracellular Matrix for Nerve Regeneration. Topics in tissue engineering 3.

Antoine, E.E., Vlachos, P.P., Rylander, M.N., 2014. Review of Collagen I Hydrogels for Bioengineered Tissue Microenvironments: Characterization of Mechanics, Structure, and Transport. Tissue Engineering Part B: Reviews 20, 683–696. https://doi.org/10.1089/ten.teb.2014.0086

Athanasiou, K., 1996. Sterilization, toxicity, biocompatibility and clinical applications of polylactic acid/ polyglycolic acid copolymers. Biomaterials 17, 93–102. https://doi.org/10.1016/0142-9612(96)85754-1

Badylak, S., Freytes, D., Gilbert, T., 2009. Extracellular matrix as a biological scaffold material: Structure and function. Acta Biomaterialia 5, 1–13. https://doi.org/10.1016/j.actbio.2008.09.013

Balint, R., Cassidy, N.J., Cartmell, S.H., 2014. Conductive polymers: Towards a smart biomaterial for tissue engineering. Acta Biomaterialia 10, 2341–2353. https://doi.org/10.1016/j.actbio.2014.02.015

Bano, I., Arshad, M., Yasin, T., Ghauri, M.A., Younus, M., 2017. Chitosan: A potential biopolymer for wound management. International Journal of Biological Macromolecules 102, 380–383. https://doi.org/10.1016/j.ijbiomac.2017.04.047

Bektas, N., Şenel, B., Yenilmez, E., Özatik, O., Arslan, R., 2020. Evaluation of wound healing effect of chitosan-based gel formulation containing vitexin. Saudi Pharmaceutical Journal 28, 87–94. https://doi.org/10.1016/j.jsps.2019.11.008

Bian, S., He, M., Sui, J., Cai, H., Sun, Y., Liang, J., Fan, Y., Zhang, X., 2016. The self-crosslinking smart hyaluronic acid hydrogels as injectable three-dimensional scaffolds for cells culture. Colloids and Surfaces B: Biointerfaces 140, 392–402. https://doi.org/10.1016/j.colsurfb.2016.01.008

Bierbrauer, F., 2005. Hydrogel drug delivery: diffusion models, internal report.

Bordbar-Khiabani, A., Gasik, M., 2022. Smart Hydrogels for Advanced Drug Delivery Systems. IJMS 23, 3665. https://doi.org/10.3390/ijms23073665

Bothiraja, C., Shinde, M.B., Rajalakshmi, S., Pawar, A.P., 2010. Evaluation of molecular pharmaceutical and in-vivo properties of spray-dried isolated andrographolide—PVP. Journal of Pharmacy and Pharmacology 61, 1465–1472. https://doi.org/10.1211/jpp.61.11.0005

Bouhadir, K.H., Hausman, D.S., Mooney, D.J., 1999. Synthesis of cross-linked poly(aldehyde guluronate) hydrogels. Polymer 40, 3575–3584. https://doi.org/10.1016/S0032-3861(98)00550-3

Boyan, B., 1996. Role of material surfaces in regulating bone and cartilage cell response. Biomaterials 17, 137–146. https://doi.org/10.1016/0142-9612(96)85758-9

Brannon-Peppas, L., Peppas, N.A., 1991. Equilibrium swelling behavior of pH-sensitive hydrogels. Chemical Engineering Science 46, 715–722. https://doi.org/10.1016/0009-2509(91)80177-Z

Brauker, J.H., Carr-Brendel, V.E., Martinson, L.A., Crudele, J., Johnston, W.D., Johnson, R.C., 1995. Neovascularization of synthetic membranes directed by membrane microarchitecture. J. Biomed. Mater. Res. 29, 1517–1524. https://doi.org/10.1002/jbm.820291208

Bryant, S.J., Anseth, K.S., 2001. The effects of scaffold thickness on tissue engineered cartilage in photocrosslinked poly(ethylene oxide) hydrogels. Biomaterials 22, 619–626. https://doi.org/10.1016/S0142-9612(00)00225-8

Bulpitt, P., Aeschlimann, D., 1999. New strategy for chemical modification of hyaluronic acid: preparation of functionalized derivatives and their use in the formation of novel biocompatible hydrogels. J Biomed Mater Res 47, 152–169. https://doi.org/10.1002/(sici)1097-4636(199911)47:2<152::aid-jbm5>3.0.co;2-i

Burdick, J.A., Prestwich, G.D., 2011. Hyaluronic Acid Hydrogels for Biomedical Applications. Adv. Mater. 23, H41–H56. https://doi.org/10.1002/adma.201003963

Caló, E., Khutoryanskiy, V.V., 2015. Biomedical applications of hydrogels: A review of patents and commercial products. European Polymer Journal 65, 252–267. https://doi.org/10.1016/j.eurpolymj.2014.11.024

Cao, W., Sui, J., Ma, M., Xu, Y., Lin, W., Chen, Y., Man, Y., Sun, Y., Fan, Y., Zhang, X., 2019. The preparation and biocompatible evaluation of injectable dual crosslinking hyaluronic acid hydrogels as cytoprotective agents. J. Mater. Chem. B 7, 4413–4423. https://doi.org/10.1039/C9TB00839J

Cecen, B., Kozaci, D., Yuksel, M., Erdemli, D., Bagriyanik, A., Havitcioglu, H., 2015. Biocompatibility of MG-63 Cells on Collagen, Poly-L-Lactic Acid, Hydroxyapatite Scaffolds with Different Parameters. Journal of Applied Biomaterials & Functional Materials 13, 10–16. https://doi.org/10.5301/jabfm.5000182

Cervidil [WWW Document], 2021. URL https://www.cervidil.com/

Chamkouri, H., 2021. A Review of Hydrogels, Their Properties and Applications in Medicine. AJBSR 11, 485–493. https://doi.org/10.34297/AJBSR.2021.11.001682

Chandra, R., 1998. Biodegradable polymers. Progress in Polymer Science 23, 1273–1335. https://doi.org/10.1016/S0079-6700(97)00039-7

Chen, C.T., Chang, Y.J., Chen, M.C., Tobolsky, A.V., 1973. Formalized poly(vinyl alcohol) membranes for reverse osmosis. J. Appl. Polym. Sci. 17, 789–796. https://doi.org/10.1002/app.1973.070170311

Choi, Y.S., Hong, S.R., Lee, Y.M., Song, K.W., Park, M.H., Nam, Y.S., 1999. Studies on gelatin-containing artificial skin: II. Preparation and characterization of cross-linked gelatin-hyaluronate sponge. J Biomed Mater Res 48, 631–639. https://doi.org/10.1002/(sici)1097-4636(1999)48:5<631::aid-jbm6>3.0.co;2-y

Courtney, T., Sacks, M., Stankus, J., Guan, J., Wagner, W., 2006. Design and analysis of tissue engineering scaffolds that mimic soft tissue mechanical anisotropy. Biomaterials S0142961206001645. https://doi.org/10.1016/j.biomaterials.2006.02.024

Cruise, G.M., Scharp, D.S., Hubbell, J.A., 1998. Characterization of permeability and network structure of interfacially photopolymerized poly(ethylene glycol) diacrylate

hydrogels. Biomaterials 19, 1287–1294. https://doi.org/10.1016/S0142-9612(98)00025-8

Cui, P., Pan, P., Qin, L., Wang, X., Chen, X., Deng, Y., Zhang, X., 2023. Nanoengineered hydrogels as 3D biomimetic extracellular matrix with injectable and sustained delivery capability for cartilage regeneration. Bioactive Materials 19, 487–498. https://doi.org/10.1016/j.bioactmat.2022.03.032

Das, S., Baker, A.B., 2016. Biomaterials and Nanotherapeutics for Enhancing Skin Wound Healing. Front. Bioeng. Biotechnol. 4. https://doi.org/10.3389/fbioe.2016.00082

Day, A.J., Sheehan, J.K., 2001. Hyaluronan: polysaccharide chaos to protein organisation. Current Opinion in Structural Biology 11, 617–622. https://doi.org/10.1016/S0959-440X(00)00256-6

De, P., Dey, N., Leyland-Jones, B., 2013. Growth Factor and Signaling Networks, in: Brenner's Encyclopedia of Genetics. Elsevier, pp. 365–369. https://doi.org/10.1016/B978-0-12-374984-0.00664-1

Dev, A., Mohan, J.C., Sreeja, V., Tamura, H., Patzke, G.R., Hussain, F., Weyeneth, S., Nair, S.V., Jayakumar, R., 2010. Novel carboxymethyl chitin nanoparticles for cancer drug delivery applications. Carbohydrate Polymers 79, 1073–1079. https://doi.org/10.1016/j.carbpol.2009.10.038

Devarasetty, M., Mazzocchi, A.R., Skardal, A., 2018. Applications of Bioengineered 3D Tissue and Tumor Organoids in Drug Development and Precision Medicine: Current and Future. BioDrugs 32, 53–68. https://doi.org/10.1007/s40259-017-0258-x

Dhandayuthapani, B., Yoshida, Y., Maekawa, T., Kumar, D.S., 2011. Polymeric Scaffolds in Tissue Engineering Application: A Review. International Journal of Polymer Science 2011, 1–19. https://doi.org/10.1155/2011/290602

Dinescu, S., Albu Kaya, M., Chitoiu, L., Ignat, S., Kaya, D.A., Costache, M., 2019. Collagen-Based Hydrogels and Their Applications for Tissue Engineering and Regenerative Medicine, in: Mondal, Md.I.H. (Ed.), Cellulose-Based Superabsorbent Hydrogels, Polymers and Polymeric Composites: A Reference Series. Springer International Publishing, Cham, pp. 1643–1664. https://doi.org/10.1007/978-3-319-77830-3_54

Dovedytis, M., Liu, Z.J., Bartlett, S., 2020. Hyaluronic acid and its biomedical applications: A review. Engineered Regeneration 1, 102–113. https://doi.org/10.1016/j.engreg.2020.10.001

Drumheller, P.D., Elbert, D.L., Hubbell, J.A., 1994. Multifunctional poly(ethylene glycol) semi-interpenetrating polymer networks as highly selective adhesive substrates for bioadhesive peptide grafting. Biotechnol. Bioeng. 43, 772–780. https://doi.org/10.1002/bit.260430812

Drury, J.L., Mooney, D.J., 2003. Hydrogels for tissue engineering: scaffold design variables and applications. Biomaterials 24, 4337–4351. https://doi.org/10.1016/S0142-9612(03)00340-5

Duck, F.A., 1990. Electrical Properties of Tissue, in: Physical Properties of Tissues. Elsevier, pp. 167–223. https://doi.org/10.1016/B978-0-12-222800-1.50010-3

Dunnill, C., Patton, T., Brennan, J., Barrett, J., Dryden, M., Cooke, J., Leaper, D., Georgopoulos, N.T., 2017. Reactive oxygen species (ROS) and wound healing: the functional role of ROS and emerging ROS-modulating technologies for augmentation of the healing process: Reactive oxygen species and wound healing. Int Wound J 14, 89–96. https://doi.org/10.1111/iwj.12557

Ebhodaghe, S.O., 2020. Hydrogel – based biopolymers for regenerative medicine applications: a critical review. International Journal of Polymeric Materials and Polymeric Biomaterials 1–18. https://doi.org/10.1080/00914037.2020.1809409

Echave, M.C., Burgo, L.S., Pedraz, J.L., Orive, G., 2017. Gelatin as Biomaterial for Tissue Engineering. CPD 23. https://doi.org/10.2174/0929867324666170511123101

Ekdahl, K.N., Lambris, J.D., Elwing, H., Ricklin, D., Nilsson, P.H., Teramura, Y., Nicholls, I.A., Nilsson, B., 2011. Innate immunity activation on biomaterial surfaces: A mechanistic model and coping strategies. Advanced Drug Delivery Reviews 63, 1042–1050. https://doi.org/10.1016/j.addr.2011.06.012

Elbert, D.L., Hubbell, J.A., 1996. Surface Treatments of Polymers for Biocompatibility. Annu. Rev. Mater. Sci. 26, 365–394. https://doi.org/10.1146/annurev.ms.26.080196.002053

Ellman, G.L., 1959. Tissue sulfhydryl groups. Archives of Biochemistry and Biophysics 82, 70–77. https://doi.org/10.1016/0003-9861(59)90090-6

El-Sherbiny, I.M., Yacoub, M.H., 2013. Hydrogel scaffolds for tissue engineering: Progress and challenges. Global Cardiology Science and Practice 2013, 38. https://doi.org/10.5339/gcsp.2013.38

Elvira, C., Mano, J.F., San Román, J., Reis, R.L., 2002. Starch-based biodegradable hydrogels with potential biomedical applications as drug delivery systems. Biomaterials 23, 1955–1966. https://doi.org/10.1016/S0142-9612(01)00322-2

Engler, A.J., Sen, S., Sweeney, H.L., Discher, D.E., 2006. Matrix Elasticity Directs Stem Cell Lineage Specification. Cell 126, 677–689. https://doi.org/10.1016/j.cell.2006.06.044

Fadilah, N.I.M., Phang, S.J., Kamaruzaman, N., Salleh, A., Zawani, M., Sanyal, A., Maarof, M., Fauzi, M.B., 2023. Antioxidant Biomaterials in Cutaneous Wound Healing and Tissue Regeneration: A Critical Review. Antioxidants 12, 787. https://doi.org/10.3390/antiox12040787

Feng, T., Du, Y., Li, J., Wei, Y., Yao, P., 2007. Antioxidant activity of half N-acetylated water-soluble chitosan in vitro. Eur Food Res Technol 225, 133. https://doi.org/10.1007/s00217-006-0391-0

Fiorati, A., Linciano, C., Galante, C., Raucci, M.G., Altomare, L., 2021. Bioactive Hydrogels: Design and Characterization of Cellulose-Derived Injectable Composites. Materials 14, 4511. https://doi.org/10.3390/ma14164511

Firlar, I., Altunbek, M., McCarthy, C., Ramalingam, M., Camci-Unal, G., 2022. Functional Hydrogels for Treatment of Chronic Wounds. Gels 8, 127. https://doi.org/10.3390/gels8020127

Franco, P., De Marco, I., 2020. The Use of Poly(N-vinyl pyrrolidone) in the Delivery of Drugs: A Review. Polymers 12, 1114. https://doi.org/10.3390/polym12051114

Fraser, J.R.E., Laurent, T.C., Laurent, U.B.G., 1997. Hyaluronan: its nature, distribution, functions and turnover. Journal of Internal Medicine 242, 27–33. https://doi.org/10.1046/j.1365-2796.1997.00170.x

Freimoser, F.M., Jakob, C.A., Aebi, M., Tuor, U., 1999. The MTT [3-(4,5-Dimethylthiazol-2-yl)-2,5-Diphenyltetrazolium Bromide] Assay Is a Fast and Reliable Method for Colorimetric Determination of Fungal Cell Densities. Appl Environ Microbiol 65, 3727–3729. https://doi.org/10.1128/AEM.65.8.3727-3729.1999

Gangopadhyay, R., Molla, M.R., 2011. Polypyrrole-polyvinyl alcohol stable nanodispersion: A prospective conducting black ink: Please Provide Copy. J. Polym. Sci. B Polym. Phys. 49, 792–800. https://doi.org/10.1002/polb.22216

Gao, Y., Liu, Q., Kong, W., Wang, J., He, L., Guo, L., Lin, H., Fan, H., Fan, Y., Zhang, X., 2020. Activated hyaluronic acid/collagen composite hydrogel with tunable physical properties and improved biological properties. International Journal of Biological Macromolecules 164, 2186–2196. https://doi.org/10.1016/j.ijbiomac.2020.07.319

Gentile, P., Chiono, V., Carmagnola, I., Hatton, P., 2014. An Overview of Poly(lactic-co-glycolic) Acid (PLGA)-Based Biomaterials for Bone Tissue Engineering. IJMS 15, 3640–3659. https://doi.org/10.3390/ijms15033640

Gomez-Florit, M., Pardo, A., Domingues, R.M.A., Graça, A.L., Babo, P.S., Reis, R.L., Gomes, M.E., 2020. Natural-Based Hydrogels for Tissue Engineering Applications. Molecules 25, 5858. https://doi.org/10.3390/molecules25245858

Griffon, D., Sedighi, M., Schaeffer, D., Eurell, J., Johnson, A., 2006. Chitosan scaffolds: Interconnective pore size and cartilage engineering. Acta Biomaterialia 2, 313–320. https://doi.org/10.1016/j.actbio.2005.12.007

Guan, X., Avci-Adali, M., Alarçin, E., Cheng, H., Kashaf, S.S., Li, Y., Chawla, A., Jang, H.L., Khademhosseini, A., 2017. Development of hydrogels for regenerative engineering. Biotechnol. J. 12, 1600394. https://doi.org/10.1002/biot.201600394

Guimard, N.K., Gomez, N., Schmidt, C.E., 2007. Conducting polymers in biomedical engineering. Progress in Polymer Science 32, 876–921. https://doi.org/10.1016/j.progpolymsci.2007.05.012

Guo, B., Zhao, J., Wu, C., Zheng, Y., Ye, C., Huang, M., Wang, S., 2019. One-pot synthesis of polypyrrole nanoparticles with tunable photothermal conversion and drug loading capacity. Colloids and Surfaces B: Biointerfaces 177, 346–355. https://doi.org/10.1016/j.colsurfb.2019.02.016

Gurski, L.A., Jha, A.K., Zhang, C., Jia, X., Farach-Carson, M.C., 2009. Hyaluronic acid-based hydrogels as 3D matrices for in vitro evaluation of chemotherapeutic drugs using poorly adherent prostate cancer cells. Biomaterials 30, 6076–6085. https://doi.org/10.1016/j.biomaterials.2009.07.054

Halfter, W., Dong, S., Schurer, B., Cole, G.J., 1998. Collagen XVIII Is a Basement Membrane Heparan Sulfate Proteoglycan. Journal of Biological Chemistry 273, 25404–25412. https://doi.org/10.1074/jbc.273.39.25404

Han, G., Ceilley, R., 2017. Chronic Wound Healing: A Review of Current Management and Treatments. Adv Ther 34, 599–610. https://doi.org/10.1007/s12325-017-0478-y

Hansen, J.K., Thibeault, S.L., Walsh, J.F., Shu, X.Z., Prestwich, G.D., 2005. In Vivo Engineering of the Vocal Fold Extracellular Matrix with Injectable Hyaluronic Acid Hydrogels: Early Effects on Tissue Repair and Biomechanics in a Rabbit Model. Ann Otol Rhinol Laryngol 114, 662–670. https://doi.org/10.1177/000348940511400902

He, J., Shi, M., Liang, Y., Guo, B., 2020. Conductive adhesive self-healing nanocomposite hydrogel wound dressing for photothermal therapy of infected full-thickness skin wounds. Chemical Engineering Journal 394, 124888. https://doi.org/10.1016/j.cej.2020.124888

Heath, C.A., 2000. Cells for tissue engineering. Trends in Biotechnology 18, 17–19. https://doi.org/10.1016/S0167-7799(99)01396-7

Hernandez-Gordillo, V., Chmielewski, J., 2014. Mimicking the extracellular matrix with functionalized, metal-assembled collagen peptide scaffolds. Biomaterials 35, 7363–7373. https://doi.org/10.1016/j.biomaterials.2014.05.019

Hoare, T.R., Kohane, D.S., 2008. Hydrogels in drug delivery: Progress and challenges. Polymer 49, 1993–2007. https://doi.org/10.1016/j.polymer.2008.01.027

Holback, H., Yeo, Y., Park, K., 2011. Hydrogel swelling behavior and its biomedical applications, in: Biomedical Hydrogels. Elsevier, pp. 3–24. https://doi.org/10.1533/9780857091383.1.3

Howard, D., Buttery, L.D., Shakesheff, K.M., Roberts, S.J., 2008. Tissue engineering: strategies, stem cells and scaffolds. Journal of Anatomy 213, 66–72. https://doi.org/10.1111/j.1469-7580.2008.00878.x

Hu, W., Wang, Z., Xiao, Y., Zhang, S., Wang, J., 2019. Advances in crosslinking strategies of biomedical hydrogels. Biomater. Sci. 7, 843–855. https://doi.org/10.1039/C8BM01246F

Huang, C., Dong, L., Zhao, B., Lu, Y., Huang, S., Yuan, Z., Luo, G., Xu, Y., Qian, W., 2022. Anti-inflammatory hydrogel dressings and skin wound healing. Clinical & Translational Med 12. https://doi.org/10.1002/ctm2.1094

Humpolíček, P., Kašpárková, V., Pacherník, J., Stejskal, J., Bober, P., Capáková, Z., Radaszkiewicz, K.A., Junkar, I., Lehocký, M., 2018. The biocompatibility of polyaniline and polypyrrole: A comparative study of their cytotoxicity, embryotoxicity and impurity profile. Materials Science and Engineering: C 91, 303–310. https://doi.org/10.1016/j.msec.2018.05.037

Icardo, J.M., Colvee, E., 1995. Atrioventricular valves of the mouse: III. Collagenous skeleton and myotendinous junction. Anat. Rec. 243, 367–375. https://doi.org/10.1002/ar.1092430311

Ingber, D.E., 2006. Cellular mechanotransduction: putting all the pieces together again. FASEB j. 20, 811–827. https://doi.org/10.1096/fj.05-5424rev

J. Peters, G. Stinstra, M. Hendriks, M., 2001. Estimation of the Electrical Conductivity of Human Tissue. Electromagnetics 21, 545–557. https://doi.org/10.1080/027263401752246199

Jain, D., Mattiassi, S., Goh, E., Yim, EvelynK.F., 2020. Extracellular matrix and biomimetic engineering microenvironment for neuronal differentiation. Neural Regen Res 15, 573. https://doi.org/10.4103/1673-5374.266907

Janmey, P.A., Winer, J.P., Weisel, J.W., 2009. Fibrin gels and their clinical and bioengineering applications. J. R. Soc. Interface. 6, 1–10. https://doi.org/10.1098/rsif.2008.0327

Jasenská, D., Kašpárková, V., Radaszkiewicz, K.A., Capáková, Z., Pacherník, J., Trchová, M., Minařík, A., Vajďák, J., Bárta, T., Stejskal, J., Lehocký, M., Truong, T.H., Moučka, R., Humpolíček, P., 2021. Conducting composite films based on chitosan or sodium hyaluronate. Properties and cytocompatibility with human induced pluripotent stem cells. Carbohydrate Polymers 253, 117244. https://doi.org/10.1016/j.carbpol.2020.117244

Jeong, S.I., Kim, B.-S., Lee, Y.M., Ihn, K.J., Kim, S.H., Kim, Y.H., 2004. Morphology of Elastic Poly(L -lactide- *co* -ε-caprolactone) Copolymers and in Vitro and in Vivo Degradation Behavior of Their Scaffolds. Biomacromolecules 5, 1303–1309. https://doi.org/10.1021/bm049921i

Jia, X., Burdick, J.A., Kobler, J., Clifton, R.J., Rosowski, J.J., Zeitels, S.M., Langer, R., 2004. Synthesis and Characterization of in Situ Cross-Linkable Hyaluronic Acid-Based Hydrogels with Potential Application for Vocal Fold Regeneration. Macromolecules 37, 3239–3248. https://doi.org/10.1021/ma035970w

Jian, S., Xiao Ming, S., 1987. Crosslinked PVA-PS thin-film composite membrane for reverse osmosis. Desalination 62, 395–403. https://doi.org/10.1016/0011-9164(87)87040-6

Jiang, S., Liu, S., Feng, W., 2011. PVA hydrogel properties for biomedical application. Journal of the Mechanical Behavior of Biomedical Materials 4, 1228–1233. https://doi.org/10.1016/j.jmbbm.2011.04.005

Kafedjiiski, K., Jetti, R., Foger, F., Hoyer, H., Werle, M., Hoffer, M., Bernkopschnurch, A., 2007. Synthesis and in vitro evaluation of thiolated hyaluronic acid for mucoadhesive drug delivery. International Journal of Pharmaceutics 343, 48–58. https://doi.org/10.1016/j.ijpharm.2007.04.019

Kandarova, H., Willoughby, J.A., De Jong, W.H., Letasiova, S., Milasova, T., Bachelor, M.A., Breyfogle, B., Handa, Y., De La Fonteyne, L., Coleman, K.P., 2018. Pre-validation of an in vitro skin irritation test for medical devices using the reconstructed human tissue model EpiDerm™. Toxicology in Vitro 50, 407–417. https://doi.org/10.1016/j.tiv.2018.02.007

Kang, H., Peng, J., Lu, S., Liu, S., Zhang, L., Huang, J., Sui, X., Zhao, B., Wang, A., Xu, W., Luo, Z., Guo, Q., 2014. *In vivo* cartilage repair using adipose-derived stem cell-loaded decellularized cartilage ECM scaffolds: *In vivo* cartilage repair using ADSC-loaded decellularized cartilage ECM scaffolds. J Tissue Eng Regen Med 8, 442–453. https://doi.org/10.1002/term.1538

Kasaai, M.R., 2010. Determination of the degree of N-acetylation for chitin and chitosan by various NMR spectroscopy techniques: A review. Carbohydrate Polymers 79, 801–810. https://doi.org/10.1016/j.carbpol.2009.10.051

Kern, C.B., Twal, W.O., Mjaatvedt, C.H., Fairey, S.E., Toole, B.P., Iruela-Arispe, M.L., Argraves, W.S., 2006. Proteolytic cleavage of versican during cardiac cushion morphogenesis. Dev. Dyn. 235, 2238–2247. https://doi.org/10.1002/dvdy.20838

Khor, E., Lim, L.Y., 2003. Implantable applications of chitin and chitosan. Biomaterials 24, 2339–2349. https://doi.org/10.1016/S0142-9612(03)00026-7

Kim, M.H., Park, H., Nam, H.C., Park, S.R., Jung, J.-Y., Park, W.H., 2018. Injectable methylcellulose hydrogel containing silver oxide nanoparticles for burn wound healing. Carbohydrate Polymers 181, 579–586. https://doi.org/10.1016/j.carbpol.2017.11.109

Kim, S., Cui, Z.-K., Koo, B., Zheng, J., Aghaloo, T., Lee, M., 2018. Chitosan–Lysozyme Conjugates for Enzyme-Triggered Hydrogel Degradation in Tissue Engineering Applications. ACS Appl. Mater. Interfaces 10, 41138–41145. https://doi.org/10.1021/acsami.8b15591

Kim, S.-H., Turnbull, J., Guimond, S., 2011. Extracellular matrix and cell signalling: the dynamic cooperation of integrin, proteoglycan and growth factor receptor. Journal of Endocrinology 209, 139–151. https://doi.org/10.1530/JOE-10-0377

Kim, Y., Zharkinbekov, Z., Raziyeva, K., Tabyldiyeva, L., Berikova, K., Zhumagul, D., Temirkhanova, K., Saparov, A., 2023. Chitosan-Based Biomaterials for Tissue Regeneration. Pharmaceutics 15, 807. https://doi.org/10.3390/pharmaceutics15030807

Klawitter, J.J., Hulbert, S.F., 1971. Application of porous ceramics for the attachment of load bearing internal orthopedic applications. J. Biomed. Mater. Res. 5, 161–229. https://doi.org/10.1002/jbm.820050613

Konno, T., Ishihara, K., 2007. Temporal and spatially controllable cell encapsulation using a water-soluble phospholipid polymer with phenylboronic acid moiety. Biomaterials 28, 1770–1777. https://doi.org/10.1016/j.biomaterials.2006.12.017

Kraehenbuehl, T.P., Ferreira, L.S., Zammaretti, P., Hubbell, J.A., Langer, R., 2009. Cell-responsive hydrogel for encapsulation of vascular cells. Biomaterials 30, 4318–4324. https://doi.org/10.1016/j.biomaterials.2009.04.057

Kubota, N., Tatsumoto, N., Sano, T., Toya, K., 2000. A simple preparation of half N-acetylated chitosan highly soluble in water and aqueous organic solvents. Carbohydrate Research 324, 268–274. https://doi.org/10.1016/S0008-6215(99)00263-3

Kuo, C.K., Ma, P.X., 2001. Ionically crosslinked alginate hydrogels as scaffolds for tissue engineering: Part 1. Structure, gelation rate and mechanical properties. Biomaterials 22, 511–521. https://doi.org/10.1016/S0142-9612(00)00201-5

Lau, L.W., Cua, R., Keough, M.B., Haylock-Jacobs, S., Yong, V.W., 2013. Pathophysiology of the brain extracellular matrix: a new target for remyelination. Nat Rev Neurosci 14, 722–729. https://doi.org/10.1038/nrn3550

Lee, C.H., Singla, A., Lee, Y., 2001. Biomedical applications of collagen. International Journal of Pharmaceutics 221, 1–22. https://doi.org/10.1016/S0378-5173(01)00691-3

Lee, J., Lee, H., Andrade, J., 1995. Blood compatibility of polyethylene oxide surfaces. Progress in Polymer Science 20, 1043–1079. https://doi.org/10.1016/0079-6700(95)00011-4

Lee, K.Y., Kong, H.J., Larson, R.G., Mooney, D.J., 2003. Hydrogel Formation via Cell Crosslinking. Adv. Mater. 15, 1828–1832. https://doi.org/10.1002/adma.200305406

Lee, K.Y., Mooney, D.J., 2012. Alginate: Properties and biomedical applications. Progress in Polymer Science 37, 106–126. https://doi.org/10.1016/j.progpolymsci.2011.06.003

Lee, K.Y., Mooney, D.J., 2001. Hydrogels for Tissue Engineering. Chem. Rev. 101, 1869–1880. https://doi.org/10.1021/cr000108x

Lee, S., Valmikinathan, C.M., Byun, J., Kim, S., Lee, G., Mokarram, N., Pai, S.B., Um, E., Bellamkonda, R.V., Yoon, Y., 2015. Enhanced therapeutic neovascularization by CD31-expressing cells and embryonic stem cell-derived endothelial cells engineered with chitosan hydrogel containing VEGF-releasing microtubes. Biomaterials 63, 158–167. https://doi.org/10.1016/j.biomaterials.2015.06.009

Li, Y., Bober, P., Apaydin, D.H., Syrový, T., Sariciftci, N.S., Hromádková, J., Sapurina, I., Trchová, M., Stejskal, J., 2016. Colloids of polypyrrole nanotubes/nanorods: A promising conducting ink. Synthetic Metals 221, 67–74. https://doi.org/10.1016/j.synthmet.2016.10.007

Liang, C.-C., Park, A.Y., Guan, J.-L., 2007. In vitro scratch assay: a convenient and inexpensive method for analysis of cell migration in vitro. Nat Protoc 2, 329–333. https://doi.org/10.1038/nprot.2007.30

Liang, Y., Zhao, X., Ma, P.X., Guo, B., Du, Y., Han, X., 2019. pH-responsive injectable hydrogels with mucosal adhesiveness based on chitosan-grafted-dihydrocaffeic acid and oxidized pullulan for localized drug delivery. Journal of Colloid and Interface Science 536, 224–234. https://doi.org/10.1016/j.jcis.2018.10.056

Liu, H., Slamovich, E.B., Webster, T.J., 2006. Less harmful acidic degradation of poly(lactic-co-glycolic acid) bone tissue engineering scaffolds through titania nanoparticle addition. International Journal of Nanomedicine 1, 541–545. https://doi.org/10.2147/nano.2006.1.4.541

L-Mesitran [WWW Document], 2023. URL https://mesitran.com/

Lockhart, M., Wirrig, E., Phelps, A., Wessels, A., 2011. Extracellular matrix and heart development. Birth Defects Research Part A: Clinical and Molecular Teratology 91, 535–550. https://doi.org/10.1002/bdra.20810

Lu, Y., Wang, Yanan, Zhang, J., Hu, X., Yang, Z., Guo, Y., Wang, Yunbing, 2019. In-situ doping of a conductive hydrogel with low protein absorption and bacterial adhesion for electrical stimulation of chronic wounds. Acta Biomaterialia 89, 217–226. https://doi.org/10.1016/j.actbio.2019.03.018

Luong, H., Singh, S., Patil, M., Krishnamurthy, P., 2021. Cardiac glycosaminoglycans and structural alterations during chronic stress-induced depression-like behavior in mice. American Journal of Physiology-Heart and Circulatory Physiology 320, H2044–H2057. https://doi.org/10.1152/ajpheart.00635.2020

Lutolf, M.P., Hubbell, J.A., 2005. Synthetic biomaterials as instructive extracellular microenvironments for morphogenesis in tissue engineering. Nat Biotechnol 23, 47–55. https://doi.org/10.1038/nbt1055

Maccarone, T.J., Eijnden, J. van den, Russell, T.D., Degenaar, N., 2020. Eclipses of jets and discs of X-ray binaries as a powerful tool for understanding jet physics and binary parameters. Monthly Notices of the Royal Astronomical Society 499, 957–973. https://doi.org/10.1093/mnras/staa2674

Madihally, S.V., Matthew, H.W.T., 1999. Porous chitosan scaffolds for tissue engineering. Biomaterials 20, 1133–1142. https://doi.org/10.1016/S0142-9612(99)00011-3

Maitra, J., Shukla, V.K., 2014. Cross-linking in Hydrogels - A Review. American Journal of Polymer Science 4, 25–31. https://doi.org/10.5923/j.ajps.20140402.01

Maleki, A., Kjøniksen, A.-L., Nyström, B., 2008. Effect of pH on the Behavior of Hyaluronic Acid in Dilute and Semidilute Aqueous Solutions. Macromol. Symp. 274, 131–140. https://doi.org/10.1002/masy.200851418

Mantha, S., Pillai, S., Khayambashi, P., Upadhyay, A., Zhang, Y., Tao, O., Pham, H.M., Tran, S.D., 2019. Smart Hydrogels in Tissue Engineering and Regenerative Medicine. Materials 12, 3323. https://doi.org/10.3390/ma12203323

Massia, S.P., Hubbell, J.A., 1991. An RGD spacing of 440 nm is sufficient for integrin alpha V beta 3-mediated fibroblast spreading and 140 nm for focal contact and stress fiber formation. Journal of Cell Biology 114, 1089–1100. https://doi.org/10.1083/jcb.114.5.1089

Middleton, J.C., Tipton, A.J., 2000. Synthetic biodegradable polymers as orthopedic devices. Biomaterials 21, 2335–2346. https://doi.org/10.1016/S0142-9612(00)00101-0

Milner, R., Campbell, I.L., 2002. The integrin family of cell adhesion molecules has multiple functions within the CNS. J. Neurosci. Res. 69, 286–291. https://doi.org/10.1002/jnr.10321

Mohd Zohdi, R., Abu Bakar Zakaria, Z., Yusof, N., Mohamed Mustapha, N., Abdullah, M.N.H., 2012. Gelam (*Melaleuca* spp.) Honey-Based Hydrogel as Burn Wound Dressing. Evidence-Based Complementary and Alternative Medicine 2012, 1–7. https://doi.org/10.1155/2012/843025

Mouw, J.K., Ou, G., Weaver, V.M., 2014. Extracellular matrix assembly: a multiscale deconstruction. Nat Rev Mol Cell Biol 15, 771–785. https://doi.org/10.1038/nrm3902

Muchová, M., Münster, L., Capáková, Z., Mikulcová, V., Kuřitka, I., Vícha, J., 2020. Design of dialdehyde cellulose crosslinked poly(vinyl alcohol) hydrogels for transdermal drug delivery and wound dressings. Materials Science and Engineering: C 116, 111242. https://doi.org/10.1016/j.msec.2020.111242

Münster, L., Vícha, J., Klofáč, J., Masař, M., Hurajová, A., Kuřitka, I., 2018. Dialdehyde cellulose crosslinked poly(vinyl alcohol) hydrogels: Influence of catalyst and crosslinker shelf life. Carbohydrate Polymers 198, 181–190. https://doi.org/10.1016/j.carbpol.2018.06.035

Münster, L., Vícha, J., Klofáč, J., Masař, M., Kucharczyk, P., Kuřitka, I., 2017. Stability and aging of solubilized dialdehyde cellulose. Cellulose 24, 2753–2766. https://doi.org/10.1007/s10570-017-1314-x

Naahidi, S., Jafari, M., Logan, M., Wang, Y., Yuan, Y., Bae, H., Dixon, B., Chen, P., 2017. Biocompatibility of hydrogel-based scaffolds for tissue engineering applications. Biotechnology Advances 35, 530–544. https://doi.org/10.1016/j.biotechadv.2017.05.006

Neff, J., 1999. Surface modification for controlled studies of cell–ligand interactions. Biomaterials 20, 2377–2393. https://doi.org/10.1016/S0142-9612(99)00166-0

Nerem, R.M., 1991. Cellular engineering. Ann Biomed Eng 19, 529–545. https://doi.org/10.1007/BF02367396

Nho, Y., Kim, Y., Lim, Y., 2007. Therapeutic hydrogel for atopic dermatitis and preparation method thereof. EP1889608B1.

Nuttelman, C.R., Mortisen, D.J., Henry, S.M., Anseth, K.S., 2001. Attachment of fibronectin to poly(vinyl alcohol) hydrogels promotes NIH3T3 cell adhesion, proliferation, and migration. J Biomed Mater Res 57, 217–223. https://doi.org/10.1002/1097-4636(200111)57:2<217::aid-jbm1161>3.0.co;2-i

O'Brien, F.J., 2011. Biomaterials & scaffolds for tissue engineering. Materials Today 14, 88–95. https://doi.org/10.1016/S1369-7021(11)70058-X

Ocular TherapeutixTM [WWW Document], 2021. URL https://www.ocutx.com/

Oda, H., Konno, T., Ishihara, K., 2015. Efficient differentiation of stem cells encapsulated in a cytocompatible phospholipid polymer hydrogel with tunable physical properties. Biomaterials 56, 86–91. https://doi.org/10.1016/j.biomaterials.2015.03.051

OECD, 2021. Test No. 439: In Vitro Skin Irritation: Reconstructed Human Epidermis Test Method, OECD Guidelines for the Testing of Chemicals, Section 4. OECD. https://doi.org/10.1787/9789264242845-en

Ono, K., Saito, Y., Yura, H., Ishikawa, K., Kurita, A., Akaike, T., Ishihara, M., 2000. Photocrosslinkable chitosan as a biological adhesive. J Biomed Mater Res 49, 289–295. https://doi.org/10.1002/(sici)1097-4636(200002)49:2<289::aid-jbm18>3.0.co;2-m

Ostuni, E., Chapman, R.G., Holmlin, R.E., Takayama, S., Whitesides, G.M., 2001. A Survey of Structure−Property Relationships of Surfaces that Resist the Adsorption of Protein. Langmuir 17, 5605–5620. https://doi.org/10.1021/la010384m

Oyama, T., 2014. Cross-Linked Polymer Synthesis, in: Kobayashi, S., Müllen, K. (Eds.), Encyclopedia of Polymeric Nanomaterials. Springer Berlin Heidelberg, Berlin, Heidelberg, pp. 1–11. https://doi.org/10.1007/978-3-642-36199-9_181-1

Panduranga Rao, K., 1996. Recent developments of collagen-based materials for medical applications and drug delivery systems. Journal of Biomaterials Science, Polymer Edition 7, 623–645. https://doi.org/10.1163/156856295X00526

Peppas, N., 2000. Hydrogels in pharmaceutical formulations. European Journal of Pharmaceutics and Biopharmaceutics 50, 27–46. https://doi.org/10.1016/S0939-6411(00)00090-4

Pina, S., Ribeiro, V.P., Marques, C.F., Maia, F.R., Silva, T.H., Reis, R.L., Oliveira, J.M., 2019. Scaffolding Strategies for Tissue Engineering and Regenerative Medicine Applications. Materials 12, 1824. https://doi.org/10.3390/ma12111824

Portero, A., Teijeiro-Osorio, D., Alonso, M.J., Remuñán-López, C., 2007. Development of chitosan sponges for buccal administration of insulin. Carbohydrate Polymers 68, 617–625. https://doi.org/10.1016/j.carbpol.2006.07.028

Przekora, A., Ginalska, G., 2014. Addition of 1,3-β-d-glucan to chitosan-based composites enhances osteoblast adhesion, growth, and proliferation. International Journal of Biological Macromolecules 70, 474–481. https://doi.org/10.1016/j.ijbiomac.2014.07.035

Qin, C., Li, H., Xiao, Q., Liu, Y., Zhu, J., Du, Y., 2006. Water-solubility of chitosan and its antimicrobial activity. Carbohydrate Polymers 63, 367–374. https://doi.org/10.1016/j.carbpol.2005.09.023

Quirk, R.A., France, R.M., Shakesheff, K.M., Howdle, S.M., 2004. Supercritical fluid technologies and tissue engineering scaffolds. Current Opinion in Solid State and Materials Science 8, 313–321. https://doi.org/10.1016/j.cossms.2003.12.004

Ratner, B.D., 2013. Biomaterials science: an introduction to materials in medicine. Academic Press, Place of publication not identified.

Raval, N., Maheshwari, R., Kalyane, D., Youngren-Ortiz, S.R., Chougule, M.B., Tekade, R.K., 2019. Importance of Physicochemical Characterization of Nanoparticles in Pharmaceutical Product Development, in: Basic Fundamentals of Drug Delivery. Elsevier, pp. 369–400. https://doi.org/10.1016/B978-0-12-817909-3.00010-8

Ren, Y., Zhang, H., Wang, Y., Du, B., Yang, J., Liu, L., Zhang, Q., 2021. Hyaluronic Acid Hydrogel with Adjustable Stiffness for Mesenchymal Stem Cell 3D Culture via Related Molecular Mechanisms to Maintain Stemness and Induce Cartilage Differentiation. ACS Appl. Bio Mater. 4, 2601–2613. https://doi.org/10.1021/acsabm.0c01591

Riss, T.L., Moravec, R.A., Niles, A.L., Duellman, S., Benink, H.A., Worzella, T.J., Minor, L., 2004. Cell Viability Assays, in: Markossian, S., Grossman, A., Brimacombe, K., Arkin, M., Auld, D., Austin, C.P., Baell, J., Chung, T.D.Y., Coussens, N.P., Dahlin, J.L., Devanarayan, V., Foley, T.L., Glicksman, M., Hall, M.D., Haas, J.V., Hoare, S.R.J., Inglese, J., Iversen, P.W., Kales, S.C., Lal-Nag, M., Li, Z., McGee, J., McManus, O., Riss, T., Saradjian, P., Sittampalam, G.S., Tarselli, M., Trask, O.J., Wang, Y., Weidner, J.R., Wildey, M.J., Wilson, K., Xia, M., Xu, X. (Eds.), Assay Guidance Manual. Eli Lilly & Company and the National Center for Advancing Translational Sciences, Bethesda (MD).

Rodriguez, A.-M., Elabd, C., Amri, E.-Z., Ailhaud, G., Dani, C., 2005. The human adipose tissue is a source of multipotent stem cells. Biochimie 87, 125–128. https://doi.org/10.1016/j.biochi.2004.11.007

Roy, I., Gupta, M.N., 2003. Smart Polymeric Materials. Chemistry & Biology 10, 1161–1171. https://doi.org/10.1016/j.chembiol.2003.12.004

Sahoo, D.R., Biswal, T., 2021. Alginate and its application to tissue engineering. SN Appl. Sci. 3, 30. https://doi.org/10.1007/s42452-020-04096-w

Saltzman, W.M., 2004. Tissue engineering: engineering principles for the design of replacement organs and tissues. Oxford University Press, Oxford ; New York.

Sayyah, S.M., Mohamed, F., Shaban, M., 2014. Antibacterial activity of nano fabricated polypyrrole by cyclic voltammetry. IOSRJAC 7, 11–15. https://doi.org/10.9790/5736-07211115

Schense, J.C., Bloch, J., Aebischer, P., Hubbell, J.A., 2000. Enzymatic incorporation of bioactive peptides into fibrin matrices enhances neurite extension. Nat Biotechnol 18, 415–419. https://doi.org/10.1038/74473

Shi, C., Zhu, Y., Ran, X., Wang, M., Su, Y., Cheng, T., 2006. Therapeutic Potential of Chitosan and Its Derivatives in Regenerative Medicine. Journal of Surgical Research 133, 185–192. https://doi.org/10.1016/j.jss.2005.12.013

Shi, Y., Xiong, D., Liu, Y., Wang, N., Zhao, X., 2016. Swelling, mechanical and friction properties of PVA/PVP hydrogels after swelling in osmotic pressure solution. Materials Science and Engineering: C 65, 172–180. https://doi.org/10.1016/j.msec.2016.04.042

Shin, H., Jo, S., Mikos, A.G., 2003. Biomimetic materials for tissue engineering. Biomaterials 24, 4353–4364. https://doi.org/10.1016/S0142-9612(03)00339-9

Shin, J., Choi, E.J., Cho, J.H., Cho, A.-N., Jin, Y., Yang, K., Song, C., Cho, S.-W., 2017. Three-Dimensional Electroconductive Hyaluronic Acid Hydrogels Incorporated with Carbon Nanotubes and Polypyrrole by Catechol-Mediated Dispersion Enhance Neurogenesis of Human Neural Stem Cells. Biomacromolecules 18, 3060–3072. https://doi.org/10.1021/acs.biomac.7b00568

Shin, J., Choi, S., Kim, J.H., Cho, J.H., Jin, Y., Kim, S., Min, S., Kim, S.K., Choi, D., Cho, S., 2019. Tissue Tapes—Phenolic Hyaluronic Acid Hydrogel Patches for Off-the-Shelf Therapy. Adv. Funct. Mater. 29, 1903863. https://doi.org/10.1002/adfm.201903863

Shirwaiker, R.A., Purser, M.F., Wysk, R.A., 2014. Scaffolding hydrogels for rapid prototyping based tissue engineering, in: Rapid Prototyping of Biomaterials. Elsevier, pp. 176–200. https://doi.org/10.1533/9780857097217.176

Silva, A.K.A., Richard, C., Bessodes, M., Scherman, D., Merten, O.-W., 2009. Growth Factor Delivery Approaches in Hydrogels. Biomacromolecules 10, 9–18. https://doi.org/10.1021/bm801103c

Singh, B., Sharma, S., Dhiman, A., 2017. Acacia gum polysaccharide based hydrogel wound dressings: Synthesis, characterization, drug delivery and biomedical properties. Carbohydrate Polymers 165, 294–303. https://doi.org/10.1016/j.carbpol.2017.02.039

Singh, M.R., Patel, S., Singh, D., 2016. Natural polymer-based hydrogels as scaffolds for tissue engineering, in: Nanobiomaterials in Soft Tissue Engineering. Elsevier, pp. 231–260. https://doi.org/10.1016/B978-0-323-42865-1.00009-X

Singh, S.R., 2009. Principles of Regenerative Medicine: Edited by Anthony Atala, Robert Lanza, James Thompson and Robert Nerem, Academic Press, an imprint of Elsevier Inc., 2008, Hardcover, pp. 1448, ISBN: 978-0-12-369410-2. Ann Biomed Eng 37, 2658–2659. https://doi.org/10.1007/s10439-009-9817-8

Slaughter, B.V., Khurshid, S.S., Fisher, O.Z., Khademhosseini, A., Peppas, N.A., 2009. Hydrogels in Regenerative Medicine. Adv. Mater. 21, 3307–3329. https://doi.org/10.1002/adma.200802106

Spicer, C.D., 2020. Hydrogel scaffolds for tissue engineering: the importance of polymer choice. Polym. Chem. 11, 184–219. https://doi.org/10.1039/C9PY01021A

Stern, R., Kogan, G., Jedrzejas, M.J., Šoltés, L., 2007. The many ways to cleave hyaluronan. Biotechnology Advances 25, 537–557. https://doi.org/10.1016/j.biotechadv.2007.07.001

Stevens, K.R., Einerson, N.J., Burmania, J.A., Kao, W.J., 2002. In vivo biocompatibility of gelatin-based hydrogels and interpenetrating networks. Journal of Biomaterials Science, Polymer Edition 13, 1353–1366. https://doi.org/10.1163/15685620260449741

Stokols, S., Tuszynski, M.H., 2004. The fabrication and characterization of linearly oriented nerve guidance scaffolds for spinal cord injury. Biomaterials 25, 5839–5846. https://doi.org/10.1016/j.biomaterials.2004.01.041

Su, J., Li, Jiankang, Liang, J., Zhang, K., Li, Jingan, 2021. Hydrogel Preparation Methods and Biomaterials for Wound Dressing. Life 11, 1016. https://doi.org/10.3390/life11101016

Suprasorb®G [WWW Document], 2023. URL https://www.lohmann-rauscher.com/en/

SUPREME PHARMATECH, CO., LTD. [WWW Document], 2021. URL https://supremepharmatech.com/

Svensson, L., Oldberg, Å., Heinegård, D., 2001. Collagen binding proteins. Osteoarthritis and Cartilage 9, S23–S28. https://doi.org/10.1053/joca.2001.0440

Talikowska, M., Fu, X., Lisak, G., 2019. Application of conducting polymers to wound care and skin tissue engineering: A review. Biosensors and Bioelectronics 135, 50–63. https://doi.org/10.1016/j.bios.2019.04.001

Tamura, H., Furuike, T., Nair, S.V., Jayakumar, R., 2011. Biomedical applications of chitin hydrogel membranes and scaffolds. Carbohydrate Polymers 84, 820–824. https://doi.org/10.1016/j.carbpol.2010.06.001

Thomsen, M.S., Routhe, L.J., Moos, T., 2017. The vascular basement membrane in the healthy and pathological brain. J Cereb Blood Flow Metab 37, 3300–3317. https://doi.org/10.1177/0271678X17722436

Thrivikraman, G., Madras, G., Basu, B., 2014. Intermittent electrical stimuli for guidance of human mesenchymal stem cell lineage commitment towards neural-like cells on electroconductive substrates. Biomaterials 35, 6219–6235. https://doi.org/10.1016/j.biomaterials.2014.04.018

Tian, R., Chen, J., Niu, R., 2014. The development of low-molecular weight hydrogels for applications in cancer therapy. Nanoscale 6, 3474. https://doi.org/10.1039/c3nr05414d

Tibbitt, M.W., Anseth, K.S., 2009. Hydrogels as extracellular matrix mimics for 3D cell culture. Biotechnol. Bioeng. 103, 655–663. https://doi.org/10.1002/bit.22361

Tsou, Y.-H., Khoneisser, J., Huang, P.-C., Xu, X., 2016. Hydrogel as a bioactive material to regulate stem cell fate. Bioactive Materials 1, 39–55. https://doi.org/10.1016/j.bioactmat.2016.05.001

Tu, Z., Zhong, Y., Hu, H., Shao, D., Haag, R., Schirner, M., Lee, J., Sullenger, B., Leong, K.W., 2022. Design of therapeutic biomaterials to control inflammation. Nat Rev Mater 7, 557–574. https://doi.org/10.1038/s41578-022-00426-z

Upadhyay, J., Kumar, A., Gogoi, B., Buragohain, A.K., 2014. Biocompatibility and antioxidant activity of polypyrrole nanotubes. Synthetic Metals 189, 119–125. https://doi.org/10.1016/j.synthmet.2014.01.004

Vaitkuviene, A., Kaseta, V., Voronovic, J., Ramanauskaite, G., Biziuleviciene, G., Ramanaviciene, A., Ramanavicius, A., 2013. Evaluation of cytotoxicity of polypyrrole nanoparticles synthesized by oxidative polymerization. Journal of Hazardous Materials 250–251, 167–174. https://doi.org/10.1016/j.jhazmat.2013.01.038

Varesano, A., Vineis, C., Aluigi, A., Rombaldoni, F., Tonetti, C., Mazzuchetti, G., 2013. Antibacterial efficacy of polypyrrole in textile applications. Fibers Polym 14, 36–42. https://doi.org/10.1007/s12221-013-0036-4

Vashist, Arti, Vashist, Atul, Gupta, Y.K., Ahmad, S., 2014. Recent advances in hydrogel based drug delivery systems for the human body. J. Mater. Chem. B 2, 147–166. https://doi.org/10.1039/C3TB21016B

Vella, F., 1994. Molecular biology of the cell (third edition). Biochemical Education 22, 164. https://doi.org/10.1016/0307-4412(94)90059-0

Velnar, T., Bailey, T., Smrkolj, V., 2009. The Wound Healing Process: An Overview of the Cellular and Molecular Mechanisms. J Int Med Res 37, 1528–1542. https://doi.org/10.1177/147323000903700531

Vercruysse, K.P., Marecak, D.M., Marecek, J.F., Prestwich, G.D., 1997. Synthesis and *in Vitro* Degradation of New Polyvalent Hydrazide Cross-Linked Hydrogels of Hyaluronic Acid. Bioconjugate Chem. 8, 686–694. https://doi.org/10.1021/bc9701095

Walimbe, T., Panitch, A., Sivasankar, P.M., 2017. A Review of Hyaluronic Acid and Hyaluronic Acid-based Hydrogels for Vocal Fold Tissue Engineering. Journal of Voice 31, 416–423. https://doi.org/10.1016/j.jvoice.2016.11.014

Wang, P.-H., Huang, B.-S., Horng, H.-C., Yeh, C.-C., Chen, Y.-J., 2018. Wound healing. Journal of the Chinese Medical Association 81, 94–101. https://doi.org/10.1016/j.jcma.2017.11.002

Wang, Q.Z., Chen, X.G., Liu, N., Wang, S.X., Liu, C.S., Meng, X.H., Liu, C.G., 2006. Protonation constants of chitosan with different molecular weight and degree of

deacetylation. Carbohydrate Polymers 65, 194–201. https://doi.org/10.1016/j.carbpol.2006.01.001

Wang, X., Gu, X., Yuan, C., Chen, S., Zhang, P., Zhang, T., Yao, J., Chen, F., Chen, G., 2004. Evaluation of biocompatibility of polypyrrolein vitro andin vivo. J. Biomed. Mater. Res. 68A, 411–422. https://doi.org/10.1002/jbm.a.20065

Ward, P.D., Thibeault, S.L., Gray, S.D., 2002. Hyaluronic Acid. Journal of Voice 16, 303–309. https://doi.org/10.1016/S0892-1997(02)00101-7

Weadock, K.S., Miller, E.J., Bellincampi, L.D., Zawadsky, J.P., Dunn, M.G., 1995. Physical crosslinking of collagen fibers: Comparison of ultraviolet irradiation and dehydrothermal treatment. J. Biomed. Mater. Res. 29, 1373–1379. https://doi.org/10.1002/jbm.820291108

Weng, B., Shepherd, R., Chen, J., Wallace, G.G., 2011. Gemini surfactant doped polypyrrole nanodispersions: an inkjet printable formulation. J. Mater. Chem. 21, 1918–1924. https://doi.org/10.1039/C0JM02595J

Wichterle, O., Lím, D., 1960. Hydrophilic Gels for Biological Use. Nature 185, 117–118. https://doi.org/10.1038/185117a0

Williams, D.F., 2018. Biocompatibility Pathways in Tissue-Engineering Templates. Engineering 4, 286–290. https://doi.org/10.1016/j.eng.2018.03.007

Williams, D.F., 2014. There is no such thing as a biocompatible material. Biomaterials 35, 10009–10014. https://doi.org/10.1016/j.biomaterials.2014.08.035

Williams, D.F., 1999. The Williams dictionary of biomaterials.

Wolf, K., Alexander, S., Schacht, V., Coussens, L.M., von Andrian, U.H., van Rheenen, J., Deryugina, E., Friedl, P., 2009. Collagen-based cell migration models in vitro and in vivo. Seminars in Cell & Developmental Biology 20, 931–941. https://doi.org/10.1016/j.semcdb.2009.08.005

Xavier, J.R., Thakur, T., Desai, P., Jaiswal, M.K., Sears, N., Cosgriff-Hernandez, E., Kaunas, R., Gaharwar, A.K., 2015. Bioactive Nanoengineered Hydrogels for Bone Tissue Engineering: A Growth-Factor-Free Approach. ACS Nano 9, 3109–3118. https://doi.org/10.1021/nn507488s

Xu, X., Jha, A.K., Harrington, D.A., Farach-Carson, M.C., Jia, X., 2012. Hyaluronic acid-based hydrogels: from a natural polysaccharide to complex networks. Soft Matter 8, 3280. https://doi.org/10.1039/c2sm06463d

Xu, Z., Han, S., Gu, Z., Wu, J., 2020. Advances and Impact of Antioxidant Hydrogel in Chronic Wound Healing. Adv. Healthcare Mater. 9, 1901502. https://doi.org/10.1002/adhm.201901502

Yang, J., Choe, G., Yang, S., Jo, H., Lee, J.Y., 2016. Polypyrrole-incorporated conductive hyaluronic acid hydrogels. Biomater Res 20, 31. https://doi.org/10.1186/s40824-016-0078-y

Yang, S., Leong, K.-F., Du, Z., Chua, C.-K., 2001. The Design of Scaffolds for Use in Tissue Engineering. Part I. Traditional Factors. Tissue Engineering 7, 679–689. https://doi.org/10.1089/107632701753337645

Yannas, I.V., Lee, E., Orgill, D.P., Skrabut, E.M., Murphy, G.F., 1989. Synthesis and characterization of a model extracellular matrix that induces partial regeneration of adult mammalian skin. Proceedings of the National Academy of Sciences 86, 933–937. https://doi.org/10.1073/pnas.86.3.933

Yu, Q., Zhang, C., Jiang, Z., Qin, S., Zhang, A., 2020. Mussel-Inspired Adhesive Polydopamine-Functionalized Hyaluronic Acid Hydrogel with Potential Bacterial Inhibition. Global Challenges 4, 1900068. https://doi.org/10.1002/gch2.201900068

Zakrzewski, W., Dobrzyński, M., Szymonowicz, M., Rybak, Z., 2019. Stem cells: past, present, and future. Stem Cell Res Ther 10, 68. https://doi.org/10.1186/s13287-019-1165-5

Zhao, L., Weir, M.D., Xu, H.H.K., 2010. An injectable calcium phosphate-alginate hydrogel-umbilical cord mesenchymal stem cell paste for bone tissue engineering. Biomaterials 31, 6502–6510. https://doi.org/10.1016/j.biomaterials.2010.05.017

Zhao, X., Kato, K., Fukumoto, Y., Nakamae, K., 2001. Synthesis of bioadhesive hydrogels from chitin derivatives. International Journal of Adhesion and Adhesives 21, 227–232. https://doi.org/10.1016/S0143-7496(01)00003-3

Zhao, X., Wu, H., Guo, B., Dong, R., Qiu, Y., Ma, P.X., 2017. Antibacterial anti-oxidant electroactive injectable hydrogel as self-healing wound dressing with hemostasis and adhesiveness for cutaneous wound healing. Biomaterials 122, 34–47. https://doi.org/10.1016/j.biomaterials.2017.01.011

Zhu, J., 2010. Bioactive modification of poly(ethylene glycol) hydrogels for tissue engineering. Biomaterials 31, 4639–4656. https://doi.org/10.1016/j.biomaterials.2010.02.044

Zhu, J., Marchant, R.E., 2011. Design properties of hydrogel tissue-engineering scaffolds. Expert Review of Medical Devices 8, 607–626. https://doi.org/10.1586/erd.11.27

Zong, C., Qian, X., Tang, Z., Hu, Q., Chen, J., Gao, C., Tang, R., Tong, X., Wang, J., 2014. Biocompatibility and Bone-Repairing Effects: Comparison Between Porous Poly-Lactic-Co-Glycolic Acid and Nano-Hydroxyapatite/Poly(lactic acid) Scaffolds. Journal of Biomedical Nanotechnology 10, 1091–1104. https://doi.org/10.1166/jbn.2014.1696

LIST OF FIGURES

LIST OF ABBREVIATIONS AND SYMBOLS

Alphabetically ordered

2D	Two-dimensional
3D	Three-dimensional
ADH	Adipic acid dihydrazide
BM	Basement membrane
BMSCs	Bone marrow mesenchymal stem cells
CNS	Central nervous system
CPs	Conductive polymers
CNTs	Carbon nanotubes
CSA·HCl	Cysteamine hydrochloride
DAC	Dialdehyde cellulose
ECM	Extracellular matrix
c-ECM	Cardiac extracellular matrix
n-ECM	Neural extracellular matrix
EDCl	1-Ethyl-3-(3-dimethylaminopropyl)carbodiimide hydrochloride
FDA	Food and Drug Administration
GAGs	Glucosaminoglycans
GF	Growth factors
GSH	Glutathione
HA	Hyaluronic acid
HA-SH	Thiolated hyaluronic acid
IKVAV	Ile-Lys-Val-Ala-Val
IL-6	Interleukin 6

iPSC	Induced pluripotent stem cells
MAAM	N-allylmethylamine
MSCs	Mesenchymal stem cells
MTT	3-(4,5-dimethylthiazol-2-yl)-2,5-diphenyltetrazolium bromide
NHS	N-hydroxysuccinimide
NO	Nitric oxide
NSCs	Neural stem cells
OZP	Opsonized zymosan particles
PANI	Polyaniline
PDI	Polydispersity index
PEG	Poly(ethylene glycol)
PEO	Poly(ethylene oxide)
PET	Poly(ethylene terephthalate)
PGA	Poly(glycolic acid)
PLA	Polylactide
PLGA	Poly(lactide-*co*-glycolide)
PNS	Peripheral nervous system
PPy	Polypyrrole
PVA	Poly(vinyl alcohol)
PVP	Polyvinylpyrrolidon
RGD	Tripeptide Arg-Gly-Asp
RM	Regenerative medicine
ROS	Reactive oxygen species
SC	Stem cells

SCN	Soluble chitosan
SIT	Small intestine tissue
TE	Tissue engineering
TRPV4	Transient receptor potential vanilloid 4
UPW	Ultrapure water
YIGSR	Tyr-Ile-Gly-Ser-Arg

LIST OF PUBLICATIONS

Articles published in journals indexed on Web of Science:

Jasenská, D., Kašpárková, V., Vašíček, O., Münster, L., Minařík, A., **Káčerová, S.**, Korábková, E., Urbánková, L., Vícha, J., Capáková, Z., Falleta, E., Della Pina, C., Lehocký, M., Skopalová, K., Humpolíček, P., 2022. Enzyme-Catalyzed Polymerization Process: A Novel Approach to the Preparation of Polyaniline Colloidal Dispersions with an Immunomodulatory Effect. Biomacromolecules 23, 3359–3370. https://doi.org/10.1021/acs.biomac.2c00371

Martínková, M., Hausnerová, B., Huba, J., Martínek, T., **Káčerová, S.**, Kašpárková, V., Humpolíček, P., 2022. Powder injection molded ceramic scaffolds: The role of pores size and surface functionalization on the cytocompatibility. Materials & Design 224, 111274. https://doi.org/10.1016/j.matdes.2022.111274

Münster, L., Fojtů, M., Muchová, M., Latečka, F., **Káčerová, S.**, Capáková, Z., Juriňáková, T., Kuřitka, I., Masařík, M., Vícha, J., 2021. Enhancing cisplatin anticancer effectivity and migrastatic potential by modulation of molecular weight of oxidized dextran carrier. Carbohydrate Polymers 272, 118461. https://doi.org/10.1016/j.carbpol.2021.118461

Štěpánková, K., Ozaltin, K., Pelková, J., Pištěková, H., Karakurt, I., **Káčerová, S.**, Lehocky, M., Humpolicek, P., Vesel, A., Mozetic, M., 2022. Furcellaran Surface Deposition and Its Potential in Biomedical Applications. IJMS 23, 7439. https://doi.org/10.3390/ijms23137439

Articles ready for submission to the editors of international journals with an impact factor:

Káčerová S., Valášková K., Humpolíček P., Vícha J., Vašíček O., Kašpárková V., Víchová Z. Biocompatibility of polypyrrole based colloidal dispersions

Káčerová S., Muchová M., Doudová H., Münster L., Hanulíková B., Víchová Z., Valášková K., Kašpárková V., Kuřitka I., Humpolíček P., Vašíček O., Vícha J. Antibacterial, anti-oxidant, conductive, and anti-inflammatory polypyrrole/chitosan/dialdehyde cellulose hydrogel wound dressings

CURRICULUM VITAE

Personal information

Simona Káčerová, Ing.

Address: Lidečko 26, 75615 (Czech Republic)

Contact: s_kacerova@utb.cz

Sex: Female | Date of birth: 10/3/94 | Nationality: Czech

Education

2019 – present
Doctoral degree
Centre of polymer systems, Tomas Bata University in Zlin (Czech Republic)
Biomaterials and Biocomposites

2017 – 2019
Master´s degree
Faculty of Technology, Tomas Bata University in Zlin (Czech Republic)
Chemistry of Food and Bioactive Compounds

2014 – 2017
Bachelor´s degree
Faculty of Technology, Tomas Bata University in Zlin (Czech Republic)
Chemistry and Food Technology

Education stays

November 2022
MatTek in vitro life science laboratories, Bratislava, Slovakia; Practical training course on In vitro skin irritation test according to the OECD TG 439 using reconstructed human epidermis model Epiderm (EPI-200) in order to receive a certificate

April – June 2022
CICECO – Aveiro Institute od Materials, Aveiro, Portugal traineeship – Preparation of microneedle patches based on polysaccharides

November 2021
Institute of Biophysics of the Czech Academy of Sciences, Brno, Czech Republic; Trainship focused on the isolation of mouse intestinal crypts

---

Work on projects

2023
Project IGA/CPS/2023/001, Development of advanced biomaterials and their future application
Member of the project team

2022
Project IGA/CPS/2022/001, Preparation of advanced biomaterials and their application
Member of the project team

2022 April – May
Project RP/CPS/2022/001
Member of the project team

2021 – 2023
Project Jung-2020-001, Smart biomaterials based on conducting polymers
Member of the project team

2021
Project IGA/CPS/2021/001, Biocompatibility of materials
Investigator

2020
Project IGA/CPS/2020/001, Biocompatibility and antimicrobial activity of materials
Member of the project team

2020
Project GAČR 20-28732S, Colloidal systems for topical formulations. Pickering emulsions and polymer-based colloids.
Member of the project team

2019
Project IGA/CPS/2019/004, Biological properties of materials
Member of the project team

2019
Project GAČR 19-16861S, Interactions between materials and stem cells in simulated *in vivo* conditions
Member of the project team

Pedagogic activities	Participation in teaching laboratory classes of Laboratory of cellular biology and genetics

Mentoring the bachelor thesis:

Hydrogel based on hyaluronic acid and their biological properties

Preparation and characterization of hydrogels

ARTICLE I

Münster L., Fojtů M., Muchová M, Latečka F., **Káčerová S.**, Capáková Z., Juriňáková T., Kuřitka I., Masařík M., Vícha J. Enhancing cisplatin anticancer effectivity and migrastatic potential by modulation of molecular weight of oxidized dextran carrier. Carbohydrate Polymers. 2021, 272, 118461. Doi: 10.1016/j.carbpol.2021.118461

Carbohydrate Polymers 272 (2021) 118461

Contents lists available at ScienceDirect

Carbohydrate Polymers

journal homepage: www.elsevier.com/locate/carbpol

Enhancing cisplatin anticancer effectivity and migrastatic potential by modulation of molecular weight of oxidized dextran carrier

L. Münster [a], M. Fojtů [b,c,d], M. Muchová [a], F. Latečka [a], S. Káčerová [a], Z. Capáková [a], T. Juriňáková [b,d], I. Kuřitka [a], M. Masařík [b,c,d,e,*], J. Vícha [a,**]

[a] Centre of Polymer Systems, Tomas Bata University in Zlín, tř. Tomáše Bati 5678, CZ-760 01 Zlín, Czech Republic
[b] Department of Physiology, Faculty of Medicine, Masaryk University, Kamenice 5, CZ-625 00, Brno, Czech Republic
[c] Center for Advanced Functional Nanorobots, Department of Inorganic Chemistry, Faculty of Chemical Technology, University of Chemistry and Technology in Prague, Technická 5, Prague CZ-166 28, Czech Republic
[d] Department of Pathological Physiology, Faculty of Medicine, Masaryk University, Kamenice 5, CZ-625 00 Brno, Czech Republic
[e] BIOCEV, First Faculty of Medicine, Charles University, Průmyslová 595, 252 50, Vestec, Czech Republic

ARTICLE INFO

Keywords:
Drug-delivery
Dextran
Periodate oxidation
Molecular weight
Cisplatin
Carrier

ABSTRACT

The molecular weight (M_w) of dextran derivatives, such as regioselectively oxidized dicarboxydextran (DXA), is greatly influencing their faith in an organism, which could be possibly used to improve anticancer drug delivery. Here we present a modified method of sulfonation-induced chain scission allowing direct and accurate control over the M_w of DXA without increasing its polydispersity. Prepared DXA derivatives (M_w = 10–185 kDa) have been conjugated to cisplatin and the M_w of the carrier found to have a significant impact on cisplatin release rates, *in vitro* cytotoxicity, and migrastatic potential. Conjugates with the high-M_w DXA showed particularly increased anticancer efficacy. The best conjugate was four times more effective against malignant prostatic cell lines than free cisplatin and significantly inhibited the ovarian cancer cell migration. This was traced to the characteristics of spontaneously formed cisplatin-crosslinked DXA nanogels influenced by M_w of DXA and amount of loaded cisplatin.

1. Introduction

Over the last several decades, intensive efforts have been made to design and develop advanced drug delivery systems which would improve the targeting and effectivity of platinum anticancer drugs such as cisplatin, *cis*-$[Pt(NH_3)_2Cl_2]$. Glycoconjugation of platinum anticancer drugs to various carbohydrates has been shown to improve their anticancer efficacy and targeting of malignancies due to the increased requirements of cancer cells for carbohydrates (Warburg effect) (Annunziata, Amoresano, et al., 2020; Annunziata, Cucciolito, et al., 2020; Bononi et al., 2021). Conjugation of platinum anticancer drugs to polysaccharides prolongs the circulation time of the drug in the blood, reduces its systemic toxicity, and improves its passive accumulation in the tumor due to the enhanced permeability and retention (EPR) effect (Haxton & Burt, 2009; Liechty et al., 2010; Vilar et al., 2012).

Dextrans are α-(1→6) bonded glucans produced by *Leuconostoc* and *Streptococcus* genus of bacteria with a variable degree of α-(1→3) branching, which, together with their molecular weight, depends not only on the bacterial genus but also on its strain (Dhaneshwar et al., 2006; Sarwat et al., 2008). Since the 1950s, dextrans have been used in clinical praxis as plasma volume expanders, for blood flow promotion, or as antithrombotic agents (Thorén, 1980). The plasma kinetics, renal clearance, the rate of degradation, and tissue distribution of dextrans were thus intensively studied and found to depend on the molecular weight as well as on the charge and the degree of substitution of the dextran chains (Goodarzi et al., 2013; Mehvar, 2000, 2003; Varshosaz, 2012). The impact of molecular weight is particularly pronounced; dextrans with weight-average molecular weight (M_w) below 10 kDa are rapidly eliminated from the organism because of their very high rate of renal clearance (Chang et al., 1975). Higher molecular weight dextrans (M_w > 70 kDa) spontaneously accumulate in the liver and spleen, where they can persist up to 96 h before being metabolized (Mehvar et al., 1994). High-M_w dextrans (M_w > 150 kDa) also tend to accumulate in the lymph nodes to a significant degree (Terry et al., 1953). The ratio of

* Correspondence to: M. Masařík, Department of Physiology, Faculty of Medicine, Masaryk University, Kamenice 5, CZ-625 00 Brno, Czech Republic.
** Corresponding author.
E-mail addresses: masarik@med.muni.cz (M. Masařík), jvicha@utb.cz (J. Vícha).

https://doi.org/10.1016/j.carbpol.2021.118461
Received 17 May 2021; Received in revised form 27 June 2021; Accepted 18 July 2021
Available online 21 July 2021

dextran accumulation between individual organs and tissues thus largely depends on its M_w (Mehvar et al., 1994). These properties make dextran derivatives potentially very interesting as an anticancer drugs carrier because the liver and lymphatic nodes are often among the first tissues invaded by metastases and thus represent the primary target for chemotherapy. Hypothetically, obtaining control over the molecular weight of dextran derivatives may significantly enhance their drug delivery characteristics and thus improve the efficacy of anticancer drugs.

Over the years, dextran and its derivatives had been intensively studied as anticancer drug carriers (Dhaneshwar et al., 2006; Goodarzi et al., 2013; Schechter, Neumann, et al., 1989; Varshosaz, 2012). Modification of dextran for anticancer drug binding is often achieved by the introduction of carboxylic groups to the polysaccharide chain. Advantageously, such negatively charged dextran derivatives persist in plasma much longer than neutral or positively charged ones (Mehvar, 2000), which may enhance the EPR effect because the carrier has more time to accumulate in the tumor due to the leaky vasculature. This is attributed to the negative charge of most biological membranes, which impede the uptake of molecules with the same charge, thus prolonging their residence in the vascular system (Mehvar, 2000). Chemical modifications of dextran chains were also reported to improve their overall stability in the body, *i.e.* while unmodified dextrans are depolymerized by α-1-glucosidases (dextranases) in few hours, any modification would generally reduce the rate of depolymerization (Mehvar, 2000). For instance, periodate-oxidized dextran derivatives with a degree of oxidation (*DO*) above 90% were shown to be largely resistant to dextranase hydrolysis (Ahmad et al., 2006).

Modification of dextran for binding of platinum drugs can be achieved for instance by sequential oxidation of vicinal –OH groups of anhydroglucose units (AGU) to aldehydes by periodate and subsequent oxidation of formed aldehydes to carboxylates by chlorite salt, which leads to the preparation of a mixture of 2,4- and 3,4-dicarboxydextrans (Ishak & Painter, 1978; Khomyakov et al., 1965; Kristiansen et al., 2010) collectively referred to as DXA in this work, see Fig. 1. The third potential product, 2,3-dicarboxydextran, is significantly less abundant (Khomyakov et al., 1965) and was not observed in NMR spectra of DXA (Münster et al., 2021). Hence, it is not further discussed. Note, that the periodate oxidation requires two –OH groups on neighboring (vicinal) carbons, which are oxidized simultaneously. Hence, branched DXA units are resistant to oxidation as they do not contain required vicinal diols because their –OH groups at C1, C3, and C6 engaged in glycosidic bonds (Fig. 1) (Khomyakov et al., 1965; Kristiansen et al., 2010).

Other methods of derivatization of dextran chain include carboxymethylation or dicarboxymethylation of dextran –OH groups resulting in the preparation of carboxymethyl dextran (CMD) or dicarboxymethyl dextran (DMD), respectively (Ohya et al., 1996b; Schechter et al., 1986).

Schlechter et al. studied the synthesis (Schechter et al., 1986), biological activity (Schechter et al., 1987), and blood levels (Schechter, Rosing, et al., 1989) of CMD conjugates with CP. Although the studied CP-CMD conjugates (M_w = 10 and 40 kDa) did not differ in their *in vitro* activity, both being less cytotoxic than free CP, *in vivo* tests revealed that both conjugates had higher plasma concentrations and longer half-lives than the free drug, depending on their M_w. While the content of free CP in mouse serum decreased to only 2–6% of its initial concentration already after 15 min since the i.v. administration, 14% of 10 kDa CP-CMD and 64% of 40 kDa CP-CMD conjugate remained after the same time. Even after six hours, about 11% of 40 kDa CP-CMD was still detected in the serum (Schechter, Rosing, et al., 1989). In the same work, Schechter et al. investigated also CMD with M_w = 250 kDa, which was found to retain the blood levels of platinum drug the longest (100% after 15 min, 47% after 100 min, and 14% after 6 h).

Later on, Ohya et al. compared DXA, CMD, and DMD as carriers for a derivative of oxaliplatin (Ohya et al., 1996a, 1996b). Both DXA and DMD-based conjugates were found superior to CMD one; their cytotoxicity against malignant cells was higher (comparable to a free drug) and they showed a lower decrease of cytotoxic activity after the pre-incubation in a medium containing fetal bovine serum. The DXA and DMD carriers thus provided better protection of the carried drug from the deactivating factors in serum than CMD, likely due to bidentate binding of the complex to the carrier (Ohya et al., 1996a). In follow-up work, Nakashima et al. (Nakashima et al., 1999) compared the DMD and DXA with identical M_w of 30 kDa as carriers for CP. Although CP-DXA conjugate showed higher cytotoxic activity, the cytotoxicity of CP-DMD was better retained after 36 h of pre-incubation in the presence of fetal bovine serum. Observed faster loss of activity of CP-DXA might however be a result of considerably higher platinum content (22 wt%) in CP-DXA compared to CP-DMD (9 wt%), which led to a faster release of the drug from the former. Recently, we have included DXA (M_w = 87 kDa) in the comparison of selectively oxidized polysaccharides as carriers for CP (Münster et al., 2021); established structures of CP-DXA conjugate are given in Fig. 1. Despite certain drawbacks, in particular the fast drug release rates in comparison to other carriers, DXA was deemed to be a potentially interesting carrier for CP given the highest overall cellular uptake and high cytotoxicity towards malignant cell lines, comparable or better to that of free drug (depending on the cell line). The CP-DXA also featured the lowest cytotoxicity towards non-cancerous cell line NIH-3T3 from all anhydroglucose-based carriers, including the oxidized cellulose and oxidized dextrin. Encouraged by these results, we have decided to investigate DXAs with different M_w as carriers for CP and to identify possible benefits and drawbacks related to the modulation of its M_w.

Hence, the recently developed method for direct control over the M_w of selectively oxidized polysaccharides with 1–4 glycosidic bonds (Münster et al., 2020; Münster, Fojtů, et al., 2019) was modified to prepare series of DXA derivatives with a broad range of M_w (10–184 kDa). Subsequently, prepared dextran derivatives were characterized by

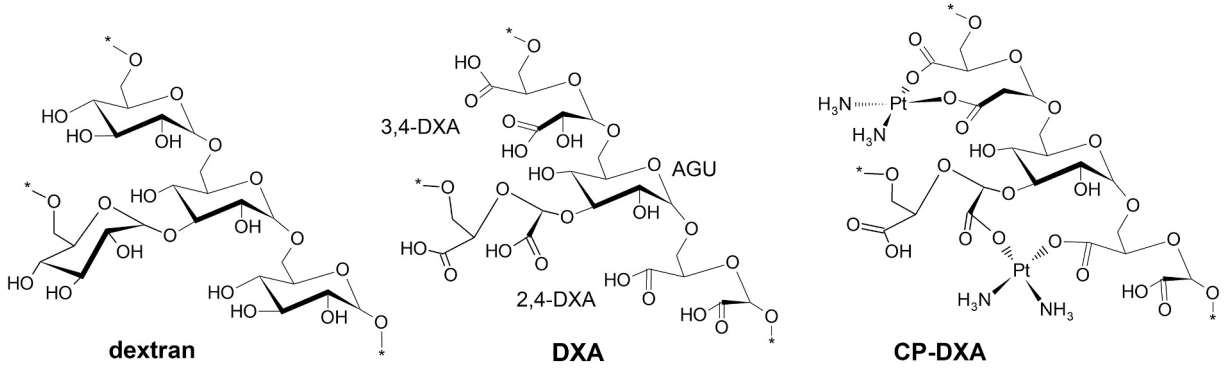

Fig. 1. Structure of dextran and 2,4- and 3,4-oxidized dextran (DXA) prepared by sequential periodate-chlorite oxidation; structure of cisplatin-DXA (CP-DXA) conjugate showing two main binding modes of CP, *i.e.* the bidentate binding of CP in single DXA unit and CP crosslinking of nearby oxidized DXA units (Münster et al., 2021).

FT-IR, GPC, and NMR spectroscopies and loaded with different amounts of CP (15, 30, and 45 wt%). Dependence of drug release rates, *in vitro* cytotoxicity, and migrastatic potential on M_w of CP-DXA conjugates have been investigated and results compared to the free CP. CP was selected as a model drug because it is currently still used as a first-line drug for the therapy of patients diagnosed with lung, ovarian, cervix, bladder, testicular, or head and neck cancer. As a first-generation platinum chemotherapeutic, it also causes adverse side effects such as nausea, neurotoxicity, nephrotoxicity, and ototoxicity, mostly due to its non-specific mechanisms of action and accumulation in healthy tissues. Conjugation of CP to DXA with variable M_w should provide better organ/tumor targeting, thus reducing its off-target toxicity. Conjugation should also protect the drug during its transport in the body and prevent its reactions with various targets of opportunity, such as thiol-containing proteins. Besides, conjugation to macromolecular carriers allows CP to avoid renal clearance, increase its plasma half-life, and accumulate in the tumor (EPR effect).

2. Materials and methods

2.1. Materials

Dextran from *Leuconostoc spp.* (Sigma Aldrich Co., M_w = 106 kDa, *PDI* = 5.59, estimated by GPC using setup described in Section 2.3) was used as a source polysaccharide. The primary oxidation was performed by sodium periodate ($NaIO_4$) and ethylene glycol (Penta, Czech Republic). The secondary oxidation of dialdehyde polysaccharides was carried out using sodium chlorite ($NaClO_2$, RT 80%), acetic acid (CH_3COOH, ≥99.8%), sulfamic acid (H_3NSO_3, 99.3%) (Sigma Aldrich, Co.), sodium hydroxide (NaOH, ≥98%) (Lachner, Czech Republic) and hydrochloric acid (HCl, 35%) (Penta, Czech Republic). Other chemicals involved in the characterization of source and resulting materials included sodium nitrate ($NaNO_3$, 99.8%) (Lachner, Czech Republic), disodium phosphate dodecahydrate ($Na_2HPO_4{\cdot}12H_2O$, 99.6%) (VWR, Czech Republic), deuterium oxide (D_2O, Sigma Aldrich, Co.) and phosphate-buffered saline pH 7.4 (PBS 7.4, Invitrogen, USA). Reagents used for the biological experiments included RPMI-1640 medium, fetal bovine serum (FBS) (mycoplasma-free), penicillin-streptomycin, trypsin, MTT reagent, ethylenediaminetetraacetic acid (EDTA), dimethyl sulfoxide (DMSO), glycine buffer, and hydroxyethylpiperazine-ethane-sulfonic acid buffer (HEPES) (Merck, Germany). All chemicals were of analytical grade and were used without further purification. Demineralized water (conductivity >0.1 μS/cm) was used throughout the experiments.

2.2. Preparation of DXA with variable M_w

The first step of selective oxidation of dextran follows well-established methods of periodate oxidation (Khomyakov et al., 1965; Maia et al., 2011; Münster et al., 2017; Münster et al., 2021; Münster, Capáková, et al., 2019). Briefly, 5 g of dextran was pre-dissolved for 1 h in 150 mL of water at laboratory temperature. Then, 8.25 g of $NaIO_4$ dissolved in 100 mL of water was added dropwise to the solution. The primary oxidation ran at 30 °C for 4 h under mild stirring (300 rpm) in the dark to prevent spontaneous periodate decomposition. The duration of primary oxidation was previously optimized based on periodate consumption estimated by UV–Vis spectroscopy (Münster et al., 2021) and it is sufficient to obtain fully oxidized dextran chains. After this period, the oxidation reaction was terminated by the addition of an excess of ethylene glycol. The prepared dialdehydedextran was then dialyzed against demineralized water using 14 kDa molecular weight cut-off (*MWCO*) dialysis tubing (Sigma Aldrich, Co.) for 4 days with regular water exchange. Next, the product was collected, filtered (0.22 μm filter), flash-frozen at −80 °C using an ethanol ice bath, and lyophilized.

The second step of DXA preparation involves oxidation of dialdehydedextran by $NaClO_2$ in the presence of CH_3COOH. The reaction mixture was composed of 0.45 g of the prepared dialdehydedextran, which was dissolved in 45 mL of 0.5 M CH_3COOH. The secondary oxidation started by dropwise addition of concentrated $NaClO_2$ solution (0.25 g/mL) to the acidified dialdehydedextran solution (final concentration 0.5 M). The molar ratio of –CHO: $NaClO_2$ was set to 1:4. The mixture was gently stirred for 7 h at laboratory temperature in the dark. After this period, the oxidation reaction was terminated by the addition of a concentrated NaOH solution (pH = 8). Then, the product solution was thoroughly dialyzed against water using a 14 kDa *MWCO* dialysis membrane. Diluted (0.1 M) NaOH and HCl solutions were then used to set the pH of the solution to 7.4. The resulting purified dicarboxydextran sodium salt (DXA) solution was filtered (0.22 μm filter), flash-frozen, and lyophilized.

To prepare DXA of various M_w, sulfonation-induced scission was initiated by the addition of sulfamic acid into the reaction mixture before the secondary oxidation to control the M_w of the final product (Münster et al., 2020; Münster, Fojtů, et al., 2019). In the first set of experiments, the standard protocol of sulfonation-induced scission used previously for M_w modulation of cellulose and dextrin was employed, *i.e.* H_3NSO_3 (0.11 g/mL) was added to the dialdehydedextran solutions immediately before the start of the secondary oxidation by the addition of $NaClO_2$ (Münster et al., 2020; Münster, Fojtů, et al., 2019). Different molar ratios of –CHO: H_3NSO_3 (from 1:0 to 1:0.5) were tested. The rest of the process parameters and methodology of secondary oxidation remained the same as described in the previous paragraph. Because of unsatisfactory results, a modified methodology featuring a presulfonation of various lengths was used in the second set of experiments. Briefly, the solution of H_3NSO_3 was added dropwise to the set of acidified dialdehydedextran sample solutions (molar ratio of –CHO: H_3NSO_3 set to 1:0.5, final H_3NSO_3 concentration was 0.0625 M) prior to the start of the secondary oxidation as before. However, these reaction mixtures were stirred for 0.5–6 h (*i.e.* the presulfonation) before the initiation of secondary oxidation by addition of $NaClO_2$ solution. Subsequent steps in the preparation methodology remained the same as above. All of the DXA samples were prepared in the form of their sodium salt. Results are discussed in Section 3.1.

2.3. Characterization of prepared DXA

Spectral FT-IR analysis was performed using a Nicolet 6700 (Thermo Scientific, USA). Spectra were collected in the range of 4000–400 cm^{-1} with 64 scans and a resolution of 2 cm^{-1} with atmosphere gas suppression enabled. Energy dispersive spectroscopic (EDS) analysis of prepared samples was conducted by using scanning electron microscope Vega II/LMU (Tescan, Czech Republic) operated at 30 keV equipped with energy dispersive X-Ray (EDX) detector Inca X-act (Oxford Instruments, UK). Molecular weight distribution was analyzed by the gel permeation chromatography (GPC) using a Waters HPLC Breeze chromatographic system (Waters, USA) coupled with a Waters 2414 refractive index detector (drift tube T = 60 °C), Tosoh TSK gel $GMPW_{XL}$ column (300 mm × 7.8 mm × 13 μm, column T = 30 °C). A mixture of 0.1 M $NaNO_3$ and 0.05 M $Na_2HPO_4{\cdot}12\ H_2O$ was used as a mobile phase. A calibration kit of pullulan standards SAC-10 (Agilent Technologies, USA) in a span of M_w 342–805000 g/mol was employed. ^{1}H NMR spectra were measured using Bruker Avance III HD 700 MHz NMR spectrometer (Bruker, USA) equipped with a triple-resonance cryoprobe at 298 K in D_2O.

2.4. Preparation and characterization of cisplatin-DXA conjugates

CP was prepared according to the literature (Wilson & Lippard, 2014). It was then dissolved in water (2 mg/mL) and added dropwise to the 4 mg/mL aqueous solution of the DXA at room temperature. The reaction mixture was then gently shaken for 72 h in the absence of light, dialyzed against water for 4 h using a 3.5 kDa *MWCO* membrane to

remove unbound CP, filtered, and lyophilized. Reactions were performed using CP: carrier *w/w* loading ratio of 2:10, 5:10, and 8:10, respectively. CP release was investigated using a setup mimicking *in vitro* conditions (Münster, Fojtů, et al., 2019); 10 mg of each conjugate was dissolved at 37 °C in 5 mL of PBS 7.4 and dialyzed (3.5 kDa *MWCO* membrane) against 95 mL of the same medium. Aliquots of 5 mL were collected throughout 48 h and replaced with 5 mL of fresh media to conserve the volume. Released cisplatin residuum, *cis*-$[Pt(NH_3)_2(H_2O)_2]^{2+}$ is in the following text referred to as cisplatin (CP) to simplify the discussion. The amount of bonded platinum was measured by the energy-dispersive X-ray fluorescence (XRF) spectrometer ARL Quant'X EDXRF Analyzer (Thermo Scientific, USA) using the calibration standards prepared by dissolving a known amount of CP in PBS 7.4. The morphology of selected CP-DXA conjugates was analyzed by transmission electron microscopy (TEM) using JEM 2100 microscope (Jeol, Japan) operated at 160 kV. Samples were drop-cast onto Formvar coated 300 mesh copper grids from diluted solution (0.01 mg/mL) and gently dried. The stability (ζ-potential) and hydrodynamic radius of selected diluted samples (1 mg/mL) were analyzed by dynamic light scattering (DLS) analysis carried out using Zetasizer Nano ZS90 instrument (Malvern Instruments, UK) operated at 25 °C, coupled with DTS1070 cells and the Smoluchowski model.

2.5. Cytotoxicity evaluation

Six tumor cell lines originating from different tissues were used in this study: i) A2780 - epithelial ovarian cancer cells established from tumor tissue of an untreated patient and ii) corresponding CP-resistant subline A2780/CP, iii) A549 - human cell line derived from pulmonary adenocarcinoma, iv) 22Rv1 - cell line representing human prostate carcinoma, and v) PC-3 - human prostate cancer cell line established from bone metastasis. Cell lines were purchased from the European Collection of Authenticated Cell Cultures (ECACC, UK) and were cultivated in RPMI-1640 medium, supplemented with 10% FBS, antibiotics (penicillin 100 U/mL and streptomycin 0.1 mg/mL), and HEPES. The cells were grown in the incubator at 37 °C in a humidified 5% CO_2 mixture with ambient air and subsequently seeded on a 96-well plate at a density ensuring 70% confluence on the day of the treatment. After 48 h, the medium was removed and replaced with a fresh culture medium containing CP-DXA conjugates in the concentration ranging from 0 to 500 μM (200 μL per well). After 24 and 48 h of the treatment, the cell culture medium with CP-carrier conjugates was removed and the cells were incubated with a fresh medium containing 1 mg/mL of MTT reagent (200 μL per well) for another 4 h. Plates with the cells were wrapped in aluminum foil and kept in a humidified atmosphere at 37 °C. Next, the culture medium with MTT was replaced by DMSO (200 μL per well) to dissolve the formazan crystals. Then, glycine buffer (25 μL per well) was added to DMSO, gently shaken and the absorbance value at 570 nm was recorded. Cytation 3 Imaging reader (BioTek Instruments, USA) was used for the determination of absorbance values. The IC_{50} values were then calculated by fitting the data with the logistic function to create a sigmoidal dose-response curve. All measurements were performed in tetraplicates.

2.6. Migration assay

A2780 cells were seeded on the tissue culture dishes at a density 2×10^5 per mL of media and incubated until they reached a confluent monolayer, which was then scratched using a sterile 200 μL pipette tip. The cellular debris was removed by washing with PBS five times and images of scratches were acquired. Subsequently, a medium containing selected samples in concentrations corresponding to their respective IC_{50} (established by MTT, see Section 2.5) was added to the cells. Cells in Petri dishes were placed in the incubator, kept at 37 °C, examined periodically and images were taken at the same position after 24 and 48 h using the phase-contrast Olympus IX81 microscope (Olympus, Japan). The results were analyzed using T-Scratch software (CSElab, Switzerland) and are presented as a percentage of open wound area remained after 24 and 48 h.

3. Results and discussion

3.1. Synthesis and characterization of DXA with a different molecular weight

Sequential oxidation of dextran from *Leuconostoc* spp. was performed as described in Section 2.2. The yield of primary oxidation was nearly quantitative (96.7%); the yields of all secondary oxidations were above 90%.

The original method of sulfonation-induced chain scission, which relies on the addition of different amounts of sulfamic acid (H_3NSO_3) just before the secondary oxidation (Münster et al., 2020; Münster, Fojtů, et al., 2019), was initially tested to prepare DXA derivatives with different M_w. It is based on the addition of acidic $–SO_3H$ groups to aldehydes introduced during the periodate oxidation. Attached $–SO_3H$ groups can efficiently protonate nearby glycosidic bonds, thus initiating their acidic hydrolysis. The $–SO_3H$ groups are eliminated during the oxidation of aldehydes to carboxylates, see ref. (Münster et al., 2020) for the detailed reaction mechanism. This approach allows the preparation of dicarboxylated polysaccharides with different M_w using the same starting material. It can be also used to decrease the polydispersity index (*PDI*) of products compared to source polysaccharide (Münster et al., 2020; Münster, Fojtů, et al., 2019). This saves resources and provides better control over the results than alternative approaches based on the oxidation of different source materials with various molecular weights or thermal degradation of prepared dicarboxylated polysaccharides, both of which offer only limited (if any) control over the M_w and *PDI* of the products.

However, the original method, developed for (1→4) bonded polysaccharides (namely cellulose), was found to be unsuitable for dextran (see Fig. 2>A and Table S1). The addition of H_3NSO_3 up to 0.25 M concentration had virtually no impact on the M_w of DXA, which started to decrease only in a presence of 0.5 M H_3NSO_3. The likely reason lies in the structure of DXA, which is formed mostly by 2,4- and 3,4-oxidized units connected by α-(1→6) glycosidic bonds. The $–SO_3H$ groups attached to C3 and C4 are thus relatively distant from α-(1→6) linkages and only sulfonation at C2 can lead to their effective protonation, see Scheme 1 for the reaction mechanism. This slows down the kinetics of the chain scission for DXA in comparison to β-(1→4) bonded cellulose units.

Hence, instead of further increasing the H_3NSO_3 concentration, which would decrease the pH and increase the risk of side reactions, a presulfonation step was introduced, *i.e.* H_3NSO_3 was added to the solution of dialdehydedextran and the mixture stirred in the dark for several hours before the secondary oxidation was initiated, see Section 2.2. This novel setup prioritizes the process of macromolecular chain scission over the competitive oxidative elimination of $–SO_3H$ groups during aldehyde oxidation. By changing the duration of presulfonation, M_w of DXA can be modulated between 5 and 100% of that of DXA prepared without presulfonation, see Fig. 2B. DXA derivatives with M_w between 184 kDa (prepared without presulfonation, $PDI = 3.54$) and 10 kDa (6 h of presulfonation, $PDI = 1.43$) were obtained, see Table S1 in Supporting Information. Moreover, the *PDIs* of DXA samples are significantly lower than that of source dextran (5.59) even without any additional purification steps, which is another benefit of the sulfonation-induced chain scission method. It should be noted, however, that the degree of polymerization of DXA prepared without the presence of sulfamic acid is about 37% higher compared to source dextran polysaccharide (DP 911 *vs.* DP 664). This is likely caused by the formation of a dense network of rather stable intermolecular hemiacetal bonds after the periodate oxidation previously described for oxidized dextran (Ishak & Painter, 1978; Maia et al., 2011), which may survive even through

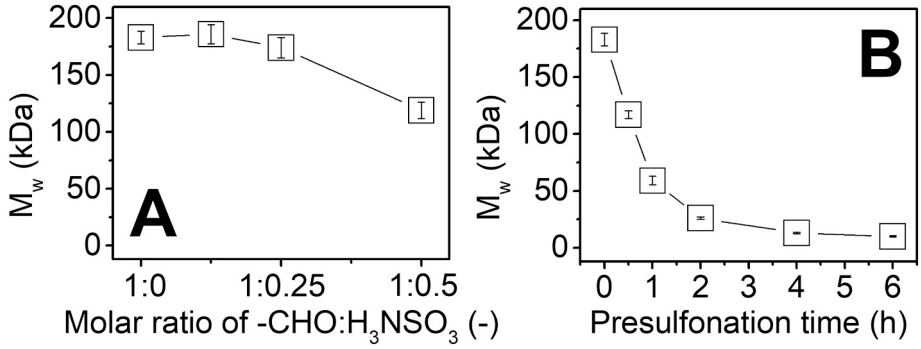

Fig. 2. Weight-average molecular weight (M_w) of dicarboxydextran (DXA) prepared using A) of various molar ratios of sulfamic acid (H_3NSO_3), B) different presulfonation times (0–6 h). All measurements were performed in triplicates, error bars represent *SD*

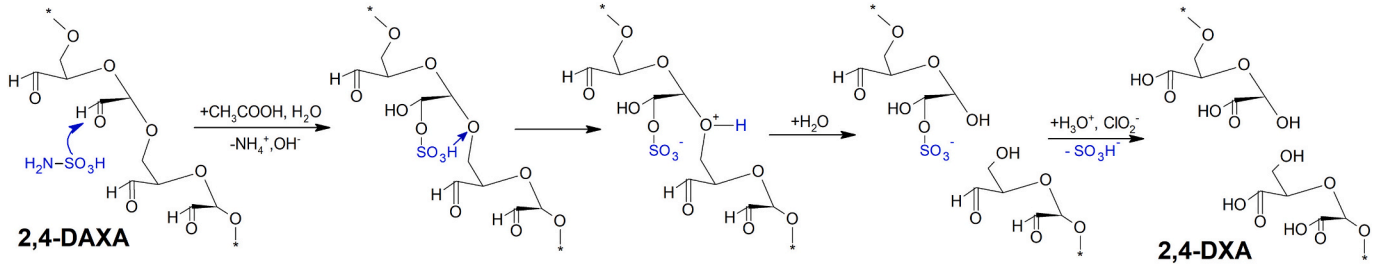

Scheme 1. Mechanism of sulfonation-induced chain scission on the example of 2,4-dialdehydedextran (2,4-DAXA).

secondary oxidation (Münster et al., 2020).

Prepared materials were characterized by EDS, FT-IR, and ^{1}H NMR spectroscopy, see Supporting Information. EDS analysis confirmed the successful elimination of –SO_3H groups during the secondary oxidation. The residual sulfur content was between 0.14 and 0.50 at.% depending on the presulfonation length, see Table S2. To further reduce the amount of residual sulfur, one may decrease the concentration of H_3NSO_3 and increase the duration of secondary oxidation (Münster et al., 2020).

The FT-IR and ^{1}H NMR spectra of species prepared using 0–6 h of presulfonation can be found in Figs. S1 and S2. All FT-IR spectra are nearly identical with dominant bands belonging to vibrations of carboxylic (~1605 cm^{-1}) and C—O groups (1000–1200 cm^{-1}). The ^{1}H NMR spectra in Fig. S2 are dominated by several partially overlapping signals, which position remains the same disregarding the duration of the presulfonation step. Increasing intensity of the signal at 4.14 ppm, which overlaps with signals of H4 from 2,4-dicarboxydextran (4.12 ppm) and H4 from 3,4-dicarboxydextran (4.11 ppm) (Münster et al., 2021) is attributed to the presence of an increased number of end groups in low-M_w derivatives, *i.e.* those prepared using longer presulfonation times. The degree of oxidation of all species is assumed to be ~85% due to the presence of approximately 15% of α-(1→3) branched units resistant to oxidation (*e.g.* signal at 3.45 ppm in Fig. S2) (Khomyakov et al., 1965; Münster et al., 2021). For full signal assignment see our recent work (Münster et al., 2021).

3.2. Cisplatin loading and release studies

Three DXA derivatives prepared using 0, 1, and 4 h of presulfonation and having M_w of 184, 59, and 13 kDa, respectively, were selected for further studies. These were loaded by CP using 2:10, 5:10, and 8:10 CP: DXA *w*/w reaction ratio, see Section 2.4 for more details. CP loading effectiveness was about 90% in all cases, resulting in 15, 30, or 45 wt% of bound CP in the conjugates (established by XRF spectroscopy). Investigated conjugates are in the following text designated by letters H, M, and L which stands for High, Medium, and Low molecular weight (184, 59, and 13 kDa), respectively, and by the number representing the amount of loaded CP in wt% (15, 30, 45). Hence, H-15 stands for DXA sample prepared without presulfonation (M_w = 184 kDa) carrying 15 wt % of CP. L-45 represents a sample with 4 h of presulfonation of M_w = 13 kDa carrying 45 wt% of CP and so on.

Cumulative drug release results of selected H-, M- and L- conjugates are given in Table S3 in Supporting Information. Here we discuss only the H- and L-series samples, where the largest differences in drug release kinetics were observed, see Fig. 3. Both M_w of the carrier and the amount of loaded CP significantly influence the CP release kinetics. Samples containing only 15 wt% of CP feature slower drug release than corresponding 45-series ones, particularly early on, see Fig. 3. An increase of DXA M_w, from 13 to 184 kDa, slows down the CP release rate significantly; about 40% less CP is released after 24 h from the H-15 sample in comparison with the L-15 sample and about 20% less from H-45 compared to the L-45 sample, see Table S3 in Supporting Information. A combination of lower drug loading and higher M_w of the carrier leads to about 50% slower release of CP from the H-15 sample after 24 h compared to the L-45 sample. The increased molecular weight of DXA in combination with optimization of drug loading can thus be used to (at least partially) counter the reported rapid drug release rates of DXA conjugates (Nakashima et al., 1999).

3.3. Cytotoxicity evaluations

Cytotoxicity of the H-15, H-45, M-30, and L-15 samples was investigated by *in vitro* study on the panel of five cell lines representing three types of carcinomas often treated with CP - ovarian carcinoma represented by A2780 human cells and its CP-resistant subline A2780/CP, lung cancer represented by A549 human adenocarcinoma cells and prostate cancer represented by 22Rv1 and metastatic PC-3 human cell lines. The cytotoxicity of carriers and their conjugates was established by MTT assay, see Section 2.5. Presented IC_{50} values (μM) are defined as a concentration of cisplatin required to inhibit the cell growth of the given cell line by 50%. The IC_{50} values of free carriers are not provided because all carriers were non-toxic in the whole range of concentrations (up to 500 μM) and IC_{50} thus could not be calculated. It should be

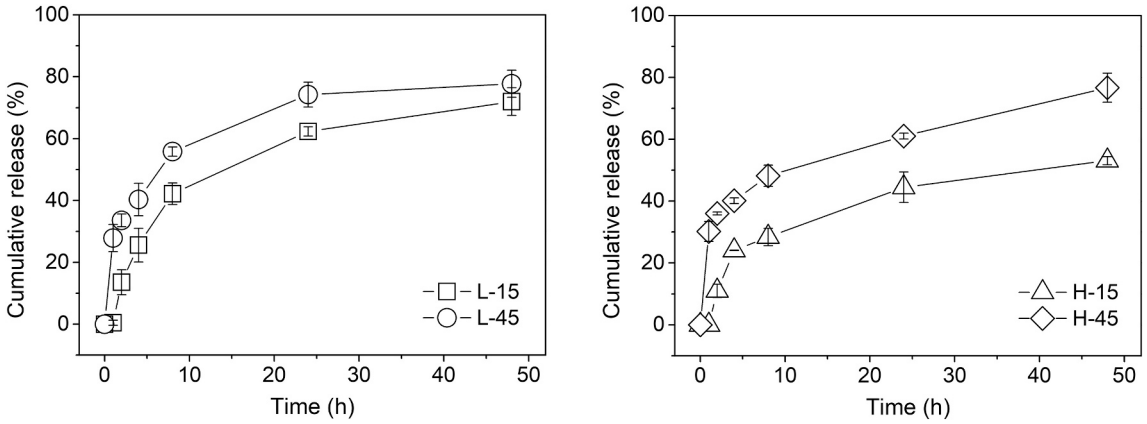

Fig. 3. Cumulative release of CP from L-15, L-45, and H-15 and H-45 DXA carriers for 48 h, error bars correspond to *SD*

stressed out that reported IC_{50} values correspond to the *total* concentration of CP in a culture media (100% release of CP from conjugates is assumed); applied doses of different conjugates were thus modified to contain the same total amount of CP as the sample of free CP. This allows to directly compare the efficacy of the free drug and individual conjugates and highlight the differences between individual carriers. The IC_{50} values are given in Tables S3 and S4 and compared in Fig. 4.

Obtained IC_{50} values differ considerably between the cell lines as well as between incubation times (note different scaling on the y-axes in Fig. 4). For detailed statistical analysis see Fig. S3. Overall cytotoxicity profiles of conjugates across the panel of cell lines follow that of free CP; all compounds were the most effective towards ovarian cell lines and prostatic cell line 22Rv1. Contrary, much higher doses were required to inhibit the growth of lung cancer cell line A549 as well as prostatic PC-3 cell line after 24 h of incubation. Nevertheless, differences between cytotoxicity of individual conjugates and the free drug could still be determined and benefits of CP conjugation to carriers with different M_w evaluated.

After 24 h of incubation, cytotoxicity of all conjugates is comparable or lower than that of free CP. This is a common feature of macromolecular carriers attributable to the slower penetration of macromolecules into the cells compared to a free drug. Distinct differences between individual carriers and the free CP are, however, observable after 48 h of incubation. Notably, observed differences do not correspond to the drug release rates as one may expect. Instead, they depend on the M_w of the carrier, although the dependence is not linear. While L-15, H-15, and particularly H-45 conjugate are significantly more cytotoxic than free CP towards several cancerous cell lines, the cytotoxicity of M-30 is comparable or lower than that of free CP in 4 out of 5 cases, see Fig. S3. Overall, H-45 conjugate offers the highest CP anticancer efficacy enhancement, being more effective than free drug in four out of five cases, and comparable to free CP only for A2780/CP cell line, see Fig. 4. The H-45 conjugate is nearly four times more effective than free CP for both prostatic cell lines and about twice more for A2780 and A549 cell lines, see Fig. 4. It is thus the most cytotoxic from all tested compounds by far, even in comparison to the H-15 derivative of the same molecular weight. The reasons for increased cytotoxicity due to higher CP loading are further discussed in Section 3.5 below.

3.4. Migrastatic potential

Wound healing migration assay was performed on A2780 cells, which were treated with free CP and two of the most effective conjugates, the L-15 and the H-45, which are prepared using DXAs of different molecular weights. Drug and conjugates were applied in doses corresponding to their respective IC_{50} values determined in the previous section. Cells were incubated for 24 and 48 h, respectively, see Fig. 5 and Table S5 in Supporting information. For detailed statistical analysis see Fig. S4.

Interestingly, after 24 h of incubation with free CP, A2780 cells showed a great increase in migration potential, covering roughly 80% of the original wound area. This is significantly more than the untreated control, see Fig. 5 and representative micrographs of the wound healing assay in Fig. 6. Treating the cells with CP-DXA conjugates, particularly

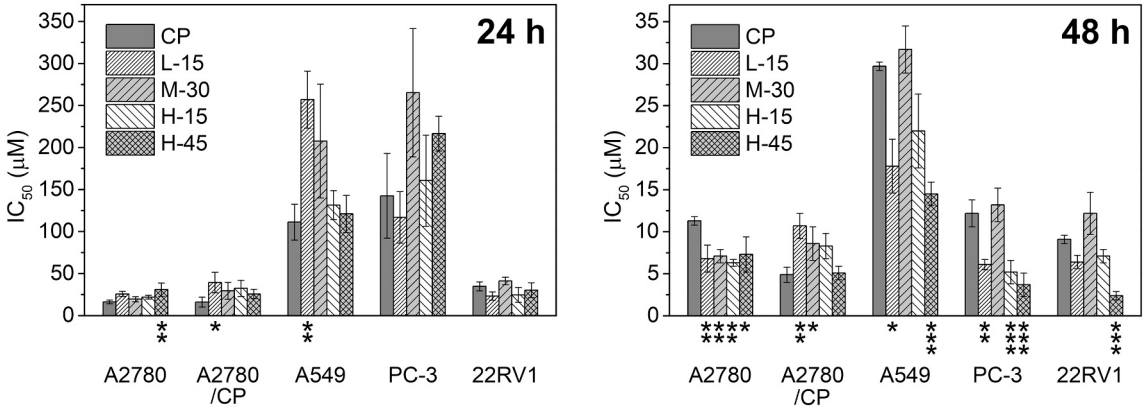

Fig. 4. Comparison of IC_{50} values (μM) for free CP and CP-DXA conjugates after 24 h and 48 h of incubation with a panel of cancer cell lines. Values are the average of four independent measurements. Data are displayed as IC_{50} means ± *SD*. The IC_{50} values of CP carriers were related to the CP IC_{50} value for each cell line and duration of treatment. Stars indicate statistical significance of the result: absent stars - not significant, $*p < 0.05$, $**p < 0.01$, $***p < 0.001$. Statistical analysis was performed using one-way ANOVA followed by Tukey *post-hoc* test.

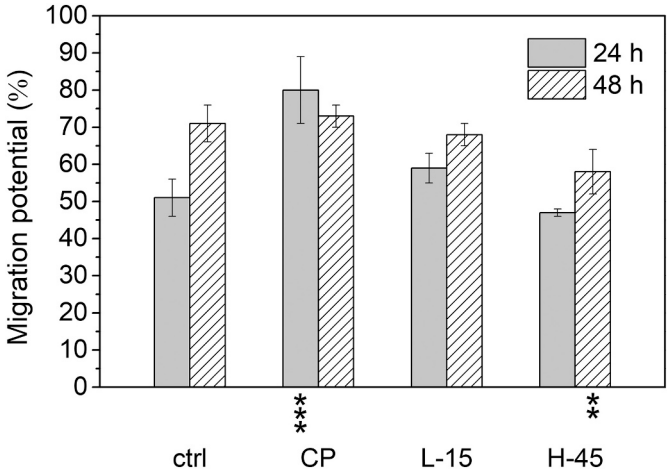

Fig. 5. Migration potential of A2780 cells (%), *i.e.* the percentage of wound area covered after 24 h and 48 h by untreated cells (ctrl) and cells treated with free CP, L-15, and H-45; applied concentrations correspond to their respective IC_{50} values. All experiments were performed in triplicates; error bars correspond to *SD*. Statistical analysis was performed using one-way ANOVA followed by Tukey *post-hoc* test with respect to untreated control; stars indicate statistical significance of the result: absent stars - not significant, $*p < 0.05$, $**p < 0.01$, $***p < 0.001$.

the H-45, led to significantly better results; only between 50 and 60% of the area healed after 24 h. In other words, conjugates showed a statistically significant reduction of migration potential compared to free CP (see Fig. S4 for statistical comparison), although their effect on cell migration is not statistically significant when compared to the untreated cells after 24 h. There is, however, a statistically significant decrease of cell migration after 48 h treatment of A2780 cells by H-45 conjugate, when only about 60% of wound area is healed, compared to 70–80% in case of untreated control and free CP, respectively, see Fig. 5. Once again, H-45 was the most effective from all tested compounds.

3.5. The role of cisplatin loading to conjugate nanoassemblies

The biological evaluation revealed that the efficacy of CP-DXA conjugates depends not only on the molecular weight of DXA but also on the amount of conjugated CP. We emphasize once more that the dose of each conjugate was set to contain an equal amount of CP; the increased cytotoxic effect of H-45 conjugate thus cannot be attributed to the higher amount of CP in applied doses and the main reason has to be found elsewhere.

It is a known fact that CP can form interstrand crosslinks between the polysaccharide chains. This behavior was used to prepare CP-loaded nanoparticles (Cai et al., 2008) or nanogels (Ohta et al., 2016) in the past. Hence, a higher amount of conjugated platinum may influence characteristics of nanostructures formed by macromolecular DXA conjugates in solution, which would, in turn, alter the cell internalization and thus also the efficacy of the conjugated drug. To investigate, H-15 and H-45 conjugates, prepared using the DXA of the same M_w but with different amounts of CP, were studied by TEM and DLS analysis. Fig. 7 shows the TEM micrographs of H-15 (part A) and H-45 (part B). Interestingly, both samples contain roughly similar spherical particles of approximately 3.5 ± 1 nm in diameter. Contrary, DLS measurements of hydrodynamic radii revealed significantly larger values (252 ± 8 nm for H-15 and 151 ± 9 nm for H-45). Conjugate nanoassemblies thus could be best described as nanogels, based on following reasoning: The small and rather uniform size of particles observed by TEM can be explained as a result of nanogel structure collapsing (shrinking) during drying. This process is similar for both samples because they are formed by DXA macromolecules of the same size. Much larger hydrodynamic radii of particles measured in colloidal solutions than indicate significant swelling of both nanoassemblies in water, which is one of the main characteristics of nanogels.

The difference in hydrodynamic radii (swelling) between H-15 and H-45 samples is then attributed to i) higher swelling due to a more sparsely crosslinked network (lower amount of loaded CP) in the H-15 sample and ii) the presence of larger ionic corona due to a higher amount of residual -COO^- groups in H-15 sample, because of the lower number of carboxyl groups being used for CP binding in H-15 than in H-

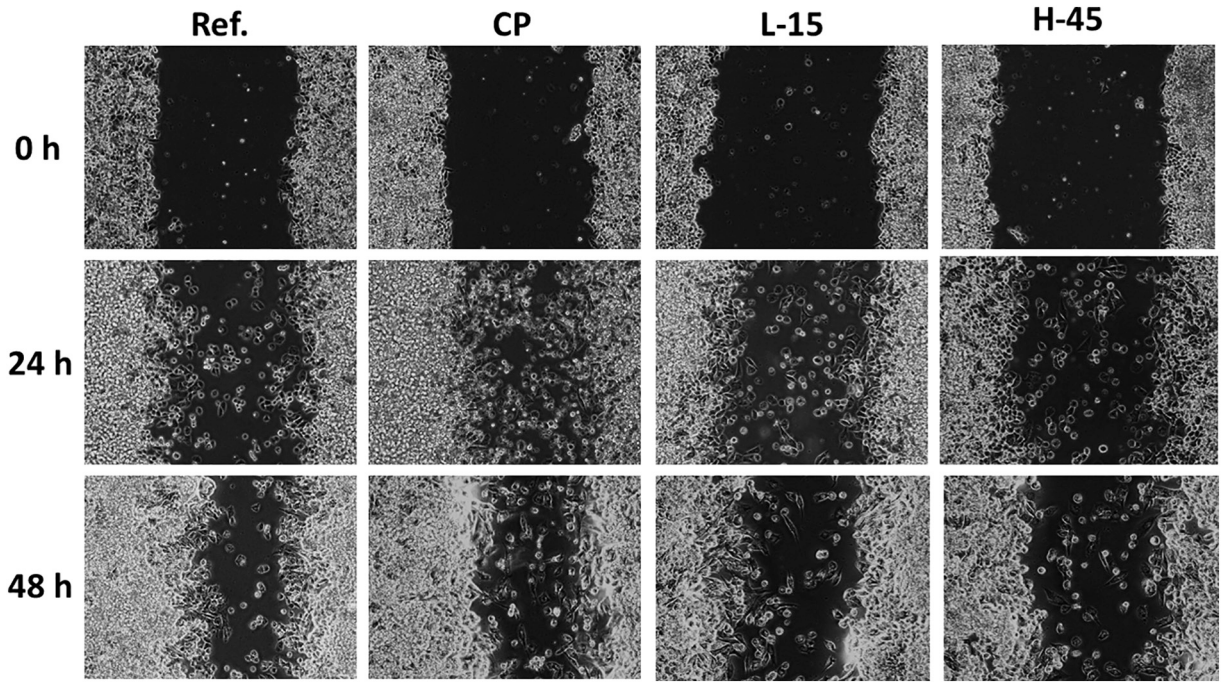

Fig. 6. Micrographs of the wound healing migration assay of A2780 cell line after 0, 24, and 48 h of incubation. All compounds were applied in IC_{50} doses established previously by the MTT assay. Ref. – untreated, CP – treated with free CP, L-15 – low-M_w DXA with 15 wt% of CP, H-45 – high-M_w DXA with 45 wt% of CP.

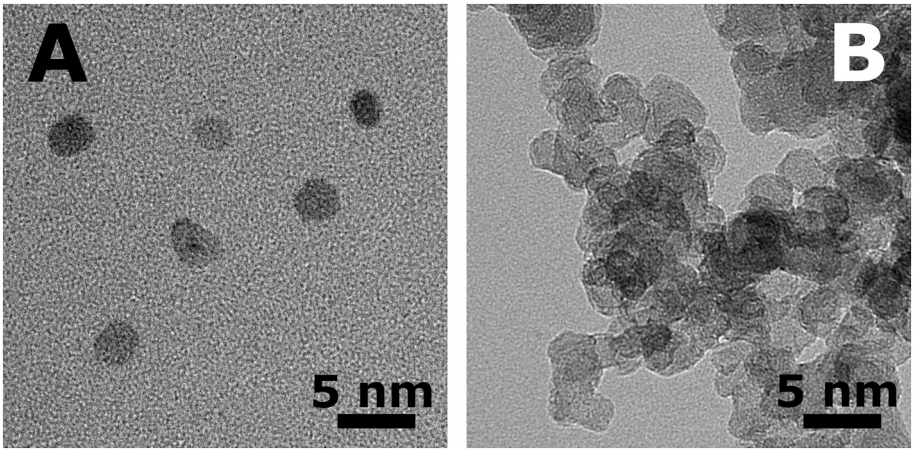

Fig. 7. TEM micrographs of H-15 (part A) and L-45 (part B).

45. This assumption is supported by the measured ζ-potential values (-34.2 ± 1.3 mV for H-15 and -21.3 $\pm$ 0.9 mV for L-45). The characteristics of CP-DXA nanogels thus depend on the amount of loaded CP and are likely responsible for the observed influencing of the biological properties. To further support this conclusion, the sample M-30, which showed the lowest anticancer efficacy from all species tested, has been also investigated using DLS. The M-30 nanogel particles were found to have a hydrodynamic radius of 374 ± 40 nm, more than twice the size of H-45 nanoparticles (ζ-potential $= -33.7 \pm 2.6$ mV). This is likely a result of a combination of shorter (yet still relatively large) DXA chains, which offer fewer crosslinking spots per macromolecule than larger H-type chains, and relatively low CP loading (5: 10). Both factors thus result in a more sparsely crosslinked nanogel network compared to H-species which would also swell more significantly in solution - hence the larger size of M-30 nanogel particles. The large dimensions of the M-30 nanogel particles are also a likely reason for their poor biological efficacy, as they likely impact the cellular uptake and thus the amount of the drug that crosses the cellular membrane.

4. Conclusions

DXAs of different molecular weights had been prepared by the modification of the recently developed method for controlled chain scission of oxidized polysaccharides using sulfamic acid. This allows to advantageously use the same starting material to prepare DXA with desired M_w and decreased polydispersity (compared to source dextran). To investigate the possible gains of control over the M_w of DXA, selected derivatives with M_w between 13 and 184 kDa were loaded with 15, 30, or 45 wt% of CP, respectively, and their drug release rates, *in vitro* cytotoxicity profiles, and suppression of cancer cell migration were compared with free CP.

Increasing M_w of the carriers significantly decreases the CP release rates, and thus partially counters the main issue of DXA carriers – fast drug release rates. For instance, a high-M_w carrier with 15 wt% of CP released about 40% less CP after 24 h than its low-M_w counterpart.

The *in vitro* cytotoxicity of CP towards malignant cell lines was enhanced by its binding to low- (13 kDa) and particularly to the high-M_w DXA (184 kDa), while its conjugation to medium-M_w DXA (59 kDa) attenuated its cytotoxicity in comparison with a free drug. Biological properties of CP-DXA conjugates are, besides the M_w of DXA, also influenced by the amount of loaded CP, which crosslinks macromolecular DXA chains into nanogels. The larger the amount of loaded CP, the denser the crosslinking. The combination of a high-M_w carrier and high drug loading (H-45 sample) led to a spontaneous formation of nanogel particles with a hydrodynamic radius of ~150 nm, which shows the highest anticancer efficacy from all samples tested. The potency of this conjugate is on average two times higher than that of a free drug across the whole panel of tested cancer cell lines and up to four times higher against both malignant prostatic cell lines. Further, H-45 conjugate showed statistically significant inhibition of the ovarian cancer cell migration when compared both to free cisplatin and untreated control. H-45 was also significantly more effective than H-15 conjugate, which is formed by the same DXA chains, yet more sparsely crosslinked (hydrodynamic radius of ~250 nm), and particularly the M-30 conjugate (hydrodynamic radius of ~375 nm), presumably because of the smaller size (and lower negative charge) of H-45 nanogel particles facilitates easier crossing over the cellular membrane.

To summarize, the study demonstrates the potential of DXA nanogels prepared using DXA of different M_w as anticancer drug carriers capable to enhance therapeutic response and suppress metastatic spreading by improving the characteristics of the drugs already established in the clinical setting. The observed relationship between biological efficacy and physical characteristics of cisplatin-crosslinked nanogel formulations is also interesting. Possibly, optimization of their parameters might improve the biological characteristics of dextran nanogels even further.

CRediT authorship contribution statement

L. Münster: Methodology, Investigation, Validation, Visualization, Writing – original draft, Writing – review & editing. **M. Fojtů:** Investigation, Validation, Visualization, Formal analysis, Writing – original draft, Writing – review & editing. **M. Muchová:** Investigation, Validation, Formal analysis. **F. Latečka:** Investigation. **S. Káčerová:** Investigation, Validation, Formal analysis. **Z. Capáková:** Investigation, Validation, Formal analysis. **T. Juriňáková:** Investigation, Validation, Formal analysis. **I. Kuřitka:** Funding acquisition, Resources, Writing – original draft. **M. Masařík:** Conceptualization, Methodology, Resources, Supervision, Funding acquisition, Writing – original draft, Writing – review & editing. **J. Vícha:** Methodology, Investigation, Visualization, Writing – original draft, Writing – review & editing, Conceptualization, Supervision, Project administration.

Declaration of competing interest

The authors declare no competing financial interest.

Acknowledgments

This work was supported by the Ministry of Education, Youth, and Sports of the Czech Republic – DKRVO (RP/CPS/2020/006). M. Fojtů and M. Masařík were supported by the Ministry of Education, Youth and Sports of the Czech Republic, project Advanced Functional Nanorobots

reg. No. CZ.02.1.01/0.0/0.0/15_003/0000444. M. Fojtů was further supported by the start-up grant InGA/SUP/08/2020 from the Masaryk University in Brno. Z. Capáková acknowledges Czech Science Foundation grant 19-16861S. CIISB research infrastructure project LM2018127 funded by the Ministry of Education, Youth and Sports of the Czech Republic is gratefully acknowledged for the financial support of the NMR measurements at the Josef Dadok CEITEC core facility in Brno. This work was supported also by funds from Specific University Research Grant, as provided by the Ministry of Education, Youth and Sports of the Czech Republic in the year 2021 (MUNI/A/1698/2020 and MUNI/A/1246/2020) and by projects of Charles University in Prague (Progress Q26/LF1 and Q27/LF1).

Appendix A. Supplementary data

Supporting Information. Molecular weight distributions, FT-IR and 1H NMR spectra of DXA derivatives; EDS analysis results; Drug-release data; IC_{50} values of CP and individual CP-DXA conjugates and their statistical analysis; Open-wound area evaluation and statistical analysis.

References

Ahmad, S., Tester, R. F., Corbett, A., & Karkalas, J. (2006). Dextran and 5-aminosalicylic acid (5-ASA) conjugates: synthesis, characterisation and enzymic hydrolysis. *Carbohydrate Research, 341*(16), 2694–2701. https://doi.org/10.1016/j.carres.2006.08.015.

Annunziata, A., Amoresano, A., Cucciolito, M. E., Esposito, R., Ferraro, G., Iacobucci, I., … Ruffo, F. (2020). Pt(II) versus Pt(IV) in carbene glycoconjugate antitumor agents: minimal structural variations and great performance changes. *Inorganic Chemistry, 59*(6), 4002–4014. https://doi.org/10.1021/acs.inorgchem.9b03683

Annunziata, A., Cucciolito, M. E., Esposito, R., Ferraro, G., Monti, D. M., Merlino, A., & Ruffo, F. (2020). Five-coordinate platinum(II) compounds as potential anticancer agents. *European Journal of Inorganic Chemistry, 2020*(11–12), 918–929. https://doi.org/10.1002/ejic.201900771

Bononi, G., Iacopini, D., Cicio, G., Pietro, S. D., Granchi, C., Bussolo, V. D., & Minutolo, F. (2021). Glycoconjugated metal complexes as cancer diagnostic and therapeutic agents. *ChemMedChem, 16*(1), 30–64. https://doi.org/10.1002/cmdc.202000456.

Cai, S., Xie, Y., Bagby, T. R., Cohen, M. S., & Forrest, M. L. (2008). Intralymphatic chemotherapy using a hyaluronan–cisplatin conjugate. *Journal of Surgical Research, 147*(2), 247–252. https://doi.org/10.1016/j.jss.2008.02.048

Chang, R. L., Ueki, I. F., Troy, J. L., Deen, W. M., Robertson, C. R., & Brenner, B. M. (1975). Permselectivity of the glomerular capillary wall to macromolecules. II. Experimental studies in rats using neutral dextran. *Biophysical Journal, 15*(9), 887–906. https://doi.org/10.1016/S0006-3495(75)85863-2

Dhaneshwar, S. S., Kandpal, M., Gairola, N., & Kadam, S. S. (2006). Dextran: a promising macromolecular drug carrier. *Indian Journal of Pharmaceutical Sciences, 68*(6), 705. https://doi.org/10.4103/0250-474X.31000

Goodarzi, N., Varshochian, R., Kamalinia, G., Atyabi, F., & Dinarvand, R. (2013). A review of polysaccharide cytotoxic drug conjugates for cancer therapy. *Carbohydrate Polymers, 92*(2), 1280–1293. https://doi.org/10.1016/j.carbpol.2012.10.036

Haxton, K. J., & Burt, H. M. (2009). Polymeric drug delivery of platinum-based anticancer agents. *Journal of Pharmaceutical Sciences, 98*(7), 2299–2316. https://doi.org/10.1002/jps.21611

Ishak, M. F., & Painter, T. J. (1978). Kinetic evidence for hemiacetal formation during the oxidation of dextran in aqueous periodate. *Carbohydrate Research, 64*, 189–197. https://doi.org/10.1016/S0008-6215(00)83700-3

Khomyakov, K. P., Penenzhik, M. A., Virnik, A. D., & Rogovin, Z. A. (1965). Synthesis of dialdehydo- and dicarboxydextran. *Polymer Science U.S.S.R., 7*(6), 1140–1145. https://doi.org/10.1016/0032-3950(65)90394-1

Kristiansen, K. A., Potthast, A., & Christensen, B. E. (2010). Periodate oxidation of polysaccharides for modification of chemical and physical properties. *Carbohydrate Research, 345*(10), 1264–1271. https://doi.org/10.1016/j.carres.2010.02.011.

Liechty, W. B., Kryscio, D. R., Slaughter, B. V., & Peppas, N. A. (2010). Polymers for drug delivery systems. *Annual Review of Chemical and Biomolecular Engineering, 1*(1), 149–173. https://doi.org/10.1146/annurev-chembioeng-073009-100847

Maia, J., Carvalho, R. A., Coelho, J. F. J., Simões, P. N., & Gil, M. H. (2011). Insight on the periodate oxidation of dextran and its structural vicissitudes. *Polymer, 52*(2), 258–265. https://doi.org/10.1016/j.polymer.2010.11.058

Mehvar, R. (2000). Dextrans for targeted and sustained delivery of therapeutic and imaging agents. *Journal of Controlled Release, 69*(1), 1–25. https://doi.org/10.1016/S0168-3659(00)00302-3

Mehvar, R. (2003). Recent trends in the use of polysaccharides for improved delivery of therapeutic agents: pharmacokinetic and pharmacodynamic perspectives. *Current Pharmaceutical Biotechnology, 4*(5), 283–302. https://doi.org/10.2174/1389201033489685

Mehvar, R., Robinson, M. A., & Reynolds, J. M. (1994). Molecular weight dependent tissue accumulation of dextrans: In vivo studies in rats. *Journal of Pharmaceutical Sciences, 83*(10), 1495–1499. https://doi.org/10.1002/jps.2600831024

Münster, L., Capáková, Z., Fišera, M., Kuřitka, I., & Vícha, J. (2019). Biocompatible dialdehyde cellulose/poly(vinyl alcohol) hydrogels with tunable properties. *Carbohydrate Polymers, 218*, 333–342. https://doi.org/10.1016/j.carbpol.2019.04.091

Münster, L., Fojtů, M., Capáková, Z., Muchová, M., Musilová, L., Vaculovič, T., Balvan, J., Kuřitka, I., Masařík, M., & Vícha, J. (2021). Oxidized polysaccharides for anticancer-drug delivery: what is the role of structure? *Carbohydrate Polymers, 257*, Article 117562. https://doi.org/10.1016/j.carbpol.2020.117562

Münster, L., Fojtů, M., Capáková, Z., Vaculovič, T., Tvrdoňová, M., Kuřitka, I., Masařík, M., & Vícha, J. (2019). Selectively oxidized cellulose with adjustable molecular weight for controlled release of platinum anticancer drugs. *Biomacromolecules, 20*(4), 1623–1634. https://doi.org/10.1021/acs.biomac.8b01807

Münster, L., Hanulíková, B., Machovský, M., Latečka, F., Kuřitka, I., & Vícha, J. (2020). Mechanism of sulfonation-induced chain scission of selectively oxidized polysaccharides. *Carbohydrate Polymers, 229*, Article 115503. https://doi.org/10.1016/j.carbpol.2019.115503

Münster, L., Vícha, J., Klofáč, J., Masař, M., Kucharczyk, P., & Kuřitka, I. (2017). Stability and aging of solubilized dialdehyde cellulose. *Cellulose, 24*(7), 2753–2766. https://doi.org/10.1007/s10570-017-1314-x

Nakashima, M., Ichinose, K., Kanematsu, T., Masunaga, T., Ohya, Y., Ouchi, T., Tomiyama, N., Sasaki, H., & Ichikawa, M. (1999). In vitro characteristics and in vivo plasma disposition of cisplatin conjugated with oxidized and dicarboxymethylated dextrans. *Biological & Pharmaceutical Bulletin, 22*(7), 756–761. https://doi.org/10.1248/bpb.22.756

Ohta, S., Hiramoto, S., Amano, Y., Sato, M., Suzuki, Y., Shinohara, M., … Ito, T. (2016). Production of cisplatin-incorporating hyaluronan nanogels via chelating ligand–metal coordination. *Bioconjugate Chemistry, 27*(3), 504–508. https://doi.org/10.1021/acs.bioconjchem.5b00674

Ohya, Y., Masunaga, T., Baba, T., & Ouchi, T. (1996a). Synthesis and cytotoxic activity of dextran carrying cis-dichloro(cyclohexane-trans-l-1,2-diamine)platinum(II) complex. *Journal of Biomaterials Science, Polymer Edition, 7*(12), 1085–1096. https://doi.org/10.1163/156856296X00570

Ohya, Y., Masunaga, T., Baba, T., & Ouchi, T. (1996b). Synthesis and cytotoxic activity of dextran-immobilizing platinum(II) complex through chelate-type coordination bond. *Journal of Macromolecular Science, Part A, 33*(8), 1005–1016. https://doi.org/10.1080/10601329608010901

Sarwat, F., Qader, S. A. U., Aman, A., & Ahmed, N. (2008). Production & characterization of a unique dextran from an indigenous Leuconostoc mesenteroides CMG713. *International Journal of Biological Sciences, 379–386*. https://doi.org/10.7150/ijbs.4.379

Schechter, B., Neumann, A., Wilchek, M., & Arnon, R. (1989). Soluble polymers as carriers of cis-platinum. *Journal of Controlled Release, 10*(1), 75–87. https://doi.org/10.1016/0168-3659(89)90019-9

Schechter, B., Pauzner, R., Arnon, R., Haimovich, J., & Wilchek, M. (1987). Selective cytotoxicity against tumor cells by cisplatin complexed to antitumor antibodies via carboxymethyl dextran. *Cancer Immunology, Immunotherapy, 25*(3). https://doi.org/10.1007/BF00199151

Schechter, B., Pauzner, R., Wilchek, M., & Arnon, R. (1986). Cis-platinum (II) complexes of carboxymethyl-dextran as potential antitumor agents. II. In vitro and in vivo activity. *Cancer Biochemistry Biophysics, 8*(4), 289–298.

Schechter, B., Rosing, M. A., Wilchek, M., & Arnon, R. (1989). Blood levels and serum protein binding of cis-platinum(II) complexed to carboxymethyl-dextran. *Cancer Chemotherapy and Pharmacology, 24*(3), 161–166. https://doi.org/10.1007/BF00300236

Terry, R., Yuile, C. L., Golodetz, A., Phillips, C. E., & White, R. R. (1953). Metabolism of dextran; a plasma volume expander; studies of radioactive carbon-labeled dextran in dogs. *The Journal of Laboratory and Clinical Medicine, 42*(1), 6–15.

Thorén, L. (1980). The dextrans—Clinical data. *Developments in Biological Standardization, 48*, 157–167.

Varshosaz, J. (2012). Dextran conjugates in drug delivery. *Expert Opinion on Drug Delivery, 9*(5), 509–523. https://doi.org/10.1517/17425247.2012.673580

Vilar, G., Tulla-Puche, J., & Albericio, F. (2012). Polymers and drug delivery systems. *Current Drug Delivery, 9*(4), 367–394. https://doi.org/10.2174/156720112801323053

Wilson, J. J., & Lippard, S. J. (2014). Synthetic methods for the preparation of platinum anticancer complexes. *Chemical Reviews, 114*(8), 4470–4495. https://doi.org/10.1021/cr4004314

ARTICLE II

Štěpánková K., Ozaltin K., Pelková J., Pištěková H., Karakurt I., **Káčerová S**., Lehocký M., Humpolíček P., Vesel A., Mozetic M. Furcellaran surface deposition and its potential in biomedical applications. International Journal of Molecular Sciences. 2022, 23(13),7439. Doi: 10.3390/ijms23137439

International Journal of
Molecular Sciences

MDPI

Article

Furcellaran Surface Deposition and Its Potential in Biomedical Applications

Kateřina Štěpánková [1], Kadir Ozaltin [1], Jana Pelková [2,3], Hana Pištěková [1], Ilkay Karakurt [1], Simona Káčerová [1], Marian Lehocky [1,4,*], Petr Humpolicek [1,4], Alenka Vesel [5] and Miran Mozetic [5]

1 Centre of Polymer Systems, University Institute, Tomas Bata University in Zlín, Trida Tomase Bati 5678, 76001 Zlin, Czech Republic; k1_stepankova@utb.cz (K.Š.); ozaltin@utb.cz (K.O.); pistekova@utb.cz (H.P.); ykarakurt@utb.cz (I.K.); s_kacerova@utb.cz (S.K.); humpolicek@utb.cz (P.H.)
2 Department of Haematology, Tomas Bata Regional Hospital, Havlickovo Nabrezi 2916, 76001 Zlin, Czech Republic; pelkova@utb.cz
3 Faculty of Humanities, Tomas Bata University in Zlín, Stefanikova 5670, 76001 Zlin, Czech Republic
4 Faculty of Technology, Tomas Bata University in Zlín, Vavreckova 5669, 76001 Zlin, Czech Republic
5 Department of Surface Engineering, Jozef Stefan Institute, Jamova cesta 39, 1000 Ljubljana, Slovenia; alenka.vesel@ijs.si (A.V.); miran.mozetic@ijs.si (M.M.)
* Correspondence: lehocky@utb.cz; Tel.: +420-608-616-048

Abstract: Surface coatings of materials by polysaccharide polymers are an acknowledged strategy to modulate interfacial biocompatibility. Polysaccharides from various algal species represent an attractive source of structurally diverse compounds that have found application in the biomedical field. Furcellaran obtained from the red algae *Furcellaria lumbricalis* is a potential candidate for biomedical applications due to its gelation properties and mechanical strength. In the present study, immobilization of furcellaran onto polyethylene terephthalate surfaces by a multistep approach was studied. In this approach, N-allylmethylamine was grafted onto a functionalized polyethylene terephthalate (PET) surface via air plasma treatment. Furcellaran, as a bioactive agent, was anchored on such substrates. Surface characteristics were measured by means of contact angle measurements, X-ray photoelectron spectroscopy (XPS) and scanning electron microscopy (SEM). Subsequently, samples were subjected to selected cell interaction assays, such as antibacterial activity, anticoagulant activity, fibroblasts and stem cell cytocompatibility, to investigate the Furcellaran potential in biomedical applications. Based on these results, furcellaran-coated PET films showed significantly improved embryonic stem cell (ESC) proliferation compared to the initial untreated material.

Keywords: furcellaran; polysaccharide; biopolymer; deposition; cell-surface interaction

Citation: Štěpánková, K.; Ozaltin, K.; Pelková, J.; Pištěková, H.; Karakurt, I.; Káčerová, S.; Lehocky, M.; Humpolicek, P.; Vesel, A.; Mozetic, M. Furcellaran Surface Deposition and Its Potential in Biomedical Applications. *Int. J. Mol. Sci.* **2022**, *23*, 7439. https://doi.org/10.3390/ijms23137439

Academic Editor: Bruce Milthorpe

Received: 7 June 2022
Accepted: 2 July 2022
Published: 4 July 2022

1. Introduction

Polysaccharides, in general, have increasingly attracted attention owing to their excellent antitumor, antioxidant, antibacterial, anti-inflammatory and anticoagulant activities [1]. Moreover, polysaccharides possess remarkable structural specifics for immobilization due to their strong binding to created brushes [2,3]. Coatings containing certain polysaccharides have improved cell adhesion and proliferation [4]. Furcellaran is a typical hybrid carrageenan extracted from the red algae *Furcellaria lumbricalis*. It is negatively charged and composed of units consisting of a fragment (1→3) β-D-galactopyranose with a sulfate group at C-4 and (1→4)-3,6-anhydro-α-D-galactopyranose. Structurally, furcellaran resembles the algal polysaccharide κ-carrageenan, with a major structural difference that only approximately 60% of the D-galactose units are 4-sulfated [5]. The number and position of ester sulfate groups and the content of 3,6-anhydrogalactose (3,6-AG) are the main differences that affect the properties of different carrageenans [6]. Anticoagulant activity and cell proliferation appear to decrease with the presence of a sulfate group in the G-6S position. The positional influence on the anticoagulant activity is ordered

A-2, G-2 > G-4 > G-6. The order of the cytotoxicity of sulfate groups is supposed to be G-6 > G-4 > G-2 > A-2 [7]. Higher levels of ester sulfate results in lower solubility temperature and lower gel strength. One of the important characteristics of these polysaccharides is their ability to form gels in the presence of specific ions, which is associated with a molecular conformational change from the coil to helix [8] and is potentially able to interact with globular proteins, including bovine serum albumin [9] and β-lactoglobulin [10], and fibrous proteins, such as gelatine [11]. The interactions with oppositely charged macroions have gained much attention in biomedical applications. One of the most prominent examples are chitosan based polyelectrolyte complexes which have been revealed to be applicable in drug delivery systems [12,13]. The film-forming ability and the anionic nature of furcellaran also make it possible to establish a binary polyelectrolyte complex with chitosan to obtain binary biopolymer films [14,15]. The properties of biopolymer films can be enriched by the addition of active ingredients, such as plant extracts [16], essential oils [17] and nanomaterials [18].

Polymeric biomaterials that are intended for clinical use must have excellent mechanical properties, as well as adequate surface properties to ensure biocompatibility while interacting with living tissue. The current problem that can be encountered with biomaterials used for implants and other devices may be acute and chronic inflammatory responses, ultimately leading to fibrous capsule formation and thereby impairing normal tissue growth [19,20]. Furthermore, insufficient hemocompatibility due to surface-induced thrombosis or restenosis must be taken into account [21,22]. Further improvements of given materials rely on the precise control of cellular interactions in terms of cell adhesion and proliferation via modification of the biomaterial surface [23]. The surface modification of polymers consists of changes in surface energy, polarity, charge, topography, etc. [24,25].

Therefore, activation procedures have been carried out to make the polymer surface more hydrophilic and obtain specific features by introducing functional groups (carboxylic, hydroxyl, carbonyl, hydroperoxide, etc.) for further covalent bonding with selected agents [26]. The typical surface modification techniques used include chemical vapor deposition, wet chemical methods, UV light radiation, ozone-induced treatment and plasma exposure. Among the physical and chemical methods used to obtain required surfaces without affecting the bulk properties, plasma treatment is an appropriate and efficient technique [27–29]. In addition to the efficiency of immobilization, plasma treatment is able to enhance hydrophilicity and create a high density of functional groups on the surface without the use of toxic chemicals and heat processing. Thus, this method is suitable for many immobilization techniques with biologically active molecules and chemically unstable substrates (including polysaccharides) [30,31].

The plasma-treated polymer results in a negatively charged surface; therefore, subsequent immobilization of a potential anionic polysaccharide is challenging. The negative charge prevents the formation of covalent bonds between the molecule interfaces and polymer surface embedded radicals due to electrostatic repulsive forces. The binding affinity can be increased by reducing the negative charge of the polymer surface. One promising solution might be introducing more positively charged groups through mediators, such as N-allylmethylamine (MAAM). This liquid chemical is able to graft onto a plasma-treated polymer surface by a copolymerization process to create a polymer brush structure with a high density of positively charged amino groups via a radical “surface from” reaction in the gaseous phase [32,33]. Such amine-rich coatings have been studied to control cell behavior, demonstrating a positive effect on cell adhesion, proliferation, and differentiation for different cell types, such as osteoblast-like cells and fibroblasts [34]. Moreover, the advantage of using these functional groups is the possibility of exploiting them for the immobilization of bioactive molecules [35–38].

In the present study, poly(ethylene terephthalate) (PET) was used as a substrate due to its unique mechanical properties, biostability and its moderate inflammatory response. The Biostability of PET is mainly due to the presence of hydrophobic aromatic groups with high crystallinity which restricts hydrolytic breakdown. The low degradability of the PET offers enduring support over time along with ultimate performance during the patient's lifetime. This can also surmount the problems of asynchronous degradation with new tissue regeneration and harmful end products of degraded polymers [39]. Hence, due to these favorable properties, this polyester has been found to be suitable in many biomedical applications, including vascular prostheses, artificial heart valve sewing cuffs, and sutures [40]. However, the hydrophobic nature of PET can be a disadvantage in the case of insufficient cellular interactions at the tissue/biomaterial interface. Furthermore, the biocompatibility of their surfaces is limited due to the lack of reactive functional groups and related long-term anti-thrombogenic demands for in vivo applications [40,41].

This research is the first study dedicated to the description of various furcellaran applications in biomedicine. Moreover, to the best of our knowledge, no study using furcellaran as a polysaccharide film layer for PET functionalization has been reported. The objective of this study is to represent a method for immobilizing furcellaran onto PET surfaces. For this purpose, RF plasma discharge is applied onto the PET surface to create oxidative functional groups for further covalent binding with selected agents. First, MAAM is grafted onto plasma-treated PET to create a high-density polymer brush for improved adhesion interaction properties. Consequently, furcellaran immobilization on such a treated surface is performed. As-prepared substrates are subjected to various selected cell interactions. Namely, the antibacterial activity, anticoagulant activity, fibroblasts and stem cell cytocompatibility of the samples were investigated.

2. Materials and Methods

2.1. Materials and Preparation of PET Films

Polyethylene terephthalate (PET) in rectangle form sheets (55 × 30 mm) was rinsed with distilled water and subsequently dried at room temperature. Monomer N-allylmethylamine (MAAM) was purchased from Sigma–Aldrich (St. Louis, MO, USA). κ-carrageenan (κ-CA) and furcellaran (FUR) of different water gel strengths (Estgel 1000, Estgel 8500) were obtained from Est-Agar AS (Karla, Estonia). The solution was prepared by dissolving 0.1% (*w*/*v*) furcellaran and κ-carrageenan in distilled water. Diiodomethane (99.0%, reagentplus) and formamide (99.5%, molecular biology grade) were supplied by Sigma–Aldrich (St. Louis, MO, USA).

2.2. Plasma Surface Modification and MAAM Grafting

Both sides of the PET films were treated by low-pressure plasma equipment (Diener Electronic, Nagold, Germany) for 60 s at a radio frequency of 13.56 MHz. The discharge matching power was set to 50 W, and the applied air feed rate was 20 sccm (standard cubic centimeter per minute). The pressure inside the chamber was approximately 60 Pa. Some of the plasma-treated PET samples were subsequently immediately exposed to saturated MAAM vapors to achieve radical graft monomer polymerization towards polymer brushes, which are suitable for biological agent immobilization (including polysaccharides). For comparison, the characterization and ensuing treatments of PET samples were also performed without previous MAAM grafting (Figure 1).

2.3. Furcerallan and κ-Carrageenan Immobilization

MAAM grafted and nongrafted PET samples were immersed into a 0.1% (*w*/*v*) solution of κ-CA and FUR for 24 h at room temperature for their immobilization onto a previously prepared polymer brush. After deposition, the samples were removed from the solution and washed in distilled water to remove residual unbound polysaccharide content. Finally, the samples with immobilized polysaccharide layers were dried overnight at room temperature.

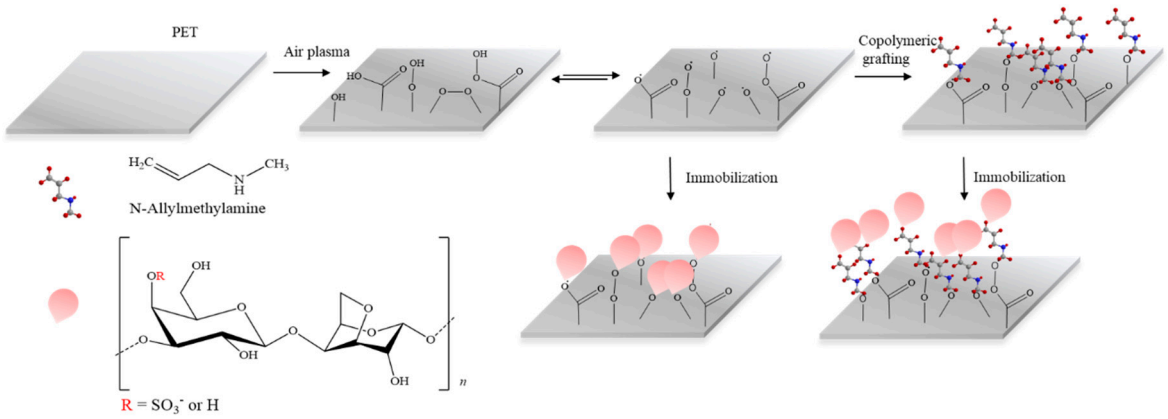

Figure 1. Schematic representation of plasma postirradiation grafting of N-allylmethylamine onto a PET surface followed by immobilization of FUR or κ-CA polysaccharide.

2.4. Contact Angle Measurement and Surface Energy Evaluation

The surface wettability was evaluated by the water sessile drop contact angle method via a SEE system (by Advex Instruments, Brno, Czech Republic). Lewis acid-base parameters of the surface free energy of the samples were evaluated from contact angle values using appropriate testing liquids, i.e., water, diiodomethane, formamide [42]. Five separate readings for each liquid were averaged to obtain representative contact angle values, which were used for surface free energy evaluation for each surface.

Droplets of testing liquid with a volume of 5 μL were placed onto each sample and captured by a CCD camera system. This droplet volume was set for several reasons. The most important factor was the fact that larger drops are deformed by gravity. Smaller drops give results with higher measurement errors.

2.5. X-ray Photoelectron Spectroscopy

The chemical composition was analyzed with X-ray photoelectron spectroscopy (XPS) using TFA (Physical Electronics, Chanhassen, MN, USA) with MultiPak software to determine the concentration of elements. The samples were irradiated with X-rays with a 400 μm spot size generated with monochromatic Al Kα1,2 radiation at 1486.6 eV. The emitted photoelectrons were detected with a hemispherical analyzer placed at an angle of 45° relative to the normal plane of the sample surfaces.

2.6. SEM Evaluation

The surface morphology of each sample was monitored by a NANOSEM 450 (FEI, Thermo Fisher Scientific, Hillsboro, OR, USA) scanning electron microscope operated at 5 kV with an Everhart–Thomley detector (ETD). The images were obtained at a magnification of 20,000×. The samples were coated with Au/Pt prior to observation.

2.7. Evaluation of Antibacterial Activity

The antibacterial activity was determined according to a modified version of the ISO 22196 standard for investigation of the antibacterial effect on modified plastic materials. First, all samples were sterilized by UV radiation and then placed in sterile Petri dishes. Standardized bacterial suspensions of *Escherichia coli* (CCM 4517) and *Staphylococcus aureus* (CCM 2022) were prepared in 1/500 nutrient broth and diluted to obtain a certain bacterial concentration between 2.5×10^5 cells/ml and 10×10^5 cells/ml. Thus, the prepared solutions were used as the test inoculum, which was dispensed onto each sample (25×25 mm) in a volume of 0.4 mL. Subsequently, the samples were covered with ethanol-disinfected polypropylene foil (PP) (20×20 mm^2) and incubated at 35 °C and 95% relative humidity for 24 h. After the incubation period, each sample with PP films was washed with 10 mL of SCDLP broth (HiMedia Laboratories, Mumbai, India) to determine the recovery

rate of the bacteria. The recovered bacterial suspensions were subjected to 10-fold serial dilutions. The viable bacteria count was evaluated by the pour plate culture method after 24 h of incubation.

2.8. Evaluation of Anticoagulant Activity

Blood was obtained by venous puncture from a healthy donor in accordance with the Helsinki Declaration and placed into blood collection tubes (VACUETTE, Greiner Bio-One, Kremsmünster, Austria) covered by prepared PET samples. The obtained human blood plasma was treated with 3.2% citric acid (109 mmol/L) and then centrifuged at room temperature for 15 min at 3000 min. The anticoagulant activity was determined by means of prothrombin time (PT), thrombin time (TT) and activated partial thromboplastin time (aPTT) using a SYSMEX CA-1500 (Siemens, Munich, Germany) instrument. Each of the samples was examined three times.

2.9. In Vitro Fibroblast Cytocompatibility

The cytotoxicity was tested using a mouse embryonic fibroblast cell line (NIH/3T3, ATCC®CRL-1658TM, Manassas, VA, USA) according to the EN ISO 10993-5 standard with some modifications. The tested samples with dimensions of 10 × 10 mm were exposed to UV radiation (wavelength of 253.7 nm; 30 min) for sterilization. ATCC-formulated Dulbecco's modified Eagle's medium (BioSera, Nuaille, France) containing 10% calf serum (BioSera, Nuaille, France) and 100 U mL^{-1} penicillin/streptomycin (BioSera, Nuaille, France) was used as the culture medium. The cells were seeded onto samples at a concentration of 2 × 10^4 cells per mm^2 and incubated at 37 ± 1 °C for 72 h. After 72 h of cell culture, the cell viability was evaluated using the 3-(4,5-dimethylthiazol-2-yl)-2,5-diphenyltetrazolium bromide (MTT) assay (Duchefa Biochemie, Amsterdam, The Netherlands). First, the culture medium was removed, and 100 µL of growth medium containing MTT dye solution (5 mg/mL in PBS) was added to the cultures. Then, the cells were incubated at 37 °C in a humidified atmosphere for 4 h. Following the removal of the growth medium, DMSO (Sigma–Aldrich, St. Louis, MO, USA) was added to dissolve the formed formazan crystals on the sample surface. The absorbance was measured using an Infinite M200 Pro NanoQuant absorbance reader (Tecan, Männedorf, Switzerland) at wavelengths of 570 nm (test) and 690 nm (reference). The reported values are the means of three replicates and are expressed as percentages of the control value.

2.10. In Vitro Stem Cell Cytocompatibility

The embryonic stem cell line ES R1 was propagated in an undifferentiated state by culturing on two series of prepared samples. One series was coated with 0.1% gelatine, and the other was not. Dulbecco's Modified Eagle's Medium with high glucose, pyruvate, 16.5% calf serum (all from Gibco, Thermo Fisher Scientific, Inc., Waltham, MA, USA), 1% penicillin/streptomycin (GE Healthcare HyClone, HyClone Ltd., Cramlington, UK), 100 mM nonessential amino acids (Gibco, Thermo Fisher Scientific, Inc., Waltham, MA, USA), 0.05 mM b-mercaptoethanol (Sigma–Aldrich, St. Louis, MO, USA), and leukemia inhibitory factor (Chemicon International, Temecula, CA, USA) at a concentration of 5 ng.mL-1 was used as the culture medium. First, both sides of the prepared samples were sterilized by UV light for 30 min. Then, the cell suspension was seeded on the tested samples at a concentration of 20,000 cells per mL and incubated at 37 °C in 5% CO_2 in humidified air. After 120 h (5 days) of proliferation, the cells were fixed and stained to visualize the DNA with Hoechst 33258 (Molecular Probes, Carlsbad, CA, USA) and observed by fluorescence microscopy using an Olympus IX 81 inverted phase-contrast microscope (Olympus, Hamburg, Germany). An MTT proliferation test was performed. All tests were performed in four separate sets. Statistical significance was determined by ANOVA with post hoc Tukey's multiple comparison test, * $p < 0.05$, ** $p < 0.01$, *** $p < 0.001$

3. Results and Discussion

3.1. Surface Wettability Investigations

Wettability changes resulting from surface modifications were determined from contact angle data for various testing liquids and are shown in Table 1. The hydrophobic nature and lack of functional groups of untreated PET are reflected in the high values of the contact angle. After air plasma treatment, the contact angle values sharply decreased due to the presence of oxidative functional groups introduced onto the PET surface and tailoring of the surface morphology, referring to the increased hydrophilicity and surface energy suitable for further immobilization. The hydrophobicity of immobilized FUR and κ-CA samples grafted onto polymer brushes increased but remained less hydrophobic than untreated PET. In comparison to the films without MAAM, no noticeable change occurred. In addition, modification effects on the surface were observed with respect to the Lewis acid-base properties of the samples. For the γ_s of untreated PET foil, low values were calculated due to its low surface wettability. The value of γ_s after air plasma exposure seemed to be distinctly higher, indicating that the surface had a relatively significant polarity. Variations between the γ_s values of plasma-treated PET and immobilized PET were not significant. The results indicate successful immobilization of FUR and κ-CAR onto the PET surface, as subsequently demonstrated in detail by XPS.

Table 1. Contact angles (θ) (w: deionized water; d: diiodomethane; f: formamide) and surface free energy parameters of probe liquids used in the acid-base method (γg total surface fee energy, apolar γsLW, polar γsAB, Lewis acid γs+ and base γs- components). PET is the virgin polyethylene terephthalate sample, PET_DC is the PET sample treated in discharge and PET_MAAM is the PET_DC sample after grafting with N-allylmethylamine. MAAM_1000, MAAM_8500 and MAAM_KAPA are samples in which selected polysaccharides were immobilized on the PET_MAAM sample. DC_1000, DC_8500 and DC_KAPA indicate samples in which selected polysaccharides were immobilized on the PET_DC sample.

	Contact Angles (°) for Liquids			Surface Free Energy Parameters (mJ/m^2)				
SAMPLE	θ_w	θ_d	θ_f	γ_s	γ_s^{LW}	γ_s^{AB}	γ_s^{+}	γ_s^{-}
PET	63.27 ± 3.08	26.63 ± 0.54	53.72 ± 0.95	50.17	45.55	4.62	0.24	22.10
PET_DC	30.25 ± 3.40	25.57 ± 0.61	8.97 ± 1.15	57.64	45.95	11.72	0.88	38.80
PET_MAAM	33.71 ± 1.83	30.76 ± 0.38	12.22 ± 2.62	57.08	43.90	13.18	1.22	35.70
MAAM_1000	40.94 ± 1.74	27.78 ± 2.91	17.8 ± 2.81	56.28	45.11	11.17	1.07	29.27
MAAM_8500	47.33 ± 1.95	32.02 ± 2.36	20.18 ± 2.05	55.32	43.36	11.96	1.59	22.52
MAAM_KAPA	49.19 ± 2.0	28.16 ± 1.15	18.73 ± 2.28	56.11	44.98	11.13	1.55	20.02
DC_1000	36.75 ± 1.35	18.06 ± 1.55	12.08 ± 2.03	57.98	48.33	9.65	0.71	32.62
DC_8500	47.08 ± 2.25	21.67 ± 0.80	10.99 ± 1.46	58.35	47.27	11.07	1.49	20.61
DC_KAPA	46.71 ± 0.99	26.82 ± 1.94	11.28 ± 1.69	57.72	45.48	12.24	1.79	20.97

3.2. Surface Chemistry Investigations

The prepared samples with the different surface treatments were investigated by the XPS method, and their elemental compositions are shown in Table 2. As expected, the surface of reference PET revealed a maximum content of carbon of 74.6% and an oxygen level of 25.4%. The chemical composition induced by plasma treatment showed a considerable increase in the level of oxygen due to the incorporation of oxidized functionalities. Nitrogen content of 1.5% might be formed during the plasma treatment process. Nevertheless, the highest contents of nitrogen were observed for MAAM-grafted samples as a result of the amine groups present in the reagent, but a proportional decrease in the oxygen level was noted. In contrast, the specimens that were not treated with MAAM had slightly higher oxygen levels. The most important result was the sulfur content presence, which was detected for the samples MAAM_KAPA, DC_1000, DC_8500 and DC_KAPA. The sulfur and oxygen contents indicate the successful immobilization of polysaccharides despite the sulfur quantities being relatively low.

Table 2. Surface elemental compositions of the samples (%) from XPS measurements.

SAMPLE	C	N	O	S
PET	74.6		25.4	
PET_DC	69.3	1.5	29.3	
PET_MAAM	69.8	2.1	28.1	
MAAM_8500	73.7	1.0	25.3	
MAAM_1000	74.6	1.0	24.5	
MAAM_KAPA	74.2	0.9	24.8	0.2
DC_1000	70.0		29.7	0.3
DC_8500	73.9	0.6	25.5	0.1
DC_KAPA	72.7	0.7	26.5	0.1

3.3. SEM Imaging

The surface morphology was examined by means of SEM performed with an Everhart–Thomley detector without a conductive coating of the samples and represented at a 10 µm resolution. The results are shown in Figure 2a–i, where the reference PET exhibits a homogenous, relatively smooth surface morphology. Among the polysaccharide-immobilized surfaces, the furcellaran-coated PET (Figure 2d,e,g,h) showed a more homogenously distributed layer, which allowed uniform adhesion of fibroblasts and their proliferation on the surface [43]. In contrast, the PET surface coated with κ-carrageenan (Figure 2i) had a rather heterogeneous nature, which may alter the behavior of cells adhering to the substrates. Similarly, an inhomogeneous and rough morphology was observed on the MAAM-grafted PET surface, where such characteristics are desired for further immobilization [44].

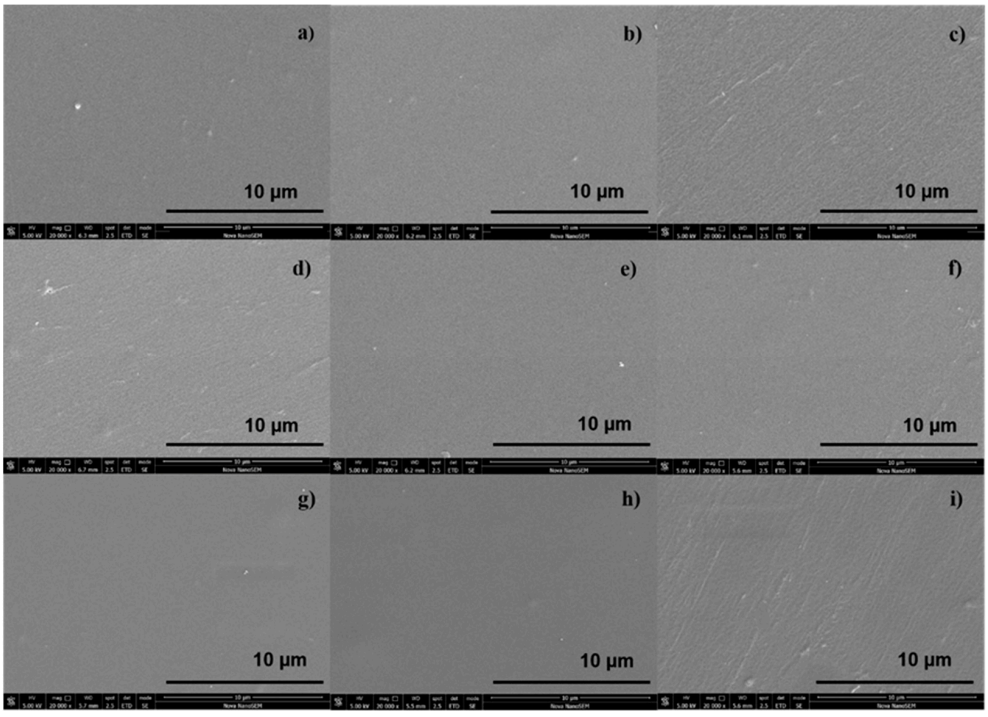

Figure 2. SEM images of (**a**) untreated PET, (**b**) PET_DC, (**c**) DC_MAAM, (**d**) MAAM_1000, (**e**) MAAM_8500, (**f**) MAAM_KAPA, (**g**) DC_1000, (**h**) DC_8500 and (**i**) DC_KAPA.

3.4. Antibacterial Analysis

The antibacterial activity levels of PET films against *Staphylococcus aureus* and *Escherichia coli* strains were evaluated by the number of viable cells calculated in the agar plates after 24 h of incubation. As shown in Table 3, a very low antibacterial effect was displayed by the immobilized samples compared to the PET reference. There are few reports about the antimicrobial effects of carrageenans. Yamashita et al. evaluated the antimicrobial

actions of three types of carrageenans (ι, λ, κ) and showed their significant inhibitory effect on almost all bacterial strains studied. The study also indicated that the removal of sulfate residues eliminates the bacteriostatic effect of ι-carrageenan, suggesting that the sulfate residues in carrageenans play an essential role in this effect. Furthermore, the addition of carrageenan significantly lowered the growth rate of bacteria in a concentration-dependent manner, although the effect was bacteriostatic rather than bactericidal. However, the inhibitory activity is unlikely to have been dependent on the sulfate content alone but on the inhibitory mechanism itself, which needs to be studied further. Another study [45] showed that oxidized κ-carrageenan could suppress the growth of both gram-positive and gram-negative bacteria. However, this was not the case for natural κ-carrageenan, which does not exhibit any antibacterial activity. PVA-κ-carrageenan films crosslinked with glutaraldehyde have no effect on the antibacterial performance unless they are loaded with antibacterial drugs [46]. Based on the mentioned studies, the lower sulfate content of furcellaran and the unmodified nature of immobilized polysaccharides overall may contribute only to the reduced growth-inhibitory effect. In addition, the amounts of immobilized furcellaran and κ-carrageenan on the PET surface associated with the minimum inhibitory concentration (MIC) might also be the reason for the insufficient antibacterial activity.

Table 3. Viable bacteria numbers on PET surfaces; antibacterial effect (R) values are expressed in CFU.

SAMPLE	*Staphylococcus aureus* CCM 2020		*Escherichia coli* CCM 4517	
	N (cfu/cm^2)	R	N (cfu/cm^2)	R
PET	1.1×10^4	0	9.8×10^5	0
PET_DC	1.1×10^4	−0.02	8.9×10^5	0.05
PET_MAAM	1.1×10^4	−0.02	8.3×10^5	0.07
MAAM_1000	1.2×10^4	−0.04	5.8×10^5	0.22
MAAM_8500	1.2×10^4	−0.05	8.6×10^5	0.05
MAAM_KAPA	4.6×10^3	0.38	9.5×10^5	0.01
DC_1000	8.1×10^3	0.14	8.2×10^5	0.07
DC_8500	2.4×10^4	−0.34	7.1×10^5	0.14
DC_KAPA	8.6×10^3	0.11	5.8×10^5	0.12

Along with the presence of the sulfate group, the antibacterial activity of polysaccharides can be enhanced via chemical modification by incorporating other functional groups, such as carboxylic and carboxymethyl groups, aldehyde, amine, alkylamine, and quaternary ammonium groups. The hydroxyl groups can be also grafted with organic moieties offering extra functional groups to improve bioactivities according to the given application [47,48]. Based on these results, furcellaran is not considered as promising an antibacterial component as some natural polysaccharides, for instance, chitosan [49], chondroitin sulfate [27] or fucoidan [50].

3.5. Anticoagulant Activity Assessment

The anticoagulant activity of PET samples was evaluated by thrombin time (TT), prothrombin time (PT) and activated partial thromboplastin time (aPTT) coagulation assays, and the obtained results are summarized in Table 4.

In general, the blood coagulation system is divided into two initiating pathways: the tissue factor (extrinsic) pathway and the contact factor (intrinsic) pathway. These pathways meet in a final common pathway where factor Xa converts prothrombin to thrombin, which then cleaves fibrinogen to fibrin monomers.

PT is a functional measure of the extrinsic and common pathways, and the physiological value is in the range of 11–13.5 s. As seen, all samples are within the range, meaning that the extrinsic pathway of coagulation was not inhibited by any of the tested samples. These data are consistent with a study on the anticoagulant activity of major types of carrageenans [6].

Table 4. Anticoagulation activity results; PT: prothrombin time; aPTT: activated partial thromboplastin time; TT: thrombin time.

SAMPLE	PT (s)	aPTT (s)	TT (s)
PET	12.0	29.1	18.0
PET_DC	12.6	32.8	20.1
PET_MAAM	12.6	30.5	18.5
MAAM_1000	12.1	28.8	18.4
MAAM_8500	12.4	30.6	18.6
MAAM_KAPA	12.3	29.7	18.9
DC_1000	13.0	32.5	18.7
DC_8500	13.3	33.4	19.7
DC_KAPA	12.3	33.9	20.5

aPPT is a functional measure of the intrinsic pathway as well as the common pathway, and the reference range is between 22 and 33 s. As the results show, the clotting times of samples PET_DC_8500 and PET_DC_KAPA were slightly prolonged, and therefore, interfered with the intrinsic coagulation process.

TT is a measure of functional fibrinogen in plasma, and for healthy donors, the clotting time range is between 12.5 and 19 s. PET_DC_KAPA displayed the highest value of clotting time and thereby mildly exceeded the threshold for anticoagulant activity. As follows, plasma-treated PET exhibited a prolonged time over the threshold. The hydrophilic surface achieved by plasma treatment may be associated with lower protein adsorption and the activation of blood components. Another factor influencing protein adsorption on hydrophilic surfaces is the type of charge. Negatively charged surfaces typically lead to a lower extent of protein adsorption than positively charged surfaces because many proteins have a net negative charge at physiological pH values [51]. These reports correspond with the fact that the presence of sulfate groups in furcellaran and κ-carrageenan might be attributed to the change in the negative charge density and influence its interactions with the coagulation proteins.

Thus, higher values were observed in plasma-treated PET and polysaccharide-immobilized samples in combination with plasma treatment, which correlated with the content of sulfates and hydrophilic surfaces [47–50]. However, samples treated with MAAM had a negative impact on anticoagulant activity. It is worth noting that none of the samples extended beyond anticoagulation action. In many cases, the prolongation of clotting time is dose-dependent [51,52]. With respect to the abovementioned, a slight anticoagulant effect was observed in the case of sample PET_DC_KAPA. However, it must be taken into account that the effect is not as significant as in the case of other sulfated polysaccharides [28].

3.6. In Vitro Fibroblast Cytocompatibility

The cytotoxicity of individual samples was evaluated using a mouse embryonic fibroblast cell line (NIH/3T3) according to the ISO 10993-5 standard. Cytotoxicity tests are the first option when the biocompatibility of materials, including polymers, is assessed. Measurements were performed in triplicate with untreated PET as a reference. Error bars represent standard deviations. Figure 3 shows that all values obtained from the relative cytotoxicity test were above 80%. Overall, the cell viability of samples functionalized with MAAM and polysaccharides (FUR, κ-CA) increased in comparison with samples treated only with plasma, and all materials can be considered nontoxic. This was also confirmed in Figure 4a–i, where cells were growing homogeneously, and all samples were assigned as cytocompatible. The biological response to any material is affected by its various surface properties. Hydrophobicity, roughness, homogeneity or functional groups belong to important factors affecting cell adhesion and proliferation. Many studies indicated that cells tended to attach to hydrophilic surfaces [44]. On the other side, it has been reported that cells adhered and proliferated at the highest rate when cultured on a hydrophobic surface or a contact angle of around 70 degrees [53]. This may be the explanation for why untreated PET showed the best proliferation results. As expected, the cell prolifera-

tion effect of furcellaran coated samples is consistent with previous studies of other seaweed polysaccharides [54–56].

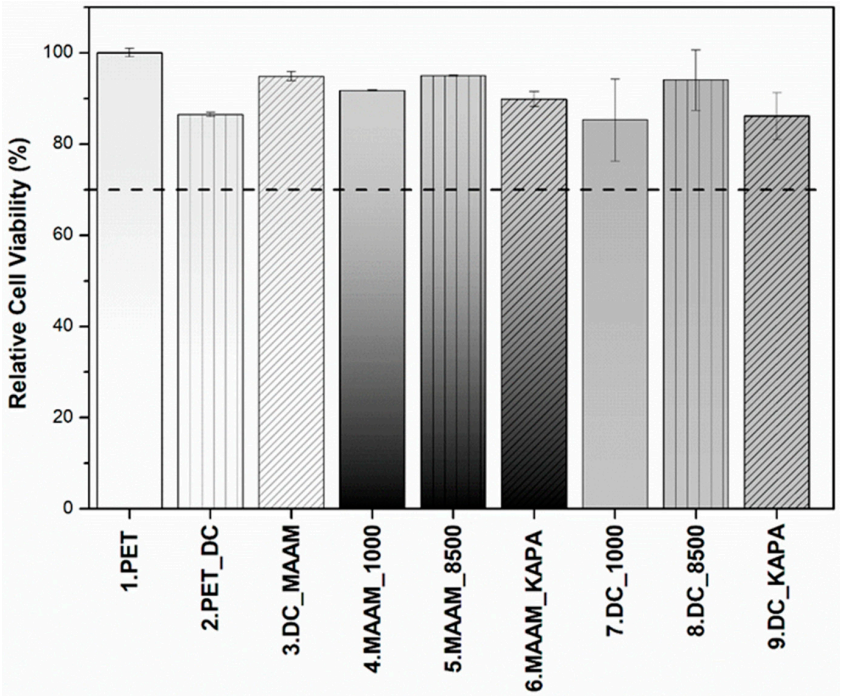

Figure 3. Relative cell viability of cells incubated with PET films coated with furcellaran of different water gel strengths (1000, 8500) and κ-carrageenan tested on a mouse embryonic fibroblast cell line (NIH/3T3).

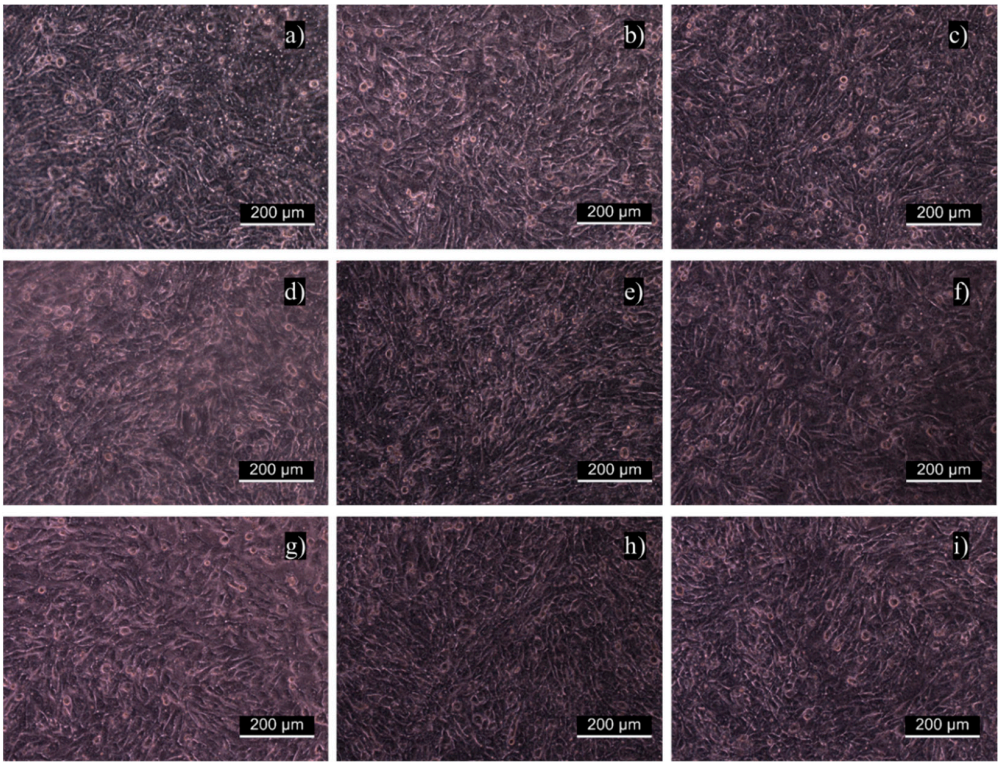

Figure 4. Fibroblast proliferation on examined samples: (**a**) untreated PET, (**b**) PET_DC, (**c**) DC_MAAM, (**d**) MAAM_1000, (**e**) MAAM_8500, (**f**) MAAM_KAPA, (**g**) DC_1000, (**h**) DC_8500 and (**i**) DC_KAPA.

3.7. Evaluation of Cell Viability in the ES R1 Cell Line

Examples of versatile, non-animal derived and inexpensive materials that are able to support the proliferation of ESCs are limited. Many of the new biomaterials used to develop stem cell microenvironments use biopolymers adsorbed or covalently immobilized to the surface to improve the biocompatibility of synthetic polymers [57]. Furcellaran coated PET samples were suggested as a potential candidate to promote the proliferation of ESC. Embryonic stem cells proliferated on uncoated and gelatine-coated samples for 5 days. As shown in Figure 5A, there was no significant difference in cell viability between the reference (cells cultivated on TPP plastic) and PET. Figure 5B shows cell viability on TPP plastic coated with gelatine (reference) and PET coated with gelatine. The results did not indicate a significant difference in cell viability. Therefore, PET was deemed to be a good material for cell cultivation and was considered a reference in subsequent testing (Figure 5C,D). The polymerization of N-allylmethylamine (MAAM) onto plasma-treated PET films was performed to introduce amine (-NH_2) functional groups and reveal the optimum polymer brush for the immobilization of the tested polysaccharides. Amine groups are known to promote cell adhesion because of their positive charges, which can attract negatively charged biomolecules, such as proteins under physiological conditions. It was expected that MAAM-treated samples would demonstrate increased cell proliferation due to a higher quantity of polysaccharide agents immobilized. As shown in Figure 5C, there was a significant reduction in cell viability on sample MAAM_8500. One possible explanation for this observation is the correlation between the gel strength of FUR 8500 and insufficient interaction with the amine groups of MAAM. The gel strength of FUR 8500 was lower than that of FUR 1000, which also corresponded to the lower content of 3,6-anhydro-D-galactose residues. The amount of these units could adversely affect the immobilization of FUR 8500. In general, the existence of MAAM polymer brushes was revealed; however, intramolecular interactions between grafted polymer brushes and polysaccharides might not be sufficient for immobilization, and therefore, negatively influence subsequent interactions with ESC. However, the most important result is that for samples DC_8500 (Figure 6B) and DC_KAPA, ESC proliferation was significantly increased compared to that of the reference PET (Figure 5A). This might be a result of sufficient polysaccharide immobilization. Thus, more polysaccharide on the surface is able to enhance the proliferation of ESCs. All of the samples coated with gelatine (Figure 6D) did not show a cytotoxic effect, except sample MAAM_8500_G.

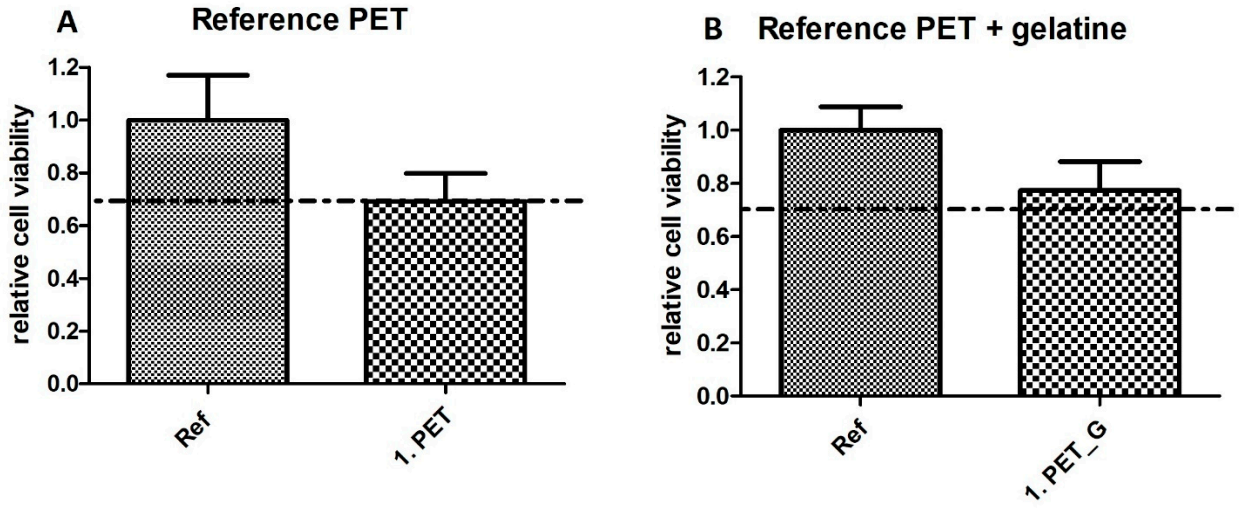

Figure 5. *Cont.*

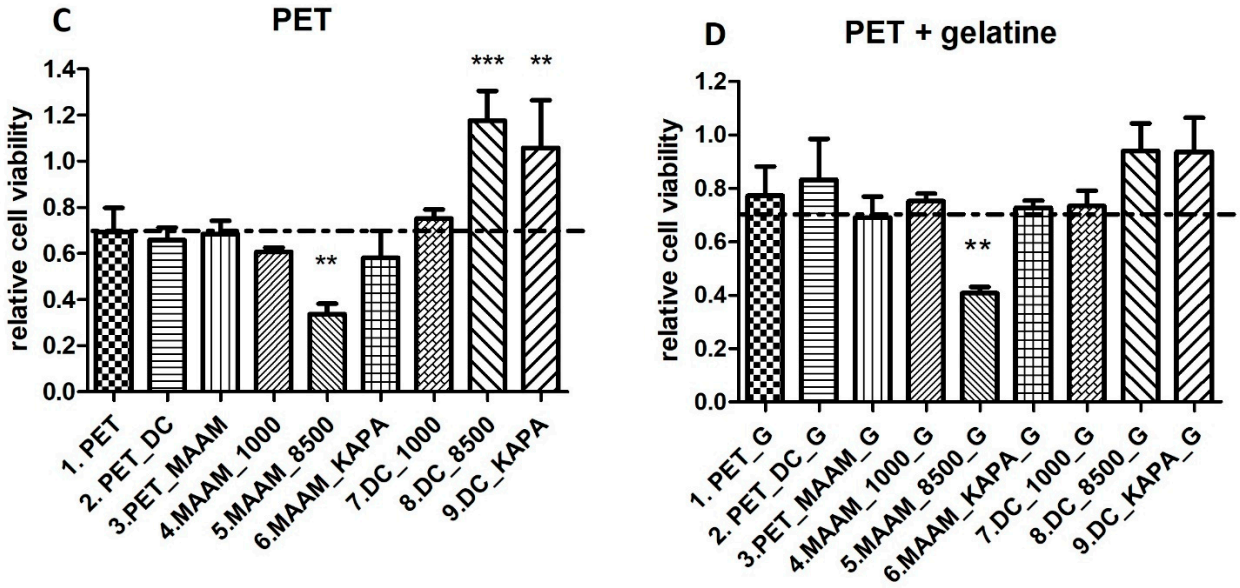

Figure 5. Cell viability of individual samples. The dashed line highlights the limit of viability according to EN ISO 10993-5: viability < 0.7 corresponds to a cytotoxic effect. (**A**) Comparison of reference (cells on TPP plastic) and PET; (**B**) Comparison of reference (cells on TPP plastic coated with gelatine) and PET coated with gelatine; (**C**) Comparison of PET as a reference and samples; (**D**) Comparison of PET coated with gelatine as a reference and samples also coated with gelatine. Data are reported as the means and standard deviations from a minimum of four independent experiments. To determine significant differences between samples ANOVA with post hoc Tukey's Multiple Comparison test was used; ** $p < 0.01$, *** $p < 0.001$.

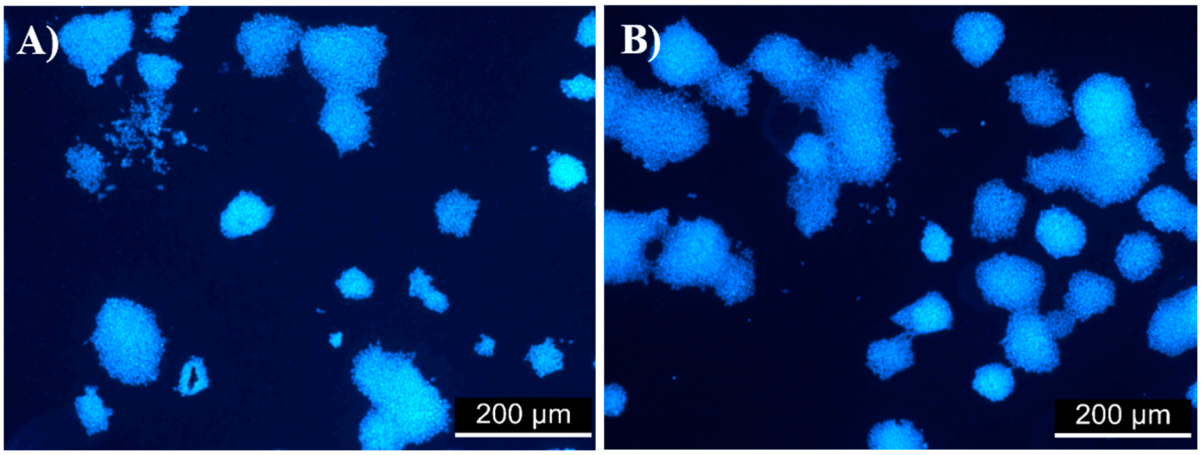

Figure 6. Mouse embryonic cells (Line R1) on (**A**) PET uncoated with 0.1% gelatine and (**B**) DC 8500 uncoated with 0.1% gelatine after 120 h of cultivation.

4. Conclusions

In this work, furcellaran deposition onto a PET surface via RF air plasma discharge activation followed by grafting of a MAAM monomer was studied. The successful immobilization of polysaccharides onto grafted and nongrafted MAAM monomer brushes was confirmed by the contact angle and XPS results, where the surface wettability of the resultant films increased compared to the PET reference, and the sulfur content characteristic of the tested polysaccharides was detected. SEM images of coated PET samples demonstrated a rather microtextured homogenously distributed layer, which had positive effects on the uniform adhesion and proliferation of fibroblasts and thus exhibited nontoxicity for all

functionalized samples. All samples had minor effects on the antibacterial activity and blood coagulation, as indicated by the clotting times of APPT, PT and TT.

However, MAAM nongrafted samples of immobilized FUR significantly increased ESC proliferation, in contrast to the MAAM grafted ones. The low ESC proliferation rate for MAAM grafted samples might be due to the insufficient interaction of polysaccharides with amine groups. The obtained data for furcellaran were compared with the results for κ-carrageenan. These preliminary results show that furcellaran itself has significant biomedical application prospects and paves the way for future investigations.

Author Contributions: Conceptualization, K.O., M.M., P.H. and M.L.; Methodology, K.O., J.P., H.P., M.M., I.K. and P.H.; Formal analysis, K.Š., K.O., S.K., J.P., H.P. and A.V.; investigation, I.K., K.Š, K.O., S.K., J.P., H.P. and A.V.; data curation, K.Š., S.K., H.P., J.P. and A.V.; writing—original draft preparation, K.Š. and M.L.; writing—review and editing, K.Š. and M.M.; supervision, M.L.; project administration, M.L.; funding acquisition, M.L., P.H. and M.M. All authors have read and agreed to the published version of the manuscript.

Funding: The authors thank the Internal Grant Agency of Tomas Bata University in Zlín, Czech Republic (IGA/CPS/2022/001), and the Ministry of Education, Youth and Sports of the Czech Republic, projects: DKRVO (RP/CPS/2022/001) and (RP/CPS/2022/002). Authors M.M. and A.V. acknowledge the financial support from the Slovenian Research Agency (research core funding No. P2-0082 and project L2-3163 "DemoCat"). Author P.H. acknowledges the Czech Science Foundation grant (20-28732S).

Institutional Review Board Statement: Not applicable.

Informed Consent Statement: Not applicable.

Data Availability Statement: The data presented in this study are available upon reasonable request from the corresponding author.

Conflicts of Interest: The authors declare no conflict of interest.

References

1. Fasl, H.; Stana, J.; Stropnik, D.; Strnad, S.; Stana-Kleinschek, K.; Ribitsch, V. Improvement of the Hemocompatibility of PET Surfaces Using Different Sulphated Polysaccharides as Coating Materials. *Biomacromolecules* **2010**, *11*, 377–381. [CrossRef] [PubMed]
2. Muhamad, I.I.; Zulkifli, N.; Selvakumaran, S.A.P.; Lazim, N.A.M. Bioactive Algal-Derived Polysaccharides: Multi-Functionalization, Therapeutic Potential and Biomedical Applications. *CPD Curr. Pharm. Des.* **2019**, *25*, 1147–1162. [CrossRef] [PubMed]
3. Xu, S.-Y.; Huang, X.; Cheong, K.-L. Recent Advances in Marine Algae Polysaccharides: Isolation, Structure, and Activities. *Mar. Drugs* **2017**, *15*, 388. [CrossRef]
4. Lee, Y.-E.; Kim, H.; Seo, C.; Park, T.; Lee, K.B.; Yoo, S.-Y.; Hong, S.-C.; Kim, J.T.; Lee, J. Marine Polysaccharides: Therapeutic Efficacy and Biomedical Applications. *Arch. Pharm. Res.* **2017**, *40*, 1006–1020. [CrossRef] [PubMed]
5. Ghanbarzadeh, M.; Golmoradizadeh, A.; Homaei, A. Carrageenans and Carrageenases: Versatile Polysaccharides and Promising Marine Enzymes. *Phytochem. Rev.* **2018**, *17*, 535–571. [CrossRef]
6. Silva, F.R.F.; Dore, C.M.P.G.; Marques, C.T.; Nascimento, M.S.; Benevides, N.M.B.; Rocha, H.A.O.; Chavante, S.F.; Leite, E.L. Anticoagulant Activity, Paw Edema and Pleurisy Induced Carrageenan: Action of Major Types of Commercial Carrageenans. *Carbohydr. Polym.* **2010**, *79*, 26–33. [CrossRef]
7. Liang, W.; Mao, X.; Peng, X.; Tang, S. Effects of Sulfate Group in Red Seaweed Polysaccharides on Anticoagulant Activity and Cytotoxicity. *Carbohydr. Polym.* **2014**, *101*, 776–785. [CrossRef]
8. van de Velde, F.; Rollema, H.S.; Grinberg, N.V.; Burova, T.V.; Grinberg, V.Y.; Tromp, R.H. Coil-Helix Transition of ?-Carrageenan as a Function of Chain Regularity. *Biopolymers* **2002**, *65*, 299–312. [CrossRef]
9. Jamróz, E.; Para, G.; Jachimska, B.; Szczepanowicz, K.; Warszyński, P.; Para, A. Albumin–Furcellaran Complexes as Cores for Nanoencapsulation. *Colloids Surf. A Physicochem. Eng. Asp.* **2014**, *441*, 880–884. [CrossRef]
10. Laos, K.; Brownsey, G.; Ring, S. Interactions between Furcellaran and the Globular Proteins Bovine Serum Albumin and β-Lactoglobulin. *Carbohydr. Polym.* **2007**, *67*, 116–123. [CrossRef]
11. Jamroz, E.; Konieczna-Molenda, A.; Para, A. Ternary Potato Starch-Furcellaran-Gelatin Film—A New Generation of Biodegradable Foils. *Polimery* **2017**, *62*, 673–679. [CrossRef]
12. Alsharabasy, A.M.; Moghannem, S.A.; El-Mazny, W.N. Physical Preparation of Alginate/Chitosan Polyelectrolyte Complexes for Biomedical Applications. *J. Biomater. Appl.* **2016**, *30*, 1071–1079. [CrossRef] [PubMed]

13. Seal, B.L.; Panitch, A. Physical Polymer Matrices Based on Affinity Interactions between Peptides and Polysaccharides. *Biomacromolecules* **2003**, *4*, 1572–1582. [CrossRef] [PubMed]
14. Jamróz, E.; Janik, M.; Juszczak, L.; Kruk, T.; Kulawik, P.; Szuwarzyński, M.; Kawecka, A.; Khachatryan, K. Composite Biopolymer Films Based on a Polyelectrolyte Complex of Furcellaran and Chitosan. *Carbohydr. Polym.* **2021**, *274*, 118627. [CrossRef]
15. Meka, V.S.; Sing, M.K.G.; Pichika, M.R.; Nali, S.R.; Kolapalli, V.R.M.; Kesharwani, P. A Comprehensive Review on Polyelectrolyte Complexes. *Drug Discov. Today* **2017**, *22*, 1697–1706. [CrossRef]
16. Jamróz, E.; Kulawik, P.; Guzik, P.; Duda, I. The Verification of Intelligent Properties of Furcellaran Films with Plant Extracts on the Stored Fresh Atlantic Mackerel during Storage at 2 °C. *Food Hydrocoll.* **2019**, *97*, 105211. [CrossRef]
17. Jamróz, E.; Juszczak, L.; Kucharek, M. Investigation of the Physical Properties, Antioxidant and Antimicrobial Activity of Ternary Potato Starch-Furcellaran-Gelatin Films Incorporated with Lavender Essential Oil. *Int. J. Biol. Macromol.* **2018**, *114*, 1094–1101. [CrossRef]
18. Jamróz, E.; Khachatryan, G.; Kopel, P.; Juszczak, L.; Kawecka, A.; Krzyściak, P.; Kucharek, M.; Bębenek, Z.; Zimowska, M. Furcellaran Nanocomposite Films: The Effect of Nanofillers on the Structural, Thermal, Mechanical and Antimicrobial Properties of Biopolymer Films. *Carbohydr. Polym.* **2020**, *240*, 116244. [CrossRef]
19. Anderson, J.M.; Miller, K.M. Biomaterial Biocompatibility and the Macrophage. *Biomaterials* **1984**, *5*, 5–10. [CrossRef]
20. Hubbell, J.A. Biomaterials in Tissue Engineering. *Biotechnology* **1995**, *13*, 565–576. [CrossRef]
21. Jaffer, I.H.; Fredenburgh, J.C.; Hirsh, J.; Weitz, J.I. Medical Device-Induced Thrombosis: What Causes It and How Can We Prevent It? *J. Thromb. Haemost.* **2015**, *13*, S72–S81. [CrossRef] [PubMed]
22. Ren, X.; Feng, Y.; Guo, J.; Wang, H.; Li, Q.; Yang, J.; Hao, X.; Lv, J.; Ma, N.; Li, W. Surface Modification and Endothelialization of Biomaterials as Potential Scaffolds for Vascular Tissue Engineering Applications. *Chem. Soc. Rev.* **2015**, *44*, 5680–5742. [CrossRef]
23. Massia, S.P.; Stark, J.; Letbetter, D.S. Surface-Immobilized Dextran Limits Cell Adhesion and Spreading. *Biomaterials* **2000**, *21*, 2253–2261. [CrossRef]
24. Jacobs, T.; Morent, R.; De Geyter, N.; Dubruel, P.; Leys, C. Plasma Surface Modification of Biomedical Polymers: Influence on Cell-Material Interaction. *Plasma Chem. Plasma Process.* **2012**, *32*, 1039–1073. [CrossRef]
25. Ferreira, P.; Alves, P.; Coimbra, P.; Gil, M.H. Improving Polymeric Surfaces for Biomedical Applications: A Review. *J Coat Technol. Res.* **2015**, *12*, 463–475. [CrossRef]
26. Drobota, M.; Trandabat, A.; Pislaru, M. Surface Modification of Poly(Ethylene Terephthalate) in Air Plasma. *Acta Chem. Iasi* **2019**, *27*, 128–136. [CrossRef]
27. Karakurt, I.; Ozaltin, K.; Vesela, D.; Lehocky, M.; Humpolíček, P.; Mozetič, M. Antibacterial Activity and Cytotoxicity of Immobilized Glucosamine/Chondroitin Sulfate on Polylactic Acid Films. *Polymers* **2019**, *11*, 1186. [CrossRef]
28. Ozaltin, K.; Lehocky, M.; Humpolicek, P.; Pelkova, J.; Di Martino, A.; Karakurt, I.; Saha, P. Anticoagulant Polyethylene Terephthalate Surface by Plasma-Mediated Fucoidan Immobilization. *Polymers* **2019**, *11*, 750. [CrossRef]
29. Tkavc, T.; Petrinič, I.; Luxbacher, T.; Vesel, A.; Ristić, T.; Zemljič, L.F. Influence of O2 and CO2 Plasma Treatment on the Deposition of Chitosan onto Polyethylene Terephthalate (PET) Surfaces. *Int. J. Adhes. Adhes.* **2014**, *48*, 168–176. [CrossRef]
30. Popelka, A.; Novák, I.; Lehocký, M.; Junkar, I.; Mozetič, M.; Kleinová, A.; Janigová, I.; Šlouf, M.; Bílek, F.; Chodák, I. A New Route for Chitosan Immobilization onto Polyethylene Surface. *Carbohydr. Polym.* **2012**, *90*, 1501–1508. [CrossRef]
31. Popelka, A.; Kronek, J.; Novák, I.; Kleinová, A.; Mičušík, M.; Špírková, M.; Omastová, M. Surface Modification of Low-Density Polyethylene with Poly(2-Ethyl-2-Oxazoline) Using a Low-Pressure Plasma Treatment. *Vacuum* **2014**, *100*, 53–56. [CrossRef]
32. Bílek, F.; Křížová, T.; Lehocký, M. Preparation of Active Antibacterial LDPE Surface through Multistep Physicochemical Approach: I. Allylamine Grafting, Attachment of Antibacterial Agent and Antibacterial Activity Assessment. *Colloids Surf. B Biointerfaces* **2011**, *88*, 440–447. [CrossRef] [PubMed]
33. Ozaltin, K.; Lehocký, M.; Humpolíček, P.; Pelková, J.; Sáha, P. A New Route of Fucoidan Immobilization on Low Density Polyethylene and Its Blood Compatibility and Anticoagulation Activity. *Int. J. Mol. Sci.* **2016**, *17*, 908. [CrossRef] [PubMed]
34. Martocq, L.; Douglas, T.E.L. Amine-Rich Coatings to Potentially Promote Cell Adhesion, Proliferation and Differentiation, and Reduce Microbial Colonization: Strategies for Generation and Characterization. *Coatings* **2021**, *11*, 983. [CrossRef]
35. Bílek, F.; Sulovská, K.; Lehocký, M.; Sáha, P.; Humpolíček, P.; Mozetič, M.; Junkar, I. Preparation of Active Antibacterial LDPE Surface through Multistep Physicochemical Approach II: Graft Type Effect on Antibacterial Properties. *Colloids Surf. B Biointerfaces* **2013**, *102*, 842–848. [CrossRef]
36. Ozaltin, K.; Lehocky, M.; Humpolicek, P.; Vesela, D.; Mozetic, M.; Novak, I.; Saha, P. Preparation of Active Antibacterial Biomaterials Based on Sparfloxacin, Enrofloxacin, and Lomefloxacin Deposited on Polyethylene. *J. Appl. Polym. Sci.* **2018**, *135*, 46174. [CrossRef]
37. Yang, Z.; Wang, J.; Luo, R.; Maitz, M.F.; Jing, F.; Sun, H.; Huang, N. The Covalent Immobilization of Heparin to Pulsed-Plasma Polymeric Allylamine Films on 316L Stainless Steel and the Resulting Effects on Hemocompatibility. *Biomaterials* **2010**, *31*, 2072–2083. [CrossRef]
38. Charbonneau, C.; Ruiz, J.-C.; Lequoy, P.; Hébert, M.-J.; De Crescenzo, G.; Wertheimer, M.R.; Lerouge, S. Chondroitin Sulfate and Epidermal Growth Factor Immobilization after Plasma Polymerization: A Versatile Anti-Apoptotic Coating to Promote Healing Around Stent Grafts. *Macromol. Biosci.* **2012**, *12*, 812–821. [CrossRef]
39. Subramaniam, A.; Sethuraman, S. Biomedical Applications of Nondegradable Polymers. In *Natural and Synthetic Biomedical Polymers*; Elsevier: Amsterdam, The Netherlands, 2014; pp. 301–308, ISBN 978-0-12-396983-5.

40. Dhahri, M.; Abed, A.; Lajimi, R.H.; Mansour, M.B.; Gueguen, V.; Abdesselem, S.B.; Chaubet, F.; Letourneur, D.; Meddahi-Pellé, A.; Maaroufi, R.M. Grafting of Dermatan Sulfate on Polyethylene Terephtalate to Enhance Biointegration. *J. Biomed. Mater. Res. Part A* **2011**, *98*, 114–121. [CrossRef]
41. Pandiyaraj, K.N.; Selvarajan, V.; Rhee, Y.H.; Kim, H.W.; Shah, S.I. Glow Discharge Plasma-Induced Immobilization of Heparin and Insulin on Polyethylene Terephthalate Film Surfaces Enhances Anti-Thrombogenic Properties. *Mater. Sci. Eng. C* **2009**, *29*, 796–805. [CrossRef]
42. Gotoh, K.; Yasukawa, A.; Kobayashi, Y. Wettability Characteristics of Poly(Ethylene Terephthalate) Films Treated by Atmospheric Pressure Plasma and Ultraviolet Excimer Light. *Polym. J.* **2011**, *43*, 545–551. [CrossRef]
43. van Oss, C.J.; Wu, W.; Docoslis, A.; Giese, R.F. The Interfacial Tensions with Water and the Lewis Acid–Base Surface Tension Parameters of Polar Organic Liquids Derived from Their Aqueous Solubilities. *Colloids Surf. B Biointerfaces* **2001**, *20*, 87–91. [CrossRef]
44. Ozaltin, K.; Lehocký, M.; Kuceková, Z.; Humpolíček, P.; Sáha, P. A Novel Multistep Method for Chondroitin Sulphate Immobilization and Its Interaction with Fibroblast Cells. *Mater. Sci. Eng. C* **2017**, *70*, 94–100. [CrossRef]
45. Zhu, M.; Ge, L.; Lyu, Y.; Zi, Y.; Li, X.; Li, D.; Mu, C. Preparation, Characterization and Antibacterial Activity of Oxidized κ-Carrageenan. *Carbohydr. Polym.* **2017**, *174*, 1051–1058. [CrossRef] [PubMed]
46. Bajpai, S.K.; Daheriya, P. Kappa-Carrageenan/PVA Filmswith Antibacterial Properties: Part 1. Optimization of Preparation Conditions and Preliminary Drug Release Studies. *J. Macromol. Sci. Part A* **2014**, *51*, 286–295. [CrossRef]
47. Abdelhamid, H.N.; Mathew, A.P. Cellulose-Based Materials for Water Remediation: Adsorption, Catalysis, and Antifouling. *Front. Chem. Eng.* **2021**, *3*. [CrossRef]
48. Abdelhamid, H.N.; Mathew, A.P. Cellulose-Based Nanomaterials Advance Biomedicine: A Review. *Int. J. Mol. Sci.* **2022**, *23*, 5405. [CrossRef]
49. Liu, X.F.; Guan, Y.L.; Yang, D.Z.; Li, Z.; De Yao, K. Antibacterial Action of Chitosan and Carboxymethylated Chitosan. *J. Appl. Polym. Sci.* **2001**, *79*, 1324–1335.
50. Ayrapetyan, O.N.; Obluchinskaya, E.D.; Zhurishkina, E.V.; Skorik, Y.A.; Lebedev, D.V.; Kulminskaya, A.A.; Lapina, I.M. Antibacterial properties of fucoidans from the brown algae *Fucus vesiculosus* L. of the barents sea. *Biology* **2021**, *10*, 67. [CrossRef]
51. Kuchinka, J.; Willems, C.; Telyshev, D.V.; Groth, T. Control of Blood Coagulation by Hemocompatible Material Surfaces—A Review. *Bioengineering* **2021**, *8*, 215. [CrossRef]
52. Olson, S. Identification of Critical Molecular Interactions Mediating Heparin Activation of Antithrombin Implications for the Design of Improved Heparin Anticoagulants. *Trends Cardiovasc. Med.* **2002**, *12*, 198–205. [CrossRef]
53. Wei, J.; Yoshinari, M.; Takemoto, S.; Hattori, M.; Kawada, E.; Liu, B.; Oda, Y. Adhesion of Mouse Fibroblasts on Hexamethyldisiloxane Surfaces with Wide Range of Wettability. *J. Biomed. Mater. Res. B Appl. Biomater.* **2007**, *81*, 66–75. [CrossRef] [PubMed]
54. Ko, J.-Y.; Lee, J.-H.; Kim, H.-S.; Kim, H.-H.; Jeon, Y.-J. Cell proliferation effect of brown marine algae extracts on Mouse Fibroblast. *J. Mar. Biosci. Biotechnol.* **2015**, *7*, 28–34. [CrossRef]
55. Popa, E.; Carvalho, P.; Dias, A.; Santos, T.; Santo, V.; Marques, A.; Viegas, C.; Gomes, M.; Reis, R.L. Evaluation of the in Vitro and in Vivo Biocompatibility of Carrageenan-Based Hydrogels. *J. Biomed. Mater. Res. Part A* **2014**, *102*, 4087–4097. [CrossRef]
56. Alves, A.; Sousa, R.A.; Reis, R.L. In Vitro Cytotoxicity Assessment of Ulvan, a Polysaccharide Extracted from Green Algae. *Phytother. Res.* **2013**, *27*, 1143–1148. [CrossRef]
57. Perestrelo, A.R.; Grenha, A.; Rosa da Costa, A.M.; Belo, J.A. Locust Bean Gum as an Alternative Polymeric Coating for Embryonic Stem Cell Culture. *Mater. Sci. Eng. C Mater. Biol. Appl.* **2014**, *40*, 336–344. [CrossRef]

ARTICLE III

Jasenská D., Kašpárková V., Vašíček O., Münster L., Minařík A., **Káčerová S.**, Korábková E., Urbánková L., Vícha J., Capáková Z., Falleta E., Pina C. D., Lehocký M., Skopalová K., Humpolíček P. Enzyme-catalyzed polymerization process: a novel approach to the preparation of polyaniline colloidal dispersions with and immunomodulatory effect. Biomacromolecules. 2022, 23(8), 3359-3370. Doi: 10.1021/acs.biomac.2c00371

pubs.acs.org/Biomac

Article

Enzyme-Catalyzed Polymerization Process: A Novel Approach to the Preparation of Polyaniline Colloidal Dispersions with an Immunomodulatory Effect

Daniela Jasenská, Věra Kašpárková,* Ondřej Vašíček,* Lukáš Münster, Antonín Minařík, Simona Káčerová, Eva Korábková, Lucie Urbánková, Jan Vícha, Zdenka Capáková, Ermelinda Falleta, Cristina Della Pina, Marián Lehocký, Kateřina Skopalová, and Petr Humpolíček*

Cite This: *Biomacromolecules* 2022, 23, 3359–3370

Read Online

ACCESS | Metrics & More | Article Recommendations

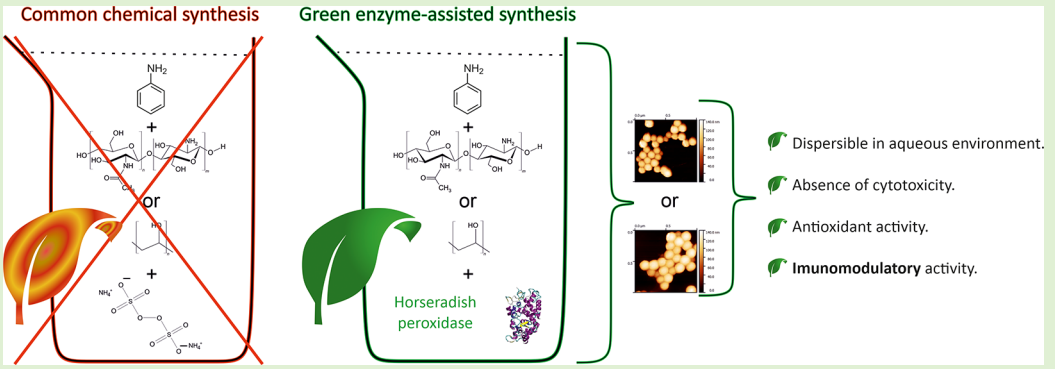

ABSTRACT: A green, nature-friendly synthesis of polyaniline colloidal particles based on enzyme-assisted oxidation of aniline with horseradish peroxidase and chitosan or poly(vinyl alcohol) as steric stabilizers was successfully employed. Physicochemical characterization revealed formation of particles containing the polyaniline emeraldine salt and demonstrated only a minor effect of polymer stabilizers on particle morphology. All tested colloidal particles showed *in vitro* antioxidation activity determined via scavenging of 1,1-diphenyl-2-picrylhydrazyl (DPPH) radicals. *In vitro*, they were able to reduce oxidative stress and inhibit the production of reactive oxygen species by neutrophils and inflammatory cytokines by macrophages. The anti-inflammatory effect observed was related to their antioxidant activity, especially in the case of neutrophils. The particles can thus be especially advantageous as active components of biomaterials modulating the early stages of inflammation. In addition to the immunomodulatory effect, the presence of intrinsically conducting polyaniline can impart cell-instructive properties to the particles. The approach to particle synthesis that we employed—an original one using environmentally friendly and biocompatible horseradish peroxidase—represents a smart way of preparing conducting particles with unique properties, which can be further modified by the stabilizers used.

INTRODUCTION

The discovery of intrinsically conducting polymers (ICPs) opened the door to research of an attractive new material exhibiting interesting properties and suggesting numerous possibilities with respect to its application. Ever-increasing numbers of papers dealing with ICPs document interest in these materials. Polyaniline (PANI) is an ICP that has been investigated with regard to many applications, including biomedicine.[1−3] This polymer exhibits advantages, such as the ease and low cost of synthesis, the ability to electrically switch between its conductive and resistive states, and stability.

PANI is commonly prepared by the reaction of ammonium persulfate with aniline in an acidic aqueous medium, where PANI precipitates as a powder.[4] Unfortunately, such PANI powder is insoluble and difficult to process. Although the solubility of PANI in an aqueous environment[5] or organic solvents[6] can be improved, the utilization of toxic organic solvents or severe functionalization conditions make these processes inconvenient for commercial purposes, increase the environmental burden, and raise concerns about the

Received: April 19, 2022
Revised: July 8, 2022
Published: July 28, 2022

biocompatibility of the product. One way to avoid these complications is to prepare water-dispersible PANI colloidal particles.

PANI colloids have received a lot of attention because of the potential use they could have in sensors, electrorheological fluids, and coatings. PANI colloids can be routinely synthesized by the polymerization of aniline in the presence of oxidizing agents and steric stabilizers, these including a wide variety of water-soluble polymers and biopolymers, such as poly(vinyl alcohol) (PVA),[7] poly(vinyl pyrrolidone),[8] and poly(2-acrylamido-2-methyl-1-propanesulfonic acid),[9] among others. In addition, some of them have shown low cytotoxicity, on the one hand,[10] and considerable antibacterial activity on the other.[11] In connection with biomedical applications, we can increasingly encounter the use of several biomacromolecules as stabilizers, such as cellulose derivatives, proteins, gelatine,[12] and chitosan,[13,14] the latter known for its unique antibacterial properties.

Application of enzymes, peroxidases, in the synthesis of colloidal PANI appears to be an efficient and environmentally friendly procedure, which can be an alternative to the chemical or electrochemical synthesis route of these systems. Recently, peroxidase-catalyzed oxidative polymerization was used by Jin et al.[15] for the preparation of a stable microemulsion or by Cruz-Silva et al.[16,17] who prepared PANI colloidal particles with chitosan and PVA. The advantages of this enzyme-catalyzed method are the milder conditions under reaction where the oxidation rate mainly depends on the amount and activity of the enzyme; on the other hand, the common chemical oxidation of aniline is a non-autocatalytic reaction.[18] In addition, during enzymatic oxidation supported by hydrogen peroxide, only a limited concentration of potentially harmful byproducts (e.g., the contamination of the reaction media with salts) is formed,[19,20] and a limited increase in acidity is observed in comparison with the chemical route of synthesis.[21]

In this work, we prepared and characterized colloidal particles of PANI by an environmentally friendly approach based on the enzyme-assisted polymerization of aniline in aqueous media with the aid of horseradish peroxidase, using either chitosan or PVA as a steric stabilizer. The main novelty and originality of the work, however, lies in the examination of the biological properties of the prepared particles. On the basis of our previous knowledge[10] and published studies,[22] we anticipated that the colloidal particles would exhibit antioxidant properties, which could induce immunomodulatory effects on macrophages and neutrophils. The biological characterization also included cytotoxicity tests conducted on two cell lines, fibroblasts (NIH/3T3) and macrophages (RAW264.7).

EXPERIMENTAL SECTION

Materials. Reagent-grade aniline (≥98%) was purchased from PENTA (Czech Republic). Partially hydrolyzed (>99%) poly(vinyl alcohol) (PVA, M_w 89 000−98 000 g moL^{-1}), *p*-toluenesulfonic acid (TSA; ≥98.5%), high-molecular-weight chitosan (CHIT; molecular weight of 310 000−375 000 g moL^{-1}), and horseradish peroxidase (HRP; type VI, activity ≥250 U g^{-1}, RZ 3.2) were acquired from Sigma-Aldrich. Hydrogen peroxide (30%) was purchased from Kittford (Czech Republic).

Preparation of Colloidal Particles. Colloidal PANI was synthesized using both PVA and CHIT as steric stabilizers. The dispersion polymerization was carried out according to Cruz-Silva et al.[14] with minor modifications. Briefly, 1.2 g of PVA, 0.215 mL of aniline, and 0.456 g of TSA were dissolved in 20 mL of water. The reaction mixture was kept under vigorous stirring in a water/ice bath for 6 h. Afterward, 2.0 mL of a freshly prepared enzyme solution in Milli-Q water (1.2 mg mL^{-1}) was added to the reaction mixture under stirring. The reaction was initiated by adding 2 mL of hydrogen peroxide (3.75 wt %). The hydrogen peroxide solution was added dropwise to the stirred reaction mixture over a time period of 2 h. The resulting polyaniline composite particles (PANI-PVA) were transferred into membrane tubing (MWCO 12 000−14 000; Spectrum Laboratories Inc.) and exhaustively dialyzed against 0.2 mol L^{-1} hydrochloric acid to remove any residual monomers and byproducts. For the production of colloidal particles stabilized with chitosan (PANI-CHIT), 0.040 g of CHIT and 0.215 mL of aniline were added to 20 mL of Milli-Q water, after which TSA was added slowly until a pH of 3.0 was achieved. The procedure for particle production was the same as that described above for PANI-PVA. A reference PANI sample (designated PANI-N) was prepared in a similar manner to PANI-PVA, however, without the PVA stabilizer.

Size and Colloidal Stability of Particles. The sizes and size distributions of the colloidal particles were determined on both freshly prepared and dialyzed samples by dynamic light scattering (DLS) using a Zetasizer Nano ZS instrument (Malvern Instruments, U.K.). Measurements of the hydrodynamic radii of colloidal particles, expressed as z-average particle diameters, were performed at 25 °C. The intensity of scattered light (λ = 633 nm) was observed at a scattering angle of 173°. The polydispersity index (PDI) was calculated by assuming a lognormal distribution of particle sizes. Samples for analysis were prepared by diluting 10 μL of the colloidal dispersion in 1 mL of 0.1 mol L^{-1} hydrochloric acid. All analyses were run in triplicate and are expressed as the mean and standard deviation (SD). Using the same procedure, the colloidal stability of the particles was determined after 24 months of storage at 5 ± 2 °C, and the z-average particle diameters and PDI were recorded and calculated.

Antioxidation Activity Determined by Scavenging of DPPH Radicals. Antioxidant activity of PANI-CHI and PANI-PVA was determined by a 1,1-diphenyl-2-picrylhydrazyl (DPPH) free-radical scavenging assay[22] using a previously published method with modifications. Freshly prepared 1 × 10^{-4} M DPPH solution in ethanol (1 mL) was added to 10 μL of each of the investigated samples. The reaction mixture was stirred for 30 s and UV spectra were recorded within a time period of 60 min. The absorbance was read at 516 nm using a Jasco V-750 spectrophotometer (Jasco Inc.), and antioxidation activity was calculated as % DPPH scavenging activity = $[(A_0 - A_1)/A_0] \times 100$, where A_0 and A_1 are absorbances of DPPH solution in the absence and the presence of tested samples, respectively. DPPH ethanolic solution served as a blank.

UV−Vis Spectroscopy. UV−vis spectra of PANI dispersions in a wavelength range of 200−800 nm were obtained on a UV−vis Varian Cary 300 instrument, Varian Inc. For sample preparation, a 10 μL sample was withdrawn and dispersed in 3.0 mL of 1.0 mol L^{-1} hydrochloric acid or in Milli-Q water. The UV−vis spectra of PANI dispersions recorded in 1.0 mol L^{-1} hydrochloric acid were used for determining the concentration of PANI in the colloidal dispersions. This data was needed for testing the biological properties of samples. The concentration of PANI in each of the samples was calculated from the local maximum of absorbance at a wavelength of 395 nm using the Lambert−Beer law, $A = \varepsilon cl$, where ε is the absorption coefficient (ε = 31 500 ± 1700 cm^2 g^{-1}),[23] c is the concentration of PANI, and l is the optical path (l = 1 cm).

Transmission Electron Microscopy. The morphology of colloidal particles was assessed by means of a JEM 2100 transmission electron microscope (JEOL, Japan) using an accelerating voltage of 160 kV. Samples were prepared by the gentle drying of a diluted (0.1 wt %) sample dispersion drop-cast on a formvar-coated copper grid.

Atomic Force Microscopy. Stock particle dispersions were diluted 20 times with Milli-Q water. In the following step, 20 μL of the diluted dispersion was deposited on a freshly cleaved mica surface. V-5 grade Mica (SPI) with an area of 10 × 10 mm^2 was used. After 5 min of exposure, mica-surface-attached colloids were gently dried using a stream of air. Dried colloids were observed with an AFM

https://doi.org/10.1021/acs.biomac.2c00371
Biomacromolecules 2022, 23, 3359−3370

microscope, using the ScanAsyst mode on a Dimension ICON instrument (Bruker Corporation). Analyses were performed under laboratory temperature and humidity. A ScanAsyst-Air silicon nitride probe (Bruker Corporation) with a spring constant of 0.4 N m^{-1} was used. The scanning rate was 0.5 Hz. Data from the AFM were processed using Gwyddion 2.5 software (Czech Metrology Institute, Czech Republic).

Cell Cultures and Cultivation Techniques. Cytotoxicity testing was performed using the NIH/3T3 mouse embryonic fibroblast cell line (ECACC 93061524, England) and RAW264.7 murine peritoneal macrophage cell line (European Collection of Authenticated Cell Cultures, U.K.). Dulbecco's modified Eagle's medium (Biosera, France) with 10% calf serum (Biosera, France) and 100 mg mL^{-1} penicillin/streptomycin (Biosera, France) was used for the cultivation of NIH/3T3 cells. Dulbecco's modified Eagle's medium (DMEM; Gibco), supplemented with 10% heat-inactivated low endotoxin fetal bovine serum (FBS; PAN, Germany) and 1% combination of penicillin/streptomycin was used for the cultivation of RAW264.7. Both cell lines were maintained at 37 °C in a humidified atmosphere containing 5% CO_2 and 95% air (incubator HERAcell 150i, Thermo Scientific).

Blood Collection and Isolation of Neutrophils. Human neutrophils were isolated from the blood (containing sodium citrate) of healthy volunteers who had given their informed consent. Volunteers were both female and male and aged between 18 and 60 years; they did not take any drugs and had been free of any signs of cold or other diseases for at least 3 weeks before blood collection. The Ethics Committee for Research at Masaryk University, Brno, Czech Republic (number EKV-2018-083) approved the collection protocol. The whole blood was mixed with 3% dextran and left at room temperature for ~30 min. The resulting buffy coat was overlaid on a Histopaque 1077 instrument and centrifuged at 390*g* for 30 min without acceleration or brake. After centrifugation, the remaining erythrocytes were lysed by water hypotonic lysis. The neutrophils were washed in cold PBS, centrifuged at 190*g* for 10 min, and finally resuspended in cold PBS. The viability of neutrophils was verified with a CASY cytometer (Roche, Switzerland) and only neutrophils with viability exceeding 95% were used for experiments.

Cytotoxicity Determination. Cytotoxicity determination was performed according to the protocol of standard EN ISO 10993-5 (2019) with modifications. Cells were seeded in a concentration of 1×10^5 cells mL^{-1} and precultivated for 24 h. Then, the culture medium was replaced with colloids freshly diluted with medium to concentrations of 1, 2.5, 5.0, 10, 15, and 20% (Table 1). In the case of RAW264.7, the cells were also activated by lipopolysaccharides (LPSs, 25 ng mL^{-1}). As a reference, cells cultivated in a medium without colloids were used. After 1 day of cultivation, the effects of colloids on cell viability were assessed by the MTT assay (Invitrogen Corporation). Absorption was measured at 570 nm using an Infinite M200 Pro NanoQuant instrument (Tecan, Switzerland).

Table 1. Concentration of PANI Colloids (μg mL^{-1}) Related to the Dilution (%) of the Parent Colloidal Dispersion

% of parent colloidal dispersion used for cytotoxicity testing	concentration of PANI in colloids (μg mL^{-1})		
	PANI-CHIT	PANI-PVA	PANI-N
100	791	308	754
20	158	61.6	150.8
15	118.7	46. 2	113.1
10	79.1	30. 8	75.4
5	39.6	15.4	37.7
2.5	19.8	7.7	18.9
1	7.9	3.1	7.5

The cell viability of the reference sample was set as 1 (100% viability). According to ISO 10993-5 (2019), a viability higher than 0.7 represents an absence of cytotoxicity, while samples with a viability lower than 0.7 are determined to be cytotoxic. The cell morphology was observed using an Olympus inverted fluorescence microscope (Olympus, CKX 41, Japan).

Apoptosis of Neutrophils. The apoptosis of neutrophils was determined with an Annexin V Apoptosis Kit-FITC (Exbio, Prague, Czech Republic). Neutrophils were incubated in a cytometric tube at a concentration of 2.5×10^5 cells per tube and incubated with tested compounds (at concentrations of 1−15%) for 2 h. After exposure, the reaction mixture of annexin V (1:150 Annexin V-FITC and 1× Annexin V binding buffer) was added and incubated for 20 min in the dark; 2 μL of propidium iodide (PI, final concentration 1 mg mL^{-1}) was added to each sample and analyzed by flow cytometry (FACSVerse, BD Bioscience, Carlsbad, CA).

Oxidative Burst of Isolated Neutrophils. The oxidative burst of isolated neutrophils was measured by luminol-enhanced chemiluminescence (CL) using an LM-01 microplate luminometer (Immunotech, Czech Republic). The principle of the method was described previously.[24] Briefly, the reaction mixture for spontaneous (non-stimulated) CL consisted of 2.5×10^5 isolated neutrophils per well, 1 mM luminol (10 mM stock solution in 0.2 mol L^{-1} borate buffer), and the tested compounds (PANI-CHIT and PANI-PVA). Furthermore, for stimulated-CL, opsonized zymosan particles (OZP; 62.5 μg mL^{-1}) were used. Hank's balanced salt solution (HBSS) was used to adjust the total reaction volume to 250 μL. The CL activity of the samples was measured immediately at 37 °C and recorded continuously for 120 min. Data were converted to a percentage of the spontaneous or activated reference to achieve final results.

Reactive Oxygen Species (ROS) Antioxidant Activity in a Luminol−HRP−H_2O_2 Cell-Free System. The principle of the method was described previously.[25] As a source of CL signals, H_2O_2 and horseradish peroxidase (HRP) were used. Aliquots of 50 μL of PANI-CHIT or PANI-PVA (final concentrations 1−15%), HRP (final concentration, 2 U mL^{-1}), and luminol (final concentration, 10 μmol L^{-1}) were mixed in a 96-well luminescence plate. The reaction was initiated by adding H_2O_2 to a final concentration of 100 μmol L^{-1}. The CL signal was measured for 120 min at 37 °C with an LM-01 microplate luminometer (Immunotech, Czech Republic). Data were converted to a percentage of the control.

Nitric Oxide (NO) Production by Murine Macrophages. Changes in NO production were measured indirectly as the accumulation of nitrites (the end product of NO metabolism) in the medium using the Griess reagent (Sigma-Aldrich) according to the method described previously.[26] RAW264.7 cells (0.5×10^5 cells per well) were incubated in a 24-well plate with PANI-CHIT or PANI-PVA (final concentrations, 1−15%) and LPSs from *Escherichia coli* (25 ng mL^{-1}) for 24 h at 37 °C in an atmosphere of 5% CO_2 and 95% air. LPS (25 ng mL^{-1}) alone was used as a positive reference. At the end of the incubation period, culture media were collected from the respective wells and centrifuged (16 000*g*, 4 °C, 5 min); 100 μL of centrifuged medium and the Griess reagent were mixed in a 96-well plate and incubated at room temperature in the dark for 30 min. The absorbance was measured at 546 nm, using sodium nitrite (in the concentration range of 0−52 μmol L^{-1}) as the standard for the calibration curve. Data were converted to a percentage of the LPS control.

IL-6 Production by Murine Macrophages. The concentration of the proinflammatory cytokine interleukine-6 (IL-6) produced by RAW264.7 cells in the cultivation medium was determined after 24 h of exposure to PANI-CHIT or PANI-PVA (final concentrations, 1−15%) and LPS (25 ng mL^{-1}) by commercially available immunoassays (Mouse IL-6 DuoSet, R&D Systems). The assays were performed according to the manufacturer's instructions as described previously.[27] For more detailed information on culturing and preparing the medium, see the section: "Nitric Oxide (NO) Production by Murine Macrophages".

https://doi.org/10.1021/acs.biomac.2c00371
Biomacromolecules 2022, 23, 3359−3370

Table 2. Size (*z*-Average Diameter ± SD) and Polydispersity Index (PDI ± SD) of Colloidal Particles Stabilized with PVA or CHIT as the Steric Stabilizer[a]

	before dialysis		after dialysis		after 24 months of storage	
sample	*z*-average (nm)	PDI	*z*-average (nm)	PDI	*z*-average (nm)	PDI
PANI-CHIT	585 ± 10	0.41 ± 0.06	655 ± 7	0.45 ± 0.03	541 ± 2	0.30 ± 0.02
PANI-PVA	206 ± 2	0.50 ± 0.04	240 ± 2	0.55 ± 0.01	175 ± 3	0.52 ± 0.02
PANI-N	2800 ± 81	0.33 ± 0.05	3500 ± 74	0.33 ± 0.13	n.d.[b]	n.d.[b]

[a]Comparison with PANI prepared without a stabilizer. [b]Not determined.

Statistical Analysis. Data of cytocompatibility experiments are presented as the mean ± standard error of the mean (SEM). All assays were performed in quadruplicate. The number of independent experiments (n) is stated in the figure legend. The data from some of the measurements were normalized to the reference in each experiment to account for the variability of individual cell passages. Statistical analysis was performed using GraphPad Prism version 6.01 for Windows, GraphPad Software, La Jolla, CA. Statistical differences were tested by one-way ANOVA, which was followed by Dunnett's multiple comparison test or by a one-sample *t*-test to compare values expressed as percentages. In the case of the one-sample *t*-test application, the Bonferroni correction of the *p*-value for multiple comparisons was performed. $p < 0.05$ was taken to indicate significant differences between data mean values.

RESULTS AND DISCUSSION

Particle Size and Stability Are Controlled by the Type of Polymer Stabilizer. The colloidal particles exhibited different sizes depending on the type of the polymer used for their stabilization (Table 2), and PANI-PVA colloids were smaller in size (206 ± 2 nm) than samples prepared in the presence of chitosan, showing a *z*-average diameter of 585 ± 10 nm. The widths of distribution expressed as PDI were 0.55 and 0.45 for PANI-PVA and PANI-CHIT afer dialysis, respectively. After dialysis, conducted with the aim of removing residual impurities, which might compromise the biological tests, the average particle size in the samples increased. In our previous study, the average size of PANI colloidal particles stabilized with PVA and synthesized by the oxidative polymerization of aniline with ammonium persulfate (APS) was 116 nm (measured by DLS).[28] The particle size of PANI-CHIT samples from the enzyme-assisted process was also comparable with previously published sizes of colloidal PANI particles stabilized with chitosan and prepared by APS oxidation;[13] however, their morphologies were different. It is clear from the results that the size of colloidal PANI-CHIT particles obtained from the enzymatic reaction is well within the range of sizes prepared by the standard reaction employing APS for oxidation.

In contrast to PANI-PVA or PANI-CHIT, the freshly prepared sample without a stabilizer, PANI-N, was not of a true colloidal character, and particles greater than 3 μm sedimenting soon after dialysis were formed. Nevertheless, after homogenization, a uniform dispersion formed again, which was stable for several hours. If we compare enzymatically prepared PANI-N with PANI prepared by polymerization with APS, both without a stabilizing polymer, the nature of the enzymatically prepared sample was different and its colloidal stability was significantly higher. The explanation for this may lie in the stabilizing effect of peroxidase. Peroxidase is a protein (molecular weight of ~44×10^3 g mol^{-1}), which in fact can act as a polymeric stabilizer.[29] The resulting sample, therefore, exhibited different properties between standard PANI powder prepared in the absence of a stabilizer using APS and true colloidal particles prepared with the stabilizing effects of polymers of higher molecular weights.

The colloidal stability of PANI-PVA and PANI-CHIT was confirmed even after 24 months of storage at 5 ± 2 °C (Table 2). For studied samples, the particle size was reduced by storage to 83% (PANI-CHIT) and 73% (PANI-PVA) of the initial values. This decrease was not surprising, as a corresponding effect was observed for CHIT-stabilized PANI colloids prepared by standard chemical oxidation.[13] A drop in the particle size during storage was also reported by Li et al.[30] for colloidal particles made of PVA-stabilized polypyrrole who suggested that this process may be driven by size changes in certain polymer agglomerates that occur during storage. Another option for the size reduction mentioned here could be time-induced changes in the polymer stabilizers used. The size distribution (expressed as PDI) of PANI-CHIT broadened after storage, but the distribution curve remained monomodal. On the contrary, the PDI value of PANI-PVA remained nearly unchanged after storage, but the initially monomodal distribution curve changed to a bimodal one, indicating the formation of two distinct particle populations.

Antioxidation Activity Depends on the PANI Concentration in Colloidal Particles. The antioxidation activity of polyaniline and its composites has previously been documented in several studies.[22,31,32] Also, the current study unambiguously confirmed the antioxidation activity of PANI-CHIT and PANI-PVA samples, which were both capable of scavenging DPPH radicals. Furthermore, the analyses revealed that the samples' activity differed. The efficacy of PANI-CHIT was higher immediately after mixing with DPPH$^{\bullet}$; however, with increasing time, the activity reduced and reached a plateau. The activity of PANI-PVA, on the other hand, was not as high as that for PANI-CHIT in short reaction times, but it gradually increased with a prolonged time of contact with radicals. The earlier onset of antioxidation activity for PANI-CHIT samples can be correlated with their higher concentration of PANI (791 μg L^{-1}) in comparison with PANI-PVA (308 μg L^{-1}). Differences in the course of PANI-PVA and PANI-CHIT scavenging activities might also be correlated with differences in their particle size. In summary, PANI-CHIT and PANI-PVA scavenging activities were 82 and 67% after 60 min, respectively. It should also be mentioned that after being exposed to ethanolic DPPH, the aqueous dispersions of PANI-CHIT and PANI-PVA gradually precipitated, forming particles on the bottom of the cuvette. This effect, however, did not compromise their antioxidation activity.

Spectra of Colloidal Particles Demonstrate the Presence of the Conducting Emeraldine PANI Salt. The process of the formation of polymer-stabilized PANI colloids and nonstabilized PANI was monitored by UV−vis spectroscopy. During synthesis, the reaction mixtures became blue. The color change confirmed the formation of polyaniline oligomers induced by hydrogen peroxide. This reaction step

https://doi.org/10.1021/acs.biomac.2c00371
Biomacromolecules 2022, 23, 3359−3370

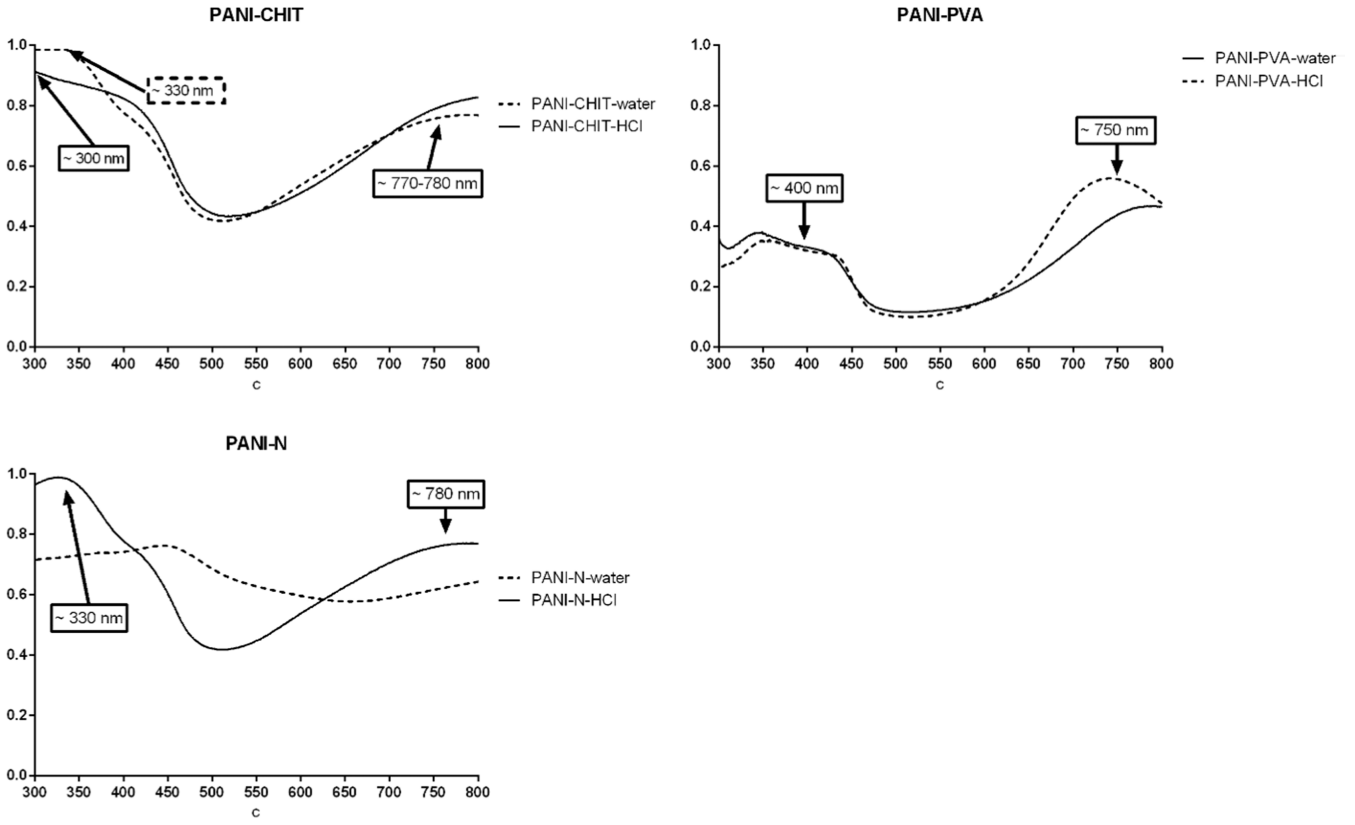

Figure 1. UV−vis spectra of enzymatically synthesized PANI stabilized with PVA and CHIT or without a stabilizer (PANI-N).

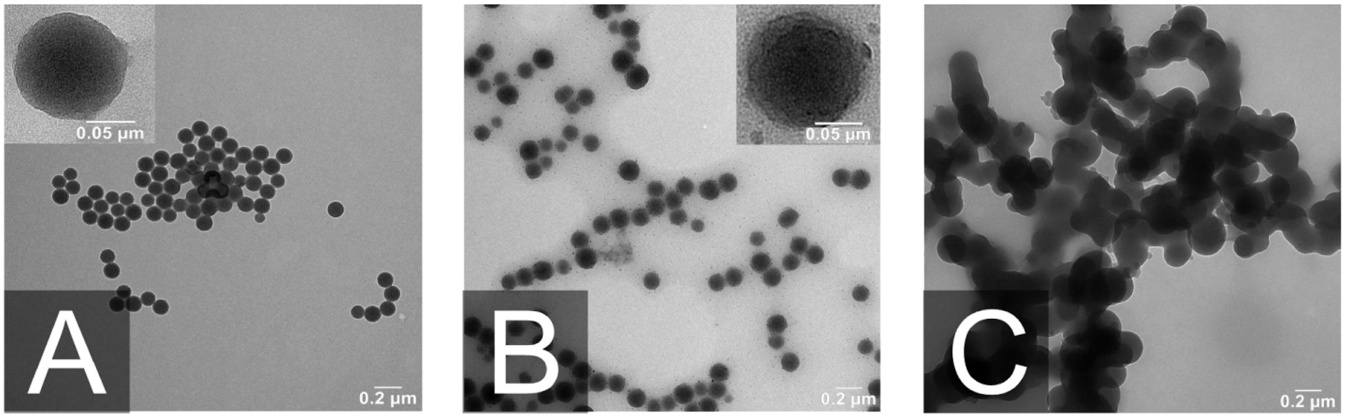

Figure 2. Transmission electron micrographs of PANI-CHIT (A), PANI-PVA (B), and PANI-N (C) colloids.

was very short, lasting for only 20 s, and was followed by a rapid change in the color of the reaction mixture to dark green, indicating thus the formation of the PANI emeraldine salt. An exception was the PANI-N sample prepared in the absence of a stabilizer, where the reaction mixture did not turn dark green but brown. The UV−vis spectra of all samples (PANI-PVA, PANI-CHIT, PANI-N) recorded in two different dilution media (1 mol L^{-1} HCl and water) within a wavelength range from 300 to 800 nm are given in Figure 1. The UV−vis spectra of the PANI-PVA colloid were similar in both media and showed a broad peak at 400 nm and a peak with a maximum at about 750 nm. The peak at ∼400 nm arose from the $\pi-\pi^*$ electron transition within the benzenoid ring and the peak at ∼750 nm evidenced the formation of a polaron structure. The λ_{max} of the latter peak shifted to 740 nm for PANI-PVA measured in HCl in comparison with spectra in water, indicating differences in polaron delocalization. When measured with the acidity of the medium fixed, i.e., in 1 mol L^{-1} HCl, the maximum absorbance in the λ range from 350 to 430 nm may be taken as an approximate measure of the concentration of PANI in the dispersion. The spectrum of PANI-CHIT colloids shows maxima at λ of ∼330 and 770 nm in water, and 300 and 780 nm in HCl. In the study,[12] PANI colloids stabilized with chitosan prepared by standard chemical oxidation with APS showed a similar course of spectra, with slightly shifted distinct maxima at 390 and 800 nm. The abovementioned difference in the color between nonstabilized PANI-N (brown) and PANI-PVA and PANI-CHIT (green) is also evident from the spectra obtained on the PANI-N sample dispersed in water, which does not show a course typical of the green PANI salt. After the dispersion medium was changed to 1 mol L^{-1} hydrochloric acid, the spectra converted to their

https://doi.org/10.1021/acs.biomac.2c00371
Biomacromolecules 2022, 23, 3359−3370

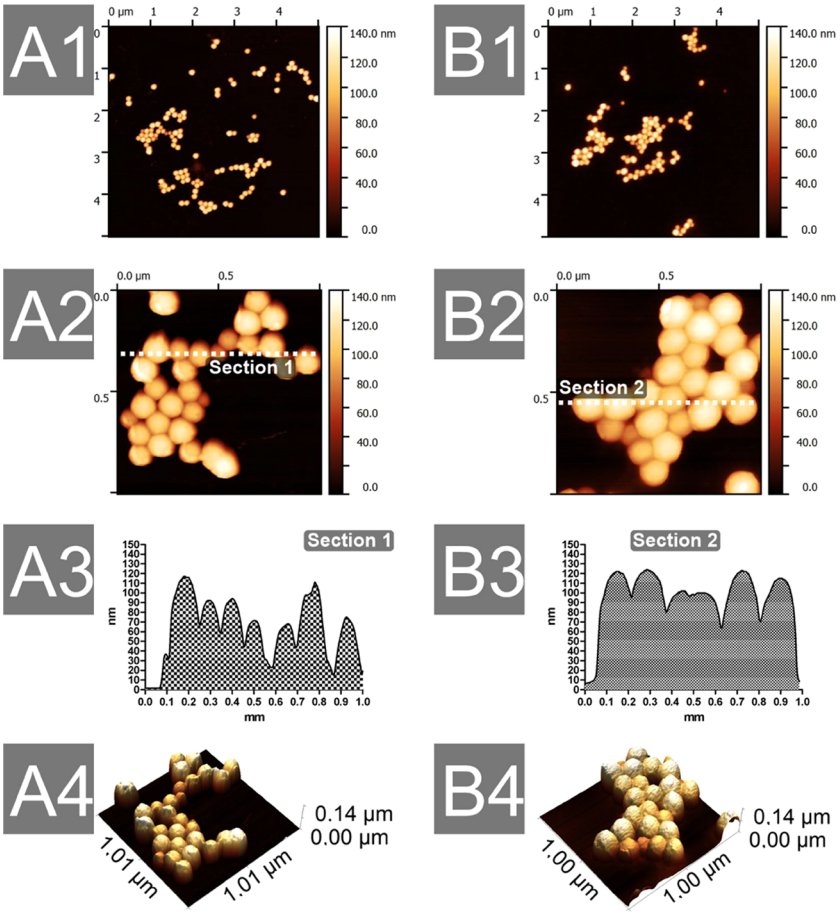

Figure 3. Colloidal particles on mica surfaces characterized by AFM. Height images and profiles of PANI-CHIT (left) and PANI-PVA (right). PANI-N formed aggregate-like structures and, thus, are not presented.

common course (Figure 1). The reason for this is obvious as experimental data published in ref 33 show that the oxidation products of PANI formed in neutral and weakly acidic media are brown in color with low conductivity but turn to the green emeraldine salt in a more strongly acidic environment.

Morphology of Colloidal Particles—Stabilizers Are a Key Factor in the Formation of Colloidal Particles. The morphology, size, and shape of the prepared PANI colloids were depicted using TEM (Figure 2). The microscopy observations revealed regular, spherical particles of similar sizes, with relatively narrow distributions for both PVA- and CHIT-stabilized samples. The average diameters estimated by TEM were 126 ± 9 and 133 ± 13 nm for PANI-CHIT and PANI-PVA, respectively. In contrast, PANI-N synthesized without a stabilizing agent was formed by particles, which were obviously bigger than those present in polymer-stabilized samples and exhibited significant aggregation caused by the absence of a stabilizing polymer. The TEM analyses roughly complied with results from the scattering measurements. However, differences between the sizes of PVA- and CHIT-stabilized samples measured by DLS were bigger in comparison with TEM measurements, thanks to the different measuring principles of the DLS technique. Bigger PANI-CHIT particles can originate from the higher molecular weight of CHIT (310 000−375 000 g mol^{-1}) compared to PVA (89 000−98 000 g mol^{-1}) stabilizers, which are detected as loose layers around the core particles by DLS but are not visible after particle drying for TEM analysis. Compared to other standard PANI-based colloids, enzymatically polymerized colloids with the CHIT or PVA stabilizer are spherically symmetrical. After deposition on a solid substrate for TEM or AFM imaging, they do not disintegrate into the randomly arranged elliptical or fibrillar structures discussed in[13] and some other papers.[16,17]

Atomic force microscopy (AFM) confirmed the spherical shapes of PANI-PVA and PANI-CHIT particles on the mica surface. In contrast, the AFM analysis of PANI-N was not feasible, as the size of the particles/agglomerates were unsuitable for such analysis. The particles stabilized by CHIT were characterized by diameters ranging from 50 to 110 nm and heights ranging from 60 to 120 nm. Colloidal particles stabilized by PVA exhibited diameters from 90 to 150 nm and heights from 100 to 130 nm. Nonstabilized PANI-N formed aggregate-like structures with an average width and height in the order of units of micrometers on the mica surfaces. The resulting sizes from AFM differed from those measured by DLS analysis. However, they fully comply with TEM (Figure 3).

Cytotoxicity Is Related to the Concentration of PANI. Cytotoxicity is one of the basic biological properties determining the applicability of materials. Here, cytotoxicity was evaluated using two different cell lines, fibroblasts (NIH/3T3) and macrophages (RAW264.7). As these cell lines differ in their phenotypes and properties (fibroblasts are the most common cells of soft tissues and are mostly used for cytotoxicity evaluation, while macrophages are immune cells,

https://doi.org/10.1021/acs.biomac.2c00371
Biomacromolecules 2022, 23, 3359−3370

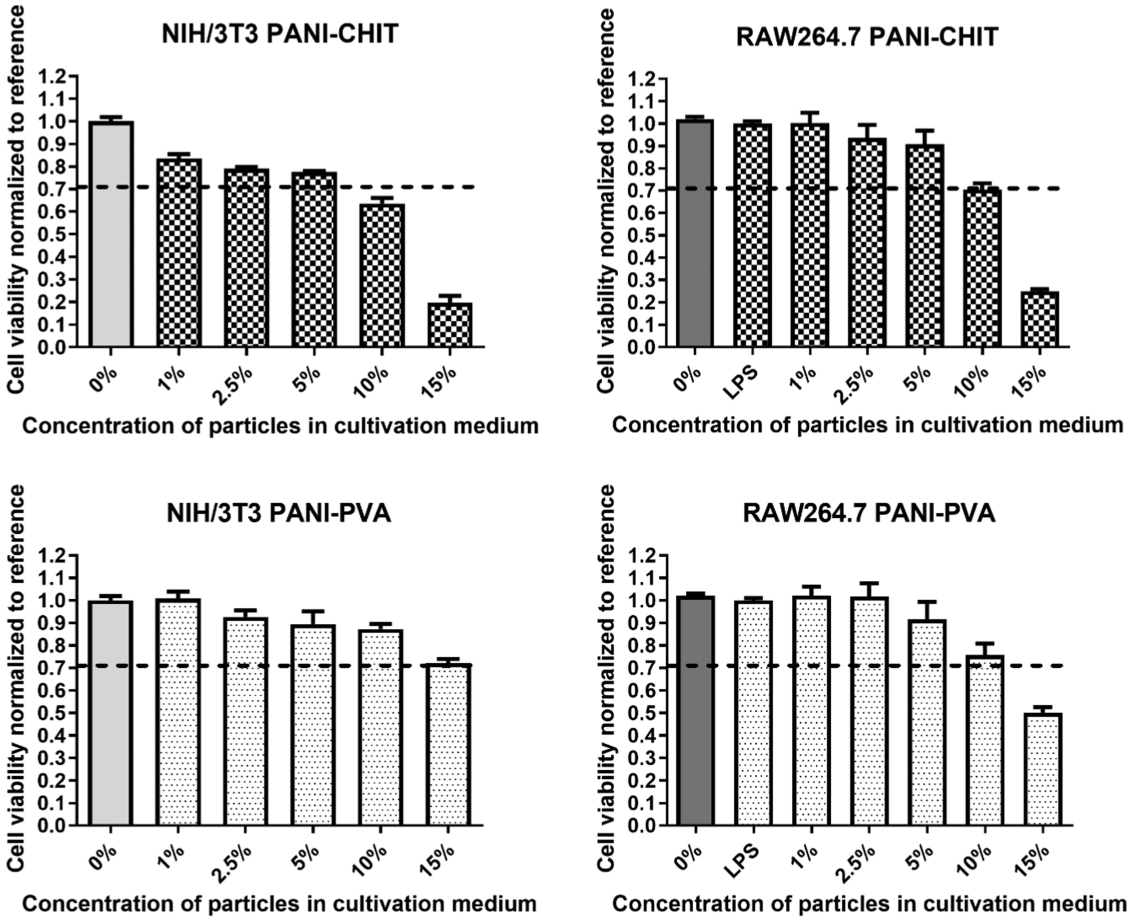

Figure 4. Cell viability in the presence of different concentrations of colloidal particles in cultivation medium. Data were converted to a relative value of the reference and expressed as the mean ± SEM (n = 3). According to EN ISO 10993-5, samples were deemed cytotoxic if the cell viability fell below a threshold value of 0.7.

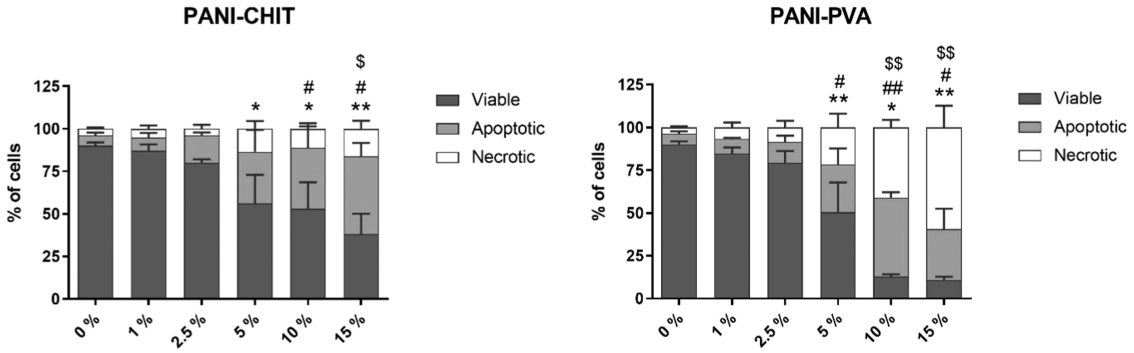

Figure 5. Effect of PANI-PVA and PANI-CHIT (1−15%) on the induction of apoptosis/necrosis in isolated neutrophils. The distribution of viable, apoptotic, and necrotic cells was determined on the basis of annexin V/PI staining after 2 h. Data were expressed as the mean ± SEM (n = 3) and analyzed by ANOVA combined with Dunnett's test ($^{**/\#\#/\$\$}p < 0.01$ and $^{*/\#/\$}p < 0.05$). * represents the statistical analysis of the viable cells, # represents the statistical analysis of the apoptotic cells, and $ represents the statistical analysis of the dead cells.

which are moreover activated by LPS before testing), the results presented here are widely representative.

For isolated and short-lived neutrophils (viable for 6−12 h), we determined the percentage of viable, apoptotic, and necrotic cells to distinguish the reason for cytotoxicity (Figure 5).

As can be seen, the cytotoxic effect was found to be very similar in the case of both cell lines (see Figures 4 and 5). The noncytotoxic threshold was achieved at dilutions of the colloidal dispersion in the cultivation medium lower than 10%, except for PANI-CHIT on NIH/3T3 cell lines. Here, cell viability slightly decreased below the noncytotoxic threshold at 10% sample dilution. In the more sensitive isolated neutrophils, the ratio of apoptotic and necrotic cells increased compared to live cells. At 5% of PANI-PVA, neutrophil viability was reduced to about 50% of the total cells, and at 10 and 15% of PANI-PVA, the viability was reduced to 15% of the total cells. In 5 and 10% of PANI-CHIT, neutrophil viability decreased to ∼50% of the total cells, and in 15% of PANI-CHIT, the viability decreased to ∼35% of the total cells. The

https://doi.org/10.1021/acs.biomac.2c00371
Biomacromolecules 2022, 23, 3359−3370

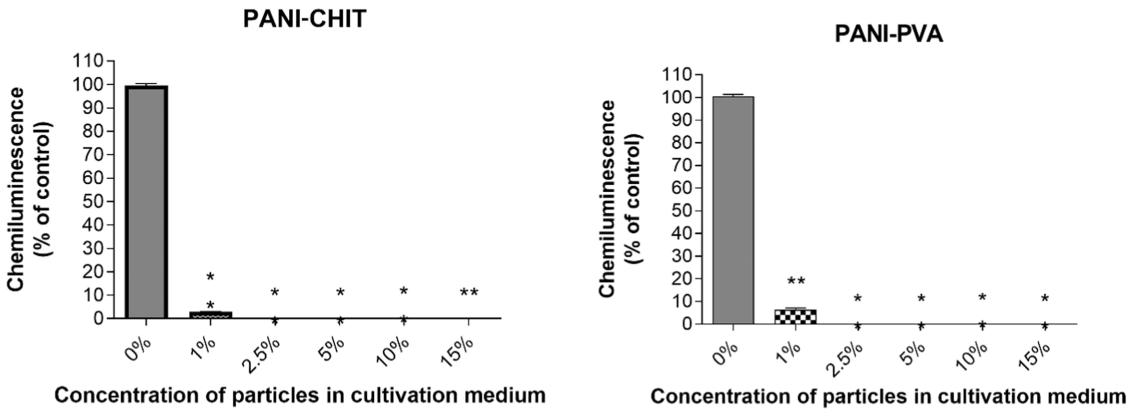

Figure 6. Antioxidant activity of PANI-PVA and PANI-CHIT. Data were converted to a percentage of the control and expressed as the mean ± SEM (n = 6). One-sample t-test was used to analyze the significance of the obtained data separately comparing the effect of each compound with the control. A Bonferroni correction of the p-value for multiple comparisons was performed (**$p < 0.01$).

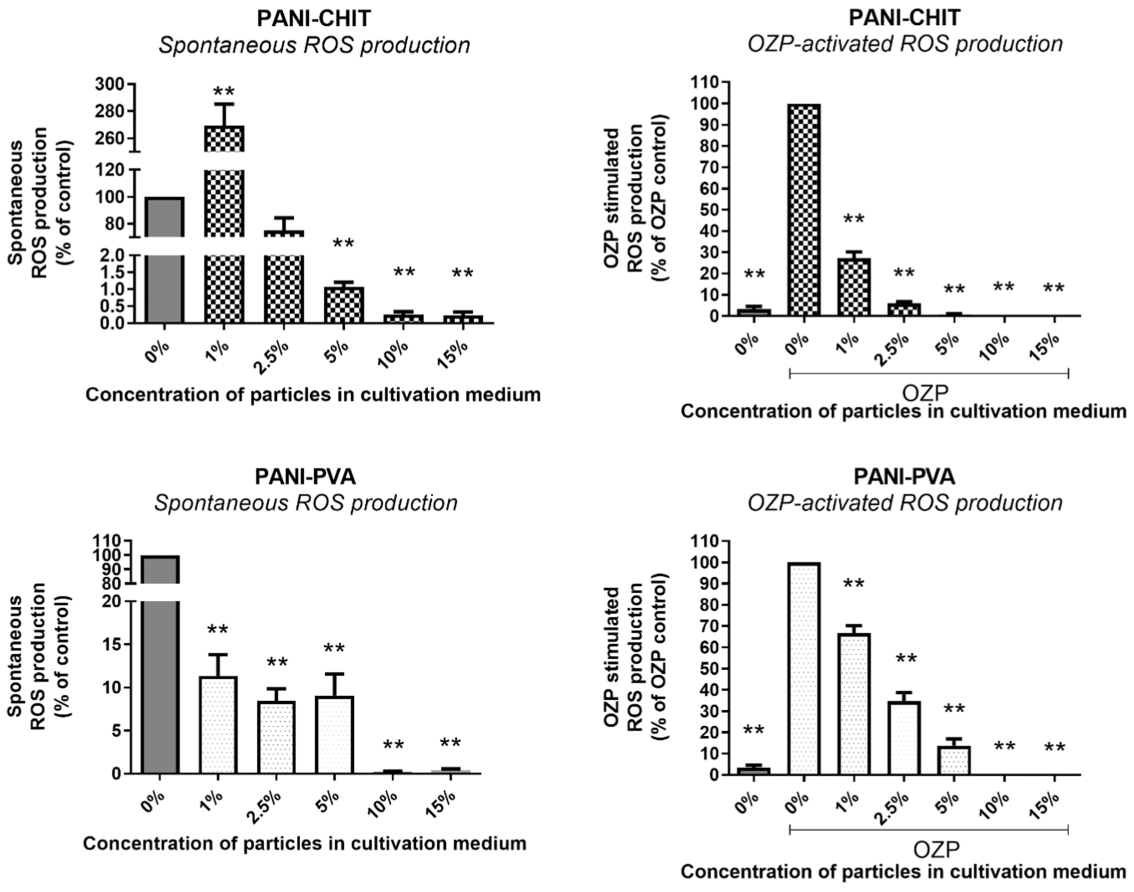

Figure 7. Effect of colloidal particles on spontaneous ROS production (left) and on OZP-activated ROS production (right) by neutrophils. Data were converted to a percentage of the control and expressed as the mean ± SEM (n = 4). One-sample t-test was used to analyze the significance of the obtained data separately comparing the effect of each compound with the control. A Bonferroni correction of the p-value for multiple comparisons was performed (**$p < 0.01$).

cytotoxic limits of the colloidal dispersions tested here obviously correlate with the contents of PANI. It has previously been reported that the cytotoxicity of PANI-based colloids could be affected not only by the concentration of PANI but also by the type of stabilizer. While the PVA stabilizer is commonly considered biocompatible,[34] the biocompatibility of CHIT is still controversial. The potential cytotoxic effect of CHIT particles was also shown to depend on the particle size[35] and could also be induced by the molecular weight of the stabilizing chitosan.[36] Kašpárková et al.[13] recently investigated the biocompatibility of PANI-CHIT colloids, and their results somewhat differ from those obtained in the current study. The absence of cytotoxicity (viability >0.8 in comparison with the reference, determined according to ISO 10993-5/2009) was observed up to a higher concentration of 90 μg mL^{-1} PANI in colloidal particles, while in the current work, the noncytotoxic threshold was 80 μg mL^{-1} PANI in colloidal particles. In this case, however, the protocol of ISO

https://doi.org/10.1021/acs.biomac.2c00371
Biomacromolecules 2022, 23, 3359−3370

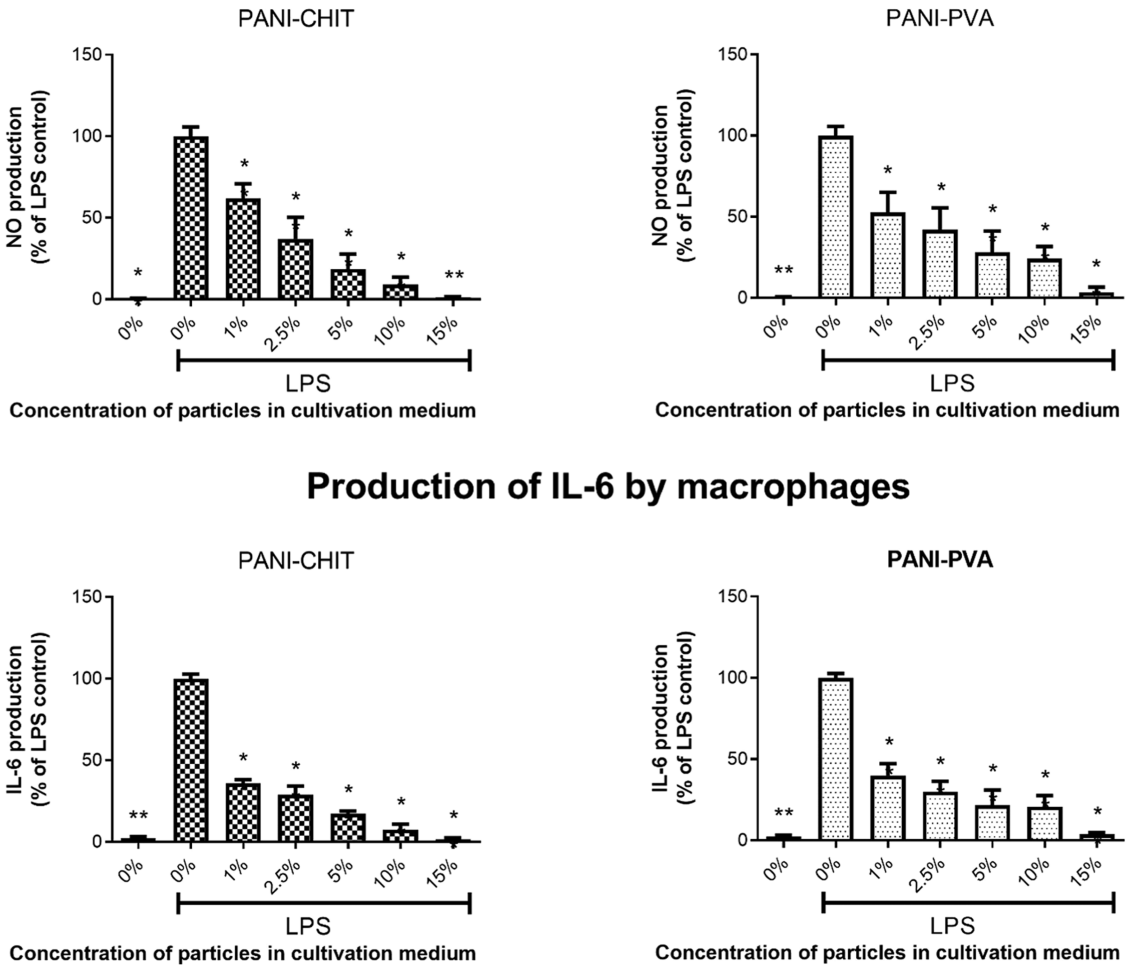

Figure 8. Effect of PANI-PVA and PANI-CHIT on NO and IL-6 production by RAW264.7 macrophages. Data were converted to a percentage of the LPS reference and expressed as the mean ± SEM (n = 3). One-sample t-test was used to analyze the significance of the obtained data separately comparing the effect of each compound with the reference. A Bonferroni correction of the p-value for multiple comparisons was performed (**p < 0.01).

10993-5 followed new limits (viability >0.7 in comparison with the reference, as given by the standard version from 2019). Based on the observations by Kašpárková et al.,[13] it can be concluded that enzymatically prepared samples are somewhat more cytotoxic in comparison with samples prepared by standard chemical oxidation.

Antioxidant Activity Contributes to Immunomodulatory Properties of Colloidal Dispersions. The immunomodulatory activity of PANI-PVA and PANI-CHIT was studied using two types of selected professional phagocytes, neutrophils (acting in blood circulation) and macrophages (acting in the tissues). The activity of both immune cell types is closely connected to the production of reactive oxygen (ROS) and nitrogen (RNS) species. Both types of phagocytic cells form an essential part of the innate immune system.

The antioxidant activity of tested compounds plays an important role in reducing the immune response and the CL signal. Therefore, we focused on detecting the antioxidant activity of PANI-PVA and PANI-CHIT.

As presented in Figure 6, both types of colloidal particles express high antioxidant activity. Even at a 1% dilution of PANI-PVA (a PANI concentration of 3.1 μg mL^{-1}) and PANI-CHIT (a PANI concentration of 7.9 μg mL^{-1}), the colloidal particles showed a significant reduction to 6.45 and 2.85% of the reference, respectively. The other tested concentrations of PANI-PVA and PANI-CHIT decreased the CL signal to 0% of the reference (Figure 5).

Colloidal Particles Significantly Reduced ROS Production in Neutrophils. First, the effect of the presence of colloidal particles on the detectable amount of ROS produced by neutrophils spontaneously and after their activation was tested.

Both types of colloidal particles significantly reduced the amount of detectable ROS produced by neutrophils spontaneously or after their activation (Figure 7). PANI-PVA significantly reduced ROS production in all tested concentrations. In contrast, 1% PANI-CHIT significantly upregulated spontaneous ROS production at other tested concentrations of PANI-CHIT, and the ROS production was reduced. At 5% dilutions of all tested samples (a PANI concentration of 15.4 μg mL^{-1} in PANI-PVA and 39.6 μg mL^{-1} in PANI-CHIT), spontaneous ROS production was reduced. When OZP was used as the activator, the tested colloidal particles were able to significantly reduce ROS production in a dose-dependent manner (Figure 6). Considering the antioxidant activity of colloidal particles (Figure 5), the effect is related to the inactivation of ROS, not to the interaction between colloidal particles and neutrophils itself.

Colloidal Particles Significantly Reduced NO and IL-6 Production in Macrophages. After their activation, for

https://doi.org/10.1021/acs.biomac.2c00371
Biomacromolecules 2022, 23, 3359−3370

example, by bacteria or parts thereof, such as LPS, many proinflammatory compounds are produced by macrophages (e.g., cytokines, chemokines, or NO). Here, the two important proinflammatory markers of macrophage activation were detected—namely, NO and IL-6.

Both tested types of colloidal particles were able to significantly reduce the production of NO and IL-6 in a dose-dependent manner (Figure 8). When compared to their potential cytotoxic activity at higher concentrations, the tested colloidal particles showed similar anti-inflammatory activity. From Figures 5−7, we can conclude that colloidal particles exhibit an anti-inflammatory effect related to their antioxidant activity, especially in the case of neutrophils.

CONCLUSIONS

Biocompatible polymers, PVA or chitosan, were used as steric stabilizers during the enzymatic polymerization of aniline in dispersed media to create PANI colloidal particles. A sample without a stabilizing component was prepared for comparison. All tested colloidal particles showed *in vitro* antioxidation activity determined via scavenging of DPPH radicals. Cytotoxicity testing demonstrated that all colloids exhibited low toxicity. Samples up to concentrations of 31 μg mL^{-1} (PANI-PVA) and 40 μg mL^{-1} (PANI-CHIT) did not show cytotoxicity (the cell viability was higher than 70%). The cytotoxicity depended mainly on the polyaniline concentration and somewhat on the type of stabilizer. All tested colloidal particles reduced oxidative stress and hindered the release of inflammatory cytokines by macrophages. The observed antioxidant capacity can be especially advantageous in the early stages of inflammation. The original approach to synthesis used here, employing environmentally friendly and biocompatible horseradish peroxidase, demonstrates a smart way of preparing conducting particles with unique properties, which can be further modified by the stabilizers used. Overall, the results of this study indicate that colloidal particles based on conducting polyaniline and chitosan (or PVA) produced by enzymatic synthesis are promising systems for biological applications.

AUTHOR INFORMATION

Corresponding Authors

Věra Kašpárková − *Centre of Polymer Systems and Faculty of Technology, Tomas Bata University in Zlín, 760 01 Zlín, Czech Republic; Faculty of Technology, Tomas Bata University in Zlín, 760 01 Zlín, Czech Republic;* Email: vkasparkova@utb.cz

Ondřej Vašíček − *Institute of Biophysics of the Czech Academy of Sciences, 612 65 Brno, Czech Republic; Institute of Experimental Biology, Faculty of Science, Masaryk University, 625 00 Brno, Czech Republic;* orcid.org/0000-0001-5892-0457; Email: ondrej.vasicek@ibp.cz

Petr Humpolíček − *Centre of Polymer Systems and Faculty of Technology, Tomas Bata University in Zlín, 760 01 Zlín, Czech Republic; Faculty of Technology, Tomas Bata University in Zlín, 760 01 Zlín, Czech Republic;* orcid.org/0000-0002-6837-6878; Email: humpolicek@utb.cz

Authors

Daniela Jasenská − *Centre of Polymer Systems and Faculty of Technology, Tomas Bata University in Zlín, 760 01 Zlín, Czech Republic*

Lukáš Münster − *Centre of Polymer Systems and Faculty of Technology, Tomas Bata University in Zlín, 760 01 Zlín, Czech Republic;* orcid.org/0000-0003-1643-2038

Antonín Minařík − *Centre of Polymer Systems and Faculty of Technology, Tomas Bata University in Zlín, 760 01 Zlín, Czech Republic;* orcid.org/0000-0002-0055-675X

Simona Káčerová − *Centre of Polymer Systems and Faculty of Technology, Tomas Bata University in Zlín, 760 01 Zlín, Czech Republic*

Eva Korábková − *Centre of Polymer Systems and Faculty of Technology, Tomas Bata University in Zlín, 760 01 Zlín, Czech Republic*

Lucie Urbánková − *Faculty of Technology, Tomas Bata University in Zlín, 760 01 Zlín, Czech Republic*

Jan Vícha − *Centre of Polymer Systems and Faculty of Technology, Tomas Bata University in Zlín, 760 01 Zlín, Czech Republic;* orcid.org/0000-0003-3698-8236

Zdenka Capáková − *Centre of Polymer Systems and Faculty of Technology, Tomas Bata University in Zlín, 760 01 Zlín, Czech Republic*

Ermelinda Falleta − *Department of Chemistry, University of Milan, 20133 Milan, Italy*

Cristina Della Pina − *Department of Chemistry, University of Milan, 20133 Milan, Italy*

Marián Lehocký − *Centre of Polymer Systems and Faculty of Technology, Tomas Bata University in Zlín, 760 01 Zlín, Czech Republic; Faculty of Technology, Tomas Bata University in Zlín, 760 01 Zlín, Czech Republic*

Kateřina Skopalová − *Centre of Polymer Systems and Faculty of Technology, Tomas Bata University in Zlín, 760 01 Zlín, Czech Republic*

Complete contact information is available at: https://pubs.acs.org/10.1021/acs.biomac.2c00371

Author Contributions

D.J.: investigation, formal analysis, and writing—original draft; V.K.: conceptualization, methodology, formal analysis, and writing—original draft and supervision; P.H.: conceptualization, methodology, and formal analysis, writing—original draft and supervision; O.V.: methodology, formal analysis, and writing—original draft; L.M.: investigation and formal analysis; A.M.: investigation and formal analysis; S.K.: investigation and formal analysis; E.K.: investigation and formal analysis; L.U.: investigation and formal analysis; M.L.: investigation, formal analysis; K.S.: investigation and formal analysis; J.V.: methodology, formal analysis, and writing—original draft; Z.C.: methodology, formal analysis, and writing—original draft; E.F.: investigation and formal analysis; and C.D.P.: investigation and formal analysis.

Funding

This work was supported by the Czech Science Foundation (20-28732S) and by the Ministry of Education, Youth and Sports of the Czech Republic—DKRVO (RP/CPS/2022/001). D.J., S.K., and E.K. also appreciate support of the Internal Grants of TBU in Zlín IGA/CPS/2022/001 funded from the resources of specific academic research. The article was supported within the project OP RDE Junior Grants of TBU in Zlín, Reg. No. CZ.02.2.69/0.0/0.0/19_073/0016941. O.V. also partially received support from European Structural and Investment Funds, Operational Program Research, Development and Education—"Preclinical Progression of New Organic Compounds with Targeted Biological Activity"

https://doi.org/10.1021/acs.biomac.2c00371
Biomacromolecules 2022, 23, 3359−3370

(Preclinprogress) CZ.02.1.01/0.0/0.0/16_025/0007381. The authors would like to thank Jan Vajďák for microbiological assessment.

Notes

The authors declare no competing financial interest.

REFERENCES

(1) Zamani, F. G.; Moulahoum, H.; Ak, M.; Demirkol, D. O.; Timur, S. Current Trends in the Development of Conducting Polymers-Based Biosensors. *TrAC, Trends Anal. Chem.* **2019**, *118*, 264−276.
(2) Wang, G.; Vivek, R.; Wang, J.-Y. Polyaniline Nanoparticles: Synthesis, Dispersion and Biomedical Applications. *Mini-Rev. Org. Chem.* **2017**, *14*, 56−64.
(3) Bagheri, B.; Zarrintaj, P.; Surwase, S. S.; Baheiraei, N.; Saeb, M. R.; Mozafari, M.; Kim, Y. C.; Park, O. O. Self-Gelling Electroactive Hydrogels Based on Chitosan−Aniline Oligomers/Agarose for Neural Tissue Engineering with on-Demand Drug Release. *Colloids Surf., B* **2019**, *184*, No. 110549.
(4) Stejskal, J.; Gilbert, R. G. Polyaniline. Preparation of a Conducting Polymer (IUPAC Technical Report). *Pure Appl. Chem.* **2002**, *74*, 857−867.
(5) Wei, X. L.; Bobeczko, C.; Epstein, A. J. *Synthesis and Physical Properties of Highly Sulfonated Polyaniline*. Technical Report; AD-A-305369/1/XAB; Department of Physics, Ohio State University: Columbus, OH; 1996.
(6) Cao, Y.; Smith, P.; Heeger, A. J. Counter-Ion Induced Processibility of Conducting Polyaniline. *Synth. Met.* **1993**, *57*, 3514−3519.
(7) Stejskal, J.; Kratochvíl, P.; Helmstedt, M. Polyaniline Dispersions. 5. Poly(Vinyl Alcohol) and Poly(N-Vinylpyrrolidone) as Steric Stabilizers. *Langmuir* **1996**, *12*, 3389−3392.
(8) Chen, F.; Liu, P. Conducting Polyaniline Nanoparticles and Their Dispersion for Waterborne Corrosion Protection Coatings. *ACS Appl. Mater. Interfaces* **2011**, *3*, 2694−2702.
(9) Yoo, J. E.; Bae, J. High-Performance Fabric-Based Supercapacitors Using Water-Dispersible Polyaniline-Poly(2-Acrylamido-2-Methyl-1-Propanesulfonic Acid). *Macromol. Res.* **2015**, *23*, 749−754.
(10) Kucekova, Z.; Humpolicek, P.; Kasparkova, V.; Perecko, T.; Lehocký, M.; Hauerlandová, I.; Sáha, P.; Stejskal, J. Colloidal Polyaniline Dispersions: Antibacterial Activity, Cytotoxicity and Neutrophil Oxidative Burst. *Colloids Surf., B* **2014**, *116*, 411−417.
(11) Boomi, P.; Poorani, G. P.; Palanisamy, S.; Selvam, S.; Ramanathan, G.; Ravikumar, S.; Barabadi, H.; Prabu, H. G.; Jeyakanthan, J.; Saravanan, M. Evaluation of Antibacterial and Anticancer Potential of Polyaniline-Bimetal Nanocomposites Synthesized from Chemical Reduction Method. *J. Cluster Sci.* **2019**, *30*, 715−726.
(12) Bober, P.; Humpolíček, P.; Syrový, T.; Capáková, Z.; Syrová, L.; Hromádková, J.; Stejskal, J. Biological Properties of Printable Polyaniline and Polyaniline−Silver Colloidal Dispersions Stabilized by Gelatin. *Synth. Met.* **2017**, *232*, 52−59.
(13) Kašpárková, V.; Jasenská, D.; Capáková, Z.; Maráková, N.; Stejskal, J.; Bober, P.; Lehocký, M.; Humpolíček, P. Polyaniline Colloids Stabilized with Bioactive Polysaccharides: Non-Cytotoxic Antibacterial Materials. *Carbohydr. Polym.* **2019**, *219*, 423−430.
(14) Jasenská, D.; Kašpárková, V.; Radaszkiewicz, K. A.; Capáková, Z.; Pacherník, J.; Trchová, M.; Minařík, A.; Vajďák, J.; Bárta, T.; Stejskal, J.; Lehocký, M.; Truong, T. H.; Moučka, R.; Humpolíček, P. Conducting Composite Films Based on Chitosan or Sodium Hyaluronate. Properties and Cytocompatibility with Human Induced Pluripotent Stem Cells. *Carbohydr. Polym.* **2021**, *253*, No. 117244.
(15) Jin, W.; Wang, R.; Huang, X. Horseradish Peroxidase-Catalyzed Oxidative Polymerization of Aniline in Bicontinuous Microemulsion Stabilized by AOT/SDS. *J. Mol. Liq.* **2020**, *302*, No. 112529.
(16) Cruz-Silva, R.; Ruiz-Flores, C.; Arizmendi, L.; Romero-García, J.; Arias-Marin, E.; Moggio, I.; Castillon, F. F.; Farias, M. H. Enzymatic Synthesis of Colloidal Polyaniline Particles. *Polymer* **2006**, *47*, 1563−1568.
(17) Cruz-Silva, R.; Escamilla, A.; Nicho, M. E.; Padron, G.; Ledezma-Perez, A.; Arias-Marin, E.; Moggio, I.; Romero-Garcia, J. Enzymatic Synthesis of PH-Responsive Polyaniline Colloids by Using Chitosan as Steric Stabilizer. *Eur. Polym. J.* **2007**, *43*, 3471−3479.
(18) Cruz-Silva, R.; Romero-García, J.; Angulo-Sánchez, J. L.; Ledezma-Pérez, A.; Arias-Marín, E.; Moggio, I.; Flores-Loyola, E. Template-Free Enzymatic Synthesis of Electrically Conducting Polyaniline Using Soybean Peroxidase. *Eur. Polym. J.* **2005**, *41*, 1129−1135.
(19) Junker, K.; Gitsov, I.; Quade, N.; Walde, P. Preparation of Aqueous Polyaniline-Vesicle Suspensions with Class III Peroxidases. Comparison between Horseradish Peroxidase Isoenzyme C and Soybean Peroxidase. *Chem. Pap.* **2013**, *67*, 1028−1047.
(20) Junker, K.; Kissner, R.; Rakvin, B.; Guo, Z.; Willeke, M.; Busato, S.; Weber, T.; Walde, P. The Use of Trametes Versicolor Laccase for the Polymerization of Aniline in the Presence of Vesicles as Templates. *Enzyme Microb. Technol.* **2014**, *55*, 72−84.
(21) Kurisu, M.; Kissner, R.; Imai, M.; Peter, W. Application of an Enzymatic Cascade Reaction for the Synthesis of the Emeraldine Salt Form of Polyaniline. *Chem. Pap.* **2021**, *75*, 5071−5085.
(22) Gizdavic-Nikolaidis, M.; Travas-Sejdic, J.; Kilmartin, P. A.; Bowmaker, G. A.; Cooney, R. P. Evaluation of Antioxidant Activity of Aniline and Polyaniline. *Curr. Appl. Phys.* **2004**, *4*, 343−346.
(23) Stejskal, J.; Kratochvíl, P.; Radhakrishnan, N. Polyaniline Dispersions 2. UV—Vis Absorption Spectra. *Synth. Met.* **1993**, *61*, 225−231.
(24) Georgiev, Y. N.; Paulsen, B. S.; Kiyohara, H.; Ciz, M.; Ognyanov, M. H.; Vasicek, O.; Rise, F.; Denev, P. N.; Yamada, H.; Lojek, A.; Kussovski, V.; Barsett, H.; Krastanov, A. I.; Yanakieva, I. Z.; Kratchanova, M. G. The Common Lavender (Lavandula Angustifolia Mill.) Pectic Polysaccharides Modulate Phagocytic Leukocytes and Intestinal Peyer's Patch Cells. *Carbohydr. Polym.* **2017**, *174*, 948−959.
(25) Vasicek, O.; Lojek, A.; Jancinova, V.; Nosal, R.; Ciz, M. Role of Histamine Receptors in the Effects of Histamine on the Production of Reactive Oxygen Species by Whole Blood Phagocytes. *Life Sci.* **2014**, *100*, 67−72.
(26) Vašíček, O.; Lojek, A.; Číž, M. Serotonin and Its Metabolites Reduce Oxidative Stress in Murine RAW264.7 Macrophages and Prevent Inflammation. *J. Physiol. Biochem.* **2020**, *76*, 49−60.
(27) Vasicek, O.; Rubanova, D.; Chytkova, B.; Kubala, L. Natural Pseurotins Inhibit Proliferation and Inflammatory Responses through the Inactivation of STAT Signaling Pathways in Macrophages. *Food Chem. Toxicol.* **2020**, *141*, No. 111348.
(28) Stejskal, J.; Kratochvíl, P.; Gospodinova, N.; Terlemezyan, L.; Mokreva, P. Polyaniline Dispersions: Preparation of Spherical Particles and Their Light-Scattering Characterization. *Polymer* **1992**, *33*, 4857−4858.
(29) Banci, L. Structural Properties of Peroxidases. *J. Biotechnol.* **1997**, *53*, 253−263.
(30) Li, Y.; Bober, P.; Apaydin, D. H.; Syrový, T.; Sariciftci, N. S.; Hromádková, J.; Sapurina, I.; Trchová, M.; Stejskal, J. Colloids of Polypyrrole Nanotubes/Nanorods: A Promising Conducting Ink. *Synth. Met.* **2016**, *221*, 67−74.
(31) Zare, E. N.; Lakouraj, M. M. Biodegradable Polyaniline/Dextrin Conductive Nanocomposites: Synthesis, Characterization, and Study of Antioxidant Activity and Sorption of Heavy Metal Ions. *Iran. Polym. J.* **2014**, *23*, 257−266.
(32) Karimi-Soflou, R.; Nejati, S.; Karkhaneh, A. Electroactive and Antioxidant Injectable In-Situ Forming Hydrogels with Tunable Properties by Polyethylenimine and Polyaniline for Nerve Tissue Engineering. *Colloids Surf., B* **2021**, *199*, No. 111565.
(33) Sapurina, I. Y.; Shishov, M. A. *Oxidative Polymerization of Aniline: Molecular Synthesis of Polyaniline and the Formation of Supramolecular Structures*, IntechOpen, 2012.
(34) Alexandre, N.; Ribeiro, J.; Gärtner, A.; Pereira, T.; Amorim, I.; Fragoso, J.; Lopes, A.; Fernandes, J.; Costa, E.; Santos-Silva, A.; Rodrigues, M.; Santos, J. D.; Maurício, A. C.; Luís, A. L. Biocompatibility and Hemocompatibility of Polyvinyl Alcohol

https://doi.org/10.1021/acs.biomac.2c00371
Biomacromolecules 2022, 23, 3359−3370

Hydrogel Used for Vascular Grafting–In Vitro and in Vivo Studies. *J. Biomed. Mater. Res., Part A* **2014**, *102*, 4262−4275.
(35) Alhomrany, R.; Zhang, C.; Chou, L. Cytotoxic Effect of Chitosan Nanoparticles on Normal Human Dental Pulp Cells. *Nanosci. Nanotechnol.* **2019**, *3*, 940.
(36) Zaki, S. S. O.; Ibrahim, M. N.; Katas, H. Particle Size Affects Concentration-Dependent Cytotoxicity of Chitosan Nanoparticles towards Mouse Hematopoietic Stem Cells. *J. Nanotechnol.* **2015**, *2015*, No. 919658.

https://doi.org/10.1021/acs.biomac.2c00371
Biomacromolecules 2022, 23, 3359−3370

ARTICLE IV

Martínková M., Hausnerová B., Huba J., Martínek T., **Káčerová S.**, Kašpárková V., Humpolíček P. Powder injection molded ceramic scaffolds: The role of pores size and surface functionalization on the cytocompatibility. Materials and Design. 2022, 224, 111274. Doi: 10.1016/j.matdes.2022.111274

Materials & Design 224 (2022) 111274

Contents lists available at ScienceDirect

Materials & Design

journal homepage: www.elsevier.com/locate/matdes

Powder injection molded ceramic scaffolds: The role of pores size and surface functionalization on the cytocompatibility

Martina Martínková [a,*], Berenika Hausnerová [a,b], Jakub Huba [b], Tomáš Martínek [c], Simona Káčerová [a], Věra Kašpárková [a,b], Petr Humpolíček [a,b,*]

[a] Tomas Bata University in Zlin, Centre of Polymer Systems, tr. Tomase Bati 5678, Zlin 76001, Czech Republic
[b] Tomas Bata University in Zlin, Faculty of Technology, Vavreckova, 275, Zlin 76001, Czech Republic
[c] Tomas Bata University in Zlin, Faculty of Applied Informatics, Nad Stranemi, 4511, Zlin 76005, Czech Republic

GRAPHICAL ABSTRACT

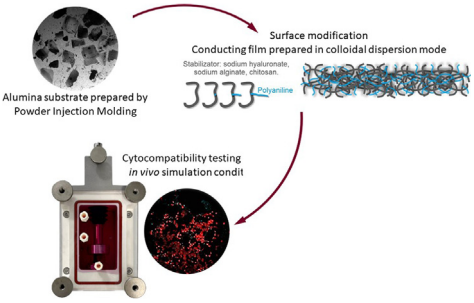

ARTICLE INFO

Article history:
Received 6 April 2022
Revised 5 October 2022
Accepted 19 October 2022
Available online 20 October 2022

Keywords:
Powder Injection Molding
Surface Modification
Polyaniline
Alumina
Tissue Engineering
Cytocompatibility

ABSTRACT

The alumina-based scaffolds prepared by powder injection molding can be preferentially used for preparation of bone grafts. Here, the final architecture of alumina scaffolds was efficiently controlled by powder space holder size and volume ratio. The alumina is not intrinsically cell-instructive material and thus the coating with electrically-conducting polyaniline or polyaniline/biopolymer films prepared in a colloidal dispersion mode was used to provide this advanced property. The component of the extracellular matrix, sodium hyaluronate, or natural biopolymers (sodium alginate or chitosan) were employed, and, subsequently, the cytocompatibility of the native and functionalized alumina scaffolds were determined. Both the absence of cytotoxicity and the cytocompatibility that were revealed demonstrate the application potential of these composites. The scaffolds with pore size greater than 250 μm were more cytocompatibility than those with pores size between 125 and 250 μm. The cytocompatibility was confirmed under *in vivo*-mimicking dynamic cultivation conditions which further improve the cell distribution and growth.

1. Introduction

Personalized medical devices such as dental prostheses, bone grafts or personalised medical devices often require the preparation of precisely designed scaffolds. While 3D printing techniques are applicable for polymer-based scaffolds, Powder Injection Molding (PIM) allows the preparation of precisely designed ceramics-

Abbreviations: CBS, ceramic-based scaffold; CH, chitosan; SA, sodium alginate; SH, sodium hyaluronate; AH, aniline hydrochloride; APS, ammonium persulfate.

* Corresponding authors.
E-mail addresses: martinkova@utb.cz (M. Martínková), hausnerova@utb.cz (B. Hausnerová), jhuba@utb.cz (J. Huba), tmartinek@utb.cz (T. Martínek), s_kacerova@utb.cz (S. Káčerová), vkasparova@utb.cz (V. Kašpárková), humpolicek@utb.cz (P. Humpolíček).

https://doi.org/10.1016/j.matdes.2022.111274
0264-1275/

based products made. The precise design together with homogeneous chemical composition [1] is considered as main advantages of PIM made materials. PIM allow to fabricate the personalised medical devices made of ceramics which can be especially advantageous in bone or dental engineering. The resulting porous PIM structures have a different internal structure to those fabricated by additive manufacturing plus allows to control the porosity [2].

Aluminum oxide (alumina) has good biocompatibility [3], excellent corrosion resistance, high wear resistance and strength, and is chemically bioinert [4]. In addition, its price is substantially lower in comparison to, for example, titanium alloys. It should also be mentioned that the production of porous alumina structures is not as demanding as in the case of titanium and its alloys, which are highly reactive and thus must be mixed, molded, and also debound/sintered carefully under protective atmospheres.

Both, the bulk and surface properties must be considered when the cytocompatibility of scaffolds are considered. From the bulk properties, the pore shape is known to affect cell behavior, as in the bone tissue regeneration process, the size and interconnection of pores affect the cell migration, proliferation, and ingrowth into the scaffold [5]. Another bulk properties such porosity [6], thermal conductivity [7], and elasticity [8] is not limited the ceramic-based scaffolds (CBS) application, but the surface characteristics are. Thus, the composites combining the appropriate bulk characteristics with stimuli-responsive surface coatings seems to be the most appropriate way for preparation of desired cell-instructive scaffolds.

One of the most suitable materials for the preparation of stimuli-responsive, and thus cell-instructive coatings is polyaniline (PANI) [5]. PANI is a widely studied conducting polymer that possesses some unique properties. For example, the coating by PANI itself is not adequately cytocompatible, but can be combined with a variety of biomolecules, by the preparation of thin films based on colloidal dispersions, to produce cytocompatible films [9,10]. PANI also intrinsically combines electronic and ionic conductivities, which is advantageous for material/cell communication. As mentioned, PANI can be stabilized by biopolymers that influence the cellular physiology [11,12]. The following compounds can be used as stabilizers: sodium hyaluronate, which can provide final material-specific bioactivity, especially changes in stem cell gene expression [13]; chitosan, which is well known for its antibacterial properties [14]; and alginate, which is widely used in a variety of biomedical applications including tissue engineering [15].

There have been studies devoted to the space-holder-assisted PIM of metal powders such as 316 L stainless steel and several titanium alloys, but there has hitherto been no report on aluminum oxide. Considering the shape of the pores, polymethyl methacrylate (PMMA) was used as a spherical space-holder for 316 L stainless steel [16,17] and Ti6Al4V [18], while sodium chloride (NaCl) and potassium chloride (KCl) have been employed in cases where an irregular shape of particles or fibers with a high L/D ratio is desired. Thus, one of the novelties of presented study is the use of KCl as space holder for aluminium oxide. Another innovative feature of the approach used in the present study is the colloidal-based coating of surfaces. Concretely, the surfaces of a substrate were coated with various films based on polyaniline (PANI) stabilized by biopolymers – in this case, sodium hyaluronate, chitosan, and sodium alginate. Using these biopolymers, cell compatibility, or more generally the biocompatibility of materials, might be controlled.

2. Materials and methods

2.1. Preparation of native ceramic-based substrates

The powder components of the PIM compound were aluminum oxide (Martinswerk – Huber Corporation, USA) (ρ = 3.98 g/cm^3, size range 0.1–3.0 μm) and a powder space holder (PSH), potassium chloride (KCl, Sigma Aldrich, Germany) (ρ = 1.98 g/cm^3, size range 125–500 μm). The powders were admixed into a partially water-soluble binder (Licomont EK 583, ρ = 1.08 g/cm^3, viscosity 1.5 mPa.s at 130 °C) in a batch mixer (Plasti-Corder, Brabender, Germany) with counter-rotating blades. The powder content was kept at 60 vol%, the powder: PSH ratio varied from 20:40 to 50:10, and two size ranges of the PSH were tested, see Table 1 (samples marked as CBS – Ceramic Based Substrates).

Injection molding was performed on an injection molding machine (Allrounder 370S, Arburg, ARBURG GmbH + Co KG, Lössburg, Germany) with a universal tooling frame. The inserts for test samples were made by machining EN AW 7022 aluminum alloy. The test geometry consisted of a round plate (diameter 45 mm) with a highly-drafted angle due to the absence of an ejector system. The molding pressures were optimized to obtain defect-free samples, (see Table 1).

Afterwards, the water-soluble binder component and part of the PSH were removed by immersion in distilled water (60 °C) for 24 h. The remaining binder (the backbone) was debound thermally (280 °C) at atmospheric pressure. Sintering was carried out in a PIM furnace (CLASIC CZ s.r.o., Revnice, Czech Republic) up to a maximum temperature of 1670 °C and for a holding time of 1 h. The surface of CBS were inspected using SEM microscopy (VEGA, Tescan).

2.2. Surface functionalization of native substrate

The surface of native CBS was further coated to become bioactive. Four different compositions of the coating were tested. Firstly, polyaniline (PANI) was used for coating. This coating can provide electroactivity but according to previous studies does not provide adequate cytocompatibility. Another three coatings were therefore prepared *via* the innovative *in-situ* polymerization of aniline hydrochloride in the presence of stabilizers – concretely, sodium hyaluronate (SH), sodium alginate (SA), and chitosan (CH) [11]. The final composite coating is denominated either as PANI/SH, PANI/SA, or PANI/CH. In all cases, aniline hydrochloride (AH, Sigma Aldrich, Germany) and ammonium persulfate (APS, Sigma Aldrich, Germany) were used for the preparation of each coating.

Preparation of PANI coating. PANI films were prepared by mixing 0.2 M AH and 0.25 M APS solutions and then pouring the reaction mixture over samples and into Petri dishes. After 1 h of polymerization, the surfaces were washed with 0.2 M HCl (Penta, Czech Republic) and rinsed with methanol (Penta, Czech Republic).

Preparation of PANI/SH coating. For the preparation of PANI with SH, 0.2 M AH, 0.1 M APS, and 1 % SH (Contipro a.s., Czech Republic) were used. SH in demineralized water was shaken at 55 °C overnight. Then, the AH solution was added, followed by the APS solution. The reaction mixture was poured over samples and into Petri dishes, and polymerization carried out for 4 h.. As before, this step was followed by washing with 0.2 M HCl and rinsing with methanol.

Preparation of PANI/SA coating. PANI film stabilized with sodium alginate (IPL, Czech Republic) was prepared using 0.2 M AH, 0.25 M APS, and 2 % SA. The solution of SA was made in demineralized water and shaken at 37 °C overnight. Afterward, AH was added, followed by APS; thereafter, samples and the Petri dishes were coated with the PANI/SA mixture. The polymer films were allowed to polymerize for 4 h. The last step was the fixation of films with 0.2 M HCl and methanol.

Preparation of PANI/CH coating. This surface modification was made with 0.2 M AH, 0.01 M APS, and 2 % chitosan (Sigma Aldrich, Germany). Firstly, a solution of CH was prepared by dissolving it in 1 M HCl and shaking the solution at 55 °C overnight. After filtration of the solution, AH was added, followed by APS. The surfaces were

Table 1
Composition of mixture and parameters of powder injection moulding process. Two ranges of PSH grain sizes were used in this study, firstly grains in the size range of 125–250 ($^{\leq 250}$) μm and grains of 250–500 μm ($^{\geq 250}$).

Abbreviation	Powder Space Holder		Powder	Pressure [bar]	
	size [μm]	[vol.%]	[vol.%]	Injection	Holding
$CBS^{\geq 250\_A}$	250–500	20	40	2100	1650
$CBS^{\geq 250\_B}$		30	30	1500	1200
$CBS^{\geq 250\_C}$		40	20	1900	1500
$CBS^{\geq 250\_D}$		50	10	2100	1650
$CBS^{\leq 250\text{-}E}$	125–250	20	40	2100	1650
$CBS^{\leq 250\text{-}F}$		30	30	1500	1200
$CBS^{\leq 250\text{-}G}$		40	20	1900	1500
$CBS^{\leq 250\text{-}H}$		50	10	2100	1650

covered with the resulting mixture and the film was left to polymerize for 12 h. Subsequently, the films were washed with 0.2 M HCl and rinsed with methanol.

2.3. Cytotoxicity determination

In the tests, a mouse embryonic fibroblast cell line (ATCC CRL-1658 NIH/3T3, USA) was used. The cultivation medium consisted of Dulbecco's Modified Eagle's Medium (PAA Laboratories GmbH, Austria) containing 10 % bovine calf serum (BioSera, France) and 1 % of Penicillin/Streptomycin (GE Healthcare HyClone, United Kingdom). The test was repeated twice, each with five repetitions per sample. Cells were incubated at 37 °C in 5 % CO_2 in humidified air.

Cytotoxicity of the native substrate. Native CBS were crushed and extracted according to ISO standard 10993–12 in media with a concentration of 0.2 g/mL. The tested samples were extracted in a culture medium for 24 h at 37 °C with stirring. The parent extracts (100 vol%) were then diluted in the culture medium to achieve final concentrations of 75, 50, 25, 10, and 1 vol%. All extracts were used within 24 h.

Cytotoxicity testing itself was performed according to ISO protocol 10 993–5. Cells were preincubated in 96 well plates (TPP, Switzerland) at a concentration of 10^5 cells per mL. The extracts were added to pre-cultivated cells for another 24 h. All tests were performed in quadruplicates. The evaluation of cell viability at the end of exposure was performed using Tetrazolium (MTT cell proliferation assay kit, Duchefa Biochemie, Netherlands). The absorbance was measured at 570 nm with an Infinite M200 Pro NanoQuant instrument (Tecan, Switzerland) and the reference wavelength was adjusted to 690 nm. The results are presented as the cell viability (%) in NIH/3T3 culture compared to that in medium without PIM extracts (reference cell viability corresponds to 1). The morphology of cells from the culture plates was assessed after their cultivation in CBS extracts by using an inverted Olympus IX 81 phase contrast microscope (Olympus, Germany).

2.4. Cytocompatibility determination

The cytocompatibility study began with the determination of cell adhesion, growth, and proliferation on (1) native CBS and (2) the films used for its functionalization. The results from these initial steps allowed us to design and perform (3) bioactivity studies in which cell growth and ingrowth under static or dynamic conditions with electrical stimulation were investigated.

The cultivation conditions for experiments 1 and 2 were the same: the cells were incubated at 37 °C in humidified air with 5 % CO_2 for 2 days. The differences were in the concentrations of seeded cells: 2×10^5 per mL for experiment 1, and half that concentration (10^5 per mL) for experiment 2. The experimental setup and cultivation conditions for experiment 3 were adjusted as follows: A concentration of 2×10^5 cells per mL was seeded on substrates with a functionalized surface. After 3 days of proliferation, samples were transferred to a bioreactor enabling electrical stimulation. The bioreactor was run for 6 h per day for a total run-time of 72 h, each successive hour-long period alternating between electrical stimulation and no stimulation. The medium flow was 54 RPM. The pulse had a rectangular waveform with a width of 3000 ms, and the voltage was set at 0.1 V. Cells were visualised through nuclei counterstaining by Hoechst 33,258 (Invitrogen, USA) and actin filaments were visualized by counterstaining with ActinRed™ 555 (Thermo Fisher Scientific, USA).

3. Results and discussion

3.1. Space holder size and volume determine the architecture of CBS

Substrate composition, architecture, pore size, and porosity all play important roles in the context of designing materials for use within biomedicine. Here, we used different sizes of space holder, different space holder *vs* powder ratios, and different processing parameters. Scaffold porosity increases with increasing additions of the powder space holder. In addition, the shape of the pores can be influenced by the shape of the PSH grains. As can be clearly seen in Fig. 1, the critical parameter determining the material properties is the space holder size and its ratio to powder, while processing parameters seems to be less important. Using these two components, the architecture, porosity, and especially the pore size can be easily controlled.

3.2. Native CBS do not induce cytotoxicity

The level of cytotoxicity predetermines any application of a material in biomedicine. Here, the ISO procedure was used to determine the cytotoxicity of the native substrate. The cytotoxicity evaluation is based on the determination of effect of soluble impurities leaching from the material, thus the cytotoxicity of substrates with functionalized surfaces was not determined, as the volume ratio of coatings was very low and could not thus induce cytotoxicity. The surface functionalization can however influence the cytocompatibility due to receptor-based interaction with cells. This issue is determined and discussed further.

As presented in Fig. 2, the native CBS did not induce cytotoxicity. Only in the case of two samples, $CBS^{\geq 250\_B,}$ $CBS^{\leq 250\text{-}F}$ marked as B and F, the cell viability slightly decreased bellow the 70 %, and thus approach the cytotoxicity threshold. If the standard deviations and cytotoxicity of higher concentrations (in case of sample B) are considered, the cytotoxicity of those concentrations was not clearly proved. It can thus be concluded that native CBS are applicable in biomedicine and can be further functionalized to become bioactive.

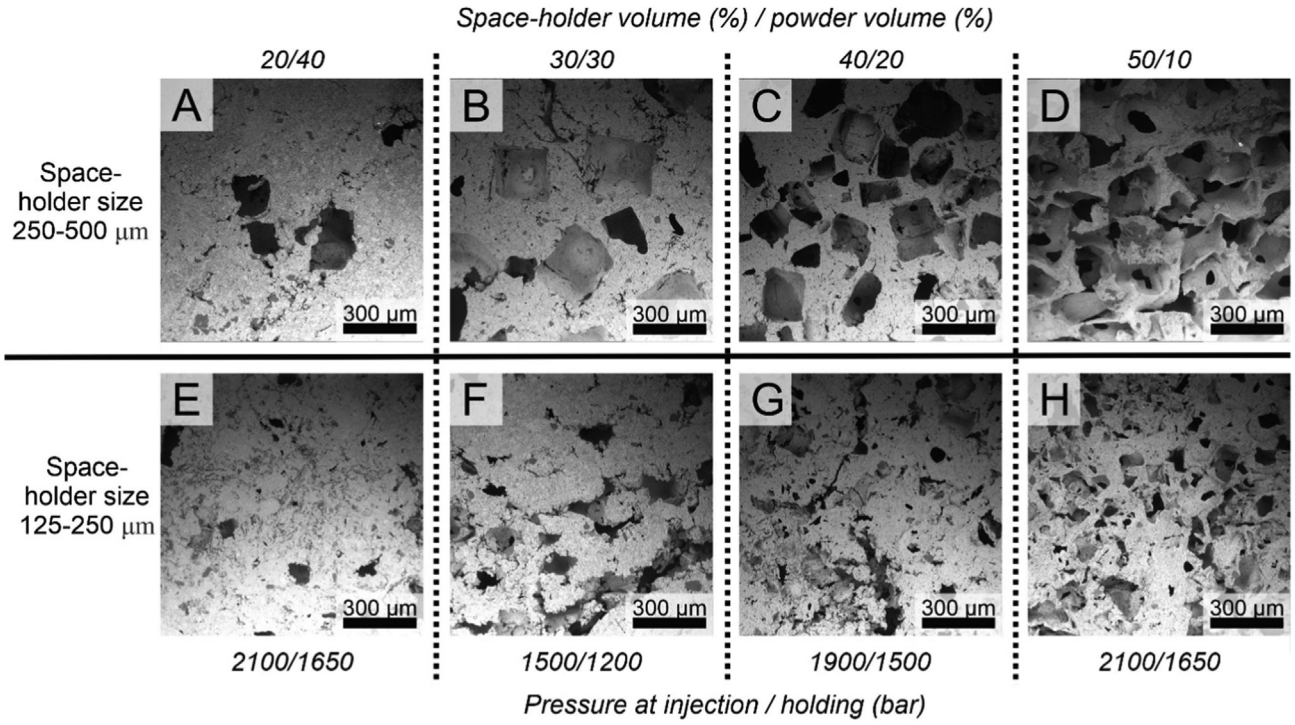

Fig. 1. SEM images of the structure of native CBS prepared using different compositions and preparation parameters. The effect of the size of the space-holder as well as the ratio between space and powder volume on the final structure of the substrate can be clearly seen. The pore size is highly correlated to the size of space holder, while the space holder / powder volume ration predetermine the porosity and pore interconnection. A = $CBS^{\geq 250\_A}$ B = $CBS^{\geq 250\_B}$, C = $CBS^{\geq 250\_C}$, D = $CBS^{\geq 250\_D}$, E = $CBS^{\leq 250\text{-}E}$, F = $CBS^{\leq 250\text{-}F}$, G = $CBS^{\leq 250\text{-}G}$, H = $CBS^{\leq 250\text{-}H.}$

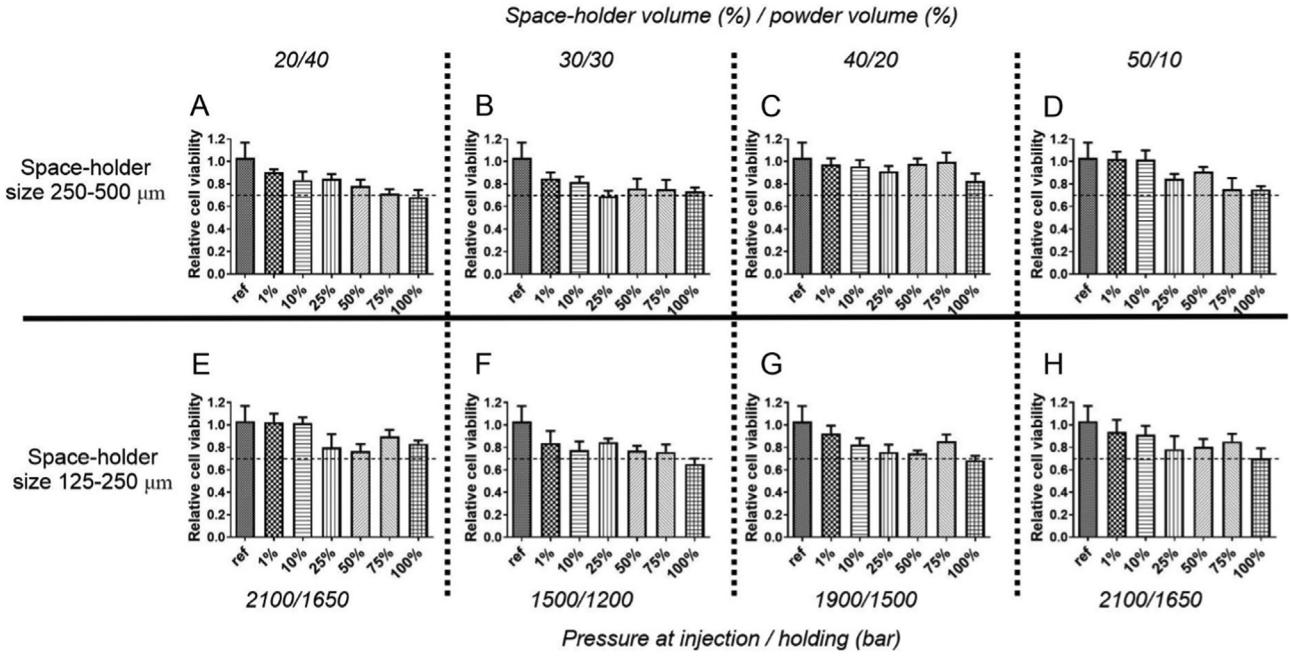

Fig. 2. The cytotoxicity of native CBS determined by a decrease in cell viability compared to the reference (data were converted to a percentage of the control and expressed as the mean ± standard deviation, n = 5). The ISO 10–993 procedure, concretely the testing of extracts, was used. The cytotoxicity threshold is marked by dashed lines; when the viability falls below 70 %, samples are considered to induce cytotoxicity. None of the tested native substrates induced cytotoxicity. A = $CBS^{\geq 250\_A}$; B = $CBS^{\geq 250\_B}$, C = $CBS^{\geq 250\_C}$, D = $CBS^{\geq 250\_D}$, E = $CBS^{\leq 250\text{-}E}$, F = $CBS^{\leq 250\text{-}F}$, G = $CBS^{\leq 250\text{-}G}$, H = $CBS^{\leq 250\text{-}H.}$

3.3. Bioactive coatings prepared in colloidal dispersion mode are cytocompatible

The conductivity is one of the crucial properties when the bioactivity of bone scaffolds and grafts are considered [19]. The conductivity can be achieved by incorporation of conducting polymers. It was, however, previously determined that native PANI does not provide an adequate cell response, which was also confirmed by this study (see Fig. 3B). Functionalization was therefore performed by means of an innovative procedure combining the

synthetic conducting polymer (providing stimuli-responsivity) with biopolymers (providing cytocompatibility). The procedure is based on the preparation of thin films in colloidal dispersion mode [10]. The final composite coating can thus provide both bioactivity and cytocompatibility.

To confirm the cytocompatibility of the surface functionalization employed here, cells were seeded onto surfaces and their proliferation and morphology were determined. The quantification of cells on the individual surfaces was not determined due to both the interaction of films with reagents used for cell viability evaluation (especially the MTT assay results can be biased) and due to the fact, that cell quantity does not provide relevant information about the real cytocompatibility which depends on cell physiology and morphology. It is clearly shown that cells on the PANI films were not capable of proliferation (see Fig. 3B). From the study [11], it is known that the addition of biocompatible polysaccharides to colloidal films changes the surface energy and surface topography, which can also lead to a change in cytocompatibility. Fig. 3C show that the number of cells on the surface modified with PANI/SA was smaller than the numbers of cells on the surfaces modified with PANI/SH (Fig. 3E) and PANI/CH (Fig. 3D) film. Also, on PANI/SA (Fig. 3C), round cells could be observed that were capable of adhering onto the surface, but they could not proliferate. The number of cells on the surface stabilized by alginate was smaller in comparison to the other stabilized films. Fig. 3E shows the cell on the surface coated with PANI/SH are present in higher quantity and especially their morphology is more physiological. This could be because of SH, which can support not only cell adhesion and proliferation but mainly their physiological state according to the type of adhered cells. The actin cytoskeleton of cells on this film was more fibrous compared to the reference sample (Fig. 3A). The proliferation rate on the PANI/CH film (Fig. 3D) was similar to that on the PANI/SH film and also the morphology of actin fibers was similar in these two cases. It can be clearly seen that the best cytocompatibility was offered by the PANI/SH and PANI/CH coatings. From those, the PANI/SH was later chosen as the most promising treatment for the determination of bioactivity under dynamic cultivation conditions. Sodium hyaluronate was chosen with regard to bioactivity related to stem cell differentiation [20].

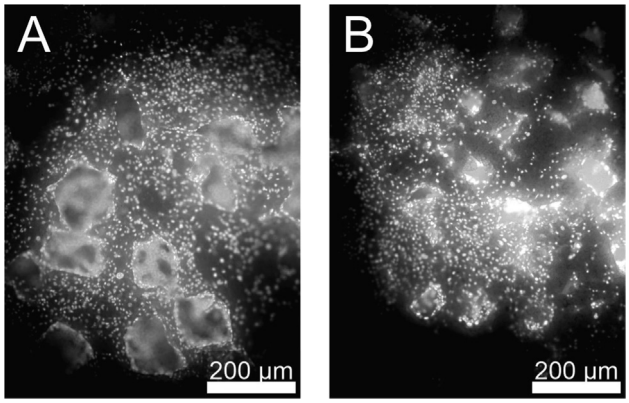

Fig. 4. Cell growth on the surface and within the pores of native $CBS^{\geq 250\_B}$ (A) and $CBS^{\leq 250\_F}$ (B) prepared with 30 vol% of space holder. The cells were seeded in a concentration of 2×10^5 cells per mL and cultivated for 2 days. Individual cells were visualised through nuclei counterstaining by Hoechst (white). There were no significant differences between any of native CBS. The $CBS^{\geq 250\_D}$ were chosen as the most appropriate for other experiments.

3.4. Cells can grow on the surface and within the pores of CBS under static cultivation conditions

In addition, cell growth on the surface of the sample, as well as cell ingrowth into the pores were investigated on native as well functionalized CBS. Cells were able to attach to, and subsequently grow on all mentioned samples.

Fig. 4 provides a detailed view of the surface of the native CBS without any surface treatment and with different pores sizes (A 250 μm and more, B 125–250 μm). Overall, the growth of cells was better on samples with a pore size greater than 250 μm than on samples with a pore size between 125 and 250 μm. The lowest viability was observed for CBS functionalized with PANI. In contrast, functionalization by films prepared in colloidal dispersion mode improved cell growth on PIM samples in the case of all stabilizers. Also, there were no significant differences in cell growth between $CBS^{PANI/SH}$, $CBSP^{PANI/SA}$, and $CBS^{PANI/CH}$. Moreover, the cell

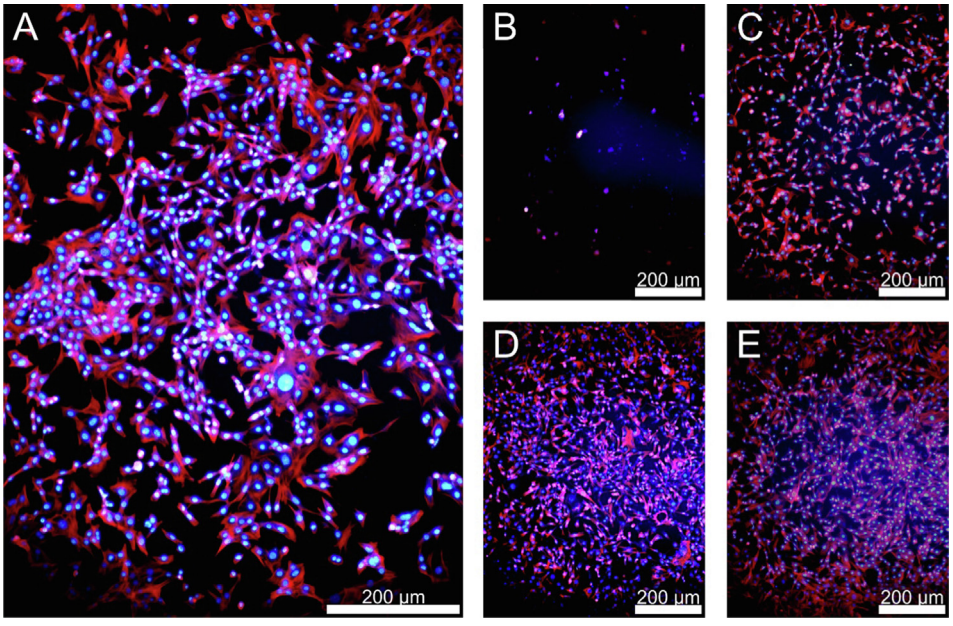

Fig. 3. Cell proliferation on reference – the cell culture polystyrene without surface modification (A); PANI (B), PANI/SA (C); PANI/CH (D); and PANI/SH (E). Cells were seeded in a concentration of 10^5 cells per mL and cultivated for 2 days. Cell nuclei were visualized by counterstaining with Hoechst; actin filaments were visualized by counterstaining with ActinRed™ 555 The appropriate cytocompatibility was observed in the case of the PANI/CH and PANI/SH coating.

quantity was very similar to that observed for pure PIM samples. Based on microscopic observations it can be concluded, that cells were able to ingrowth deeper into the pores in all of the samples.

Due to the best cytocompatibility of CBS with pores higher than 250 μm and most promising properties of PANI/SH based coating the only CBS$^{\geq 250_D_PANI/SH}$ was used for further experiments.

3.5. Dynamic conditions and electrical stimulation improve cytocompatibility

The final goal of the here presented study was to prepare a CBS which is not only cytocompatible but also possess stimuli-responsive and thus even cell-instructive potential. The importance of *in vivo* occurred dynamic condition is often omitted within the cytocompatibility study. In this context, the mechanotransduction which integrates various physical cues from a cell's surrounding microenvironment and converts them into biochemical intracellular signaling responses are most important. The flow of cultivation medium (shear stress) is main part of mechanotransduction when the bone scaffolds are considered. Here we apply the media flow 54 RPMI. Except of mechanotransduction, the instructive role of electroconductivity is obviously of great importance. Especially in case of bone tissue, the role of electroconductivity of materials is discussed [21].

There are no generally accepted protocols used for the electrical stimulation of cells, the set-ups vary not only in the applied voltage (from ~ 4–5 mV to 150 mV) but also pulse duration (mostly from 2 ms to 200 ms), frequency (mostly between 2 and 6 Hz), and waveform (e.g. monophasic, square) [19,22,23]. In here presented experiments the commercial equipment was used and the electrical stimulation parameters were as follows: voltage 0.1 V, pulse width 3000 ms, arrangement on square-wave.

As mentioned, the CBS with a pore size above 250 μm was chosen for the experiments under dynamic conditions. The preferential cytocompatibility of materials with pore size of about 200 to 300 μm is generally considered as ideal for bone tissue replacements [24] and was confirmed even on the CBS (see Fig. 4A). The coating with PANI/SH was chosen as the most promising, mainly due to the bioactivity of SH.

Both described cell-stimuli external factors, shear stress and external electrical stimuli, were applied together, and the results are presented in Fig. 5. It is obvious that application of shear stress and external electrical stimulation has an important effect on few cellular parameters (please compare the Fig. 5A and 5B versus 5C and 5D). Firstly, the cell quantity is higher on the surfaces exposed to dynamic conditions, and more importantly the cell distribution is more homogeneous. This is critical for the scaffold acceptance after implantation [25]. In addition, a slightly different cell morphology and structure of cytoskeleton can be observed under dynamic conditions with electrical pulses than under static conditions. This can be connected to both the applied shear stress and electrostimulation [26,27].

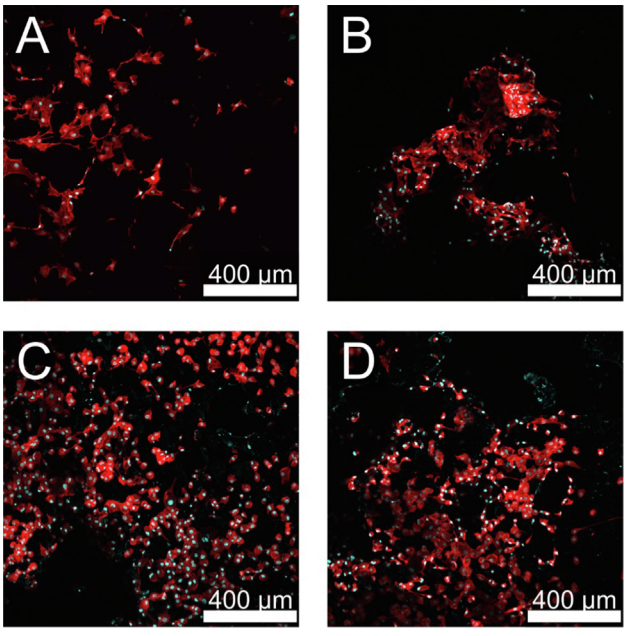

Fig. 5. Cell distribution and cell morphology on CBS$^{\geq 250_D_PANI/SH}$ under static (A,B) or dynamic (C,D) cultivation conditions. Cells were seeded in a concentration of 2 × 10^5 cells per mL and precultivated in static conditions for 3 days and subsequently cultivated in dynamic conditions for another 3 days. Cell nuclei are visualized by counterstaining with Hoechst, actin filaments are visualized by counterstaining with ActinRed. Parameters of dynamic conditions: Media flow 54 RPMI, pulse width 3000 ms, square waveform, voltage 0.1 V.

4. Conclusion

Ceramic-based scaffolds prepared by Powder Injection Molding are promising candidates for use as medical scaffolds, especially in bone regeneration and restoration. The composition of the PIM mixture as well as the processing parameters were tested to reveal their impact on the architecture of the porous material. It was found that the final architecture can be efficiently controlled by the powder space holder size and the volume ratio. However, alumina itself does not provide adequate cytocompatibility, or, especially, bioactivity. None of the prepared ceramic-based scaffolds induced cytotoxicity, and more importantly, cells were able to grow on their surface and ingrowth into the pores. The scaffolds surfaces were therefore subsequently functionalized by stimuli-responsive polyaniline-based films. To improve the cytocompatibility, coatings were innovatively prepared in colloidal dispersion mode and combined the synthetic conducting polymer with biopolymer stabilizers (sodium hyaluronate, chitosan, and sodium alginate). This functionalization further significantly improved the cytocompatibility of the ceramic-based scaffolds. The bioactivity of the prepared scaffolds was confirmed by an improvement in cytocompatibility when dynamic cultivation conditions and electrical impulses were applied. The *in vivo* mimicking conditions improve the cytocompatibility of scaffolds, especially in context of cell distribution and growth.

Data availability

Data will be made available on request.

Declaration of Competing Interest

The authors declare that they have no known competing financial interests or personal relationships that could have appeared to influence the work reported in this paper.

Acknowledgements

The work was supported within the project OP RDE Junior Grants of TBU in Zlin, Reg. No. CZ.02.2.69/0.0/0.0/19_073/0016941 (JUNG-2020-001), Czech Science Foundation (20-28732S) and Ministry of Education, Youth and Sports of the Czech Republic – DKRVO (RP/CPS/2022/001 and RP/CPS/2022/003).

Appendix A. Supplementary material

Supplementary data to this article can be found online at https://doi.org/10.1016/j.matdes.2022.111274.

References

[1] G. Matula, A. Szatkowska, K. Matus, B. Tomiczek, M. Pawlyta, Structure and properties of Co-Cr-Mo alloy manufactured by powder injection molding method, Materials 14 (8) (Apr. 2021) 2010, https://doi.org/10.3390/ma14082010.

[2] D. Zhao et al., Surface topography and cytocompatibility of metal injection molded Ti–22Nb alloy as biomaterial, Trans. Nonferrous Metals Soc. China 28 (7) (Jul. 2018) 1342–1350, https://doi.org/10.1016/S1003-6326(18)64772-7.

[3] M. Rahmati, M. Mozafari, Biocompatibility of alumina-based biomaterials–a review, J. Cell Physiol. 234 (4) (Apr. 2019) 3321–3335, https://doi.org/10.1002/jcp.27292.

[4] D.F. Heaney, J.D. Gurosik, C. Binet, Isotropic forming of porous structures via metal injection molding, J. Mater. Sci. 40 (4) (Feb. 2005) 973–981, https://doi.org/10.1007/s10853-005-6516-1.

[5] Y. Arteshi, A. Aghanejad, S. Davaran, Y. Omidi, Biocompatible and electroconductive polyaniline-based biomaterials for electrical stimulation, Eur. Polym. J. 108 (Nov. 2018) 150–170, https://doi.org/10.1016/j.eurpolymj.2018.08.036.

[6] J.L. Hernandez, K.A. Woodrow, Medical Applications of Porous Biomaterials: Features of Porosity and Tissue-Specific Implications for Biocompatibility, Adv Healthcare Materials 11 (9) (May 2022) 2102087, https://doi.org/10.1002/adhm.202102087.

[7] M.S. Zafar et al., "Properties of dental biomaterials", in *Advanced Dental Biomaterials*, Elsevier (2019) 7–35, https://doi.org/10.1016/B978-0-08-102476-8.00002-5.

[8] A.M.J. Coenen, K.V. Bernaerts, J.A.W. Harings, S. Jockenhoevel, S. Ghazanfari, Elastic materials for tissue engineering applications: Natural, synthetic, and hybrid polymers, Acta. Biomater. 79 (Oct. 2018) 60–82, https://doi.org/10.1016/j.actbio.2018.08.027.

[9] P. Bober, P. Humpolíček, J. Pacherník, J. Stejskal, T. Lindfors, Conducting polyaniline based cell culture substrate for embryonic stem cells and embryoid bodies, RSC Adv. 5 (62) (2015) 50328–50335, https://doi.org/10.1039/C5RA07504A.

[10] V. Kašpárková et al., Cell-compatible conducting polyaniline films prepared in colloidal dispersion mode, Colloids Surf., B 157 (Sep. 2017) 309–316, https://doi.org/10.1016/j.colsurfb.2017.05.066.

[11] D. Jasenská et al., Conducting composite films based on chitosan or sodium hyaluronate. Properties and cytocompatibility with human induced pluripotent stem cells, Carbohydr. Polym. 253 (Feb. 2021), https://doi.org/10.1016/j.carbpol.2020.117244 117244.

[12] V. Kašpárková et al., Polyaniline colloids stabilized with bioactive polysaccharides: Non-cytotoxic antibacterial materials, Carbohydr. Polym. 219 (Sep. 2019) 423–430, https://doi.org/10.1016/j.carbpol.2019.05.038.

[13] M. Hemshekhar, R.M. Thushara, S. Chandranayaka, L.S. Sherman, K. Kemparaju, K.S. Girish, Emerging roles of hyaluronic acid bioscaffolds in tissue engineering and regenerative medicine, Int. J. Biol. Macromol. 86 (May 2016) 917–928, https://doi.org/10.1016/j.ijbiomac.2016.02.032.

[14] F. Croisier, C. Jérôme, Chitosan-based biomaterials for tissue engineering, Eur. Polym. J. 49 (4) (Apr. 2013) 780–792, https://doi.org/10.1016/j.eurpolymj.2012.12.009.

[15] J. Sun, H. Tan, Alginate-Based Biomaterials for Regenerative Medicine Applications, Materials 6 (4) (Mar. 2013) 1285–1309, https://doi.org/10.3390/ma6041285.

[16] H.Ö. Gülsoy, R.M. German, Production of micro-porous austenitic stainless steel by powder injection molding, Scr. Mater. 58 (4) (Feb. 2008) 295–298, https://doi.org/10.1016/j.scriptamat.2007.10.004.

[17] K. Nishiyabu, S. Matsuzaki, S. Tanaka, Net-Shape Manufacturing of Micro Porous Metal Components by Powder Injection Molding, MSF 534–536 (Jan. 2007) 981–984, https://doi.org/10.4028/www.scientific.net/MSF.534-536.981.

[18] G. Engin, B. Aydemir, H.Ö. Gülsoy, Injection molding of micro-porous titanium alloy with space holder technique, Rare Met. 30 (6) (Dec. 2011) 565–571, https://doi.org/10.1007/s12598-011-0430-2.

[19] L. Leppik et al., Combining electrical stimulation and tissue engineering to treat large bone defects in a rat model, Sci. Rep. 8 (1) (Dec. 2018) 6307, https://doi.org/10.1038/s41598-018-24892-0.

[20] M.B. Asparuhova, V. Chappuis, A. Stähli, D. Buser, A. Sculean, Role of hyaluronan in regulating self-renewal and osteogenic differentiation of mesenchymal stromal cells and pre-osteoblasts, Clin. Oral. Invest. 24 (11) (Nov. 2020) 3923–3937, https://doi.org/10.1007/s00784-020-03259-8.

[21] D.T. Dixon, C.T. Gomillion, Conductive Scaffolds for Bone Tissue Engineering: Current State and Future Outlook, JFB 13 (1) (Dec. 2021) 1, https://doi.org/10.3390/jfb13010001.

[22] K. Ronaldson-Bouchard et al., Advanced maturation of human cardiac tissue grown from pluripotent stem cells, Nature 556 (7700) (Apr. 2018) 239–243, https://doi.org/10.1038/s41586-018-0016-3.

[23] Z. Zhao et al., Optimization of Electrical Stimulation for Safe and Effective Guidance of Human Cells, Bioelectricity 2 (4) (Dec. 2020) 372–381, https://doi.org/10.1089/bioe.2020.0019.

[24] C.M. Murphy, M.G. Haugh, F.J. O'Brien, The effect of mean pore size on cell attachment, proliferation and migration in collagen–glycosaminoglycan scaffolds for bone tissue engineering, Biomaterials 31 (3) (Jan. 2010) 461–466, https://doi.org/10.1016/j.biomaterials.2009.09.063.

[25] C. Kleinhans et al., A perfusion bioreactor system efficiently generates cell-loaded bone substitute materials for addressing critical size bone defects, Biotechnol. J. 10 (11) (Sep. 2015) 1727–1738, https://doi.org/10.1002/biot.201400813.

[26] C. Chen, X. Bai, Y. Ding, I.-S. Lee, Electrical stimulation as a novel tool for regulating cell behavior in tissue engineering, Biomater. Res. 23 (1) (Dec. 2019) 25, https://doi.org/10.1186/s40824-019-0176-8.

[27] J. Hansmann, F. Groeber, A. Kahlig, C. Kleinhans, H. Walles, Bioreactors in tissue engineering-principles, applications and commercial constraints, Biotechnol. J. 8 (3) (Mar. 2013) 298–307, https://doi.org/10.1002/biot.201200162.